INFORMATION TO USERS

This manuscript has been reproduced from the microfilm master. UMI films the text directly from the original or copy submitted. Thus, some thesis and dissertation copies are in typewriter face, while others may be from any type of computer printer.

The quality of this reproduction is dependent upon the quality of the copy submitted. Broken or indistinct print, colored or poor quality illustrations and photographs, print bleedthrough, substandard margins, and improper alignment can adversely affect reproduction.

In the unlikely event that the author did not send UMI a complete manuscript and there are missing pages, these will be noted. Also, if unauthorized copyright material had to be removed, a note will indicate the deletion.

Oversize materials (e.g., maps, drawings, charts) are reproduced by sectioning the original, beginning at the upper left-hand corner and continuing from left to right in equal sections with small overlaps.

Photographs included in the original manuscript have been reproduced xerographically in this copy. Higher quality 6" x 9" black and white photographic prints are available for any photographs or illustrations appearing in this copy for an additional charge. Contact UMI directly to order.

UMI®

Computational Studies on Topics of Environmental Interest:

From Kinetics to Excited States

by

Nelaine M. Mora Diez

Submitted in partial fulfillment of the requirements
for the degree of Doctor of Philosophy

at

Dalhousie University
Halifax, Nova Scotia
August, 2001

DALHOUSIE UNIVERSITY

FACULTY OF GRADUATE STUDIES

The undersigned hereby certify that they have read and recommend to the
Faculty of Graduate Studies for acceptance a thesis entitled "Computational
Studies on Topics of Environmental Interest: From Kinetics to Excited States" by
Nelaine M. Mora Diez in partial fulfillment of the requirements for the degree of
Doctor of Philosophy.

Dated: _____September 7, 2001_____

External Examiner:

Research Supervisor:

Examining Committee:
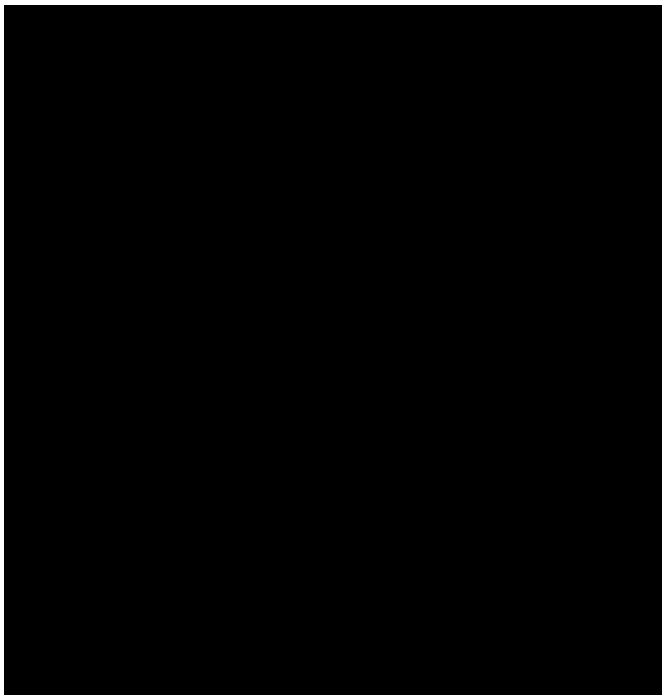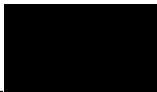
DALHOUSIE UNIVERSITY

Date: September 7, 2001

Author: _____ Nelaine M. Mora Diez _____

Title: _____ Computational Studies on Topics of Environmental Interest: _____

_____ From Kinetics to Excited States _____

Department or School: _____ Department of Chemistry _____

Degree: Ph. D.   Convocation: October   Year: 2001

Permission is herewith granted to Dalhousie University to circulate and to have copied for non-commercial purposes, at its discretion, the above title upon the request of individuals or institutions.

_____
Signature of Author

The author reserves other publication rights, and neither the thesis nor extensive extracts from it may be printed or otherwise reproduced without the author's written permission.

The author attests that permission has been obtained for the use of any copyrighted material appearing in this thesis (other than brief excerpts requiring only proper acknowledgement in scholarly writing), and that all such use is clearly acknowledged.

To you, my dear sister,
because your path was always there
to illuminate my own.

To my parents,
for all their love, support,
encouragement and trust
through these years.

To my dearest professors,
because in me there is a little
of every one of you.

Table of Contents

List of Figures

List of Tables

Abstract

There are a number of critical environmental issues associated with a changing atmosphere and a great deal of research and development activity is aimed at understanding and solving some of the problems that arise from industrial development. This thesis concentrates on computational studies on systems of environmental interest, covering aspects related to the calculation of kinetic parameters and excited states.

Aldehydes, known to play an important role in the pollution of the troposphere, are emitted as primary pollutants from partial oxidation of hydrocarbon fuels and arise as secondary pollutants from the oxidation of volatile organic compounds. Once in the atmosphere, aldehydes either photolyse or react further with OH radicals during the day, or with NO_3 radicals during the night. High-level *ab initio* calculations have been performed to examine the OH and NO_3 hydrogen-abstraction reactions from a series of aldehydes (XCHO, X = F, Cl, H, CH_3). In addition, classical transition state theory has been applied for the calculation of the rate constants. The importance of considering the reactant complex formation in the kinetics of some of these reactions is discussed, and new theoretical predictions for kinetic data are reported.

Polycyclic aromatic compounds (PACs) are of great interest to the petroleum industry since they interfere with refining operations, and federal environmental regulations have been created to reduce their emission to the atmosphere. The characterization of PACs in petroleum-related samples is extremely difficult. Theoretical semi-empirical methods have been used to study the effects of methyl and reduced-ring substitution on the excited states of naphthalene, the smallest polycyclic aromatic hydrocarbon. Regularities are found and an explanation is given for an "anomalous" behaviour.

List of Acronyms

AM1	Austin model 1
AO	Atomic orbital
au	Atomic units
BH&H	Becke half and half
BSSE	Basis set superposition error
B3LYP	Hybrid DFT functional B3 + LYP
B3P86	Hybrid DFT functional B3 + P86
B3PW91	Hybrid DFT functional B3 + PW91
BLYP	GGA functional B + LYP
BH&HLYP	Hybrid DFT functional BH&H + LYP
CASSCF	Complete active-space self-consistent field
CC	Coupled cluster
CCSD(T)	Coupled cluster including single, doubles and triplets (perturbative way)
CF	Configuration function
CI	Configuration interaction
CIS	Configuration interaction including singly excited determinants
CNDO	Complete neglect of differential overlap
CNDO/S	Spectroscopic CNDO
CP	Counterpoise
CPU	Central processor unit
DFP	Davidson-Fletcher-Powell
DFT	Density functional theory
EF	Eigenvector following
GDIIS	Geometric direct inversion of the iterative subspace
GGA	Generalized gradient approximation
GTO	Gaussian-type orbital
HA	Hydrogen affinity
HF	Hartree-Fock
HMO	Hückel molecular orbital theory
HOMO	Highest occupied MO

HPLC	High performance liquid chromatography
H, H1, H2	HOMO, HOMO-1, HOMO-2 orbitals
INDO	Intermediate neglect of differential overlap
INDO/S	Spectroscopic INDO
IRC	Intrinsic reaction coordinate
JT	Jahn-Teller
LSDA	Local spin density approximation
LDA	Local density approximation
LUMO	Lowest unoccupied MO
L, L1, L2	LUMO, LUMO+1, LUMO+2 orbitals
MEE	Maximum excitation energy
MNDO	Modified neglect of differential overlap
MO	Molecular orbital
MP	Møller-Plesset
MR-CI	Multi-reference CI
MRD-CI	Multi-reference double excitation CI
NDDO	Neglect of diatomic differential overlap
PACs	Polycyclic aromatic compounds
PAHs	Polycyclic aromatic hydrocarbons
PAN	Peroxyacetyl nitrate
PCA	Principal component analysis
PEH	Potential energy hypersurface
PMP2	Projected Spin-unrestricted Møller-Plesset (second order)
PPP	Pariser-Parr-Pople method
PT	Perturbation theory
Prod	Products
PUHF	Projected spin-unrestricted Hartree-Fock
RC	Reactant complex
React	Reactants
RH	Roothaan-Hall
ROHF	Spin-restricted open-shell calculation

RPA	Random phase approximation
RRKM/QET	Rice-Ramsperger-Kassel-Marcus/quasi-equilibrium theory
SAM1	Semi-*ab initio* method 1
SCF	Self-consistent-field
SCRF	Self-consistent reaction field
SINDO1	Symmetrically orthogonalized INDO
STO	Slater-type orbital
TCE	Thermal correction to the energy
TD-HF	Time-dependent HF
TD-DFT	Time-dependent DFT
TNDO	Typed neglect of differential overlap
TS	Transition state
TST	Transition state theory
UHF	Spin-unrestricted Hartree-Fock
UMP	Spin-unrestricted Møller-Plesset
UV-vis	Ultraviolet-visible
VTST	Variational TST
ZDO	Zero differential overlap
ZINDO	see INDO/S
ZINDO/S	see INDO/S
ZPE	Zero-point energy correction
(FC)	Using the frozen-core approximation

List of Symbols

$\hat{H}$	Hamiltonian operator
Ψ	Total wavefunction
ε	Energy of the stationary states
ε_0	Exact ground state energy
ϕ	Molecular orbital
α, β	Spin functions
χ	Spin-orbital
N	Number of electrons
$\hat{F}$	HF operator
ε_i	Orbital energies
$\hat{J}$	Coulomb operator
$\hat{K}$	Exchange operator
M	Number of basis functions
Φ_0	HF ground state wavefunction
$(\mu\nu|\lambda\sigma)$	Two-electron integrals: $(ij|kl)$, $(aa|bb)$, $(ab|ba)$
Φ_S	Configuration functions
ρ	Electron probability density
E_{xc}	Exchange-correlation energy
δ_{ij}	Kronecker delta symbol, $\delta_{ij} = \begin{cases} 1 & i = j \\ 0 & i \neq j \end{cases}$
Q	Molecular partition function
g	Degeneracy factor
i	Index that numbers the states or energy levels
Q_{trans}	Translational partition function
Q_{rot}	Rotational partition function
$Q_{int-rot}$	Internal-rotational partition function
Q_{vib}	Vibrational partition function
Q_{elect}	Electronic partition function
k_B	Boltzmann's constant
T	Temperature

V	Molar volume of an ideal gas
p^0	Standard pressure
R	Ideal gas constant
h	Planck's constant
m	Mass of a molecule
I, I_X	Moments of inertia (X = A, B, C)
k	Force constant
x	Displacement
c	speed of light
$\bar{v}$	Wavenumber
V_0	Barrier to internal rotation
G	Gibbs free energy
N	Number of indistinguishable independent particles
n	number of moles
N_A	Avogadro's number
K_{eq}	Equilibrium constant
Q^X	Standard molar partition function of X (divided by N_A)
$\Delta_r E_0$	Molar reaction internal energy at T = 0 K
ΔE_0	Hypothetical energy of activation at 0 K
$v^\neq$	Imaginary frequency of the TS
$\bar{v}^\neq$	Imaginary wavenumber of the TS
k	Rate constant
κ	Tunneling factor
k(E)	Microcanonical rate constant
k_{uni}	Rate constant for a unimolecular reaction
$V^\bullet$	Potential at the maximum of the Eckart barrier
$\Delta s_{\frac{1}{2}}$	Full width of the barrier at half its height
$T^\bullet$	Characteristic tunneling temperature
E_a	Arrhenius activation energy
A	Arrhenius pre-exponential factor

E_a^{eff}	Effective activation energy (for a complex mechanism)
ΔH	Reaction enthalpy
k_{eff}	Effective rate constant (for a complex mechanism)
k_D	Direct rate constant (for an elementary or direct mechanism)
E^X	Total energy of X at 0 K
Q_{IR}^{TS}	Internal-rotational partition function of the TS
Q_{corr}^{TS}	Corrected total partition function of the TS
Å	Angström
DH_{298}	Bond enthalpy at 298 K
λ	Wavelength
J_{ab}	Molecular Coulomb integrals
K_{ab}	Molecular exchange integrals
Ψ_{CIS}	CIS wavefunction
c_i	CIS coefficients
f	Oscillator strength
μ_{fi}	Electric dipole transition moment
ε	Molar absorption or extinction coefficient
ΔE	Excitation or transition energy
f_σ, f_π	Overlap weighting factors
c_h	CIS coefficients calculated by HyperChem

Acknowledgements

I would like to take this opportunity to thank Dr. Russell J. Boyd, for giving me the opportunity to carry out my graduate studies at Dalhousie University under his supervision. These four years in Canada have been full of new experiences that have allowed me to grow in many aspects. His trust, support and constant encouragement in both research and life have been essential in the development and culmination of this thesis.

I am very grateful to Dr. J. Raúl Alvarez Idaboy, for introducing me to the fascinating world of computational kinetics, for letting me realize how gratifying working in a team is, and for many happy moments while doing science together in the distance. I am thankful for his trust and friendship.

I would like to give special thanks to Dr. Philip D. Pacey for giving me the inspiration needed to carry out the computational kinetic studies; my participation in these projects was a consequence of the graduate courses taught by him. I thank Dr. Pacey for his patience, guidance, very important comments and discussions, and for his always-happy disposition to help.

I would like to thank Dr. Annik Vivier Bunge for the invitation to visit her research group at the Autonomous Metropolitan University in Mexico City. The idea of giving a series of seminars related to the work in computational kinetics presented in this thesis was extremely stimulating.

I wish to acknowledge Dr. George Heard for all his explanations, ideas and advice in the projects concerning the calculation of excited states. I would also like to thank Lorenzo J. Vega Montoto for helpful discussions, for teaching me important skills in the work with computers, and for suggesting the application of principal component analysis to the excited states studies on methylated naphthalenes.

Chapter 1. Introduction

1.1. An overview of computational chemistry

While atomic physics is concerned with the core electrons in atoms, chemists are primarily interested in understanding the behaviour and interactions between the valence electrons in molecules. Quantum mechanical laws describe the behaviour of electrons and nuclei in atoms. Since it has been demonstrated that quantum mechanics adequately describes the physics governing chemical problems, the application of these laws to chemical phenomena gives rise to the non-experimental field of quantum chemistry.

Quantum chemistry, in principle, deals only with problems where quantum aspects are considered; it is a subfield of a wider non-experimental area of chemistry: modern theoretical chemistry. Theoretical chemistry has been traditionally associated with paper and pencil type of research, and the development of new theories and approximations. In modern research the implementation of new methods in computer programs has led to dramatic advances. Computers are used to test new methods and to investigate interesting chemical problems. The role of computers in the development of theoretical chemistry led to the emergence of the new field of computational chemistry.

Computational chemistry[1] is as wide as everything else in science, and faces challenges in many directions, e.g., reaction mechanisms and dynamics, spectroscopy, condensed-phase studies. Among other things, computer-based research has provided explanations for experimental discoveries, helped calculate parameters not yet measured experimentally and develop chemical theories (e.g., ozone depletion). Furthermore, computational chemistry has aided in our understanding of biochemical processes (e.g., enzymatic reactions, photosynthesis), assisted in the design of new drugs and chemical compounds in general with specific properties, and led to the discovery of structure-property-reactivity relationships.

1

Chapter 2 will provide a simple account of important and basic features of different methods of computational chemistry that were applied during the development of this thesis.

1.2. On the importance of environmental issues

Annual budgets for environmental research, education and scientific assessment have increased dramatically in recent years. This is clear evidence of the critical importance of environmental issues. Unfortunately, for countries with emerging economies these issues will take much longer to become important priorities.

Environmental research is a complex blend of pursuits that have several objectives, as has been recently pointed out:[2] "To some, the highest form of environmental research is that which seeks only to extend knowledge and is driven by a combination of curiosity and disciplinary traditions. It seeks to describe the structure and function of the natural world, as well as the relationship between this world and humans or human civilizations. (...) Another form of environmental research focuses on the changes that are taking place in the natural and human environments as a result of human activity, either to understand these changes or to seek solutions." Very often, the systems to deal with are extremely complicated and models have to be used to study them. The verification of such models is expensive and usually only approximate measurements and estimates can be made.[2]

Industrial wastes discharged into lakes, rivers and oceans are destroying life in these environments and also indirectly outside them. Industrial emission of toxic gases are affecting agriculture, and provoking health problems,[3] climate changes[4] and the variation of the atmosphere's chemical composition, among other disastrous consequences. In atmospheric chemistry very well known problematic situations have developed such as those associated with photochemical smog, the presence of tropospheric ozone, acid rain, the accumulation of greenhouse gases, the stratospheric ozone-layer depletion, and several others.[5] The development of solutions for these and other problems has become an important environmental challenge.[6]

One hopes there is still time to reverse or counteract the damage provoked by human activity over the many years of economic and industrial development. Definitely this task will require the creative and persistent work of multidisciplinary teams around the world.

The studies compiled in this thesis are computational chemistry applications to subjects of environmental interest. In the first part, reactions that are of interest in atmospheric chemistry are studied from the kinetic point of view. The second part is devoted to the calculation of excited states in a family of compounds whose negative environmental consequences are well known.

1.3. Kinetic calculations in atmospheric chemistry

The chemistry of the atmosphere is very complex. The life cycles of the atmospheric species (including traces) are strongly coupled, often in unexpected ways. Depending on the lifetime of atmospheric species, they can exhibit an enormous range of spatial and temporal variability, but every substance emitted into the atmosphere is eventually removed so that a biogeochemical cycle is established.[7]

In order to estimate the lifetimes of pollutants in the atmosphere different removal options have to be considered, and for this, the development of a reliable kinetic database for atmospheric reactions is of extreme importance. By knowing the activation energy and rate constant of every reaction taking place in the atmosphere, it would be possible to predict the chemical destiny of all compounds emitted to or generated in the atmosphere. This knowledge would also permit the estimation of the lifetime of every atmospheric species so that it would be possible to foresee their degree of migration into the different atmospheric regions, and their potential consequences. Unfortunately such experimental studies are often difficult to achieve and therefore theoretical predictions are an important alternative.

The OH radical is the most important oxidant species in the troposphere during the daytime. It reacts with virtually all the atmospheric species, organic (both saturated and unsaturated compounds) and inorganic, and in many instances in the first and rate

determining step.[5a,8] The hydroxyl radical is formed mainly from three routes: the photolysis of O_3 and HONO, and from the reaction between HO_2 and NO (the most important source at mid-day). In the absence of sunlight the OH radical concentration in the troposphere is very low.[7]

The NO_3 radical, as well as the OH radical, is a strong oxidizing agent that reacts with a number of atmospheric species.[9] The reaction of NO_3 radicals with atmospheric organic molecules can lead to the formation of undesirable compounds such as: HNO_3,[10] peroxyacyl nitrates (PANs)[11] and dinitrates.[12] The only primary source of NO_3 in the troposphere requires the simultaneous presence of NO_2 and O_3 in the same air mass,[7] but during the day NO_3 radicals photolize rapidly, thus its presence in the troposphere is only significant at night.

Aldehydes play an important role in the chemistry of the polluted troposphere.[5a] They are emitted as primary pollutants from partial oxidation of hydrocarbon fuels, and besides, they arise as secondary pollutants from the oxidation of volatile organic compounds. Once in the atmosphere, aldehydes either photolyse or react further with OH radicals during the day, or with NO_3 radicals during the night.

Formaldehyde (HCHO) and acetaldehyde (CH_3CHO) are the most abundant aldehydes in the atmosphere and furthermore, have been regulated as hazardous air pollutants. The reactions of CH_3CHO with OH and NO_3 lead to the formation of PAN (peroxyacetylnitrate), a strong eye irritant, with phytotoxic properties and mutagenic and carcinogenic activity,[13] that has been identified as a component of photochemical smog.[5a,14]

Formyl fluoride (FCHO) is one of the halogenated molecules in the upper stratosphere, and a major product of the degradation in the troposphere of CH_3CFH_2 (HFC-134a).[15] It is also a product of the subsequent dissociation of fluorinated radicals that originate in the atmosphere. Formyl chloride (ClCHO) is a reactive molecule that forms as an atmospheric degradation intermediate of several chlorinated hydrocarbons such as

CH_3Cl, CH_2Cl_2, $CHCl_3$, and hydrochlorofluorocarbons (HCFCs),[16] as well as from the tropospheric reaction of Cl atoms with volatile organic compounds such as isoprene.[17]

The reactions of aldehydes with OH and NO_3 radicals are supposed to be tropospheric removal routes for these compounds during the day and night, respectively.

Rate constants and Arrhenius parameters for the OH reaction with a variety of aldehydes have been measured[5a,18] but there are serious uncertainties as to the reaction mechanism. For the CH_3CHO reaction the negative temperature dependence of the rate constant is well established; the activation energy of the HCHO + OH reaction is known to be almost zero, most experimental results varying between +0.7 and -1.9 kJ/mol.[18] For the OH hydrogen-abstraction reaction from FCHO and ClCHO only experimental upper-bound rate constants have been reported and activation energy values are unknown.[19]

There have been fewer kinetic studies on the reactions of NO_3 with aldehydes than on the corresponding reactions with OH radicals. The activation energy of the NO_3 reaction with CH_3CHO has been the only one determined among the previously mentioned aldehydes. Rate constants have been reported for HCHO and CH_3CHO, but no kinetic data is available for FCHO and ClCHO.[18] Furthermore, no previous theoretical determinations of the kinetic parameters for NO_3 reactions with aldehydes have been published.

In the first part of the thesis, the OH and NO_3 hydrogen-abstraction reactions from the above mentioned aldehydes (XCHO: X = F, Cl, H, CH_3) are studied to clarify aspects concerning the reaction mechanism and to provide accurate theoretically determined kinetic parameters. High-level *ab initio* calculations are performed with large basis sets and furthermore, transition state theory (TST) including tunneling corrections is applied to the calculation of rate constants. The results for the OH reactions are presented in Chapters 4 and 5,[20] and the NO_3 kinetic results are discussed in Chapter 6.[21] Chapter 3 provides general background information to complement the kinetic calculations reported in Chapters 4 to 6, including an overview of the concepts and approximations related to TST and tunneling calculations, among other kinetic topics.

Dr. J. Raúl Alvarez-Idaboy, presently at the Mexican Petroleum Institute (IMP) co-supervised the work presented in Chapters 4 and 5. The results discussed in Chapter 4 are part of a collaboration that also included Dr. Annik Vivier-Bunge at the Autonomous Metropolitan University (UAM - Iztapalapa), in Mexico City.

1.4. Polycyclic aromatic compounds and the interest in their study

Polycyclic aromatic hydrocarbons (PAHs) are aromatic compounds containing only carbon and hydrogen atoms in a series of inter-connected rings. They are called benzenoid or non-benzenoid depending on the presence or absence of six-membered rings. Some examples are shown in Fig. 1.1. The alkyl-, amino-, halogen- and nitro-substituted derivatives, along with the mono- and poly- N, S and O heteroatomic analogues of PAHs constitute a much larger and diverse class of molecules, the polycyclic aromatic compounds (PACs).[22]

PACs are found in both natural materials such as crude oil, and man-made substances such as engine exhaust. These substances can be useful, for example, in raising the octane rating of gasoline, but they can also be quite harmful, often possessing carcinogenic or mutagenic properties.[22]

Syncrude Canada, located in Alberta, is a petroleum company which converts Athabasca oil sands into synthetic crude oil. It is the world's largest producer of oil made from oil sands, the largest known petroleum reserve in Canada. The petroleum industry is vitally interested in the identification and quantification of PACs in their source materials, final products and intermediate process streams, because these compounds interfere with petroleum refining operations, poisoning catalysts or building up in chemical reactors. They may also corrode refinery equipment and alter the odour and shelf lifetime of the final products. Federal environmental regulations to reduce toxic emissions also must be considered. This is of even greater importance in the oil sands industry since the aromatic content of these source materials is much higher than in most other forms of crude oil.
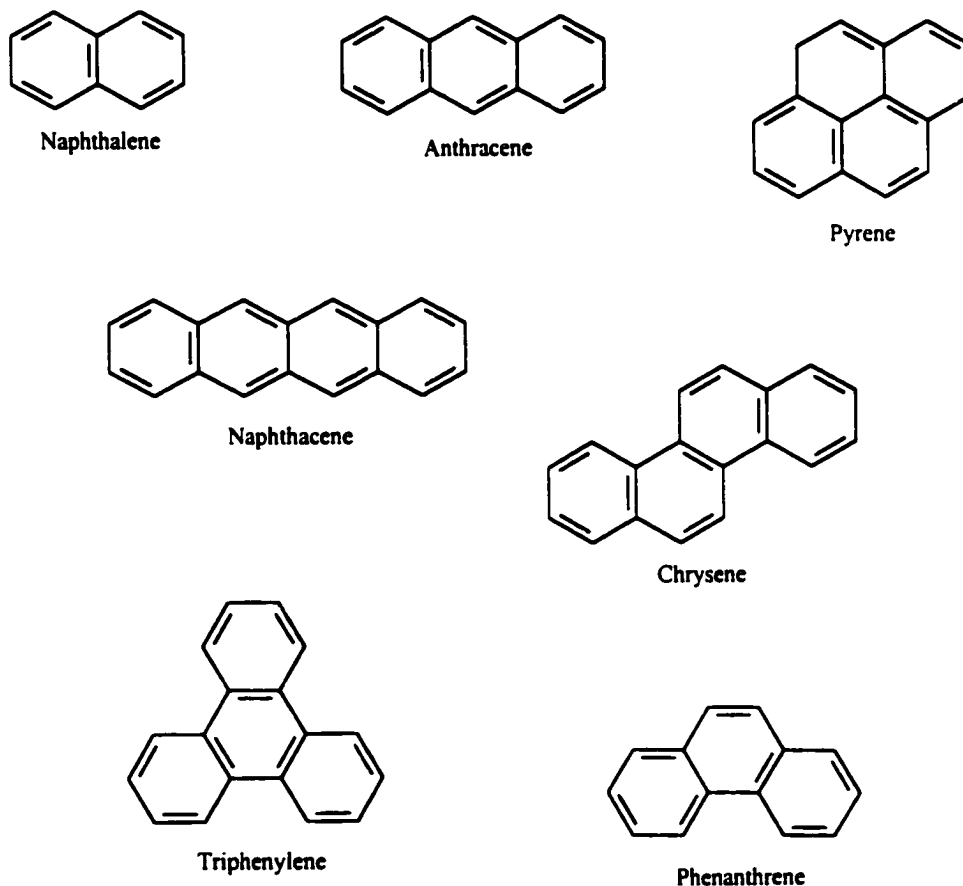
Figure 1.1. Examples of PAHs

The characterization of PACs in petroleum-related samples is extremely difficult because these samples contain thousands of such compounds which are very similar to one another and must be separated before identification. Even if complete separation were possible, identification would still be difficult because in many cases standard compounds are not available for comparison and positive identification purposes. It is in such cases that theoretical methods can play an important role as a predictive tool, since only a starting structure is needed to predict molecular properties using quantum chemistry.

It has been proposed that PACs in these samples are basically alkylated PAHs, mainly methyl- and ethyl- substituted PAHs, although it has also been suggested that partially hydrogenated PAHs may be present as a consequence of the reduction process undergone by the samples during the industrial treatment.[23] The presence of alkyl groups causes some problems in the identification of the species. The bigger the PAH the larger the number of alkylated isomers, and the greater the labour of separation, identification and quantification. State-of-the-art chromatographic methods are mainly used to separate and identify these compounds, using ultraviolet-visible (UV-vis), laser fluorescence and mass spectrometric detectors. But all these isomers are indistinguishable from each other using mass spectrometry and there are few good reference electronic spectra available.

In the second part of the thesis, Chapter 7 presents general theoretical aspects of UV-vis spectroscopy, common characteristics in the absorption spectra of PAHs, and some *ab initio* and semi-empirical methods used to calculate excited states of organic systems. The results of the calculations are outlined and discussed in Chapter 8 that focuses on the effect of alkyl substituents on the excited states of naphthalene, the smallest PAH. The effect of methyl and reduced-ring substituents (cyclic substituents which are completely reduced) on the electronic spectrum of naphthalene is examined.[24]

This study was part of a multidisciplinary project to assist Syncrude in the identification of the PACs and in tracking the progress made in improving their product. This Syncrude project was a collaboration with the research groups of Drs. R. D. Guy, L. Ramaley and P. D. Wentzell. Dr. Guy's group was responsible for the development and optimization of liquid chromatographic techniques to give the best possible separation of the compounds present in the complex test mixtures. Dr. Ramaley's group was in charge of the construction, development, calibration and optimization of the detection schemes which include a laser fluorescence detector and the use of a quadrupole mass spectrometer. The group of Dr. Wentzell uses the chromatographic data to assist in the identification of poorly resolved compounds by using chemometric methods. The theoretical contribution was intended to provide calculated data related to the chemical-physical properties of PACs, to assist or complement the work done by the other groups.

Chapter 9 will present global conclusions and plans for future work on the previously mentioned topics.

1.5. References

1.   Young, D.C. *Computational Chemistry: A Practical Guide for Applying Techniques to Real-World Problems*, John Wiley & Sons, New York, 2001.

2.   Glaze, W.H. *Environ. Sci. & Technol.* **2001**, *35*, 225A.

3.   Hogue, C. *Chem. & Eng. News* **2000**, *78*, 15.

4.   It was S. Arrhenius who first made a quantitative link between atmospheric CO_2 concentrations and temperature over 100 years ago, in 1896. (a) *Chem. in Britain*, February **2000**, 28. (b) White, B. *Can. Chem. News* **2001**, *53*, 23. (c) Hengeveld, H.G. *idem.* 15.

5.   (a) Finlayson-Pitts, B.J.; Pitts, J.N. *Atmospheric Chemistry: Fundamentals and Experimental Techniques*, Wiley Interscience, New York, 1986. (b) Brown, T.L.; LeMay, H.E., Jr., Bursten, B.E. *Chemistry: The Central Science*, 6th Ed., Prentice Hall, NJ, 1994. (c) Swaddle, T.W. *Inorganic Chemistry: An Industrial and Environmental Perspective*, Academic Press, San Diego, 1997. (d) http:// www.cac.yorku.ca/intro.html.

6.   Schoen, D. *Environ. Sci. & Technol.* **2001**, *35*, 75A.

7.   Seinfeld, J.H.; Pandis, S.N. *Atmospheric Chemistry and Physics: From Air Pollution to Climate Change*, Wiley Interscience, New York, 1998.

8.   Ehhalt, D.H. *Phys. Chem. Chem. Phys.* **1999**, *1*, 5401.

9.   Atkinson, R. *Atmos. Environ.* **2000**, *34*, 2063.

10. (a) Calvert, J.G.; Stockwell. W.R. *Environ. Sci. Technol.* **1983**, *17*, 428A. (b) Atkinson, R.; Plum, C.N.; Carter, W.P.L.; Winer, A.M.; Pitts, J.N., Jr. *J. Phys. Chem.* **1984**, *88*, 2361. (c) Seinfeld, J.H. *Science* **1989**, *243*, 745. (d) Schwartz, S.E. *ibid.*, 753. (e) McElroy, M.B.; Salawitch, R.J. *ibid.*, 763.

11. (a) Louw, R.; van Harm, J.; Nieboer, H. *J. Air Pollut. Contr. Ass.* **1973**, *23*, 716. (b) Cantrell, C.A.; Davidson, J.A.; Busarow, K.L.; Calvert, J.G. *J. Geophys. Res.* **1986**, *91*, 5347. (c) Miller, C.E.; Francisco, J.S. *J. Phys. Chem.* **2001**, *105*, 750.

12. Bandow, H.; Okuda, M.; Akimoto, H. *J. Phys. Chem.* **1980**, *84*, 3604.

13. Kleindiest, T.E.; Shepson, P.B.; Smith, D.F.; Hudgens, E.E.; Nero, C.M.; Cuppit, L.T.; Bufini, J.J.; Claxton, L.D. *Environ. Molecular Mutagen* **1990**, *16*, 70.

14. (a) Scott, W.E.; Stephens, E.R.; Hanst, P.L.; Doerr, R.C. Paper presented at the 22nd Midyear Meeting of the American Petroleum Institute, Division of Refining, Philadelphia, Pennsylvania, May 14, 1957. (b) Temple, P.J.; Taylor, O.C. *Atmos. Environ.* **1983**, *17*, 1583.

15. (a) Wallington, T.J.; Hurley, M.D.; Ball, J.C.; Kaiser, E.W. *Environ. Sci. Technol.* **1992**, *26*, 1318. (b) Hasson, A.S.; Moore, C.M.; Smith, I.W.M. *Int. J. Chem. Kinet.* **1998**, *30*, 541.

16. (a) Sanhueza, E.C.; Heicklen, J. *J. Phys. Chem.* **1975**, *79*, 7. (b) Gay, B.W.; Hanst, P.L.; Bufalini, J.J.; Noonan, R.C. *Environ. Sci. Technol.* **1976**, *10*, 58. (c) Niki, H.; Maker, P.D.; Savage, C.M.; Breitenbach, L.P. *Int. J. Chem. Kinet.* **1980**, *12*, 1001. (d) Niki, H.; Maker, P.D.; Savage, C.M.; Breitenbach, L.P.; Martinez, R.I.; Herron J.T. *J. Phys. Chem.* **1982**, *86*, 1858.

17. Fantechi, G.; Jensen, N.R.; Saastad, O.; Hjorth, J.; Peeters, J. *J. Atmos. Chem.* **1998**, *31*, 247.

18. The NIST Chemical Kinetics Database, NIST Standard Reference Database, U.S. Dept. of Commerce, Technology Administration, National Institute of Standards and Technology: Gaithersburg, MD, 17-2Q98.

19. (a) Libuda, H.G.; Zabel, F.; Fink, E.H.; Becker, K.H. *J. Phys. Chem.* **1990**, *94*, 5860. (b) Wallington, T.J.; Hurley, M.D. *Environ. Sci. Technol.* **1993**, *27*, 1448. (c) Atkinson, R.; Baulch, D.L.; Cox, R.A.; Hampson, R.F., Jr.; Kerr, J.A.; Rossi, M.J.; Troe, J. *J. Phys. Chem. Ref. Data* **1997**, *26*, 521.

20. (a) Alvarez-Idaboy, J.R.; Mora-Diez, N.; Boyd, R.J.; Vivier-Bunge, A. *J. Am. Chem. Soc.*, **2001**, *123*, 2018. (b) Mora-Diez, N.; Alvarez-Idaboy, J.R.; Boyd, R.J. *J. Phys. Chem.*, **2001**, in press.

21. Mora-Diez, N.; Boyd, R.J. *J. Phys. Chem.*, **2001**, submitted.

22. Vo-Dinh, T. *Chemical Analysis of Polycyclic Aromatic Compounds*, Wiley, New York, 1989.

23. Information obtained through private correspondence with Michael Potvin and Drs. L. Ramaley and R.D. Guy, Dalhousie University.

24. Mora-Diez, N; Boyd, R.J.; Heard, G.L. *J. Phys. Chem. A* **2000**, *104*, 1020.

Chapter 2. Theoretical Background

A qualitative overview of the basic aspects of quantum chemistry and computational methods is provided in this chapter. It is intended to give an introduction without excessive detail to the approximations and methods of computational chemistry applied throughout the thesis. These methods are neither exact nor perfect. However, qualitative or approximate computations can give useful insight into chemistry if the researcher understands what they do or do not predict.

2.1. Introduction

The energy and electronic properties of a stationary state of a molecule can be obtained by solving the time-independent Schrödinger equation.[1] This is an eigenvalue equation that cannot be solved exactly, except for simple cases:

$$\hat{H} \Psi = \varepsilon \Psi \qquad (2.1)$$

where $\hat{H}$ is a Hermitian operator called the Hamiltonian operator, Ψ is the exact wave function of the system and ε is the energy of the stationary states, with the lowest energy state being the ground state.

The Hamiltonian operator considers all possible contributions to the total energy of the system arising from the kinetic energy of electrons and nuclei, the attractive potential energy between the electrons and nuclei, and the interelectronic and internuclear repulsive potential energy. The adiabatic or Born-Oppenheimer[2] approximation is one of the most important approximations used to simplify the mathematical expression of the Hamiltonian operator. Since the electron mass is much less than that of the nuclei, the motions of the nuclei are negligible compared to those of the electrons. Hence, the nuclear kinetic term in the Hamiltonian operator can be neglected, and the internuclear repulsion term can be treated as a constant. In other words, we can consider the electrons in a molecule to be moving in a field of fixed nuclei.

The variational method[3] is based on the variational principle and is an important approach for finding approximate solutions to eigenvalue equations. The variational principle states that, given a normalized wavefunction, Ψ, that satisfies the appropriate boundary conditions, the expectation value of the Hamiltonian is an upper bound to the exact ground state energy, ε_0.

$$<\Psi|\hat{H}|\Psi> \geq \varepsilon_0 \qquad (2.2)$$

The more accurate the wave function employed, the lower the energy obtained. The variational method uses a normalized trial function Ψ which can be written as a function of a set of parameters and the coordinates of the system; through differentiation the parameters are varied to minimize the energy.

2.2. The many-electron wavefunction

Molecular orbital theory is an approach to molecular quantum mechanics that assigns individual electrons to spin-orbitals to approximate the full wavefunction. The complete wavefunction for a single electron is the product of a molecular orbital (MO) and a spin function. The MOs, $\phi(x,y,z)$, are functions of the Cartesian coordinates x, y, z, while the spin functions, $\alpha(\xi)$ or $\beta(\xi)$, depend on the spin coordinates, ξ. This product, $\phi(x,y,z)$ $\alpha(\xi)$ or $\phi(x,y,z)$ $\beta(\xi)$, is called a spin-orbital, $\chi(x,y,z,\xi)$.[4]

Since electrons are fermions, the many-electron wavefunction has to be antisymmetric with respect to the interchange of any two of them, that is:

$$\Psi(1,...,i,...,j,...,N) = -\Psi(1,...,j,...,i,...,N) \qquad (2.3)$$

The representation of an N-electron wavefunction as a Slater determinant[3,5] satisfies the antisymmetry requirement and also allows for the fact that electrons are indistinguishable:

$$\Psi(1,2,...,N) = (N!)^{-1/2} \begin{vmatrix} \chi_1(1) & \chi_2(1) & \cdots & \chi_N(1) \\ \chi_1(2) & \chi_2(2) & \cdots & \chi_N(2) \\ \vdots & \vdots & & \vdots \\ \chi_1(N) & \chi_2(N) & \cdots & \chi_N(N) \end{vmatrix} \qquad (2.4)$$

The factor $(N!)^{-1/2}$ is a normalization factor. In this representation N electrons occupy N spin-orbitals without specifying which electron is in which orbital; rows are labelled by electrons and columns are labelled by spin-orbitals. Interchanging the coordinates of two electrons corresponds to interchanging two rows of the Slater determinant, which changes its sign. This representation of the many-electron wavefunction is the simplest MO approximation to the solution of the Schrödinger equation. Within the single Slater determinant description, the motion of electrons with parallel spins is partially correlated (the probability of finding two electrons with parallel spins at the same point in space is zero) but the motion of electrons with opposite spins is not.

2.3. Basis set expansions

A basis set in a vector space is a set of vectors (basis functions) linearly independent, which are able to generate all the vectors of the vector space. The wavefunctions used in quantum chemistry are vectors of an infinite-dimensional complex vector space: the Hilbert space. A complete basis set for this vector space should contain an infinite number of basis functions, but this is impossible from a computational point of view.

Practical applications of molecular orbital theory require that the individual MOs be expressed as a linear combination of a finite set of one-electron functions known as basis functions, φ:

$$\phi_i = \sum_{\mu=1}^{M} c_{\mu i} \varphi_\mu \qquad i = 1, 2, ..., M \qquad (2.5)$$

where the $c_{\mu i}$ are the MO expansion coefficients. The larger and more complete the set of basis functions the more flexible the description of the orbitals since fewer restrictions are imposed on the location of the electrons in space.

Two types of basis functions have received widespread use: Slater-type $(STO)^6$ and Gaussian-type $(GTO)^7$ orbitals. STOs provide a reasonable representation of atomic orbitals but the evaluation of the two-electron integrals is very time consuming. The behaviour of the Gaussians near and far from the nucleus is incorrect. Thus, many more

GTOs than STOs are needed to approximate the orbitals to the same degree of accuracy, but as a consequence of the Gaussian product theorem the computation of integrals is relatively fast. In practice, linear combinations of Gaussians are used to represent the basis functions, which are called contracted basis functions.

When one basis function per atomic orbital is used the basis set is said to be minimum. If two basis functions are used (per atomic orbital) the basis set is called double-zeta; there are other variants. Additional Gaussians can also be added to extend the accuracy of the basis set. For example, polarization functions, those with higher angular momentum than are needed by the atom in its electronic ground state (p and higher on hydrogen; d and higher on heavy atoms) are added to account for distortion of the atomic orbitals in the molecular environment, giving the wavefunction more flexibility to change shape. Diffuse functions may also be added to account for large electronic clouds in systems where electrons are relatively far from the nucleus, such as molecules with lone pairs, anions, systems in their excited states, and when describing interactions at long distances in systems with van der Waals interactions. These diffuse functions are primitives with small exponents, thus describing the shape of the wavefunction far from the nucleus. The selection of the basis set is a difficult computational problem and is the focus of many research papers.[8]

2.3.1. Basis set notation

Most calculations undertaken today are performed by choosing an existing segmented GTO basis set. A popular family of basis sets, commonly referred to as the Pople basis sets, are indicated by the notation 6-31G. This notation indicates that each atomic core orbital is described by a single contraction of six GTO primitives, and each valence shell orbital is described by two contractions (basis functions), one with three primitives and the other with one primitive, allowing for more flexibility in the description of the valence electrons. This notation identifies a double-zeta basis set, and is very popular when treating organic systems of considerable size. Another Pople basis set is 6-311G, a triple-zeta basis set that will be frequently used in the following chapters.

The Pople basis set notations described above can be modified by adding polarization functions, *e.g.*, 6-311G(d,p): *d* primitives are added to atoms other than hydrogen and *p* primitives are added to hydrogen as well. Another modification in this notation accounts for the inclusion of diffuse functions, *e.g.*, 6-311++G(d,p): a single plus sign indicates that diffuse functions are added to atoms other than hydrogen and a second plus implies that these functions are used for all atoms.

2.3.2. Basis set superposition error

An artificial lowering of the interaction energy of weakly or strongly bound systems, such as dimers, systems with hydrogen bonding interactions, reactant or product complexes, and transition states, is encountered when the basis set used to optimize these systems is not big enough. It is an additional contribution to the inaccuracy of calculations when using a finite basis set. This phenomenon was discovered in 1968,[9] and five years later[10] received the name: basis set superposition error (BSSE).[11]

This phenomenon is easier to understand through an example: to calculate the dimerization energy of a certain molecule with a given basis set, it is possible to subtract the energy of the two infinitely separated monomers from the energy of the dimer, but this procedure involves an inconsistency. When the energy of a monomer is computed, only the basis set functions on its atoms are used to describe each electronic spatial orbital. On the other hand the electrons in the dimer have associated orbitals composed of linear combinations of the basis set functions for twice the number of atoms. The basis set for the dimer is larger than that of either monomer, and this enlargement of the basis results in a non-physical lowering of the energy of the dissociated dimer relative to the separated monomers. The BSSE would vanish in the limit of a complete set on each monomer.

No completely reliable scheme for either eliminating or estimating the BSSE has been given but the approach usually taken to estimate this effect is the counterpoise (CP) method.[12] In this procedure the energies of the "monomeric units" are computed by using the full basis set of the "dimer". A basis set for each nucleus of the "monomer" is used as

well as the same basis set functions centred at the points in space that would correspond to the equilibrium positions of the other nuclei in the "dimer". In the original procedure the "monomeric units" (*e.g.*, the reactants) upon forming the "dimer" or "intermolecular complex" (*e.g.*, the TS) are not further optimized, *i.e.*, the "monomers" are frozen in their supermolecular geometries.

Estimates of the effects of the BSSE by the CP method have been found to be misleading for hydrogen bonded dimers, since they do not provide quantitative information about the basis set deficiencies.[13] Furthermore, it has been shown that the use of large enough basis sets so that the CP correction is small does not guarantee accurate results and that for smaller basis sets the inclusion of this correction does not systematically improve the accuracy of the calculations.[14] The CP procedure provides only a crude estimate and not an upper bound on the error.[15] Despite these criticisms and the fact that other methods for correcting the BSSE have been discussed in the literature,[16] the CP correction continues to be the most widely used method for this purpose.[17]

2.4. The Hartree-Fock approximation

The Hartree-Fock (HF) approximation,[4,18] which is equivalent to the MO approximation, has played an important role in elucidating modern chemistry. It usually constitutes the first step towards more accurate approximations. It is an independent particle model based on the variational method, which assumes that electrons are non-interacting. The essence of the HF approximation is to replace the complicated many-electron problem, that cannot be solved exactly, by a one-electron problem in which the electronic repulsion is treated in an average way.

The HF equations are eigenvalue non-linear integro-differential equations:

$$\hat{F}\chi_i = \varepsilon_i \chi_i \qquad i = 1,2,...,N \qquad (2.6)$$

where $\hat{F}$ is an effective one-electron operator, called the HF Hamiltonian operator defined by:

$$\hat{F} = \hat{H}^{core} + \sum_{j=1}^{N}(2\hat{J}_j - \hat{K}_j) \qquad (2.7)$$

In equation (2.7), $\hat{H}^{core}$ is the core or one-electron Hamiltonian operator representing the energy of a single electron in a field of bare nuclei, $\hat{J}$ is the Coulomb operator describing the repulsion energy between two charge distributions, and $\hat{K}$ is the exchange operator arising from the antisymmetric nature of the determinantal wavefunction; it does not have a simple classical interpretation. The second term in equation (2.7) represents the average potential experienced by one electron due to the presence of the other (N-1) electrons.

The operators $\hat{J}$ and $\hat{K}$ are functions of the spin-orbitals, and since $\hat{F}$ itself depends on Coulomb and exchange operators, it also depends on the spin-orbitals which have to be found by applying the variational method. Hence these equations must be solved iteratively by a procedure called the self-consistent-field (SCF) method.[3] An initial guess of the spin-orbitals is made, the average field seen by each electron is calculated and the eigenvalue equation (2.6) for a new set of spin-orbitals is solved. Using the new spin-orbitals, one can obtain new fields and repeat the procedure until self-consistency is reached (*i.e.*, until the fields no longer change and the spin-orbitals used to construct the HF operator are the same as its eigenfunctions).

The solution of the HF eigenvalue problem yields a set of orthonormal HF spin-orbitals $\{\chi_i\}$ with orbital energies $\{\varepsilon_i\}$. The N spin-orbitals with the lowest energies are called occupied spin-orbitals; the remaining members of the set are called virtual or unoccupied spin-orbitals. The Slater determinant formed from the occupied spin-orbitals is the HF ground-state wavefunction, Φ_0, and is the best possible variational approximation to the ground state of the system from the single determinant form.

2.5. The Roothaan-Hall method

The HF equations can only be solved exactly for atoms. No practical procedures are presently available to obtain numerical solutions for molecules. The representation of the HF orbitals as a linear combination of basis functions and the application of the

variational principle lead to a set of algebraic equations, derived by Roothaan and Hall,[4,19] that increase the applicability of the HF method.

The Roothaan-Hall (RH) equations for a closed-shell system (*i.e.*, a system where all electrons are spin paired) are:

$$\sum_{\nu=1}^{M} \left(F_{\mu\nu} - \varepsilon_i S_{\mu\nu}\right) c_{\nu i} = 0 \qquad \mu = 1, \ldots, M; \; i = 1, \ldots, N \tag{2.8}$$

Here, ε_i is the one-electron energy of the MO ϕ_i, the $c_{\nu i}$ are the MO expansion coefficients, the $S_{\mu\nu}$ are the overlap matrix elements indicating the overlap between the orbitals, and the $F_{\mu\nu}$ are the elements of the HF matrix:

$$F_{\mu\nu} = H_{\mu\nu} + \sum_{\lambda,\sigma}^{M} P_{\lambda\sigma}\left[(\mu\nu \,|\, \lambda\sigma) - \frac{1}{2}(\mu\lambda \,|\, \nu\sigma)\right] \tag{2.9}$$

The $H_{\mu\nu}$ are the elements of a matrix representing the energy of a single electron in a field of bare nuclei, $(\mu\nu|\lambda\sigma)$ and $(\mu\lambda|\nu\sigma)$ represent the Coulomb and exchange two-electron integrals respectively, and $P_{\lambda\sigma}$ are the elements of the one-electron density matrix. These equations also must be solved iteratively by the SCF procedure. As the basis set approaches completeness the spin-orbitals obtained in the RH method approach the exact HF spin-orbitals.

The above method, called restricted HF (RHF), is applied only to closed-shell system. For open-shell systems, in which electrons are not completely assigned to orbitals in pairs, the RH equations need modification. The most reasonable procedure is to assign different spatial orbitals to the α and β electrons, resulting in two sets of MOs defined by two sets of coefficients. Hence, two different Fock matrices are generated. This generalization of the RH equations is called the spin-unrestricted HF (UHF) method. Another variant to treat open-shell systems is called the spin-restricted open-shell calculation (ROHF).

2.5.1. Spin contamination

In UHF calculations there are two complete sets of orbitals that use the same set of basis functions but different MO coefficients. These calculations can be performed very efficiently but have the disadvantage that the wavefunctions generated are no longer eigenfunctions of the total spin $\langle S^2 \rangle$ and an error called spin contamination, can be introduced into the calculation.[20]

The solutions to the UHF equations may not be pure spin states, but instead are often contaminated by higher spin states. Spin contaminated wavefunctions have lower total energies associated with them; unrestricted wavefunctions have lower energies than the corresponding restricted wavefunctions. A high spin contamination can affect the geometry, the population analysis, and significantly affects the spin density. Furthermore, spin contamination can slow down the convergence of Møller-Plesset (MP) calculations (*vide infra*). Calculations of transition states and high-spin transition metal complexes tend to be particularly affected by this phenomenon. Values of $\langle S^2 \rangle$ greater than 0.75 (for radicals) show spin contamination, but as derived from experience,[34] when the difference is less than 10%, *i.e.*, $\langle S^2 \rangle < 0.82$, spin contamination is negligible.

Spin contamination is often detected in unrestricted MP (UMP2, UMP3, UMP4) and UHF calculations. It is less common to find spin contamination in unrestricted density functional theory (DFT) calculations, and it has little effect on configuration interaction (CI) and coupled cluster (CC) calculations (these methods are described below). Unrestricted calculations often incorporate a spin annihilation step that removes a large percentage of spin contamination from the wavefunction, but does not prevent it.

In an ROHF procedure the orbitals are separated into two classes: doubly and singly occupied orbitals. The doubly occupied orbitals are treated under the RHF formalism while the orbitals with unpaired electrons are treated separately with more complex expressions. In ROHF calculations there is no spin contamination but they require

additional CPU time. ROHF computations give good total energies and wavefunctions, however, they do not include spin polarization and hence are not useful for some purposes.

An approach to obtaining reliable wavefunctions in cases of spin contamination is to run an unrestricted calculation and then to project out the spin contamination after the wavefunction has been obtained (PUHF, PMP2).[21] Spin projection nearly always improves *ab initio* results (except in cases of very high spin contamination) but seriously affects the accuracy of DFT calculations.

If spin contamination is small, unrestricted methods can be used preferably with spin-annihilated wavefunctions and spin projected energies. When spin contamination becomes significant, spin-restricted open-shell or highly correlated methods should be used.

2.5.2. Symmetry breaking

The symmetry breaking or 'symmetry dilemma', as named by Löwdin,[22] is an artefact caused by the inadequate approximate solution of the electronic Schrödinger equation (due to oversimplified forms assumed for the wavefuction). Apparently, this phenomenon results from a dominance of the orbital localization effect over the resonance effect and leads to different solutions for the ground electronic state of certain chemical species corresponding to equilibrium geometries that are not connected on the same potential energy surface. An example of such a case is the NO_3 radical[23] which will be discussed in Chapter 6, but this problem can also be encountered in closed-shell systems. It is usually confronted in systems of high nuclear symmetry, although completely unsymmetrical molecules can also have geometries at which there is more than one optimal wavefunction of a limited functional form with the same energy. In such cases the potential energy surface will incorrectly display a cusp, and the calculated wavefunction will be discontinuous.[24]

The benzene molecule has D_{6h} ground-state symmetry, but calculations performed a few years ago indicated the existence of single determinants associated with the D_{3h} symmetry, which has a considerably lower energy than the corresponding determinants of symmetry D_{6h}.[25] More examples of this phenomenon can be found in solid state theory.

Imposition of symmetry conditions constitutes a reduction in flexibility in the wavefunction: a variational constraint. Consequently, even though the exact wavefunction may possess certain symmetry properties, in practical calculations a variationally better result can be achieved, *i.e.*, a lower energy, by not constraining the calculation to display these properties.[26]

The Jahn-Teller (JT) effect[27] is a consequence of the degeneracy of states in a symmetric molecule. It is encountered when two or more electronic states that coincide (degenerate) or are relatively close in energy (pseudo-degenerate) become sufficiently strongly mixed when the nuclei are displaced from their initial reference configuration. The potential energy surface has a double cone structure for small displacements from the high-symmetry point. As a result of this interaction between states the symmetric system becomes distorted to a lower symmetry structure. The simplest example of a JT unstable state involves a ^2E state of a molecule with D_{3h} symmetry.[24] If the highest occupied MOs are degenerate and partially occupied, such as for the CH_3O radical, the highest symmetric structure C_{3v} will distort to a C_s structure because of the JT effect. Another example is the JT distortion ($T_d \rightarrow C_{2v}$) in the methane radical cation, CH_4^+.[28]

It should be clear that the symmetry breaking phenomenon and the JT effect are consequences of two different situations, although these topics could lead to some confusion.

2.6. The correlation energy

Electron motion is correlated, *i.e.*, the motion of every electron depends on the motion of its neighbours. HF theory describes this incompletely, considering only some correlation of the motions of electrons with the same spin ("exchange hole"). This is a consequence

of the single-determinant representation of the many-electron wavefunction and leads to calculated (HF) energies which are above the exact values, and also to a number of qualitative deficiencies in the description of electronic structures.

The SCF or HF approximation implies that an electron of the system interacts with the other electrons according to their average location. In reality, however, the electronic motion occurs according to the electrons' actual placement. The Coulomb repulsion between electrons becomes sufficiently reduced only when a correlated motion of the electronic system takes place. This aspect of the electron motion is not contained in the independent-electron or SCF approximation.[29] What is missing is the correlation hole every electron carries along to prevent other electrons from coming too close, and thus reducing their mutual Coulomb repulsion. This correlation hole can be seen as a combination of the Coulomb hole, that keeps two electrons apart due to coulombic interactions, and the Fermi hole, that prevents electrons of the same spin from being in the same point of space. The Fermi hole is a purely quantum mechanical phenomenon and is not related to the charge of electrons.

The difference between the exact N-electron wavefunction and its HF counterpart is related to the correlation aspect of the electron motion. Löwdin gave the most often used definition of the correlation energy:[30]

> *"The correlation energy for a certain state with respect to a specified Hamiltonian is the difference between the exact eigenvalue of the Hamiltonian and its expectation value in the Hartree-Fock approximation for the state under consideration."*

There are a variety of procedures for improving upon the HF approximation, which are classified as post-HF or post-SCF methods. Some of these methods are discussed in the following sections.[31]

If electron correlation is viewed as an inadequacy of the single configuration HF approximation, two different effects can be identified. The first is the influence of other

configurations that are low-lying in energy and that mix strongly with the HF configuration. These give rise to non-dynamical correlation, which can usually be dealt with by multiconfigurational SCF techniques (*vide infra*). This effect is very important when dealing with open-shell systems like excited states, radicals or transition metals. The second effect (dynamical correlation) arises from the interelectronic repulsion, described by the term (r_{ij}^{-1}) in the Hamiltonian operator, and gives rise to dynamical correlation. This term (r_{ij}^{-1}) is singular as $r_{ij} \rightarrow 0$, but mathematical studies of the properties of exact wavefunctions show that they must contain cusps in r_{ij} to cancel this singularity. Thus, the cusp behaviour must be described to properly treat dynamical electron correlation. Methods such as MP, CI and CC (*vide infra*) are frequently used for this purpose, among others. There is no sharp dividing line between non-dynamical and dynamical correlation, and methods for treating one will undoubtedly account in some part for the other.

2.6.1. Configuration interaction

The configuration interaction (CI) method[32,33] is conceptually the simplest procedure to account for correlation energy. The exact wavefunction Ψ is represented as a linear combination of N-electron trial functions (Slater determinants) often referred to as "configurations", "configuration state functions", or simply "configuration functions" (CFs):

$$\Psi = \sum_R c_R \Phi_R + \sum_S c_S \Phi_S \qquad (2.10)$$

where c_R and c_S are the variational parameters and Φ_R denotes the so-called reference CFs, *i.e.*, those CFs that are dominant from the point of view of the energy criterion. Φ_S denotes the CFs obtained from the reference CFs by replacing one or more of the occupied spin-orbitals by virtual spin-orbitals, and the collective indexes R, S indicate the orbital structure of the individual CF.

In most cases the first sum in (2.10) contains just one term, and the expansion is called "single-reference CI" or simply "CI". In this case the reference function is usually the HF-SCF wavefunction and the CI expansion can be expressed as:

$$\Psi_0 = c_0 \Phi_0 + \sum_{s>0} c_s \Phi_s \qquad (2.11)$$

Only those CFs of the same symmetry and multiplicity as the reference configuration will have nonzero coefficients in the CI expansion. They are called spin- and space-adapted configurations.

When all possible CFs are included in the CI expansion and no further approximations are made, the CI procedure is called "full CI". The full CI method represents the most complete non-relativistic treatment possible for a molecular system within a certain basis set, but it is impractical except for very small systems. There are various approximations to the full CI calculation where different subsets of all possible CFs are selected. For example, CIS includes only single excitations (but the inclusion of only single excitations does not improve upon the ground state HF energy and wave function, as stated by Brillouin's theorem),[3] CID includes only double excitations and CISD includes single and doubles, *etc.*

The most important criteria for an accurate electron correlation theory are the properties of size-consistency and size-extensivity.[34,35] A size-consistent method[36] is one in which the energy obtained for two fragments at sufficiently large separation is equal to the sum of the energies of those fragments computed separately. This property is of primary importance for correctly describing the energetics of a system relative to its separated parts. A method is size-extensive[37] if the energy is a linear function of the number of electrons. This property is very important if systems with different numbers of atoms are to be compared. Size-extensivity is a more general concept than size-consistency. While a full CI expansion is size-consistent and size-extensive, limited CI expansions are not. Improvements in the theory have been considered to account for this.[34]

The multiconfiguration self-consistent field method (MCSCF) is another CI variant in which a truncated CI expansion is used and both the expansion coefficients and the spin orbitals are determined variationally. This simultaneous optimization makes MCSCF computationally demanding, but accurate results can be obtained with the inclusion of

even a relatively small number of configurations. The complete active-space self-consistent field (CASSCF)[38] method is a special form of the MCSCF method in which the orbital space is divided into three subspaces: inactive, virtual and active orbitals. The active electrons are those that are not in the doubly occupied inactive orbital set. Within the active subspace a full CI treatment is performed.

When the first sum in the expansion (2.10) contains more than one term the CI procedure is called multi-reference CI (MR-CI).[32,39] In this method the set of reference configurations is usually determined through a previous CI calculation. All the single and double excitations from the reference configurations, often singly or doubly excited with respect to Φ_0, are included in the CI expansion. Therefore, the final MR-CI wavefunction will include determinants which are triply and quadruply excited from Φ_0. This method is computationally very expensive.

CI techniques can be classified into two categories, those that start from the SCF approximation and those that bypass the SCF level. Moreover, they can be intended just to improve ground-state wavefunctions or to complete excited-states wavefunctions.

2.6.2. Møller-Plesset perturbation theory

A different systematic procedure for finding the correlation energy that is not variational (*i.e.*, it does not give an upper bound to the exact energy), is perturbation theory (PT).[3] In this approach, the total (perturbed) Hamiltonian of the system is divided in two parts: the unperturbed (zero-order) Hamiltonian, $\hat{H}_0$, which has known eigenfunctions and eigenvalues, and the perturbation, λV, where λ is a dimensionless parameter determining the order of the expansion in the perturbation.

The appropriate solutions to the Schrödinger equation may be expanded in powers of λ:

$$\Psi_\lambda = \Psi^{(0)} + \lambda \Psi^{(1)} + \lambda^2 \Psi^{(2)} + ... + \lambda^n \Psi^{(n)} \tag{2.12}$$

$$\varepsilon_\lambda = \varepsilon^{(0)} + \lambda \varepsilon^{(1)} + \lambda^2 \varepsilon^{(2)} + ... + \lambda^n \varepsilon^{(n)} \tag{2.13}$$

If $\hat{H}_0$ is chosen wisely, the perturbation is small and the perturbation expansion, *i.e.*, the sum of the 1st, 2nd, ..., nth order energies, converges quickly. When the HF Hamiltonian is chosen as the zero-order Hamiltonian the procedure is called Møller-Plesset perturbation theory. It is the most economical multi-determinant method and furthermore, is size-extensive.

The Møller-Plesset (MP) energy to first order is the HF energy. The inclusion of the second-order energy correction is designated MP2 and gives the simplest approximate expression for the correlation energy. When third- and fourth-order energy corrections are included the procedures are then referred to as MP3 and MP4, and so on. The results of increasing the order of the MP calculation vary depending on the nature of the chemical system; monotonic, oscillating and diverging convergence can be found.

2.6.3. Coupled cluster theory

The foundations of coupled cluster (CC) theory in the context of quantum chemistry were laid by Čížek[40] in the late 1960s, but it was not until the late 1970s that practical implementations started to take place. CC calculations are similar to CI calculations in that the wavefunction is a linear combination of many determinants, but the way of choosing the determinants in a CC procedure is more complex.

The simplest practical application of the CC approach is to include only double excitations, CCD; single excitations can also be added, CCSD. There have been a variety of approaches to incorporate the effects of triplets.[41] The direct inclusion of triplets, CCSDT, is not practical for large systems. The approach used in this thesis includes the effects of triplets in a perturbative way, CCSD(T).[35,42] This method is probably the most commonly used triples correction, and is empirically observed to be the best behaved.

CC is the most accurate approach so far to treat electronic correlation. These methods are size-consistent, size-extensive and variational (as long as the excitations are included

successively, *i.e.*, CCSD is variational, but CCD is not). A full CC calculation is equivalent to a full CI calculation.

2.6.4. Density functional theory

An alternative to the HF based methods that has been growing in popularity over the past decade is density functional theory (DFT). [32,43] It can be used to do calculations on large systems in significantly less time than the methods previously discussed. Even though DFT is primarily a theory of electronic ground state structure, a variant called time-dependent DFT (TD-DFT) has proved to be successful in the calculation of excited states. [44] So far its application has been restricted to single-reference systems, although various ways to develop DFT for multi-reference systems has been discussed. [45]

Hohenberg and Kohn [46] proved that the ground state energy of an electronic system and all other ground-state electronic properties are uniquely determined by the electron probability density, ρ, although the exact functional (a function of a function) dependence of the energy on density, $E[\rho]$, remains unknown. In addition, for any trial density the energy obtained is an upper bound to the exact energy of the ground state. These are the basic principles behind DFT.

Kohn and Sham, [47] solving equations analogous to the HF equations, obtained an expression for the exact ground-state electronic energy. This energy is expressed in terms of the kinetic energy of the electrons, the attractive potential energy between electrons and nuclei, the Coulomb interaction between the total charge distribution, and the exchange-correlation energy of the system (E_{xc}).

The exchange-correlation energy is also a functional of the density and takes into account all non-classical electron-electron interactions. If E_{xc} is ignored, the physical content of the theory becomes identical to that of the HF approximation. It is the only term for which an exact expression is not known. The main source of error in DFT arises from this functional.

Since DFT depends on an adequate knowledge of $E_{xc}[\rho]$, functionals are constantly being developed, but there is no known systematic way to improve upon a calculation, *i.e.*, a lower energy by a certain DFT method does not guarantee that such a functional leads to more accurate molecular properties.[43] Some functionals are developed from fundamental quantum mechanics, while some are developed by parameterizing functions to best reproduce experimental results. Thus, there are in essence *ab initio* and semi-empirical versions of DFT. The simplest approximation, based only on the electron density, was achieved by making use of the exchange correlation energy per particle of a uniform interacting electron gas. This method is named: local spin density approximation (LSDA).[47]

A more complex generation of functionals uses the electron density and its gradient. Several gradient-corrected (or non-local) exchange and correlation functionals were developed and are known collectively as generalized gradient approximations (GGAs).[48] The most popular correlation functionals include those of Perdew (P86),[49] Lee, Yang and Parr (LYP),[50] and Perdew and Wang (PW91).[51] The exchange functionals more widely used are those derived by Perdew and Wang (PW86)[52] and Becke (B or B88).[53]

A new class of hybrid HF/GGA theories was developed, with precision surpassing that of pure GGAs.[54] These hybrid methods combine functionals from other methods with parts of a HF calculation, usually the exchange integrals. The hybrid functionals developed by Becke can be expressed as a linear combination of HF, LSDA and Becke's gradient-corrected exchange (B or B88) contributions, together with LSDA and gradient-corrected correlation functionals such as: P86, LYP or PW91. A very popular DFT method is named B3LYP. This method combines the B3 hybrid exchange functional[54] (that contains 20% of HF exchange) with the correlation functional LYP. The first exchange functional to be suggested was the Becke half-and-half (BH&H),[55] which includes 50% HF exchange. B3LYP and BH&HLYP will be the functionals used in some chapters of the thesis.

2.7. Semi-empirical methods

The main difficulty in the solution of the RH equations is the evaluation of the two-electron integrals. The bigger the molecular system, the greater the number of integrals to solve. Based on the way computational methods deal with this problem they are classified into *ab initio* and semi-empirical methods. In *ab initio* methods, the integrals are solved for all the electrons of the system and all necessary quantities are computed accurately from the very beginning. On the other hand, semi-empirical methods[32,56] usually employ a minimal basis set for the valence electrons, neglect some of the two-electron integrals and determine the others directly from experimental data, from the corresponding analytical formulae, or from suitable parametric expressions.

Semi-empirical methods were first developed for conjugated π-electron systems, ignoring the σ electrons. The most famous and simplest π-electron theory is Hückel[57] molecular orbital (HMO) theory where all two-electron integrals are set to zero and the π-electron Hamiltonian is written as a sum of one-electron terms; thus electronic repulsions are treated very poorly.

The Pariser-Parr-Pople (PPP) method[58] is a much more substantial π-electron procedure where the inter-electronic repulsions are included in the π-electron Hamiltonian. It was the first SCF scheme for molecular calculations. Some of the two-electron integrals are neglected through the zero differential overlap (ZDO) approximation:

$$(\mu\nu|\lambda\sigma) = \delta_{\mu\nu}\,\delta_{\lambda\sigma}\,(\mu\mu|\lambda\lambda) \qquad (2.14)$$

that is, all three- and four-centre two-electron integrals are neglected. For atomic orbitals centred on atoms that are not bonded together, the Hamiltonian matrix elements are set to zero, and for those centred on bonded atoms the matrix elements are taken to be empirical parameters.

Extended Hückel theory[59] is the first semi-empirical method where all the valence electrons are considered, but the two-electron repulsion integrals are neglected, among

other simplifications. Since 1965 a variety of SCF semi-empirical procedures were developed. They are generalizations of the PPP method where the ZDO approximation is applied to all the valence electrons at three different levels: CNDO, INDO and NDDO.

In the complete neglect of differential overlap (CNDO) methods,[60] the two-electron integrals (on one and two centres) that involve different atomic orbitals (AOs) centred on the same atom are neglected, and the remaining integrals are assumed to depend only on the atoms to which the AOs belong and not on the actual forms of these AOs.

In the methods based on the intermediate neglect of differential overlap (INDO) approximation,[61,62] one-centre repulsion integrals between AOs on the same atom are not neglected, and thus some exchange integrals enter the expressions for the matrix elements. As in CNDO, parameters are chosen in INDO to give as close agreement as possible to the results of minimal basis set HF-SCF calculations. Other methods (*vide infra*) were developed later with the aim of reproducing not the HF-SCF wavefunctions but rather four gas phase molecular properties, namely molecular geometries, enthalpies of formation, dipole moments and ionization energies.[63,64,65]

A variant of the INDO scheme is the Zerner's INDO method (ZINDO) that will be explained in Section 7.4.1. Another variant, SINDO1 (symmetrically orthogonalized INDO)[66] was designed for the prediction of the binding energies and geometries of compounds containing elements of the 1st and 2nd rows, as well as 3rd row transition metals.

A much less severe approximation than INDO is the neglect of diatomic differential overlap (NDDO), in which none of the one-centre integrals are neglected. The two-centre integrals $(\mu\nu|\lambda\sigma)$, where μ and ν are different orbitals on one atom, and λ and σ are different orbitals on another atom, neglected as well in the INDO methods, are also retained. The most popular NDDO methods currently used are AM1[63] (Austin method 1) and PM3[64] (parametric method 3). Both are improved versions of the MNDO[65] (modified neglect of differential overlap) method (also based on the NDDO approximation) where

the core-core repulsion function is represented by a more flexible function with several additional adjustable parameters, reducing the overestimated nonbonding repulsions in MNDO. Depending on the nature of the system and information desired, either AM1 or PM3 will usually give the most accurate results obtainable for organic molecules with semi-empirical methods.[34]

Other more recently developed semi-empirical methods are:[56] Feske-Hall (designed for the description of inorganic metal-ligand systems), TNDO (typed neglect of differential overlap, specially parameterized to reproduce NMR chemical shifts) and SAM1 (semi-*ab initio* method 1, that uses a parameterization to estimate correlation effects; this method gives results slightly more accurate than with AM1 or PM3.[67]

The Gaussian methods (G1, G2 and G3) are unique types of computations.[68] These are compound methods that combine the results of several *ab initio* calculations, carried out at relatively low levels of theory, to approximate the result of a single, high level calculation that is too expensive to be practical. These methods arose from the observation that certain *ab initio* methods tend to show a systematic error in the prediction of ground state energies of organic molecules.[34]

Semi-empirical methods continue to be developed because there is always room for improvement of the parameterization scheme and the use of experimental data. They are very practical methods for describing electronic effects in large molecules.

2.8. Geometry optimizations

A potential energy hypersurface (PEH) describes the energy of a molecule with respect to its nuclear coordinates. Stationary points are places on the PEH with a zero gradient vector (the first derivative of the energy with respect to nuclear coordinates). If all the eigenvalues of the Hessian matrix (the second derivative of the energy with respect to nuclear coordinates) are positive, the stationary point is a minimum. If there is one, and only one, negative curvature, the stationary point is a transition state (TS). Points with more than one negative curvature do exist, but are not important in chemistry. Because

vibrational frequencies are basically the square roots of the curvatures, a minimum has all real frequencies, and a saddle point (of first order) has one imaginary vibrational frequency.

All geometry optimizations[69] require an initial guess for which the SCF equations are solved and the energy gradient is calculated. The gradient indicates the direction along the PEH in which the energy decreases most rapidly from the current point as well as the steepness of that slope. The structure is then varied along the energy gradient, and the process is repeated until the gradient of each nuclear coordinate is zero or, in practice, below a pre-set threshold. At this point the geometry has converged and a stationary point has been obtained that can be characterized by a frequency analysis.

There are many different optimization algorithms for finding the set of coordinates corresponding to the minimum energy of a stationary point. Some of these methods are: simplex, Fletcher-Powell, quasi-Newton (Berny algorithm), steepest decent, scaled steepest decent, GDIIS (geometric direct inversion of the iterative subspace), EF (eigenvector following), DFP (Davidson-Fletcher-Powell) and Newton-Raphson.[70]

To find a TS structure, the Hessian matrix has to be computed. The nuclei are moved in a manner that increases the energy in directions corresponding to negative values of the Hessian and decreases energy where there are positive values of the Hessian. A transition structure is a maximum on the reaction pathway and a minimum in all the other coordinates. TSs are more difficult to describe and find than equilibrium geometries.

To verify that the desired TS has been optimized, the frequencies must be calculated. The vibrational mode associated with the negative frequency should describe the motion toward reactants in one direction and products in the other direction. If after visualizing this vibrational mode it is still not clear whether the TS is correct, an intrinsic reaction coordinate (IRC)[71] calculation should be performed; sometimes artefacts of the method employed could lead to erroneous conclusions.

TSs have been computationally determined for many years. Experimentally, it has only recently become possible to examine reaction mechanisms directly using femtosecond pulsed laser spectroscopy.[72] This technique cannot yet be applied to all the compounds that are computationally accessible, and furthermore, they yield vibrational information rather than an actual geometry for the TS.

Usually after a geometry has been optimized at a certain level of theory, the energy of the molecular system is calculated at a higher level that includes more electronic correlation. Computations that do not involve geometry optimization are called single-point calculations.

2.8.1. Notation

The conventional notation, used in this thesis, to describe a particular method or level of theory is as follows:

method 1 / basis set 1 // method 2 / basis set 2

This notation means that after a geometry optimization has been carried out using method 2 with basis set 2, a single point energy calculation is performed using method 1 with basis set 1. Method 1 generally accounts for more electronic correlation energy than method 2; basis set 1 is usually larger than basis set 2, but could also be the same. For example, the notation:

CCSD(T)/6-311G(d,p)//BH&HLYP/6-311G(d,p)

describes a CCSD(T) single-point calculation, using a geometry optimized at the BH&HLYP level, with the 6-311G(d,p) basis set.

2.9. References

1. Schrödinger, E. *Ann. Physik* **1926**, *79*, 361.

2. Born, O.; Oppenheimer, J.R. *Ann. Physik* **1927**, *84*, 457.

3. Szabo, A.; Ostlund, N.S. *Modern Quantum Chemistry: Introduction to Advanced Electronic Structure Theory*, Dover, New York, 1989.

4. Hehre, W.J.; Radom, L.; Schleyer, P.v.R.; Pople, J.A. *Ab Initio Molecular Orbital Theory*; Wiley, New York, 1986.

5. Slater, J.C. *Phys. Rev.* **1929**, *34*, 1293; **1930**, *35*, 509.

6. Slater, J.C. *Phys. Rev.* **1930**, *36*, 57.

7. Boys, S.F. *Proc. R. Soc. London* **1950**, *A200*, 542.

8. (a) Davidson, E.R.; Feller, D. *Chem. Rev.* **1986**, *86*, 681; Feller, D. (b) Davidson, E.R. in *Reviews in Computational Chemistry*, K.B. Lipkowitz and D.B. Boyd, Eds., Vol. 1, VCH, New York, p. 1, 1990.

9. Kestner, N.R. *J. Chem. Phys.* **1968**, *48*, 252.

10. Liu, B.; McLean, A.D. *J. Chem. Phys.* **1973**, *59*, 4557.

11. (a) Davidson, E.R. *Chem. Phys. Lett.* **1994**, *217*, 48. (b) *ibid.* **1995**, *241*, 146. (c) Kestner, N.R.; Combariza, J.E. in *Reviews in Computational Chemistry*, Volume 13, Lipkowitz, K.B. and Boyd, D.B., Editors, Wiley-VCH, New York, p. 99, 1999.

12. (a) Boys, S.F.; Bernardi, F. *Mol. Phys.* **1970**, *19*, 553. (b) Liu, B.; McLean, A.D. *J. Chem. Phys.* **1989**, *91*, 2348. (c) Handy, N.C.; Pople, J.A.; Shavitt, I. *J. Phys. Chem.* **1996**, *100*, 6007 (This paper gives a biographical synopsis on Boys's work).

13. Frisch, M.J.; Del Bene, J.E.; Binkley, J.S.; Schaefer III, H.F. *J. Chem. Phys.* **1986**, *84*, 2279.

14. Schwenke, D.W.; Truhlar, D.G. *J. Chem. Phys.* **1985**, *82*, 2418.

15. Frisch, Æ.; Frisch, M.J. *Gaussian 98 User's Reference*, Gaussian, Inc., p. 235, 1998.

16. For example, see: (a) Pulay, P. *Chem. Phys. Lett.* **1983**, *100*, 1884. (b) Surjan, P.R.; Mayer, I.; Lukovitz, I. *Chem. Phys. Lett.* **1983**, *119*, 538. (c) Famulari, A.; Specchio, R.; Sironi, M.; Raimondi, M. *J. Chem. Phys.* **1998**, *108*, 3296. (d) Mayer, I.; Valiron, P. *J. Chem. Phys.* **1998**, *109*, 3360.

17. For example, see: (a) Petterson, L.; Wahlgren, U. *Chem. Phys.*, **1982**, *69*, 185. (b) Bolis, G.; Clementi, E.; Wertz, D.N., Scheraga, H.A.; Tosi, C. *J. Am. Chem. Soc.*, **1983**, *105*, 355. (c) Vargas, R.; Garza, J.; Dixon, D.A.; Hay, B.P. *J. Am. Chem. Soc.*, **2000**, *122*, 4750. (d) Simon, S.; Bertran, J.; Sodupe, M. *J. Phys. Chem. A* **2001**, *105*, 4359. (e) Vargas, R.; Garza, J.; Friesner, R.A.; Stern, H.; Hay, B.P.; Dixon, D.A. *J. Phys. Chem. A* **2001**, *105*, 4963. (f) Alagona, G.; Ghio, C.; Monti, S. *Int. J. Quantum Chem.* **2001**, *83*, 128.

18. (a) Hartree, D.R. *Cambridge Phil. Soc.* **1928**, *24*, 89. (b) Fock, V. *Z. Physik* **1930**, *61*, 126.

19. (a) Roothaan, C.C.J. *Rev. Mod. Phys.* **1951**, *23*, 69. (b) Hall, G.G. *Proc. R. Soc. London* **1951**, *A205*, 541.

20. (a) Schlegel, H.B. *Encycl. Comput. Chem.* **1998**, *4*, 2665. (b) Bally, T.; Borden, W.T. in *Reviews in Computational Chemistry*, Volume 13, Lipkowitz, K.B. and Boyd, D.B., Editors, Wiley-VCH, New York, p. 1 in *Reviews in Computational Chemistry*, Volume 13, Lipkowitz, K.B. and Boyd, D.B., Editors, Wiley-VCH, New York, p. 1, 1999.

21. Schlegel, H.B. *J. Chem. Phys.* **1986**, *84*, 4530.

22. (a) Löwdin, P.-O. *Rev. Mod. Phys.* **1963**, *35*, 496. (b) Löwdin, P.-O. *Adv. Chem. Phys.* **1969**, *14*, 283.

23. Eisfeld, W.; Morokuma, K. *J. Chem. Phys.* **2000**, *113*, 5587.

24. Davidson, E.R.; Borden, W.T. *J. Phys. Chem.* **1983**, *87*, 4783.

25. Pauncz, R.; de Heer, J.; Löwdin, P.O. *J. Chem. Phys.* **1962**, *36*, 2247.

26. Taylor, P.R. in *European Summerschool in Quantum Chemistry*, Book I, B.O. Roos and P.-O. Widmark, Eds., Lund University, Sweden, p. 147, 2000.

27. (a) Jahn, H.A.; Teller, E. *Proc. R. Soc. London A*, **1937**, *161*, 220. (b) Bersuker, I.B. *Chem. Rev.* **2001**, *101*, 1067.

28. Boyd, R.J.; Darvesh, K.V.; Fricker, P.D. *J. Chem. Phys.* **1991**, *94*, 8083.

29. Fulde, P. *Electron Correlations in Molecules and Solids*, Springer-Verlag, 1995.

30. Löwdin, P.O. *Adv. Chem. Phys.* **1959**, *2*, 207.

31. (a) Raghavachari, K.; Anderson, J.B. *J. Phys. Chem.* **1996**, *100*, 12960. (b) Taylor, P.R. in *European Summerschool in Quantum Chemistry*, Book III, B.O. Roos and P.-O. Widmark, Eds., Lund University, Sweden, p. 651, 2000.

32. Atkins, P.W.; Friedman, R.S. *Molecular Quantum Mechanics*, 3rd edition, Oxford University Press, 1997.

33. Schaefer III, H.F. (Ed.) *Methods of Electronic Structure Theory*, Plenum Press, 1977.

34. Young, D.C. *Computational Chemistry: A Practical Guide for Applying Techniques to Real-World Problems*, John Wiley & Sons, New York, 2001.

35. Taylor, P.R. in *European Summerschool in Quantum Chemistry*, Book II, B.O. Roos and P.-O. Widmark, Eds., Lund University, Sweden, p. 365, 2000.

36. Pople, J.A.; Binkley, J.S.; Seeger, R. *Int. J. Quantum Chem. Symp.* **1976**, *11*, 1.

37. Bartlett, R.J.; Purvis, G.D. *Int. J. Quantum Chem.* **1978**, *14*, 561.

38. Roos, B.O. *Int. J. Quantum Chem.*: *Quantum Chem. Symp.* **1980**, *14*, 175.

39. (a) Buenker, R.J.; Peyerimoff, S.D. *Theor. Chim. Acta* **1968**, *12*, 183. (b) Buenker, R.J.; Peyerimoff, S.D. *Theor. Chim. Acta* **1975**, *39*, 217. (c) Peyerimoff, S.D.; Buenker, R.J. *Adv. Quantum Chem.* **1975**, *9*, 69.

40. Čížek, J. *J. Chem. Phys.* **1966**, *45*, 4256.

41. (a) Pople, J.A.; Head-Gordon, M.; Raghavachari, K. *J. Chem. Phys.* **1987**, *87*, 5968. (b) Noga, J.; Bartlett, R.J. *J. Chem. Phys.* **1987**, *86*, 7041 (and references therein). (c) Bartlett, R.J. *J. Phys. Chem.* **1989**, *93*, 1697. (d) Bartlett, R.J. in *Modern Electronic Structure Theory*, Part II, Vol. 2, D.R. Yarkony, Ed., World Scientific Publishing, Singapore, 1995.

42. Raghavachari, K.; Trucks, G.W.; Pople, J.A.; Head-Gordon, M. *Chem. Phys. Lett.* **1989**, *157*, 479.

43. (a) Ziegler, T. *Chem. Rev.* **1991**, *91*, 651. (b) Kohn, W.; Becke, A.D.; Parr, R.G. *J. Phys. Chem.* **1996**, *100*, 12974.

44. (a) Bauernschmitt, R.; Ahlrichs, R. *Chem. Phys. Lett.* **1996**, *256*, 454. (b) Casida, M.E.; Jamorski, C.; Casida, K.C.; Salahub, D.R. *J. Chem. Phys.* **1998**, *108*, 4439. (c) Stratmann, R.E.; Scuseria, G.E.; Frisch, M.J. *J. Chem. Phys.* **1998**, *109*, 8218.

45. Gräfenstein, J.; Cremer, D. *Phys. Chem. Chem. Phys.* **2000**, *2*, 2091.

46. Hohenberg, P.; Kohn, W. *Phys. Rev.* **1964**, *B136*, 864.

47. Kohn, W.; Sham, L.J. *Phys. Rev. A* **1965**, *140*, 1133.

48. Parr, R.G.; Yang, W. *Density Functional Theory of Atoms and Molecules*, Oxford University Press, New York, 1989.

49. (a) Perdew, J.P. *Phys. Rev. B* **1986**, *33*, 8822. (b) *ibid.* **1986**, *34*, 7406.

50. Lee, C; Yang, W.; Parr, R.G. *Phys. Rev. B* **1988**, *37*, 785.

51. Perdew, J.P.; Wang, Y. *Phys. Rev. B* **1992**, *45*, 13244.

52. Perdew, J.P.; Wang, Y. *Phys. Rev. B* **1986**, *33*, 8800.

53. Becke, A.D. *Phys. Rev. A* **1988**, *38*, 3098.

54. (a) Becke, A.D. *J. Chem. Phys.* **1993**, *98*, 5648. (b) *ibid.* **1996**, *104*, 1040.

55. Becke, A.D. *J. Chem. Phys.* **1993**, *98*, 1372.

56. (a) Thiel, W. in *Advances in Chemical Physics*, I. Prigogine and S.A. Rice, Eds., Vol. XCIII, Wiley, New York, p. 703, 1996. (b) Jug, K.; Neumann, F. *Encycl. Comput. Chem.* **1998**, *1*, 507. (c) Stewart, J.J.P. *Encycl. Comput. Chem.* **1998**, *2*, 1513. (d) *ibid.* **1998**, *3*, 2000.

57. Hückel, E.P. *Z. Physik* **1931**, *70*, 204.

58. (a) Pariser, R.; Parr, R.G. *J. Chem. Phys.* **1953**, *21*, 466, 767. (b) Pople, J.A. *Trans. Faraday Soc.* **1953**, *49*, 1475.

59. Hoffmann, R. *J. Chem. Phys.* **1963**, *39*, 1397.

60. (a) Pople, J.A.; Santry, D.F.; Segal, G.A. *J. Chem. Phys.* **1965**, *43*, S129. (b) Pople, J.A.; Segal, G.A. *J. Chem. Phys.* **1965**, *43*, S136. (c) *ibid.* **1966**, *44*, 3289. (d) Del Bene, J.; Jaffé, H.H. *J. Chem. Phys.* **1968**, *48*, 1807, 4050.

61. (a) Pople, J.A.; Beveridge, D.L.; Dobosh, P.A. *J. Chem. Phys.* **1967**, *47*, 2026. (b) Nanda, D.N.; Jug, K., *Theor. Chim. Acta* **1980**, *57*, 95. (c) Jug, K.; Iffert, R.; Schulz, J. *Int. J. Quantum Chem.* **1987**, *32*, 265.

62. (a) Ridley, J.; Zerner, M.C. *Theor. Chim. Acta* **1973**, *32*, 111. (b) *ibid.* **1976**, *42*, 223. (c) Bacon, A.D.; Zerner, M.C. *Theor. Chim. Acta* **1979**, *53*, 21. (d) Zerner, M.C.; Loew, G.H.; Kirchner, R.F.; Mueller-Westerhoff, U.T. *J. Am. Chem. Soc.* **1980**, *102*, 589.

63. (a) Dewar, M.J.S.; Zoebisch, E.; Healy, E.F.; Stewart, J.P.P. *J. Am. Chem. Soc.* **1985**, *107*, 3902. (b) Holder, A.J. *Encycl. Comput. Chem.* **1998**, *1*, 8.

64. (a) Stewart, J.J.P. *J. Comp. Chem.* **1989**, *10*, 209, 221. (b) Stewart, J.J.P. *Encycl. Comput. Chem.* **1998**, *3*, 2080.

65. (a) Dewar, M.J.S.; Thiel, W. *J. Am. Chem. Soc.* **1977**, *99*, 4899. (b) Thiel, W. *Encycl. Comput. Chem.* **1998**, *3*, 1599, 1604.

66. Jug, K.; Bredow, T. *Encycl. Comput. Chem.* **1998**, *4*, 2599.

67. Holder, A.J. *Encycl. Comput. Chem.* **1998**, *4*, 2542.

68. (a) Curtiss. L.A.; Raghavachari, K. *Encycl. Comput. Chem.* **1998**, *2*, 1104.

69. Foresman, J.B.; Frisch, Æ. *Exploring Chemistry with Electronic Structure Methods*, 2nd dition, Gaussian, Inc., 1996.

70. (a) Hehre, W.J. *Practical Strategies for Electronic Structure Calculations*, Wavefunction Inc., Irvine, 1995. (b) Schlegel, H.B. *Encycl. Comput. Chem.* **1998**, *2*, 1136. (c) Schlick, T. *Encycl. Comput. Chem.* **1998**, *2*, 1143.

71. (a) González, C.; Schlegel, H.B. *J. Chem. Phys.* **1989**, *90*, 2154. (b) González, C.; Schlegel, H.B. *J. Phys. Chem.* **1990**, *94*, 5523.

72. Zewail, A.H. *J. Phys. Chem. A* **2000**, *104*, 5660.

PART 1

Chapter 3. Kinetic Calculations

3.1. Introduction

This chapter provides general background information to complement the kinetic calculations reported in Chapters 4 to 6. The following sections will provide an overview of the concepts and approximations behind transition state theory (TST), covering essential statistical thermodynamic topics such as the molecular partition function and its components, and the calculation of equilibrium constants. Tunneling calculations will also be covered, as a complementary part of quantum kinetic calculations on systems where light particles are transferred.

The rate constants for chemical reactions can show different temperature dependencies. Some reactions are reported to have negative activation energies. Several explanations for this phenomenon will be discussed. The consideration of the reactant complex formation has been one of the ideas proposed to explain this situation.

3.2. Essential statistical thermodynamics

Statistical mechanics bridges the gap between the microscopic world of molecules, atoms, electrons and photons, and the macroscopic world of thermodynamics and the properties of materials. The goal of this branch of physics, in which mechanics and probability theory are mixed, is the understanding and prediction of macroscopic phenomena and the calculation of macroscopic properties from the properties of the individual components of the system.

Statistical mechanics is based on either classical or quantum mechanics, with equilibrium and non-equilibrium versions. The branch dealing with thermodynamic properties is known as statistical thermodynamics, or more fully as equilibrium quantum statistical mechanics.[1]

The partition function is without any doubt the most important quantity in statistical thermodynamics. Once known as a function of the temperature, volume and number of particles in a system, all thermodynamic quantities, including heat capacities, entropies and equilibrium constants, can be calculated.[2]

The molecular partition function (Q) can be expressed as a sum over states (3.1), or a sum over energy levels, in which the degeneracy factor g_i has to be considered (3.2):

$$Q_{Total} = \sum_i exp(-\frac{E_{T_i}}{k_B T})$$
(3.1)

$$Q_{Total} = \sum_i g_i \, exp(-\frac{E_{T_i}}{k_B T})$$
(3.2)

In these expressions k_B is Boltzmann's constant, T is temperature and i is the index that numbers the states (3.1) or energy levels (3.2).

The partition function indicates the average number of energy levels (or states) that are thermally accessible to a molecule at the temperature of the system. At T = 0 K only the ground state is accessible and Q equals g_0, the degeneracy of the ground state, but at very high T, virtually all states are accessible, and Q is very large.

Since in statistical thermodynamics different ensembles (*i.e.*, collections of imaginary replications of the system) such as the canonical, microcanonical and grand canonical ensembles are defined for practical use, different kinds of partition functions refer to each of them.

As mentioned in the previous chapter, the total energy of a molecule can be expressed as a sum of contributions from the kinetic energy (E_K) of the nuclei and electrons, and the potential energy (E_P) of nuclear, electronic and electron-nuclear interactions:

$$E_T = E_K (nuclei) + E_K (electrons) + E_P (nuclei) + E_P (electrons) + E_P (electrons - nuclei)$$
(3.3)

This total energy can also be expressed by the sum of contributions from the different molecular modes of motion: translational (trans), rotational (rot), internal-rotational (int-rot), vibrational (vib) and electronic (elect):

$$E_T = E_{trans} + E_{rot} + E_{int-rot} + E_{vib} + E_{elect} \tag{3.4}$$

Strictly speaking the ground state energy of the molecule should be added to the above expression but it is usually excluded in standard textbooks.[3] The above expression is an approximation since, apart from translational motion, these modes are not completely independent. However, in most cases this approximation is satisfactory. Approximations that assume that two modes of motion are not coupled, *i.e.*, that do not interchange energy, are called adiabatic approximations. One such approximation, already mentioned in Chapter 2 (the Born-Oppenheimer approximation), allows the separation of electronic and vibrational motions. Another approximation of this kind is one in which the molecule is treated as a rigid body, permitting the separation of rotations and vibrations.

By combining expressions (3.2) and (3.4), the molecular partition function can be rewritten as:

$$Q_{Total} = \left(\sum_i g_i \exp(-\frac{E'_{trans}}{k_BT}) \right) \left(\sum_i g_i \exp(-\frac{E'_{rot}}{k_BT}) \right) \left(\sum_i g_i \exp(-\frac{E'_{int-rot}}{k_BT}) \right) \left(\sum_i g_i \exp(-\frac{E'_{vib}}{k_BT}) \right) \left(\sum_i g_i \exp(-\frac{E'_{elect}}{k_BT}) \right)$$

$$Q_{Total} = Q_{trans} \, Q_{rot} \, Q_{int-rot} \, Q_{vib} \, Q_{elec} \tag{3.5}$$

The different contributions to the total molecular partition function (that is dimensionless) have magnitudes that decrease in the following order: $Q_{trans} > Q_{rot} > Q_{int-rot} > Q_{vib} > Q_{elect}$. Each contribution can be investigated separately and can be calculated, in principle, from spectroscopic data.

3.2.1. Translational partition function

The translational component of the total partition function must be calculated from a sum over all the translational energy levels available to a molecule confined to a cubic box of

volume V = RT/p (the molar volume of an ideal gas at temperature T and pressure p; R is the ideal gas constant):

$$Q_{trans} = \sum_i \exp(-\frac{E^i_{trans}}{k_B T})$$ (3.6)

If the translational energy levels are considered to be very close to each other, this sum may be approximated by an integral to obtain expression (3.7):

$$Q_{trans} = \left(\frac{2\pi m k_B T}{h^2}\right)^{3/2} V$$ (3.7)

where m is the mass of the molecule and h is Planck's constant. For the calculation of V the standard pressure, $p^0 = 1$ atm, will be used in the calculations presented in the next chapters.

Expression (3.7) is sometimes rewritten in a different form:

$$Q_{trans} = \frac{V}{\Lambda^3} \qquad\qquad \Lambda = \frac{h}{(2\pi m k_B T)^{1/2}}$$ (3.8)

The parameter Λ is called the thermal wavelength and is used to judge whether the approximation that led to the expression of Q_{trans} is valid. This is the case if many states are occupied, which requires Q_{trans} to be large. Λ must be small compared with the linear dimensions of the container. For example, for H_2 at 298 K, $\Lambda = 71$ pm and for a heavier molecule, O_2, $\Lambda = 18$ pm. The heavier the molecule the more satisfactory the approximation.

3.2.2. Rotational partition function

A model system that approximately represents the rotation of a diatomic molecule is the rigid rotor. In this model the molecule is considered a central-force system consisting of two masses with a fixed interparticle distance. In such a model it is assumed that when the molecule rotates no vibration occurs, and *vice versa*. This model, when extended to a polyatomic system, is referred to as the rigid molecule (body) system. The free rotation of

a rigid molecule is described classically in terms of the principal moments of inertia, magnitudes that are calculated relative to three mutually perpendicular axes (principal axes) that intercept in the molecular centre of mass. In order to calculate the moments of inertia the mass and Cartesian coordinates of the atoms that form the molecule are needed. If the molecule is not considered a rigid rotor, the value of these parameters would be constantly changing.

The free rotation of a rigid molecule is also quantized and the development of expression (3.9) leads to expressions (3.10), for a diatomic molecule, and (3.11), for a polyatomic system.

$$Q_{rot} = \sum_i g_i \exp(-\frac{E^i_{rot}}{k_B T}) \tag{3.9}$$

$$Q_{rot} = \frac{1}{\sigma} \cdot \frac{8\pi^2 I k_B T}{h^2} \tag{3.10}$$

$$Q_{rot} = \frac{1}{\sigma} \cdot \frac{8\pi^2 (8\pi^3 I_A I_B I_C)^{1/2} (k_B T)^{3/2}}{h^3} \tag{3.11}$$

In these expressions, I is the moment of inertia of a diatomic molecule, and I_A, I_B and I_C are the principal moments of inertia of a polyatomic molecule with respect to its principal axes. The constant σ is called the symmetry number, rotational symmetry number or external symmetry number. The inclusion of σ in the above expressions accounts for the fact that for symmetrical molecules less thermally accessible rotational states are available because of the indistinguishability of states.

A formal way of obtaining the value of σ is by determining the order (number of elements) of the rotational subgroup of the molecule, the point group of the molecule with all but the identity and the rotations removed. For example, the rotational subgroup of HCHO, a C_{2v} molecule, is $\{E, C_2\}$, so $\sigma = 2$; the rotational subgroup of NO_3 in the D_{3h} point group is $\{E, 2C_3, 3C_2\}$, so $\sigma = 6$.

To obtain expressions (3.10) and (3.11), the sum derived from expression (3.9) is replaced by an integral (as for translations) after assuming that at high temperatures many rotational levels are occupied and the separation between neighbouring states is much smaller than $k_B T$, the characteristic thermal energy.

A useful way of expressing the temperature above which the previous approximation is valid, is by means of the rotational temperature, θ_{rot}, that can be calculated using expression (3.12). For $T \gg \theta_{rot}$, the approximation is valid; some typical values are listed in Table 3.1. Heavy and big molecules have large moments of inertia and thus very large Q_{rot}. This situation reflects the closeness in energy (compared with $k_B T$) of the rotational levels and that a large number of them are accessible at room temperature.

$$\theta_{rot} = \frac{h^2 c}{8\pi^2 k_B I} \tag{3.12}$$

Table 3.1. Rotational and vibrational temperatures.[a]

Molecule	θ_{rot}/K	θ_{vib}/K
H_2	88	6330
HCl	9.4	4300
I_2	0.053	309

[a] Taken from reference 2

3.2.3. Vibrational partition function

The simplest description of a vibration is given by the harmonic oscillator. Such an oscillation occurs when a particle experiences a restoring force (k) that is proportional to its displacement (x), according to Hooke's law. The harmonic oscillator has a parabolic potential energy V ($V \propto x^2$) and the greater the curvature of the potential at the equilibrium position, the greater the force constant k (see Fig. 3.1):[4]

$$k = \left(\frac{\partial^2 V}{\partial x^2}\right)_0 \tag{3.13}$$
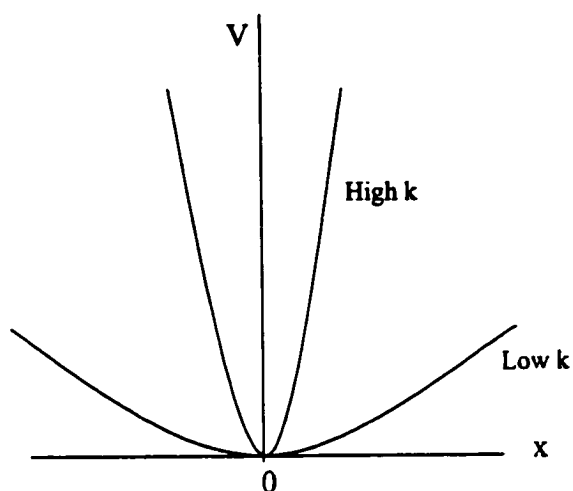
Figure 3.1. Potential energy curve for a harmonic oscillator.

The total energy computed by a geometry optimization (see Section 2.8) is the minimum on the potential energy curve. However, as an indirect consequence of the Heisenberg uncertainty principle, the molecule always has some vibrational motion, even at 0 K. This vibrational energy at 0 K is called the zero-point energy (ZPE) which is used to correct the calculated total energy of a molecule when energy differences or thermochemical data are to be calculated at 0 K. If calculations at higher temperatures are to be performed, another correction, the *thermal correction to the energy* (TCE), must be considered. The TCE contains the ZPE plus the contributions to the total energy from vibrations at temperatures higher that 0 K.

Following the harmonic approximation, the ZPE is calculated as:

$$ZPE = \frac{1}{2}hc\bar{v} \tag{3.14}$$

where c is the speed of light, and $\bar{v}$ is the wavenumber associated with the oscillation, calculated according to the following expression (μ is the reduced mass of the 'diatomic' molecule):

$$\bar{v} = \frac{1}{2\pi c} \sqrt{\frac{k}{\mu}} \qquad (3.15)$$

The quantized energy levels of the harmonic oscillator model are equally separated by an energy equal to $hc\bar{v}$. As the bond energy increases, the force constant also increases together with the separation between neighbouring vibrational energy levels.

The quantum mechanical description of a harmonic oscillator[5] does not exactly describe molecular vibrations that behave somewhat anharmonically, but does provide a useful approximate treatment for low vibrational quantum numbers.

An oscillator is mechanically anharmonic if the restoring force (k) is not strictly proportional to its displacement (x). It has a non-parabolic potential energy curve: the potential becomes less confining as x increases and the energy levels become closer together than in a harmonic oscillator; Fig. 3.2 shows the potential energy curves for the two models. Vibrations become strongly anharmonic at high excitations.

The harmonic values of $\bar{v}$ are obtained directly from the Hessian matrix (Section 2.8). One of the most direct ways to calculate anharmonic corrections to the vibrational frequencies is to compute higher-order derivatives (3rd, 4th, and so forth) of the energy with respect to the coordinates of the system; this requires considerably more computer resources.[6]
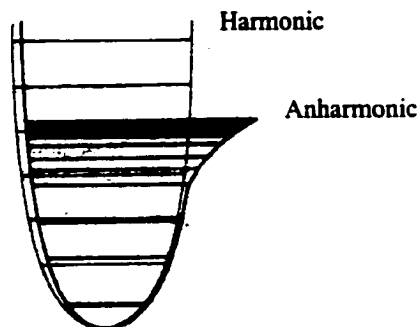
Figure 3.2. Harmonic and anharmonic potential energy curves.
Reproduced from reference 4.

In a polyatomic molecule with N atoms there are 3N-6 vibrational normal modes (3N-5, if the molecule is linear). If anharmonicities are small, these vibrational modes (each of which has its vibrational partition function) can be considered independent, and the total vibrational partition function may be expressed as:

$$Q_{vib} = \prod_{j}^{\substack{3N-6 \\ 3N-5}} Q_{vib}(j)$$

(3.16)

where $Q_{vib}(j)$ is the partition function of the jth normal mode. Normal modes of vibration may not be independent when the potential is strongly non-parabolic; the motion of one mode may stimulate another mode into vibration.

If the harmonic oscillator energy levels are incorporated into equation (3.17), the vibrational partition function of the different normal modes may be calculated as indicated in equation (3.18):

$$Q_{vib}(i) = \sum_{i} \exp(-\frac{E^i_{vib}}{k_B T})$$

(3.17)

$$Q_{vib}(j) = \frac{1}{1 - \exp\left(-\frac{hc\bar{v}_j}{k_B T}\right)}$$

(3.18)

The bigger the wavenumber of a vibrational mode, the lower its contribution to the total vibrational partition function. It is convenient to refer to the quantity $hc\bar{v}/k_B$ as the vibrational or characteristic temperature, θ_{vib} (some examples are listed in Table 3.1). Two extreme cases that lead to simplifications of equation (3.18) can be identified. When θ_{vib} is large compared with T, the fraction of molecules in vibrational excited states is small and $Q_{vib} \approx 1$. At temperatures higher than θ_{vib}, Q_{vib} can be calculated as:[7]

$$Q_{vib} = \frac{T}{\theta_{vib}}$$

(3.19)

3.2.4. Internal-rotational partition function

In polyatomic molecules, some of the 3N-6 vibrational degrees of freedom can exist as mutual rotation of the different fragments of the molecule or as more complicated mutually consistent motion. These additional degrees of freedom are called internal rotations, torsions or conformational transformations.[3]

In molecules such as ethane, the internal rotation around the single carbon-carbon bond is one of the most important internal degrees of freedom (see Fig. 3.2).
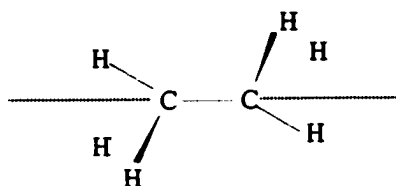
Figure 3.3. Schematic representation of the internal rotation about the C-C bond in ethane.

There are three ways to treat an internal rotation depending upon its barrier to rotation (V_0): as a free rotor, a hindered (restricted) rotor or a harmonic oscillator.[3,8,10]

If the barrier to rotation is much less than k_BT (*ca.* 2.5 kJ/mol, or about 207 cm^{-1}, at 298 K), then the internal rotation may be considered free. $Q_{int-rot}$ for such a rotor may be calculated as follows:[9,10]

$$Q_{int-rot} = \frac{\left(8\pi^3 I' k_B T\right)^{1/2}}{h\sigma_{int}} \qquad (3.20)$$

where I' is the reduced or effective moment of inertia for the internal-rotation and is given by equation (3.21):

$$I' = \frac{I_1 \cdot I_2}{I_1 + I_2} \qquad (3.21)$$

In the above expression, I_1 and I_2 are the moments of inertia of the rotating tops calculated with respect to the common axis for internal rotation:

$$I_n = \sum_i m_i r_i^2 \tag{3.22}$$

where m and r are the mass (in kilograms) of each atom and its distance (in meters) to the common axis of internal rotation, respectively.

If the barrier to internal rotation is much greater than $k_B T$, the torsion can be considered a non-rotating harmonic oscillator, and its treatment is the same as for the other vibrations. For the intermediate cases in which the torsional barrier is comparable to $k_B T$, the internal rotation may be treated as a hindered rotor for which the value of V_0 needs to be determined and there are no simple analytic solutions.[11] The internal rotation around the carbon-carbon single bond in ethane is a hindered internal rotation with a potential barrier of about 12 kJ/mol.[12] There are several reviews and monographs concerned with the calculation of internal rotations.[13]

The free and hindered rotor models require the consideration of an internal (also called effective) symmetry number, that is the symmetry number for the internal rotation, σ_{int} (see equation (3.20)). This parameter equals the number of minima (or maxima) in the torsional potential energy curve; for the torsion of a methyl group, $\sigma_{int} = 3$. The vibrational frequencies corresponding to torsions must be deleted (*i.e.*, ignored in the calculation of Q_{vib}) if the torsion is treated as a free or hindered rotation.

The centre of mass and thus, the principal moments of inertia for the overall (external) rotation will change as the torsional motion is executed. The approximation of considering these modes of motion as non-coupled could be very serious for torsions in big molecules such as polymers.

The treatment of internal rotations is especially important in TSs, where several motions may have to be treated as free or hindered rotors.[14] The harmonic oscillator treatment of

these modes of motion may cause significant error. The identification of such degrees of freedom by inspection of the normal modes in Cartesian coordinates is not an easy task, and the use of internal coordinates has been found more convenient.[15]

3.2.5. Electronic partition function

As a general case, the electronic partition function may be calculated by:

$$Q_{elect} = g_0 + \sum_i g_i \exp(-\frac{\Delta E_{elect}^i}{k_B T})$$

(3.23)

where g_0 is the degeneracy of the electronic ground state and ΔE_{elect} is the energy difference of the excited states with respect to the ground state. In the calculation of Q_{elect}, factors such as the degeneracy of the electronic states and the existence of low lying excited states, have to be considered.[1b,2,7]

The electronic levels of atoms and molecules are usually much further apart than the vibrational level in molecules. For the H atom for example, the first electronic excited state is about $1.6 \cdot 10^{-18}$ J above the ground state, and at ordinary temperatures this state makes a negligible contribution to the partition function. As a useful rule it has been said that if the difference in energy between an excited and the ground electronic state divided by k_B is greater than 5 K, the excited state can be ignored in the calculation of Q_{elect} at usual temperatures.

Another factor to consider is the degeneracy of an electronic state. If excited electronic states are ignored, $Q_{elect} = g_0$. Nearly all stable molecules are closed-shell systems and their excited states are high enough to be neglected except at very high temperatures, so for these cases the electronic partition function is unity. Important exceptions are O_2, NO, and most free radicals.

For atoms, the degeneracy of the electronic ground state is determined by the total electronic angular momentum, represented by the quantum number j. This magnitude is a combination of the spin (s) and orbital (l) angular momenta, which has positive values

between l + s and l – s. For every j there are $(2j + 1)$ possible orientations in a magnetic field, corresponding to identical energies, so $g_0 = 2j + 1$.[7]

For molecules, in addition to spin degeneracies, some states have spatial degeneracies. This situation is more common for diatomics. Linear molecules with spatial symmetry other than Σ (which has zero total angular momentum), *e.g.*, Π or Δ, have spatial degeneracy of 2. If there are both spin and spatial degeneracies, spin-orbit coupling lifts the degeneracy, often significantly.[8]

As shown in the sections above, exact analytical expressions for the calculation of the different contributions to the molecular partition function cannot be obtained. All modes of motion are considered as not being coupled and in the calculation of each contribution assumptions have to be made. These approximations are avoided by using the energy levels identified spectroscopically and by evaluating the sums explicitly, but for species that have not yet been detected or isolated, such as TS's and reactant and product complexes, among others, there is no other alternative.

The evaluation of the total molecular partition function requires only a knowledge of the mass of the system (Q_{trans}), its geometry (Q_{rot}, $Q_{int-rot}$), vibrational frequencies ($Q_{int-rot}$, Q_{vib}) and the energies of low-lying electronic excited states with respect to the ground state (Q_{elect}).

3.2.5. The calculation of equilibrium constants

One of the most important thermodynamic functions is the Gibbs free energy (G). For a system of N indistinguishable independent particles (*i.e.*, an ideal gas), G may be expressed in terms of the total molecular partition function, as follows:[2]

$$G - G(0) = -nRT \ln\left(\frac{Q}{N}\right) \tag{3.24}$$

Since $N = n \cdot N_A$ (where n is the number of moles and N_A Avogadro's number), the above expression can be conveniently rewritten in terms of the molar partition function, $Q_m = Q/n$:

$$G - G(0) = -nRT \ln\left(\frac{Q_m}{N_A}\right) \qquad (3.25)$$

For a species X, under standard conditions, *i.e.*, when $p = p^0 = 1$ atm, equation (3.25) can be written in as:

$$G_X^0 - G_X^0(0) = -nRT \ln\left(\frac{Q_{X,m}^0}{N_A}\right) \qquad (3.26)$$

where $Q_{X,m}^0$ is the standard molar partition function of X.

The equilibrium constant K_{eq} for a reaction is related to the standard Gibbs energy of reaction:

$$\Delta_r G^0 = - RT \ln K_{eq} \qquad (3.27)$$

By combining expressions (3.26) and (3.27) the equilibrium constant for a general reaction: $\qquad aA + bB \rightarrow cC + dD \qquad (3.28)$

is given by the expression:

$$K_{eq} = \frac{\left(Q_{C,m}^0/N_A\right)^c \cdot \left(Q_{D,m}^0/N_A\right)^d}{\left(Q_{A,m}^0/N_A\right)^a \cdot \left(Q_{B,m}^0/N_A\right)^b} \exp\left(-\frac{\Delta_r E_0}{RT}\right) \qquad (3.29)$$

For simplicity, equation (3.29) will be written as:

$$K_{eq} = \frac{\left(Q^C\right)^c \cdot \left(Q^D\right)^d}{\left(Q^A\right)^a \cdot \left(Q^B\right)^b} \exp\left(-\frac{\Delta_r E_0}{RT}\right) \qquad (3.30)$$

where Q^X is the standard molar partition function of X divided by N_A, and $\Delta_r E_0$ is the difference in molar energies of the ground states (including ZPEs) of the products and reactants. In other words, $\Delta_r E_0$ is the molar reaction internal energy at T = 0 K.

3.3. Transition State Theory

Collision theory and transition state theory (TST) are fundamental theories of bimolecular elementary reactions.[16] The following chapters of this part of the thesis are applications of TST to rate constant calculations.

In 1935, Eyring[17] and, independently, Evans and Polanyi,[18] developed a simple and general formulation for the calculation of reaction rates that has been called *transition state theory* (TST) and is still being used in many studies.[19] Other names have been given to this theory, such as *activated complex theory*,[2] *absolute rate theory*, *classical TST* and *conventional TST*.[16a,20]

The simplest reaction profile for an elementary reaction is represented in Fig. 3.4. As the reaction takes place, the reactants (React) make contact with the right energy and geometry, and the potential energy of the system rises to a maximum. The molecular arrangements of the reacting species in the area around the maximum (represented by a circle in Fig. 3.4) is called the *activated complex*. The climax of the reaction is at the maximum of the potential energy, the point at which the reactants have come to such a degree of closeness and distortion (called the *transition state*, TS) that a small further distortion converts them into the products of the reaction (Prod). The TS is the molecular system whose configuration corresponds to the first-order saddle point on the potential energy surface. Sometimes, the terms *activated complex* and TS are used as synonyms.[2,21]

TST focuses its attention on the TS of a bimolecular elementary reaction and calculates its concentration by making use of statistical thermodynamic concepts. As in all scientific theories, various assumptions and approximations are involved in its implementation.[16a]

It is based on the *equilibrium hypothesis* which states that even when the reactants and products are not at equilibrium with each other, the TS is always at equilibrium with the reactants, whose energy distribution is in accordance with the Maxwell-Boltzmann distribution law. Furthermore, it is assumed that once the maximum of the potential energy curve has been surmounted, such molecular systems cannot turn back and form reactant molecules again. Another approximation is the separation of the motions of the system over the maximum from the motions associated with the TS. In this theory the chemical reaction is treated in terms of classical motion over the barrier, ignoring quantum effects; although as will be discussed below this is not completely true.
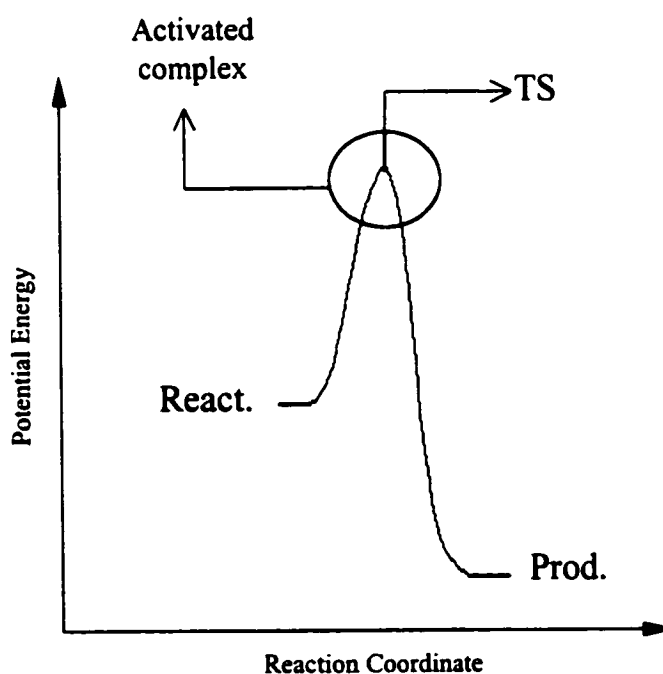
Figure 3.4. Energy profile of an elementary reaction.

For a general reaction: React $\rightleftharpoons$ [TS]* $\rightleftharpoons$ Prod

by applying basic concepts of statistical thermodynamics, the constant for the equilibrium between reactants and the TS can be written as:

$$K_{eq}^* = \frac{[TS]}{[Reac]} = \frac{Q^{TS}}{Q^{React}} \ exp\left(-\frac{\Delta E_0}{RT}\right)$$ (3.31)

where ΔE_0 is the hypothetical energy of activation at 0 K, calculated by:

$$\Delta E_0 = \left(E^{TS} + ZPE^{TS}\right) - \left(E^{React} + ZPE^{React}\right)$$ (3.32)

The partition functions and the energy difference must be calculated with respect to the same reference state, in this case the zero-point vibrational energy level.

Since the imaginary frequency of the TS (v^*) corresponds to a loose vibration without restoring force, it is supposed to be much smaller than the frequency of an arbitrary vibration, *i.e.*, $hcv^*/k_BT \ll 1$, and the expression in the exponential of equation (3.18) can be expanded in a Taylor series, so that the partition function of the vibrational component of the imaginary frequency can be calculated by:

$$Q_{vib}(\overline{v}^*) = \frac{1}{1-exp\left(-\frac{hc\overline{v}^*}{k_BT}\right)} = \frac{1}{1-\left(1-\frac{hc\overline{v}^*}{k_BT}+\cdots\right)} \approx \frac{k_BT}{hc\overline{v}^*}$$ (3.33)

Further application of the assumptions discussed above leads to the following expression for the rate constant (k has also been referred to as *specific reaction rate*[22] or *rate coefficient*):[2,16a]

$$k = \kappa\frac{k_BT}{h}\cdot\frac{Q^{TS}}{Q^{React}} \ exp\left(-\frac{\Delta E_0}{RT}\right)$$ (3.34)

In the previous expression, κ is the *tunneling factor* or *tunneling correction*, that will be discussed in Section 3.4; Q^{TS} is the standard molar partition function of the TS divided by N_A, ignoring the contribution of the imaginary frequency to the vibrational partition function.

TST, like every theory, has limitations.[16,25b] That is why there have been so many improvements and extensions to it, such as variational TST (VTST),[23] quantum TST,[24]

among others. But all the modified theories are considerably more complicated than TST and cannot be expressed in as compact a form.[16a,25,26]

3.3.1. Unimolecular reactions

Unimolecular reactions in the gas phase have been known for nearly a century.[27] Examples of such reactions are dissociations and isomerizations. In addition, unimolecular fragmentation of gas phase ions forms the basis for mass spectrometry analysis.[28]

Following the Lindemann theory, the rate constant for a unimolecular reaction k_{uni} is a function of pressure. Collisions can either energize or de-activate a gas molecule, and maintain a Boltzmann distribution of the reactant molecules throughout its energy levels. At low pressures k_{uni} is directly proportional to the total pressure, however, at high pressure k_{uni} is independent of pressure. Under high-pressure conditions collisional de-activation is much faster than the unimolecular reaction, an equilibrium distribution of the reactants is maintained, and the classical TST formula can be applied to calculate the rate constant.[16b]

Considerable experimental work concerning gas phase unimolecular reactions has been devoted to energy-selected systems.[29] All detailed statistical theories of unimolecular reactions begin with the calculation of the rate constant as a function of the internal energy, k(E), also known as the microcanonical rate constant.

The Rice-Ramsperger-Kassel-Marcus/quasi-equilibrium theory (RRKM/QET) assumes the existence of a TS. According to this theory, the expression for k(E) is given by:[29]

$$k(E) = \frac{\sigma\ N(E - E_0)}{h\rho(E)} \tag{3.35}$$

where E_0 is the critical energy of activation (not necessarily equal to the Arrhenius activation energy, see below), $\rho(E)$ is the density of vibrational states of the reactant molecule at energy E, $N(E - E_0)$ is the sum of the vibrational states from 0 to $E - E_0$ in the

TS, and σ is the reaction path degeneracy (equivalent to the rotational symmetry number, see Section 3.2.2). The application of equation (3.35) requires the knowledge of the energy barrier and the vibrational frequencies of the reactant and of the TS. Although this theory has been (and still is) widely used for the quantitative description of unimolecular reaction kinetics,[30] it is not a simple theory to be implemented; it will not be applied in the following chapters.

3.3.2. Femtochemistry

The development femtosecond pulsed lasers and their applications to chemistry in the form of femtochemistry has made possible the study of molecular motions in the ephemeral TSs of physical, chemical and biological changes.[31] The significance of these studies was manifested in the 1999 Nobel Prize, awarded to Ahmed Zewail for his groundbreaking work in femtochemistry.

In a typical experiment, a femtosecond pulse is used to excite a molecule to a dissociative state; a second pulse is fired at an interval after the first one and it is set at an absorption frequency of one of the free fragmentation products. The intensity of such absorption is a measure of the abundance of the dissociation product. In a similar study on the ICN molecule, it was possible to detect that the CN absorption signal remains zero until the fragments are separated by about 6 Å, which takes about 205 fs (1 fs $= 10^{-15}$ s).[2]

Femtosecond spectroscopy has also been used to examine analogues of the activated complex involved in bimolecular reactions; a molecular beam can be used to produce a van der Waals molecule, such as $IH\cdots OCO$. The H-I bond can be dissociated by a femtosecond pulse, in which case the H atom is ejected towards the O atom of the neighbouring CO_2 molecule to form HOCO. Hence, the van der Waals molecule acts as a source of a species that resembles the activated complex of the reaction:[2]

$$H + CO_2 \longrightarrow [HOCO]^* \longrightarrow HO + CO \qquad (3.36)$$

3.4. Tunneling calculations

It is sometimes necessary to correct the rate constant calculation by a factor that takes account of the possibility that some reactant molecules can be transformed into the products of the reaction without having surpassed the activation barrier and that not every activated complex becomes transformed into the products. Such a quantum-mechanical correction is achieved by what has been named the *tunneling correction* and will be discussed in the present section. The book by Bell[32] has been a very important material source for this topic.

The suggestion that quantum-mechanical tunneling might be a significant factor in some chemical reactions was first made more than seventy years ago by Hund.[33,34] Fig. 3.5 illustrates the meaning of the term *tunnel effect*:

(a)   (b)
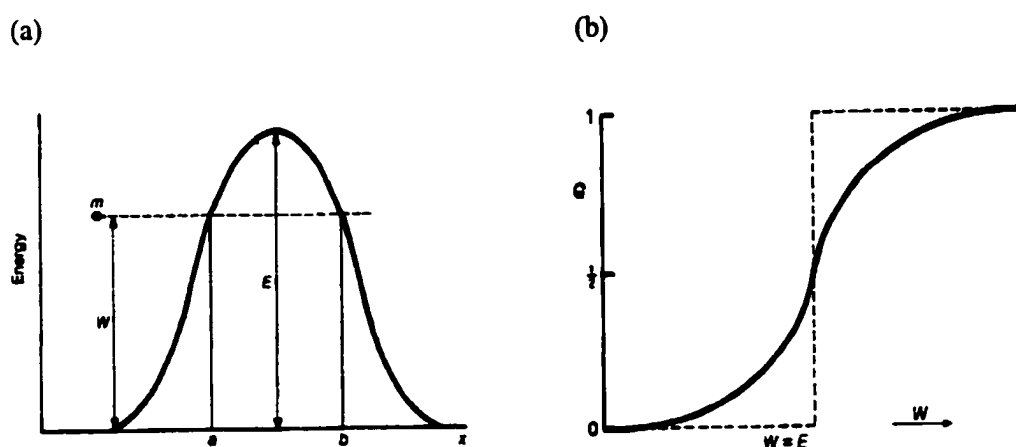
Figure 3.5. Passage of a particle across classical and quantum potential energy barriers.
(a) Particle approaching a potential energy barrier;
(b) Plot of the permeability (G) as a function of the energy of the particle (W). Reproduced from reference 32.

Fig. 3.5(a) shows a particle of mass m and energy W approaching a potential energy barrier of height E. The magnitude G, called the *permeability* or *transmission coefficient*,

represents the probability that the particle will appear on the right-hand side of the barrier. G varies with W in a way that depends on the type of barrier considered. Fig. 3.5(b) is a plot of G as a function of W. The broken line represents the predictions of classical mechanics and the everyday experience with macroscopic objects: the probability is zero as long as W < E, and rises abruptly to unity when W = E, staying at this value for all higher values of G. When going from classical to quantum mechanics, the broken line is replaced by a continuous curve, whose exact form depends not only on the height of the barrier, but also on its width and shape and on the mass of the particle.

The quantum-mechanical curve of G *vs.* W has the following limiting behaviour:

$$\lim_{W \to 0} G(W) = 0 \qquad\qquad \lim_{W \to \infty} G(W) = 1 \qquad\qquad (3.37)$$

The most impressive feature of the continuous curve is that it predicts non-zero permeabilities even when W < E (*i.e.*, the particle penetrates the barrier, it tunnels through the barrier). In addition, for some values of W > E, there is some probability that the particle be reflected by the barrier.

The tunnel effect is a consequence of the wave-particle duality of matter postulated by de Broglie in 1925,[35] and represented mathematically by the expression:

$$\lambda = \frac{h}{mv} \qquad\qquad (3.38)$$

For macroscopic systems λ is very small compared with the dimensions of the particles and classical mechanics can be applied with sufficient accuracy. For molecular systems deviations from classical behaviour take the form of quantization (*e.g.*, the existence of discrete energy levels). For a free particle (*e.g.*, e^-, H, H^+, H^-) approaching an energy barrier such deviations are manifested as the tunnel effect. However, most reacting systems may involve both quantization and the tunnel effect, but it is often convenient to treat these phenomena separately.

So far reference to the tunneling effect has been made in a qualitative manner. However, there are ways to obtain quantitative estimates of its magnitude, named the *tunneling correction* or *tunneling factor*, κ.

The tunneling correction is defined as the ratio of the quantum-mechanical (k_Q) to the classical (k_C) barrier-crossing rate, and can be calculated in terms of the previously mentioned parameters as follows:

$$\kappa = \frac{k_Q}{k_C} = \frac{\exp(\frac{E}{k_B T})}{k_B T} \int_0^\infty G(W) \exp(-\frac{W}{k_B T}) dW \qquad (3.39)$$

To obtain κ, the permeability G needs to be evaluated. To do so, the Schrödinger equation for a given potential energy barrier must be obtained, and its solutions interpreted. Usually several simplifications of the tunneling process are made: the barrier is considered unidimensional and the mass of the particle is assumed to remain constant during the process.

Several types of one-dimensional barriers have been used to model tunneling, such as rectangular, triangular and parabolic, among others. The parabolic barrier (Fig. 3.6) is of particular importance in chemical problems since it represents a more realistic representation of a real barrier (at least when tunneling involves only the upper part of the barrier). Furthermore, for the parabolic barrier an exact expression for the permeability can be obtained, that can be explicitly integrated.[36] Most types of barriers lead to expressions for G that require numerical integration, thus κ cannot be explicitly evaluated.

The Wigner correction,[37] is a very simplistic way of estimating small tunneling factors by assuming a parabolic potential for the nuclear motion near the TS:

$$\kappa = 1 + \frac{1}{24} \cdot \frac{hc\bar{v}^*}{k_B T} \qquad (3.40)$$
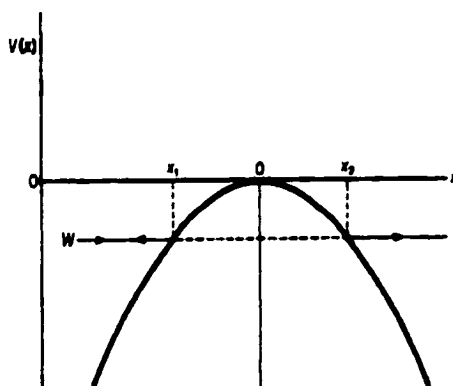
Figure 3.6. An infinite parabolic barrier.
Reproduced from reference 32.

The above expression is obtained after truncating Bell's formula for a parabolic barrier, at high temperatures or small values of $\overline{V}^*$. The Wigner correction has been used in several kinetic applications.[38]

3.4.1. The Eckart barrier

A one-dimensional barrier shape that corresponds more closely to physical reality and for which a solution of the quantum-mechanical problem is possible, was proposed by Eckart.[39] The Eckart barrier was the first realistic type of barrier for which the tunneling problem was solved, and it has been extensively used in chemical applications.[40]

The general equation for the Eckart barrier is:

$$V(x) = \frac{Ay}{(1+y)^2} + \frac{By}{(1+y)} \qquad y = \exp\left(\frac{x - x_0}{b}\right) \qquad (3.41)$$

where b is a characteristic length (thickness parameter) and x_0 indicates the origin of the barrier. The parameters A, B and b are constants related to the direct (V_1) and reverse (V_2) potential energy barriers, and to the imaginary frequency of the TS.

Fig. 3.7 shows symmetrical and unsymmetrical Eckart barriers (V^* is the potential at the maximum of the barrier, and F^* is the second derivative of the function at its maximum, calculated from $\overline{V}^*$). For the symmetrical function A is zero; B represents the endothermicity of the process for the unsymmetrical case.

A graphical comparison between symmetrical parabolic and Eckart barriers is shown in Fig. 3.8. The parabolic and Eckart barriers behave similarly at the top of the barrier, but the Eckart function shows a slower decrease of the potential away from the maximum.

For the Eckart barrier the Schrödinger equation can be solved exactly, thus an exact value of G can be obtained. The expression for the permeability of such a barrier and for the tunneling factor (3.42) are rather complicated in form and involve integrals which have to be evaluated numerically. Values of κ for a variety of conditions assuming an Eckart barrier have been reported.[41]

$$\kappa(W) = 1 - \frac{\cosh[2\pi(\alpha - \beta)] + \cosh 2\pi\delta}{\cosh[2\pi(\alpha + \beta)] + \cosh 2\pi\delta} \qquad (3.42)$$

$$\alpha = \frac{1}{2}\sqrt{\frac{W}{C}} \qquad \beta = \frac{1}{2}\sqrt{\frac{W-A}{C}} \qquad \delta = \frac{1}{2}\sqrt{\frac{B-C}{C}} \qquad C = \frac{h^2}{8ml^2}$$

Tunneling calculations considering an Eckart-type barrier are a simple (but not as simple as Wigner[37] or parabolic-type barrier[32] tunneling corrections) and practical way of accounting for tunneling. The Eckart method is still widely used in the literature, although more sophisticated methods, such as the multidimensional semiclassical zero- (ZCT) and small-curvature (SCT) tunneling methods have been developed.[42] A few years ago a study on the importance of quantum mechanical tunneling effects on the kinetics of the hydrogen exchange reaction of methane in a zeolite was published.[43] In Truong's paper,[43] the accuracy of Eckart tunneling calculations was demonstrated, in agreement with his previous work.[44] Not only were different tunneling corrections considered, but also VTST results were compared with TST calculations. The success of the TST/Eckart combination was clearly shown.
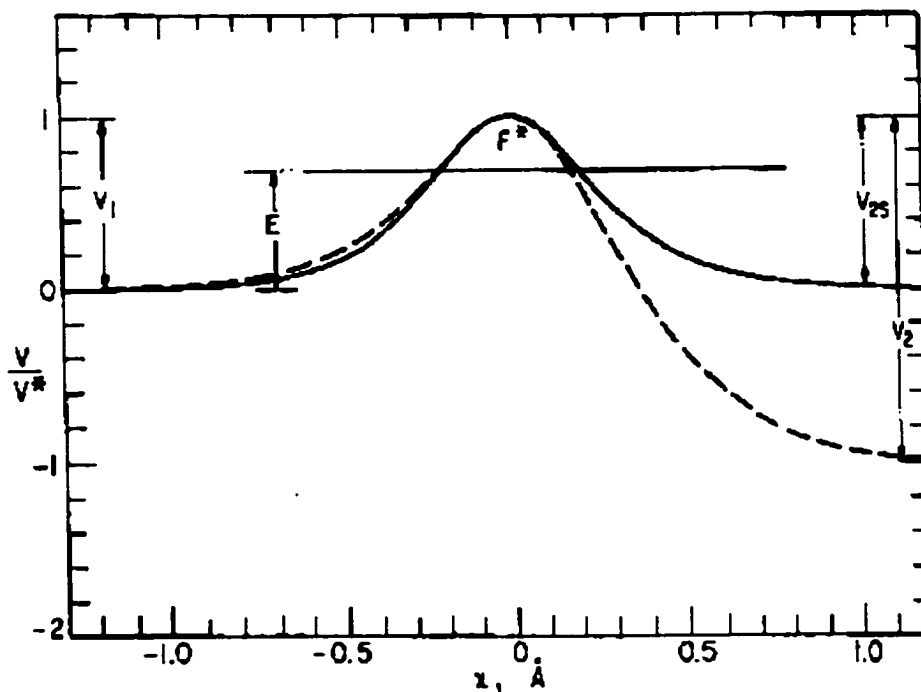
Figure 3.7. Symmetrical and unsymmetrical Eckart barriers.
Reproduced from reference 41a.
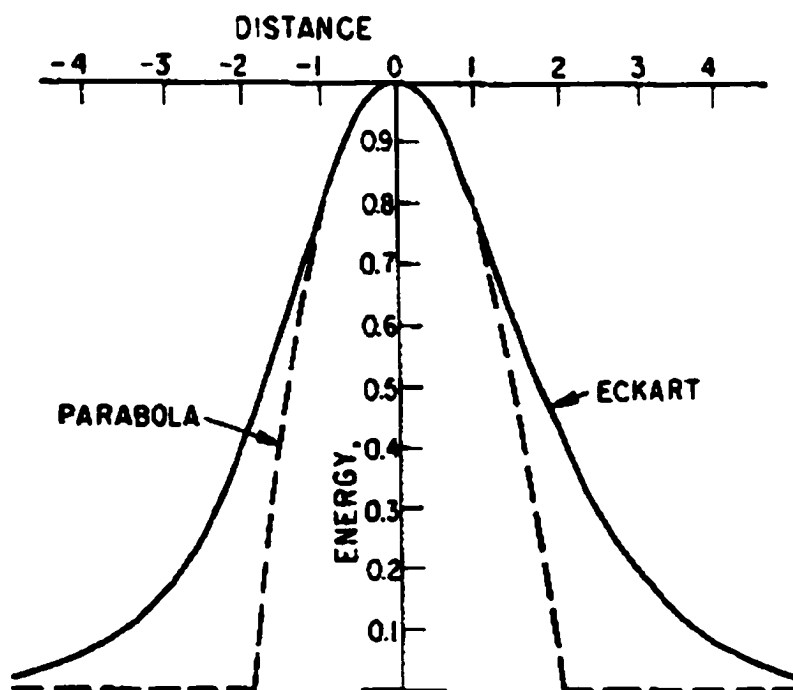
Figure 3.8. Comparison of symmetrical parabolic and Eckart barriers.
Reproduced from reference 41a.

It is well known that the Eckart method tends to overestimate the tunneling contributions especially at very low temperatures. In the papers discussed above,[43, 44] (where there is approximately the same degree of heavy-atom motion as the system moves along the reaction path, in comparison with the reactions that will be studied in Chapters 4 to 6) the Eckart corrections do not overestimate the rate constant at room temperature, as happens at much lower temperatures.

A useful measure of the barrier width is the full width of the barrier at half its height in the forward direction, $\Delta s_\frac{1}{2}$. It may be determined by setting: $V(x) = (A+B)^2/8A = V^*/2$ and obtaining the difference between the two roots of x. The magnitude of $\Delta s_\frac{1}{2}$ (usually reported in Å) depends on the direct and reverse potential energy barriers at 0 K, and on the characteristic tunneling temperature (T^*), below which tunneling is significant. This magnitude can be calculated by:

$$T^* = \frac{hc\overline{V}^*}{2\pi k_B} \tag{3.43}$$

An arbitrary general criterion for tunneling given by Bell[32] could be useful for certain applications:

Negligible tunneling: $1 < \kappa < 1.1$

Small to moderate tunneling: $1.1 < \kappa < 4$

Large tunneling: $\kappa > 4$

As a generalization on this topic it can be said that the smaller the mass of the particle to be transferred in a chemical reaction, the lower the temperature, and also that the narrower and larger the potential energy barrier, the greater the tunneling effect. The width of the potential energy barrier is given by the curvature at its maximum, determined by the imaginary frequency of the TS; the larger $\overline{V}$ the greater the curvature and κ.

3.5. Arrhenius, non-Arrhenius and anti-Arrhenius kinetic behaviours

Many rate constants show an exponential dependence on temperature that can be empirically fit by the well-known Arrhenius equation[45,46] over a relatively narrow temperature range:

$$k = A \exp\left(-\frac{E_a}{RT}\right) \tag{3.44}$$

where T is the temperature in K and R is the ideal gas constant. E_a and A have been named the Arrhenius activation energy and pre-exponential factor, respectively.

The activation energy (when referring to an elementary process) is related to the height of the energy barrier for a reaction, the energy required to transform the reacting substance into the 'active' form. The pre-exponential factor, also known formerly as the *frequency factor*, is the rate constant of a reaction without activation energy (a barrierless reaction), or at infinite temperature where all the collisions are 'effective'.

The problem of temperature dependence of reaction rates had a great deal of controversy and uncertainty for over 60 years (from 1850 to 1910)[47] and many empirical equations to describe it were developed.[48] Even though the Arrhenius equation was not empirically the best, by about 1910 it was the only one-parameter temperature-dependence equation (since one parameter, E_a, expresses the temperature dependence) accepted because of the insight it provides on how chemical reactions proceed.

To a first approximation, the Arrhenius factor A is found to be independent of temperature for many reactions over a certain temperature range. Hence, a straight line is obtained when plotting ln k *versus* 1/T; this situation has been referred to as an Arrhenius behaviour. As the temperature range over which experiments are carried out is extended, non-linear Arrhenius plots (non-Arrhenius behaviours) are observed for some reactions.[49] The failure of the Arrhenius equation in special circumstances is well known.[50] Ironically, one of the first detected reactions to fail equation (3.43) was the inversion of sucrose,[51] a reaction whose kinetic data was used by Arrhenius in his study.[45] The

Arrhenius equation can fail, for example, in a reaction with concurrent mechanisms with quite different dependencies on temperature, or in catalytic reactions where irreversible changes take place on the catalyst at high temperatures or while approaching an explosion limit. Two additional groups of reactions not obeying equation (3.44) are the diffusion-controlled reactions in aqueous glasses,[52] and reactions where a low-mass particle (*e.g.*, H, H^+ or H^-) is transferred, in solution or in the gas phase, and tunneling is significant (*vide infra*).

For reactions in which the activation energy is small or zero, the temperature dependence of A can be significant. As a result, the empirical Arrhenius equation (3.44) is not appropriate to describe the temperature dependence, and a modified equation of the form:

$$k = BT^n \exp\left(-\frac{E_0}{RT}\right)$$
(3.45)

is frequently used, where B, E_0 and n are temperature independent constants characteristic of the reaction. This is the most satisfactory two-parameter equation that can be used to describe the temperature dependence of rate constants when non-linear plots of ln k *versus* 1/T are obtained. There is a good theoretical basis for this equation arising from the temperature dependence of partition functions.

It is often convenient to define the experimental Arrhenius activation energy E_a by the equation:

$$E_a \equiv RT^2 \frac{d\ln k}{dT} \equiv -R\frac{d\ln k}{d(1/T)}$$
(3.46)

Hence, the slope of the ln k *versus* 1/T plot at any point is equal to $-E_a/R$ and the above definition applies whether or not the Arrhenius plot is linear; if it is not, E_a (and thus A) will vary with temperature.

If a reaction obeys equation (3.45), then:

$$E_a = E_0 + nRT$$
(3.47)

where E_0 is the hypothetical activation energy at absolute zero.

Hence, a non-Arrhenius behaviour (curved Arrhenius plot) implies the parameters E_a and A to be temperature-dependent. This is illustrated in Fig. 3.9.
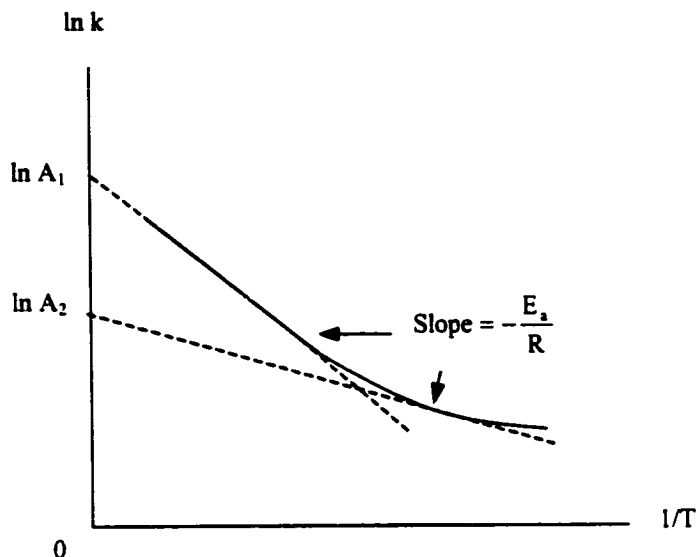
Figure 3.9. Schematic curved-Arrhenius plot showing the temperature dependence of E_a and A.

When tunneling plays an important role in the kinetics of some reactions, curved Arrhenius plots are also obtained.[32] This, of course, will be the case for temperatures below T^*.

Since $k_Q = \kappa \cdot k_C$ (see equation (3.39)), the temperature dependence of E_a and A will be established by the following expressions:

$$(E_a)_Q - (E_a)_C = RT^2 \frac{d\ln \kappa}{dT} \tag{3.48}$$

$$\ln \frac{(A)_Q}{(A)_C} = \ln \kappa + T \frac{d\ln \kappa}{dT} = \frac{d(T\ln \kappa)}{dT} \tag{3.49}$$

where $(E_a)_Q$ and $(A)_Q$ are the Arrhenius parameters considering tunneling, and $(E_a)_C$ and $(A)_C$ are the same parameters when this quantum effect is ignored.

Since tunneling decreases as temperature increases, $d\ln\kappa/dT$ is always negative. Hence, equation (3.48) predicts that tunneling will reduce the Arrhenius activation energy. The direction in which tunneling affects the pre-exponential factor is not immediately obvious, but for small tunneling corrections a reduction of the A factor is expected.[32]

For a chemical reaction where tunneling is significant, the appropriate way to theoretically or experimentally determine the Arrhenius parameters at a temperature below T^* requires the construction of a $\ln\kappa$ versus $1/T$ plot, or the determination of the corresponding analytical expression. From the slope and the intercept of the tangent to this curve at the desired temperature, the Arrhenius parameters may be determined.

Equation (3.44) is not in general obeyed in the sense that unique constants A and E_a do not exist for each reaction.

While most reactions increase in rate as the temperature increases, there are several notable exceptions for which the Arrhenius activation energy is negative. The temperature dependence of such reactions is referred to as anti-Arrhenius. This topic will be discussed further in the following section.

3.6.1. Negative Arrhenius activation energies

The above definition or interpretation of the activation energy is only valid when referring to elementary reactions; even for such systems some authors have indicated that a complete identification of the Arrhenius activation energy with the barrier height is not justified.[53] As more sophisticated experimental methods are developed, the number of accepted elementary reactions is reduced. In fact, one of the main conclusions of the following chapters related to computational kinetics refers to this topic.

Since most chemical reactions are complex, the meaning of the term *activation energy* needs to be modified. For non-elementary reactions, the Arrhenius activation energy is not in general simply related to the height of any single energy barrier, it is instead theoretically calculated by a linear combination of the activation energies of the single elementary steps of the proposed kinetic mechanism. The term Arrhenius activation energy will always refer to the experimentally determined kinetic parameter according to the operational definition (3.44). The validity of the proposed mechanism depends on how well it explains and reproduces the experimental data.

The reaction: $$2NO + Cl_2 \longrightarrow 2ONCl \qquad (3.50)$$

is a third-order process that exhibits anti-Arrhenius behaviour, i.e., the Arrhenius activation energy is negative.[54]

For an elementary process, a negative Arrhenius activation energy is inconceivable on the basis of TST or of collision theory. The above reaction is thought to occur not by a single termolecular step but instead by a complex mechanism in which an NO molecule first forms a loose reactant complex with Cl_2 in a reversible process (steps 1 and –1), followed by the reaction between such a complex and a second NO molecule (step 2). The Arrhenius activation energy is thus given by:

$$E_a = E_{a(1)} + E_{a(2)} - E_{a(-1)} \qquad (3.51)$$

The negative activation energy arises because $E_{a(-1)}$ is greater that the sum of $E_{a(1)}$ and $E_{a(2)}$. Negative E_a are normally encountered for termolecular reactions.[49]

A similar situation is found in the recombination reaction of I atoms, conventionally written as:

$$I + I + M \longrightarrow I_2 + M \qquad (3.52)$$

where M symbolizes any molecule. This reaction can also have a negative E_a.[55]

Benson and coworkers have examined some 'elementary' gas phase reactions in which negative activation energies and/or curved Arrhenius plots have been observed experimentally.[56] They have shown that activation energies as negative as –5.0 to –7.5 kJ/mol near 300 K as well as curved Arrhenius plots can be explained by the formation of an intermediate complex. These results were obtained for the reactions of OH with CO, HNO_3 and HNO_4.[49]

Another type of reaction important in atmospheric chemistry that shows this somewhat unusual inverse temperature dependence of the rate constants is that between alkenes and OH and, in some cases, $O(^3P)$.[49]

The reactions of alkenes with OH radicals are very fast. The rate constants for the larger alkenes are approximately equal to the diffusion-controlled limit (*i.e.*, the reaction occurs on every collision).[57] Several explanations have been proposed to explain the anti-Arrhenius behaviour of these reactions, one of them being the formation of a weakly bound complex (also called *reactant complex* or *pre-reactive complex*) as previously explained; Singleton and Cvetanović proposed this idea in 1976.[58] In fact the role of such complexes has received increased attention in the recent literature. Some of these studies will be discussed in the following chapter.[59] In recent studies the abundance of hydrated complexes in the atmosphere is estimated and physicochemical properties are evaluated; experimental evidence of their existence is also given.[60]

Another possible explanation for negative activation energies lies in the use of the Arrhenius equation. The data for lnk *vs.* 1/T can be fit to an expression similar to (3.44) with negative values of n that for the specific case of the alkenes + OH reaction is approximately –1.5.[49,57]

A third explanation, based on collision theory, has been given by Zellner and Lorenz.[61] A $T^{-1.5}$ temperature dependence (for the alkenes + OH reactions) is predicted if the reaction cross section is assumed to increase rapidly at the threshold energy, reach a sharp maximum, and then decrease as the energy increases.[49]

For the reaction of olefins with $O(^3P)$, Cvetanović and Singleton identified four possible explanations, some of which have aspects in common with the ones already mentioned.[62] One idea is that it is simply an elementary bimolecular reaction with an approximately zero activation energy so that the temperature dependence of the A factor becomes important. Another idea is based on the formation of a transient $O(^3P)$-alkene complex that can decompose back to the reactants or form products; in this case the complex is an electron-donor acceptor complex with the electron donor being the alkene π bond and the product is not a stable radical adduct as in the OH-alkene reactions. A third explanation refers to the existence of two or more reaction channels whose activation energies are significantly different; the addition to the double bond and atom or free radical displacement are two such reaction channels. The other explanation given by Cvetanović and Singleton refers to the crossing of potential energy surfaces: if the $O(^3P)$-olefin initial interaction has a shallow minimum and the rate determining step involves crossing in a repulsive region to an attractive potential energy surface, then intersection of the surfaces at energies lower than that of the separated reactants would result in negative activation energies.[49]

Benson explained this paradoxical result of elementary reactions having negative activation energies in terms of the different internal energies (vibrational excitation) of the reacting molecule and its dissociating fragments, which can become very pronounced at high temperatures.[9] Recently, a study by Benson and Dobis on the existence of negative activation energies in simple bimolecular metathesis reactions of the type: $R^{\bullet}$ + HX and $R^{\bullet}$ + X_2 (X = I, Br, Cl),[63] blamed the artifacts of the experimental methods for this situation.

The anti-Arrhenius behaviour of some reactions is without doubt a very interesting and somewhat frequent phenomenon that can be found in the recent literature.[64]

3.6. General aspects regarding Chapters 4 to 6

In computational chemistry the activation energy of an elementary reaction is calculated in terms of the total energies of the TS and the reactants including their respective vibrational thermal corrections to the energy (TCE) that depends on temperature:

$$E_a = (E^{TS} + TCE^{TS}) - \Sigma(E^{React} + TCE^{React}) \tag{3.53}$$

In the following chapters Arrhenius activation energies measured in a temperature range that includes 298 K are compared with calculated activation energies using thermal corrections at 298.15 K. Calculations at 0 K are also reported.

For the mechanisms considered in Chapters 4 to 6, these activation energies are calculated by expression (3.53). Reaction enthalpies (ΔH) are also calculated at 0 and 298.15 K, and reported in kJ/mol as well. The optimum situation for a theoretical calculation of E_a and ΔH is to be within chemical accuracy, *i.e.*, within *ca.* 4 kJ/mol (that is equivalent to about 1 kcal/mol), with respect to experiment. For rate constant calculations the optimum could be expected within one order of the experimental values, although this non-established criterion is subject to change as better theoretical determinations are achieved.

In Chapters 4 and 5, the calculated activation energies correspond to different mechanisms, as will be explained. When referring to the activation energy of a complex mechanism, this quantity will be named *effective activation energy* and will be denoted E_a^{eff}. Similarly, rate constants for complex mechanisms will be referred to as *effective rate constants*, k_{eff}, and for an elementary or direct mechanism this magnitude will be named *direct rate constant*, k_D. Rate constants in units of L/mol·s will be calculated at 298.15 K.

The Gaussian98[65] set of programs was used to perform the electronic calculations reported in Chapters 4 to 6. In this commercial program all the calculated harmonic frequencies are directly included in the calculation of the vibrational partition function,

hence corrections have been made to the total partition function of the TSs to account for internal rotations that were considered to be free. The character of all stationary points (minima and TSs) considered in the reactions studied was confirmed by a frequency calculation performed at the same level as for the geometry optimizations.

The tunneling factors, κ and $\Delta s_{\frac{1}{2}}$, were calculated by assuming an unsymmetrical Eckart barrier (see Section 3.4.1). A modified version of the numerical integration program of Brown[66] was used for the calculation of the tunneling factor; the Gaussian quadrature was performed at 40 points for increased accuracy. The output of the program with different input parameters was compared with the results reported by Johnston[41a] for this kind of barrier, with excellent agreement. The FORTRAN programs used to calculate κ and $\Delta s_{\frac{1}{2}}$ were kindly provided by Dr. P. D. Pacey, at Dalhousie University.

The constants and conversion factors used in the calculations reported were obtained from reference 67.

3.7. References

1. (a) Andrews, F.C. *Equilibrium Statistical Mechanics*, 2nd Ed., John Wiley & Sons, 1975. (b) McQuarrie, D.A. *Statistical Thermodynamics*, Harper & Row, New York, 1973.

2. Atkins, P.W. *Physical Chemistry*, Oxford University Press: New York, 1998.

3. Frenkel, M.; Marsh, K.N.; Wilhoit, R.C.; Kabo, G.J.; Roganov, G.N. *Thermodynamics of Organic Compounds in the Gas State*, Thermodynamics Research Centre: College Station, Texas, v. 1, 1994.

4. Atkins, W. *Quanta: A Handbook of Concepts*, 2nd Edition, Oxford University Press, 1991.

5. Hasanein, A.A. *Edu. Chem.* **1986**, *23*, 24.

6. Young, D.C. *Computational Chemistry: A Practical Guide for Applying Techniques to Real-World Problems*, John Wiley & Sons, New York, 2001.

7. Laidler, K.J.; Meiser, J.H. *Physical Chemistry*, 3rd Ed., Houghton Mifflin Company, Boston, 1999.

8. Computational Thermochemistry: Prediction and Estimation of Molecular Thermodynamics, ACS Symposium Series 677, K.K. Irikura and D.J. Frurip, Eds., ACS, Washington, D.C., 1998.

9. Benson, S.W. *Thermochemical Kinetics*, 2nd Ed., Wiley & Sons, New York, p. 43, 1976.

10. Chuang, Y-Y; Truhlar, D.G. *J. Chem. Phys.* **2000**, *112*, 1221.

11. Truhlar, D.G. *J. Comput. Chem.* **1990**, *12*, 266.

12. Kemp, J.B.; Pitzer, K.S. *J. Chem. Phys.* **1936**, *4*, 739.

13. (a) Eliel, E.L.; Allinger, N.L.; Angyal, S.J.; Morris, G.A. *Conformational Analysis*, Wiley Interscience, New York, 1965. (b) Gordy, W.; Cook, R.L. *Microwave Molecular Spectra*, Wiley Interscience, New York, 1970. (c) Rudolph, H.M. *Annu. Rev. Phys. Chem.* **1970**, *21*, 73. (d) Lehn, J.-M. *Conformational Analysis*, G. Chiurdoglu, Ed., Academic Press, New York, 1971. (e) Dashevskii, V.G. *Conformational Analysis of Organic Molecules*, Khimiya, Moscow, 1982.

14. See, for example: (a) Taylor, P.H.; Rahman, M.S.; Arif, M.; Dellinger, B.; Marshall, P. *Symp. Int. Comb. Proc.* **1996**, *26*, 497. (b) Mebel, A.M.; Lin, M.C., Morokuma, K. *Int. J. Chem. Kinet.* **1998**, *30*, 729. (c) Van Speybroeck, V.; Van Neck, D.; Waroquier, M.; Wauters, S.; Saeys, M.; Marin, G.B. *J. Phys. Chem. A* **2000**, *104*, 10939.

15. Ayala, P.Y.; Schlegel, H.B. *J. Chem. Phys.* **1998**, *108*, 2314.

16. (a) Laidler, K.J. *Chemical Kinetics*, 3rd Ed., HarperCollinsPublishers, New York, 1987. (b) Pilling, M.J.; Seakins, P.W. *Reaction Kinetics*, Oxford University Press: New York, 1996.

17. Eyring, H. *J. Chem. Phys.* **1935**, *3*, 107.

18. Evans, M.G., Polanyi, M. *Trans. Faraday Soc.* **1935**, *31*, 875.

19. See, for example: (a) Peng, J.B.; Wu, T.; Chen, X.Y.; Ju, G.Z. *Chinese. J. Inorg. Chem.* **1999**, *15*, 196. (b) Lu, X.; Musin, R.N.; Lin, M.C. *J. Phys. Chem. A* **2000**, *104*, 5141. (c) Wang, B.S.; Hou, H.; Gu, Y.S. *J. Phys. Chem. A* **2000**, *104*, 8458. (d) Lu, X.; Park, J.; Lin, M.C. *J. Phys. Chem. A* **2000**, *104*, 8730. (e) Baer, T.; Potts, A.R. *J. Phys. Chem. A* **2000**, *104*, 9397. (f) Orlando, J.J.; Tyndall, G.S.; Vereecken, L.; Peeters, J. *J. Phys. Chem. A* **2000**, *104*, 11578. (g) Arroyo, S.T.; Martin, J.A.S.; Garcia, A.H. *Chem. Phys.* **2001**, *265*, 207. (h) Barckholtz, C.;

Barckholtz, T.A.; Hadad, C.M. *J. Phys. Chem. A* **2001**, *105*, 140. (i) Wang, B.S.; Hou, H.; Gu, Y.S. *J. Phys. Chem. A* **2001**, *105*, 156. (j) Skokov, S.; Zou, S.L.; Bowman, J.M.; Allison, T.C.; Truhlar, D.G.; Lin, Y.J.; Ramachandran, B.; Garrett, B.C.; Lynch, B.J. *J. Phys. Chem. A* **2001**, *105*, 2298. (k) Jaffe, C.; Uzer, T. *J. Phys. Chem. A* **2001**, *105*, 2783.

20.   (a) Petersson, G.A. *Theor. Chem. Acc.* **2000**, *103*, 190. (b) Garret, B.C. *Theor. Chem. Acc.* **2000**, *103*, 200. (c) Laidler, K.J.; King, M.C. *J. Phys. Chem.* **1983**, *87*, 2657.

21.   Laidler, K.J. *J. Chem. Edu.* **1988**, *65*, 540.

22.   Arrhenius, S. *Z. Phys. Chem.* **1887**, *1*, 110.

23.   (a) Keck, J.C. *J. Chem. Phys.* **1960**, *32*, 1035. (b) Keck, J.C. *Adv. Chem. Phys.* **1967**, *13*, 85. (c) Garret, B.C.; Truhlar, D.G. *J. Phys. Chem.* **1979**, *83*, 1052.

24.   (a) Miller, W.H. *J. Chem. Phys.* **1971**, *55*, 3146. (b) *idem.* **1975**, *62*, 1899. (c) *idem. Acc. Chem. Res.* **1976**, *9*, 306.

25.   (a) Truhlar, D.G.; Hase, W.L.; Hynes, J.T. *J. Phys. Chem.* **1983**, *87*, 2664. (b) Steinfeld, J.I.; Francisco, J.S.; Hase, W.L. *Chemical Kinetics and Dynamics*, Prentice Hall, New Jersey, 1989. (c) Miler, W.H. *Encycl. Comput. Chem.* **1998**, *4*, 2375. (d) Quack, M.; Troe, J. *Encycl. Comput. Chem.* **1998**, *4*, 2708.

26.   (a) Truhlar, D.G.; Isaacson, A.D.; Skodje, R.T.; Garret, B.C. *J. Phys. Chem.* **1982**, *86*, 2252. (b) Garret, B.C.; Truhlar, D.G. *J. Phys. Chem.* **1991**, *95*, 10374. (c) González-Lafont, A.; Truong, T.N.; Truhlar, D.G. *J. Chem. Phys.* **1991**, *95*, 8875. (d) Melissas, V.S.; Truhlar, D.G. *J. Chem. Phys.* **1993**, *99*, 1013. (e) *idem. J. Phys. Chem.* **1994**, *98*, 875. (f) Truhlar, D.G.; Garret, B.C. *J. Phys. Chem. B* **2000**, *104*, 1069. (g) Liao, J-.L.; Pollak, E. *J. Phys. Chem. A* **2000**, *104*, 1799. (h) Rabani, E.; Krilov, G.; Berne, B.J. *J. Chem. Phys.* **2000**, *112*, 2605. (i) Robertson, S.; Wagner, A.F.; Wardlaw, D.M. *J. Chem. Phys.* **2000**, *113*, 2648. (j) Jang, S.; Voth, G.A. *J. Chem. Phys.* **2000**, *112*, 8747. (k) Liao, J-.L.; Pollak, E. *Chem. Phys.* **2001**, *268*, 295. (l) Truong, T.N. *J. Chem. Phys.* **2001**, *113*, 4957.

27.   (a) Perrin, J. *Ann. Phys.* **1919**, *11*, 5. (b) Lindemann, F.A. *Trans. Faraday Soc.* **1922**, *17*, 598.

28.   Lifshitz, C. *Chem. Soc. Rev.* **2001**, *30*, 186.

29.   Baer, T.; Hase, W.L. *Unimolecular Reaction Dynamics: Theory and Experiment*, Oxford University Press, New York, 1996.

30. See, for example: (a) Basu, S.; Knee, J.L. *J. Phys. Chem. A* **2001**, *105*, 5842. (b) Becerra, R.; Cannady, J.P.; Walsh, R. *Phys. Chem. Chem. Phys.* **2001**, *3*, 2343. (c) Hippler, H.; Striebel, F.; Viskolcz, B. *Phys. Chem. Chem. Phys.* **2001**, *3*, 2450. (d) Somnitz, H.; Zellner, R. *Phys. Chem. Chem. Phys.* **2001**, *3*, 2352. (e) Bates, R.W.; Golden, D.M.; Hanson, R.K.; Bowman, C.T. *Phys. Chem. Chem. Phys.* **2001**, *3*, 2337. (f) Gao, Y.Q.; Marcus, R.A. Science 2001, 293, 259.

31. (a) Zewail. A.H. *J. Phys. Chem. A* **2000**, *104*, 5660. (b) For a very interesting interview and the Nobel Lecture given by A. Zewail in 1999, go to: http://www.nobel.se/ chemistry/laureates/1999/zewail-video.html

32. Bell, R.P. *The Tunnel Effect in Chemistry*, Chapman and Hall, New York, 1980.

33. Hund, F. *Z. Phys.* **1927**, *43*, 805.

34. Some reviews of tunneling in chemical reactions: (a) Johnston, H.S. *Adv. Chem. Phys.* **1961**, *3*, 131. (b) Caldin, E.F. *Chem. Rev.* **1969**, *69*, 135.

35. De Broglie, L. *Ann. Phys.* **1925**, *10*, 22.

36. Bell, R.P. *Trans. Faraday Soc.*, **1959**, *55*, 1.

37. (a) Wigner, E. *Z. Phys. Chem. B* **1932**, *19*, 203. (b) Wigner, E. *J. Chem. Phys.* **1937**, *5*, 720.

38. For some applications, see: (a) Peng, J.B.; Wu, T.; Chen, X.Y.; Ju, G.Z. *Chinese J. Inorg. Chem.* **1999**, *15*, 196. (b) Chen, X.Y.; Wu, T.; Ju, Q.; Ma, J.; Ju, G.Z. *Int. J. Quantum Chem.* **1999**, *75*, 417. (c) Fang, T.D.; Taylor, P.H.; Berry, R.J. *J. Phys. Chem. A* **1999**, *103*, 2700. (d) Chen, X.Y.; Wu, T.; Peng, J.B.; Li, C.D.; Yao, T.Y.; Ju, G.Z. *Phys. Chem. Chem. Phys.* **1999**, *1*, 657.

39. Eckart, C. *Phys. Rev.* **1930**, *35*, 1303. Approximate solutions in closed form has also been given by: Shin, H. *J. Chem. Phys.* **1963**, *39*, 2934.

40. For some applications, see: (a) Yamada, T.; Fang, T.D.; Taylor, P.H.; Berry, R.J. *J. Phys. Chem. A* **2000**, *104*, 5013. (b) Cramer, C.J.; Pak, Y. *Theor. Chem. Acc.* **2001**, *105*, 477. (c) Boone, G.D.; Agyin, F.; Robichaud, D.J.; Tao, F.M.; Hewitt, S.A. *J. Phys. Chem. A* **2001**, *105*, 1456. (d) Felker, P.M.; Neuhauser, D.; Kim, W. *J. Chem. Phys.* **2001**, *114*, 1233.

41. (a) Johnston, H.S. *Gas Phase Reaction Rate Theory*, Ronald Press Company, New York, 1966. (b) Shavitt, I. *J. Chem. Phys.* **1959**, *31*, 1359. (c) Johnston, H.S.; Rapp, D. *J. Am. Chem. Soc.* **1961**, *83*, 1.

42.   Truhlar, D.G.; Isaacson, A.D.; Skodje, R.T.; Garrett, B. C. *J. Phys. Chem.* **1982**, *86*, 2252.

43.   Truong, T.N. *J. Phys. Chem.* **1997**, *101*, 2750.

44.   Truong, T.N.; Truhlar, D.G. *J. Chem. Phys.* **1990**, *93*, 1761.

45.   Arrhenius, S. *Z. Phys. Chem.* **1889**, *4*, 226. A translation of four pages that deal with the theory of teperature dependence is included in: Back, M.H.; Laidler, K.J. *Selected Readings in Chemical Kinetics*, Pergamon, Oxford, p. 31, 1967.

46.   (a) Logan, S.R. *J. Chem. Edu.* **1982**, *59*, 279. (b) Maskill, H. *Edu. Chem.* **1990**, *27*, 111.

47.   Mellor, J.W. *Chemical Statics and Dynamics*, Longmans, Green, London, 1904.

48.   See for example: (a) Wilhemy, L. *Poog. Ann.* **1850**, *81*, 453, 499. (b) Berthelot, *Ann. Chim. Phys.* **1862**, *66*, 110. (c) Hood, J.J. *Philos. Mag.* **1885**, *20*, 323. (d) van't Hoff, J.H. *Etudes de Dynamic Chimique*, Muller, Amsterdam, 1884. (e) Kooij, D.M. *Z. Phys. Chem.* **1893**, *12*, 155. (f) Harcourt, A.V.; Esson, W. *Philos. Trans. A* **1895**, *186*, 817. References taken from Ref. 1.

49.   Finlayson-Pitts, B.J.; Pitts, J.N. *Atmospheric Chemistry: Fundamentals and Experimental Techniques*, Wiley Interscience, New York, 1986.

50.   Hinshelwood, C.N. *The Kinetics of Chemical Change in Gaseous Systems*, Oxford U.P., London, p. 46, 1926.

51.   Moelwyn-Hughes, E.A. *Z. Phys. Chem.* **1934**, *B86*, 281.

52.   Dainton, F.S. *Ber. Bun. Phys. Chem.* **1971**, *75*, 608.

53.   (a) Mezinger, H.; Wolfgang, R. *Angew. Chem. (Int. Ed.)* **1969**, *8*, 438. (b) Pacey, P.D. *J. Chem. Edu.* **1981**, *58*, 612.

54.   Logan, S.R. *Edu. Chem.* **1986**, *23*, 148.

55.   Bunker, D.L.; Davidson, N. *J. Am. Chem. Soc.* **1958**, *80*, 5090.

56.   (a) Mozurkewich, M.; Benson, S.W. *J. Phys. Chem.* **1984**, *88*, 6429. (b) Mozurkewich, M.; Lamb, J.J.; Benson, S.W. *J. Phys. Chem.* **1984**, *88*, 6435. (c) Lamb, J.J.; Mozurkewich, M.; Benson, S.W. *J. Phys. Chem.* **1984**, *88*, 6441.

57. The NIST Chemical Kinetics Database, NIST Standard Reference Database, U.S. Dept. of Commerce, Technology Administration, National Institute of Standards and Technology: Gaithersburg, MD, 17-2Q98.

58. (a) Singleton, D.L.; Cvetanović, R.J. *J. Am. Chem. Soc.* **1976**, *98*, 6812. (b) Singleton, D.L.; Furuyama, S.; Cvetanović, R.J.; Irwin, R.S. *J. Chem. Phys.* **1975**, *63*, 1003.

59. (a) Sekušak, S.; Sabljić, A *Chem. Phys. Lett.* **1997**, *272*, 353. (b) Sekušak, S.; Liedl, K.R.; Sabljić, A. *J. Phys. Chem. A* **1998**, *102*, 1583. (c) Aloisio, S.; Francisco, J.S. *J. Phys. Chem. A* **2000**, *104*, 3211. (d) Vasvari, G.; Szilagyi, I.; Bencsura, A.; Dobe, S.; Berces, T.; Henon, E.; Canneaux, S.; Bohr, F. *Phys. Chem. Chem. Phys.* **2000**, *3*, 551.

60. (c) Aloisio, S.; Francisco, J.S.; Friedl, R.R. *J. Phys. Chem. A* **2000**, *104*, 6597. (d) Vaida, V.; Headrisck, J.E. *J. Phys. Chem. A* **2000**, *104*, 5401. (e) Aloisio, S.; Francisco, J.S. *Acc. Chem. Res.* **2000**, *33*, 825. (f) Goldman, N.; Fellers, R.S.; Leforestier, C.; Saykally, R.J. *J. Phys. Chem. A* **2001**, *105*, 515.

61. Zellner, R.; Lorenz, K. *J. Phys. Chem.* **1984**, *88*, 984.

62. Cvetanović, R.J.; Singleton, D.L. *Rev. Chem. Intermed.* **1984**, *5*, 183.

63. (a) Benson, S.W.; Dobis, O. *J. Phys. Chem. A* **1998**, *102*, 5175. (b) Dobis, O.; Benson, S.W. Z. Phys. Chem. 2001, 215, 283.

64. See, for example: (a) Uc, V.H.; García-Cruz, I.; Hernández-Laguna, A.; Vivier-Bunge, A. *J. Phys. Chem. A* **2000**, *104*, 7847. (b) Chuong, B.; Stevens, P.S. *J. Phys. Chem. A* **2000**, *104*, 5230. (c) Ranatunga, A.; Lasey, R.C.; Ogawa, M.Y. *Inorg. Chem. Commun.* **2001**, *4*, 30. (d) Sklyarchuk, V.; Plevachuk, Y. *Z. Phys. Chem.* **2001**, *215*, 103. (e) Olea, M.; Kunitake, M.; Shido, T.; Asakura, K.; Iwasawa, Y. Bull. Chem. Soc. Japan 2001, 74, 255.

65. Gaussian 98, (Revision A.4), Frisch, M.J.; Trucks, G.W.; Schlegel, H.B.; Scuseria, G.E.; Robb, M.A.; Cheeseman, J.R.; Zakrzewski, V.G.; Montgomery, J.A.; Stratmann, R.E.; Burant, J.C.; Dapprich, S.; Millam, J.M.; Daniels, A.D.; Kudin, K.N.; Strain, M.C.; Farkas, O.; Tomasi, J.; Barone, V.; Cossi, M.; Cammi, R.; Mennucci, B.; Pomelli, C.; Adamo, C.; Clifford, S.; Ochterski, J.; Petersson, G.A.; Ayala, P.Y.; Cui, Q.; Morokuma, K.; Malick, D.K.; Rabuck, A.D.; Raghavachari, K.; Foresman, J.B.; Cioslowski, J.; Ortiz, J.V.; Stefanov, B.B.; Liu, G.; Liashenko, A.; Piskorz, P.; Komaromi, I.; Gomperts, R.; Martin, R.L.; Fox, D.J.; Keith, T.; Al-Laham, M.A.; Peng, C.Y.; Nanayakkara, A.; Gonzalez, C.; Challacombe, M.; Gill, P.M.W.; Johnson, B.; Chen, W.; Wong, M.W.; Andres,

J.L.; Head-Gordon, M.; Replogle, E.S.; Pople, J.A. Gaussian, Inc.: Pittsburgh PA, 1998.

66.   Brown, R.L. *J. Res. Nat. Bur. Stand. (U.S.)* **1981**, *86*, 357.

67.   *Gaussian 98 Users's Reference*. Gaussian Inc.: Pittsburgh PA, 1998.

Chapter 4. OH Hydrogen-Abstraction from HCHO and CH₃CHO

4.1. Introduction

The atmosphere is a very complex chemical system that is of crucial importance to life on Earth. Aldehydes, known to play an important role in the chemistry of the polluted troposphere,[1] are directly emitted as primary pollutants from biogenic and anthropogenic sources.[2] They are also formed in large concentrations as end products of the partial oxidation of hydrocarbon fuels and arise as secondary pollutants from the oxidation of volatile organic compounds. Once in the atmosphere, aldehydes either photolyse or react further with OH radicals, the most important tropospheric daytime oxidant, or with NO_3 radicals during the night.

Since a likely route for the tropospheric removal of aldehydes in the atmosphere is by reaction with OH radicals, attention will be given to this reaction described by the following overall equation:

$$
\underset{R}{\overset{O}{\underset{\diagdown H}{\overset{\parallel}{C}}}} \quad + \quad {}^\bullet OH \quad \longrightarrow \quad \underset{R}{\overset{O}{\overset{\parallel}{C}_\bullet}} \quad + \quad H_2O
$$

(4.1)
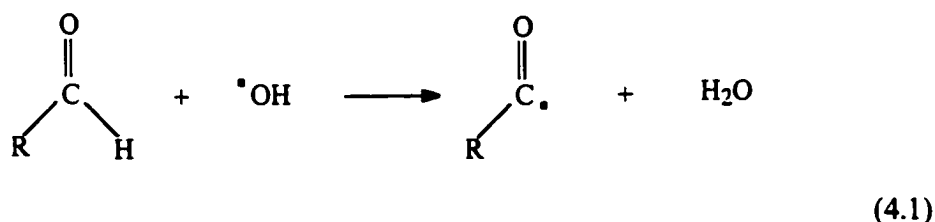
Bimolecular rate constants for the OH reaction with a variety of aldehydes have been measured and their Arrhenius parameters have been reported[1,3] but there are uncertainties as to the reaction mechanism. The negative temperature dependence of the rate constant is well established, except in HCHO, for which the activation energy is known to be almost zero, most experimental results varying between +0.7 and –1.9 kJ/mol.[3] This suggests the possibility that the reactions of aldehydes with the hydroxyl radical, in general, occur by an addition-elimination mode,[4,5] since many addition reactions of OH

show overall negative temperature dependence. Niki et al.[6] ruled out the formation of HCOOH + H but not the reaction:

$$HCHO + {}^{\bullet}OH \longrightarrow [HCHO\cdots OH]^{\bullet} \longrightarrow HCO^{\bullet} + H_2O \qquad (4.2)$$
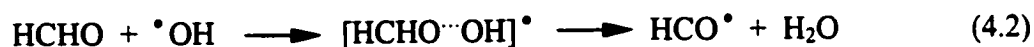
However, for HCHO it is believed that only hydrogen abstraction occurs. Recent experimental work by Butkovskaya and Setser[7] using infrared chemiluminescence confirms that the results are consistent with many polyatomic reactions in which the H atom is directly abstracted.

Michael et al.[4c] have presented a very complete mechanistic discussion of their experimental data for the CH₃CHO + OH reaction in the temperature range 244-528 K. They suggested two alternative mechanisms for this reaction, one of them being the addition-elimination mode in which CH₃COOH and H are formed. The authors suggest that this reaction proceeds through a vibrationally excited adduct radical that would be expected to undergo collisional stabilization. The other mechanistic alternative suggested by these authors is the direct aldehydic hydrogen-abstraction process. Taylor et al.[5] favour an addition-elimination mechanism at low temperatures. Atkinson[8] postulated that the reaction proceeds via overall H-atom abstraction, although the initial reaction possibly involves the OH radical addition to the C=O double bond. However, it is not clear why this hydrogen abstraction reaction presents a negative activation energy, and why the overall OH addition to the double bond does not occur.

The behaviour of reactions having a negative temperature dependence has been successfully described, for systems at low pressures, by Mozurkewich and Benson,[9] and for systems at high pressures, by Singleton and Cvetanović.[10] For this phenomenon several explanations have been proposed which are summarized in Section 3.5.1. Some of them maintain the idea of an elementary reaction but suggest a modification of the pre-exponential factor in the Arrhenius equation to allow for a term T^n. Singleton and Cvetanović[10] proposed a complex mechanism, and explained the occurrence of these negative activation energies as being due to the reversible formation of a loosely bound

reactant complex which is formed without activation energy. A second (irreversible) step follows whose TS energy is lower than the energy of the isolated reactants.

A reactant complex has, in fact, been identified in several OH-addition reactions to alkenes,[11] haloethanes[12] and aromatic hydrocarbons (toluene and xylenes).[13] In a recent study on the OH addition to substituted alkenes,[11c] by calculating the rate constants for the individual steps, it was shown that the mechanism proposed by Singleton and Cvetanović[10] provides a clear explanation of the experimental data.

Reactant complexes seem to be common in all radical-molecule reactions, and are due mainly to long-range Coulombic interactions between the reactants. In fact, in the reactant complex formed between the OH radical and an unsaturated hydrocarbon, it is the H atom of the OH radical which points towards the π electrons of the double bond, even though the OH group has to flip over in order to form the C-O bond in the adduct.[11,13] If the reaction occurs at sufficiently high pressures, the complexes are collisionally stabilized, and if the energy barriers are small, these complexes are likely to play an important role. Sekušak and Sabljić have also found that such intermediate complexes play a key role in hydrogen abstraction reactions from haloethanes.[12]

If reaction (4.1) were elementary with a negligible energy barrier, the rate constant of the aldehyde reactions with OH should depend essentially on the pre-exponential factor. Thus, because HCHO has two abstractable hydrogen atoms, one would expect its reaction with OH to be about twice as fast as the one of CH₃CHO, contrary to the observed experimental results at 298 K:[14a] $5.54 \cdot 10^9$ (HCHO) and $9.55 \cdot 10^9$ (CH₃CHO) L/mol·s. However, the experimentally determined Arrhenius parameters indicate a very small negative activation energy and a pre-exponential factor which is larger for HCHO than for CH₃CHO. Selected experimental data for these reactions are shown in Tables 4.1 and 4.2.[3,14,15] On the other hand, the greater reactivity of CH₃CHO is in line with the fact that the inductive effect of the methyl group should help stabilize the corresponding TS.

Table 4.1. Selected experimental data for the reaction $HCHO + OH = HCO + H_2O$.

Ref. (Year)	E_a [a]	A [b]	k [c]	T (K)	P (atm)
14a, b (1999, 1997)	-0.2	$5.18 \cdot 10^9$	$5.54 \cdot 10^9$	240 – 230	[d]
14c (1997)	-	-	$6.03 \cdot 10^9$	200 – 300	[d]
14d (1992) [e]	-1.9	$3.43 \cdot 10^6$	$6.07 \cdot 10^9$	300 – 3000	[d]
14e (1989)	-	-	$4.67 \cdot 10^9$	298	0.00395
14f (1988)	0.7	$1.00 \cdot 10^{10}$	$7.49 \cdot 10^9$	296 – 576	0.132
14g (1986) [e]	-1.9	$3.44 \cdot 10^6$	$6.08 \cdot 10^9$	200 – 1600	[d]
14h (1986)	-	-	$5.42 \cdot 10^9$	228 – 426	[d]
6 (1984)	-	-	$5.06 \cdot 10^9$	299	0.921
14i (1980)	-	-	$6.32 \cdot 10^9$	228 – 362	[f]
14j (1978)	-	-	$9.04 \cdot 10^9$	298	0.921
14k (1978)	0.7	$7.53 \cdot 10^9$	$5.61 \cdot 10^9$	299 – 426	0.0658
14m (1971)	-	-	$8.43 \cdot 10^9$	298	0.00132

[a] kJ/mol; [b] L/mol·s; [c] At 298 K, in L/mol·s; [d] Literature review; [e] $k = AT^{1.18} \exp(-E_a/RT)$; [f] 0.0263 – 0.0526 atm

Table 4.2. Selected experimental data for the reaction $CH_3CHO + OH = CH_3CO + H_2O$.

Ref. (Year)	E_a [a]	A [b]	k [c]	T (K)	P (atm)
14a, b (1999, 1997)	-2.6	$3.37 \cdot 10^9$	$9.55 \cdot 10^9$	240 – 530	[d]
14c (1997)	-2.2	$3.37 \cdot 10^9$	$8.35 \cdot 10^9$	200 – 300	[d]
15a (1995)	-	-	$8.73 \cdot 10^9$	298	[e]
15f (1984)	-	-	$1.00 \cdot 10^{10}$	300 – 2000	[d]

Selected experimental data for the reaction $CH_3CHO + OH = $ Products.

Ref. (Year)	E_a [a]	A [b]	k [c]	T (K)	P (atm)
5 (1996)	-2.6	$2.59 \cdot 10^9$	$7.32 \cdot 10^9$	295 – 550	0.974
15b (1993)	-	-	$9.75 \cdot 10^9$	298	[f]
14d (1992) [g]	-4.7	$2.35 \cdot 10^7$	$9.84 \cdot 10^9$	250 – 1200	[d]
15c (1992)	-	-	$1.02 \cdot 10^{10}$	298	0.0355
15d (1989)	-1.7	$5.20 \cdot 10^9$	$1.03 \cdot 10^{10}$	296 – 520	[h]
14h (1986)	-2.1	$4.14 \cdot 10^9$	$7.77 \cdot 10^9$	298 – 426	[d]
4c (1985)	-2.6	$3.33 \cdot 10^9$	$9.32 \cdot 10^9$	244 – 528	[i]
15e (1985)	-1.4	$4.28 \cdot 10^9$	$7.44 \cdot 10^9$	253 – 424	0.132
15g (1981)	-	-	$7.23 \cdot 10^9$	298	1
14j (1978)	-	-	$9.64 \cdot 10^9$	298	0.921
14k (1978)	-2.1	$4.14 \cdot 10^9$	$9.81 \cdot 10^9$	299 – 426	0.0658
15h (1971)	-	-	$9.04 \cdot 10^9$	300	0.00132

[a] kJ/mol; [b] L/mol·s; [c] At 298 K, in L/mol·s; [d] Literature review; [e] 0.00263 – 0.00395 atm; [f] 0.0961 – 0.987 atm; [g] $k = AT^{0.73} \exp(-E_a/RT)$; [h] 0.00138-0.00326; [i] 0.00132-0.00421

Using quantum chemical methods, it is possible to calculate energies of intermediate structures and TSs with a reasonable degree of accuracy, and thus to model the reaction path of a reaction. Indeed, a 0.996 correlation factor was recently obtained[11c] after plotting the logarithm of the experimental rate constants *versus* the *ab initio* calculated effective activation energies for the OH radical addition to a series of substituted alkenes.

Previous theoretical work on the HCHO + OH reaction has been reported by Dupuis and Lester[16] using HF, multiconfiguration HF and CI wavefunctions. They predicted a positive activation barrier of 23.0 kJ/mol for the OH hydrogen-abstraction reaction. Francisco[17] performed optimizations at the PMP4SDTQ(FC)/6-311++G(d,p)//MP2/ 6-311G(d,p) level with vibrational frequencies calculated at the HF/6-31G(d) level; a barrier of 6.7 kJ/mol was calculated. Francisco also calculated the rate constant, in good agreement with experiment, by means of TST; tunneling corrections were considered assuming an unsymmetrical Eckart barrier. The formation of a reactant complex was not considered in the above papers. In the present work, the results of the previous studies are included for comparison and discussion. In addition to these studies, the weakly bound complexes of the OH radical with HCHO and CH₃CHO were recently calculated by Aloisio and Francisco[18] using DFT.

In the more recent study of Takahashi *et al.*,[19] a real space *ab initio* molecular dynamic simulation of the HCHO + OH reaction was performed. Their simulation revealed that the hydrogen-abstraction reaction takes place without potential energy barrier according to gradient-corrected DFT calculations. They calculated the enthalpy of reaction to be -164.1 kJ/mol, based on LDA calculations, and -139.4 kJ/mol by means of BLYP computations.

Taylor *et al.*[5] have investigated the reaction of OH radicals with CH₃CHO in a wide temperature range with the laser photolysis/laser-induced fluorescence technique. Possible reaction pathways (OH-addition and H-atom abstraction) were evaluated with a quantum RRK model. They concluded that different reaction mechanisms occur depending on the temperature, and that OH addition followed by CH₃ elimination is the

dominant pathway for reactions occurring between 295 and 600 K. Moreover, they found that the H-atom abstraction from the CH_3 group is dominant at high temperatures. They also concluded that the aldehydic hydrogen-abstraction pathway is largely insignificant, except possibly at the lowest temperatures. However, their calculated rate constant at 298 K is about a factor of 10 too low.

HCHO and CH_3CHO are the most abundant aldehydes in the atmosphere and furthermore, have been regulated as hazardous air pollutants. As a consequence of the chain of reactions that follow after OH and CH_3CHO react in the troposphere, a very problematic compound is formed: $CH_3C(O)OONO_2$, also known as PAN, the smallest member of the family of peroxyacyl nitrates. PAN is a strong eye irritant, with phytotoxic properties and mutagenic and carcinogenic activity.[20] Moreover, in the 1950's PAN was identified as a component of photochemical smog.[1,21]

In this study, the HCHO + OH and CH_3CHO + OH reactions are characterized using several methods and large basis sets, in order to obtain an accurate reaction profile and to reproduce the experimentally observed values of the activation energy (approximately –0.2 and –2.6 kJ/mol for HCHO and CH_3CHO,[14a] respectively). With the corresponding partition functions, the effective rate constants are calculated, using TST and the proposed hydrogen-abstraction complex mechanism. The results are compared with the experimental data and with the results of previous calculations. The purpose of this study is:

(i)   To show that the complex mechanism proposed by Singleton and Cvetanovic[10] can be applied to both the formaldehyde and the acetaldehyde reactions.

(ii)   To show that consideration of the reactant complex is essential for the correct calculation of the rate constant, when the tunneling factor is significant, as is the case in hydrogen abstraction reactions.

(iii)   To define a theoretical methodology which is able to reproduce theoretically the rate constants of the two reactions.

4.2. Computational details

All geometries were fully optimized at the MP2(FC)/6-311++G(d,p) level and energies were further calculated at the CCSD(T)/6-311++G(d,p) level.

For the reactions under study two reaction mechanisms will be taken into account, a complex and a direct mechanism. For the complex mechanism the following steps are considered:

Step 1:   RCHO + OH $\overset{k_1}{\underset{k_{-1}}{\rightleftharpoons}}$ [RCHO··HO]

Step 2:   [RCHO··HO] $\overset{k_2}{\longrightarrow}$ [RCO··H₂O] $\longrightarrow$ RCO + H₂O
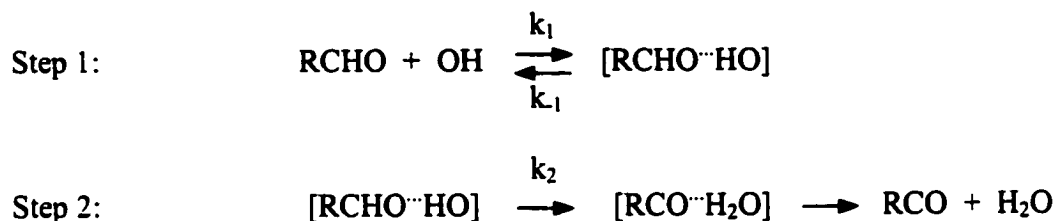
Step 1 involves a fast pre-equilibrium between the reactants and the reactant complex, followed by an internal rearrangement leading to the elimination of a water molecule in the second step.

If k_1 and k_{-1} are the forward and reverse rate constants, respectively, for the first step, and k_2 is the rate coefficient of the second step, the overall rate constant can be written as:[10]

$$k_{eff} = \frac{k_1 k_2}{k_{-1}} = \left(\frac{A_1 A_2}{A_{-1}}\right) \exp\left(-\frac{E_{a(1)} + E_{a(2)} - E_{a(-1)}}{RT}\right) \tag{4.3}$$

Since $E_{a(1)}$ is zero, the net activation energy for the overall reaction is:

$$E_a^{eff} = E_{a(2)} - E_{a(-1)} = E^{TS} - E^{React} \tag{4.4}$$

Thus, the activation energy at high pressures can be calculated as the difference between the total energy of the TS (E^{TS}) and that of the reactants (E^{React}), without having to obtain the reactant complex.

Applying basic statistical thermodynamic principles (see Section 3.1), the equilibrium constant of the fast pre-equilibrium between the reactants and the reactant complex (RC) may be obtained as:

$$K_{eq} = \frac{Q^{RC}}{Q^{React}} \exp\left(-\frac{E^{RC} - E^{React}}{RT}\right)$$ (4.5)

Under high-pressure conditions, an equilibrium distribution of the reactants (the reactant complex, for the second step of the complex mechanism) is maintained in a unimolecular process, and the TST formula can be applied to calculate k_2:

$$k_2 = \kappa \frac{k_B T}{h} \frac{Q^{TS}}{Q^{RC}} \exp\left(-\frac{E^{TS} - E^{RC}}{RT}\right)$$ (4.6)

The effective rate constant for the above mechanism may be written as:

$$k_{eff} = \frac{k_1 k_2}{k_{-1}} = K_{eq} k_2$$ (4.7)

$$k_{eff} = \kappa \frac{k_B T}{h} \frac{Q^{TS}}{Q^{React}} \exp\left(-\frac{E^{TS} - E^{React}}{RT}\right)$$ (4.8)

In the second mechanism considered the reaction is assumed to be elementary:

$$RCHO + OH \xrightarrow{k_D} RCO + H_2O$$
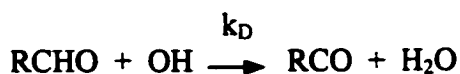
The formation of the reactant and product complexes is ignored, and the rate constant is calculated as:

$$k_D = \kappa_D \frac{k_B T}{h} \frac{Q^{TS}}{Q^{React}} \exp\left(-\frac{E^{TS} - E^{React}}{RT}\right)$$ (4.9)

It is important to notice that expressions (4.8) and (4.9) are identical except for the tunneling factor κ, which depends on the forward and reverse potential energy barriers of the elementary process in which the hydrogen atom is abstracted. For the complex mechanism these energy barriers are calculated from the energies (including ZPE) of the reactant complex, TS and product complex, while for the direct mechanism the energies of the isolated reactants and products as well as the energy of the TS are considered. The tunneling factor and $\Delta s_{\frac{1}{2}}$ were calculated by assuming an unsymmetrical Eckart barrier.[22]

4.3. Results and discussion

The OH radical attack on aldehydes appears to occur in the following way. At first, the electron-deficient hydrogen atom of the OH radical approaches a lone pair of the carbonylic oxygen atom to form a stable reactant complex, whose energy is more than 13 kJ/mol lower than the energy of the reactants (Fig. 4.1). Several such reactant complexes were identified in the case of the HCHO + OH reaction, but, in the most stable one, the OH radical lies in the plane of the CHO group. From this structure, the oxygen of the OH may flip, in the plane, towards the hydrogen to be abstracted as the energy increases to a maximum at the TS.

The geometries of the reactant complexes obtained for the HCHO + OH and CH₃CHO + OH reactions are very similar to those obtained by Aloisio and Francisco[18] using a DFT method.

Besides the aldehydic hydrogen-abstraction, another process (4.10) may also occur which leads to the OH addition to the carbonylic double bond. Starting from the same reactant complex, the OH group may flip in a plane perpendicular to the CHO plane, such that the oxygen atom may approach the carbon atom of the aldehyde from above. It will be shown below that the corresponding TS has a considerably higher energy than that for the abstraction channel.

The following complex mechanism can be considered for the OH addition reaction to HCHO:

Step 1: $RCHO + OH \rightleftharpoons [RCHO \cdots HO]$

Step 2: $[RCHO \cdots HO] \longrightarrow [RCHO(OH)]$

Step 3: $[RCHO(OH)] \longrightarrow [RCO \cdots H_2O] \longrightarrow RCO + H_2O$

(4.10)
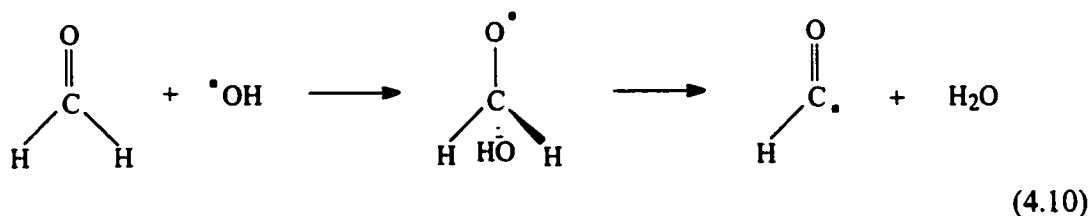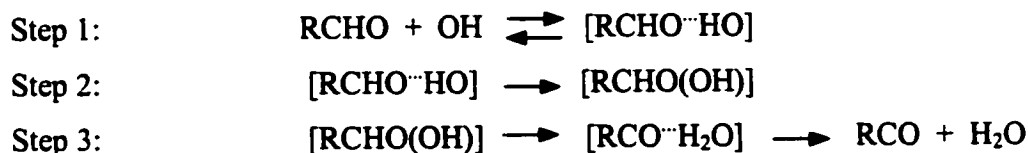
A third process could also be considered, in which the OH radical attacks CH_3CHO at the methyl group and produces the CH_2CHO radical. Indeed, this hydrogen-abstraction is about 105 kJ/mol exothermic. The energy of the methyl C-H bond is about 30 kJ/mol larger than that of the carbonyl C-H bond:

$$CH_3CHO + OH \longrightarrow CH_3CO + H_2O \qquad \Delta H_{298} = (-134.4 \pm 9.4) \text{ kJ/mol}$$

$$CH_3CHO + OH \longrightarrow CH_2CHO + H_2O \qquad \Delta H_{298} = (-104.7 \pm 9.0) \text{ kJ/mol}$$
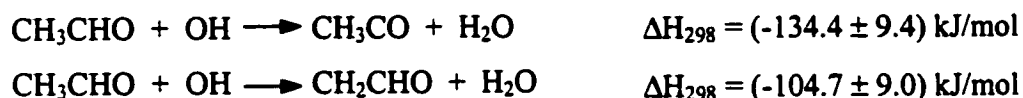
The above ΔH_{298} values were calculated from the following bond enthalpies (DH_{298} in kJ/mol) taken from Ref. 23:

$$DH_{298} (\text{H-OH}) = 499.5 \pm 0.2$$

$$DH_{298} (\text{CH}_3\text{CO-H}) = 365.1 \pm 9.6$$

$$DH_{298} (\text{H-CH}_2\text{CHO}) = 394.8 \pm 9.2$$
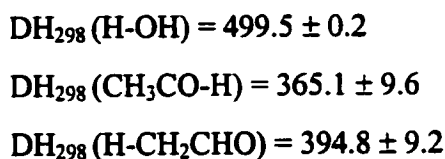
Since the aldehydic hydrogen-abstraction is more exothermic, according to Hammond's postulate its TS should resemble more closely the reactants, *i.e.*, this TS should be earlier than the methyl hydrogen-abstraction TS and thus easier to achieve. Following these

ideas the former reaction should be faster than the latter. In addition, the position of the OH hydrogen atom in the reactant complex is very far from the methyl hydrogen atoms. Indeed, it has been shown that the calculated rate constant for the methyl hydrogen-abstraction process, applying TST, is ten times smaller than the aldehydic hydrogen-abstraction reaction.[5] Moreover, in the Cl + CH₃CHO reaction the CH₃CO radicals are the only ones observed.[24] Hence, even though the methyl hydrogen-abstraction is entropically more favoured (there are three H atoms available instead of just one), other factors (energetic and dynamic) determine the lower reactivity of the methyl site in CH_3CHO.

The proposed abstraction mechanism resembles closely that described by Sekušak and Sabljić[12] for the hydrogen-abstraction reaction from haloethanes. These authors have stressed the importance of the reactant complex and the role of a strongly electronegative atom in guiding the reaction from the very beginning and in lowering the energy of the TS.

The MP2 optimized geometries of the TSs and product complexes of the hydrogen-abstraction reactions under study are shown in Figs. 4.2 and 4.3, respectively. Relevant geometric parameters have been indicated on the figures (bond distances are given in Angströms and angles in degrees). Both the hydrogen abstraction and the OH addition channels have been investigated in the case of the HCHO reaction. For CH_3CHO, however, only the abstraction channel was studied. The TS and addition product of the OH addition reaction to HCHO are shown in Figs. 4.4 and 4.5, respectively.

The C··H and O··H distances for the abstraction TS (Fig. 4.2) indicate that the TS for CH_3CHO is formed earlier than that for HCHO. This situation is a consequence of the positive inductive effect of the CH₃ group that increases the electronic density at the carbonyl carbon, favouring the abstraction of the hydrogen atom.

The symmetry of the TS for the HCHO and CH₃CHO reaction with OH is $^2A'$, implying that the unpaired electron is in the plane where the OH attack takes place. $^2A'$ is also the symmetry of the RCO radical generated. The Cartesian coordinates of the optimized species along the reaction paths of the reactions studied are available.[25]

(a)
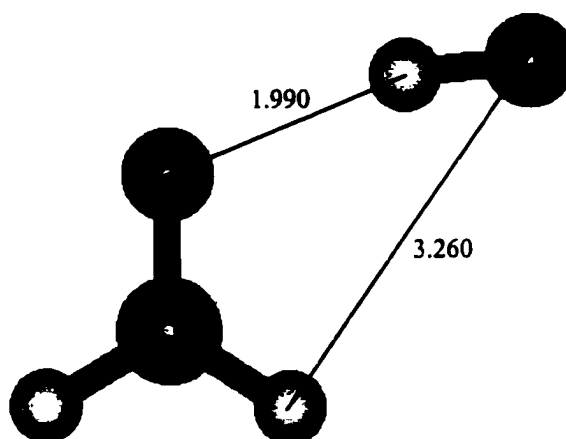
(b)
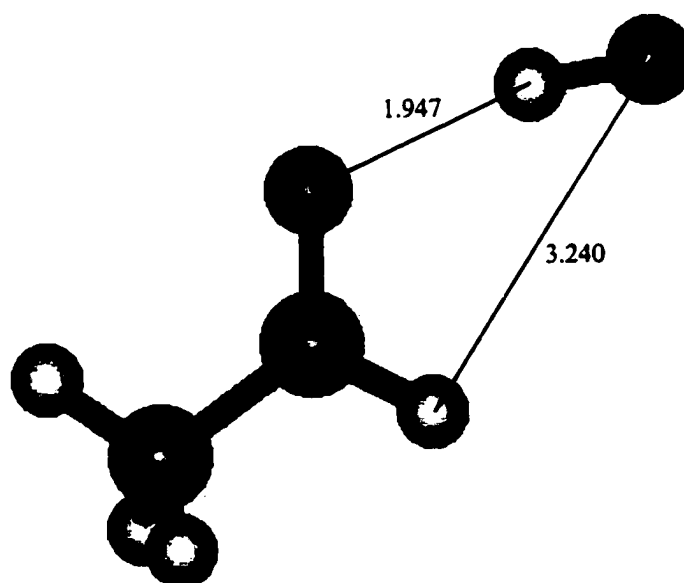
Figure 4.1. Optimized structures of the reactant complex of the (a) HCHO + OH and (b) CH₃CHO + OH hydrogen-abstraction reactions. (Bond distances are given in Å)

(a)

174.3

1.177

1.41

(b)

175.0

1.171

1.450
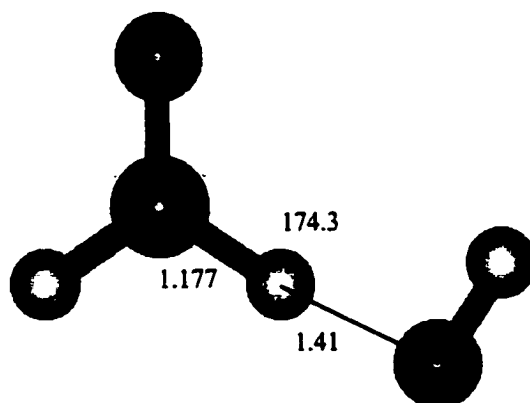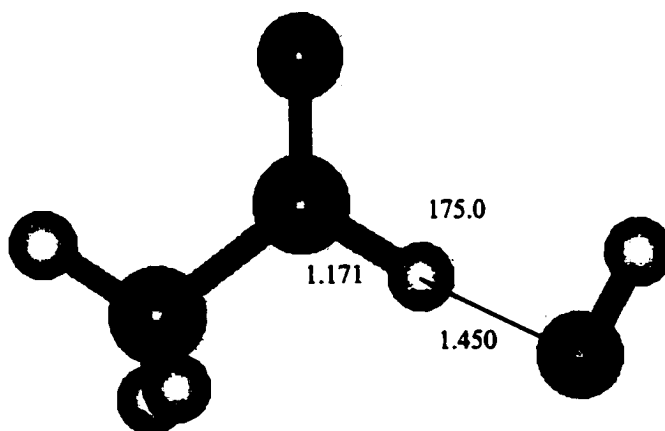
Figure 4.2. Optimized structures of the TS of the (a) HCHO + OH and
(b) CH₃CHO + OH hydrogen-abstraction reactions.
(Bond distances are given in Å and angles in degrees)

(a)
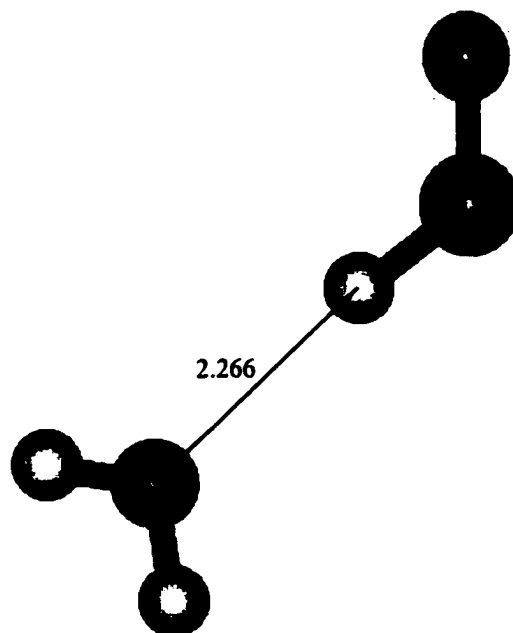
(b)
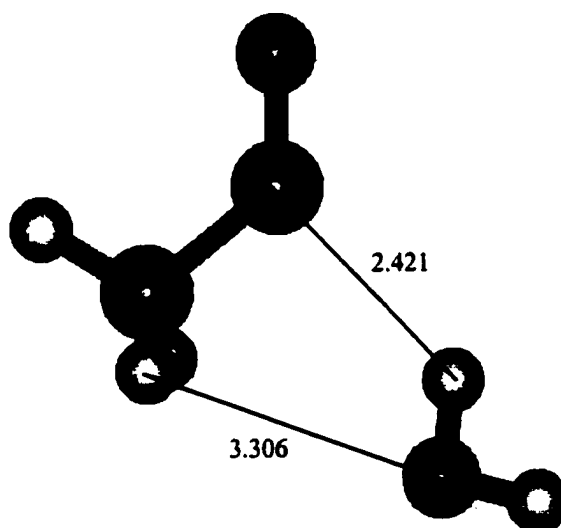
Figure 4.3. Optimized structures of the product complex of the (a) HCHO + OH and
(b) CH₃CHO + OH hydrogen-abstraction reactions.
(Bond distances are given in Å)
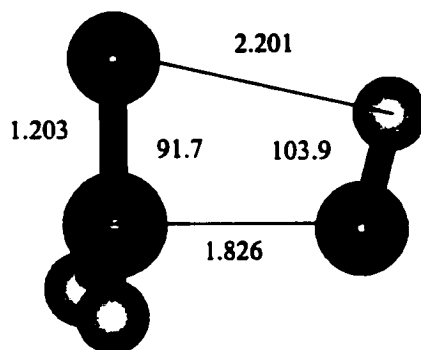
Figure 4.4. Optimized structure of the TS of the HCHO + OH addition reaction. (Bond distances are given in Å and angles in degrees)
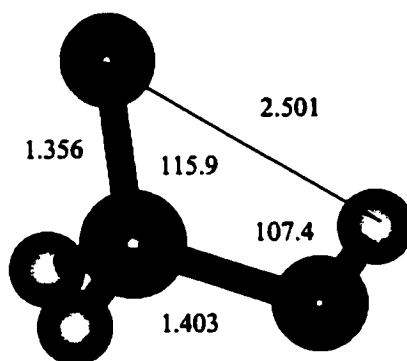
Figure 4.5. Optimized structure of the addition product of the HCHO + OH reaction. (Bond distances are given in Å and angles in degrees)

For the abstraction reactions, spin contamination is only significant (but small) at the TS: the expectation value of S^2 is 0.779 for the HCHO abstraction reaction and 0.774 for CH_3CHO, and in the MP2 calculations it is completely eliminated by projection. Thus, for these particular reactions, the CCSD(T) method applied to an MP2 optimized geometry can be expected to yield reliable energies. In contrast, results obtained in the OH addition channel indicate that spin contamination is much more important, 0.919, and it is not completely eliminated by projection, a situation that is not unusual. In fact, Sekušak et al.[11c] also observed, in the alkene + OH reactions, that single point CC calculations do not give satisfactory results, probably due to the fact that the geometry is not optimized at this level and because spin contamination is not eliminated. Thus, for the addition channel, the PMP2 results are expected to be more reliable.

The calculated total energies (PMP2, CCSD(T)), zero-point and thermal (at 298.15 K) vibrational energy corrections (calculated at the MP2 level) of the species involved in the reactions of OH with the aldehydes studied, are available.[25]

The stabilization energy of the reactant complexes (E_a (-1)), the activation barriers of the second step of the complex mechanisms (E_a (2)) and the effective activation energies (E_a^{eff}), calculated as described in equation (4.4), are given in Table 4.3 at 0 K. This table also includes reaction enthalpies (ΔH) for the addition and hydrogen-abstraction reactions for the methods employed, as well as effective activation energies, stabilization energies of the reactant complexes and reaction enthalpies at 298.15 K. Other calculated or measured values are shown for comparison. The ZPE and TCE values calculated at the MP2 level are used to obtain the CCSD(T) energy differences.

The reaction energy profiles for the OH addition and hydrogen-abstraction reactions with HCHO are shown in Fig. 4.6. The best energies were used for each reaction, i.e., PMP2 energies for the addition and CCSD(T) energies for the hydrogen-abstraction reaction (with MP2 ZPE included). The PMP2 effective activation energy of the addition reaction (32.2 kJ/mol) is considerably greater that the energy barrier calculated for the hydrogen-abstraction process (13.0 at the PMP2 level and 0.5 at the CCSD(T) level). Based on this

situation it is clear why the addition pathway is not favoured in these reactions. The difference between the CCSD(T) energies of the TSs for these two channels is more than 35 kJ/mol. It is interesting to note that almost half of this energy difference arises from the zero point correction energies. This is clearly due to the fact that the TS for the addition is expected to be much tighter than the one for the abstraction, and thus its vibrational zero point correction is larger. Even considering that the CCSD(T) method is not adequate for the addition channel, the difference in energy between the TSs for addition and abstraction is also large enough (about 20 kJ/mol) at the PMP2 level to guarantee that only the abstraction channel occurs.

The energy profiles obtained using the CCSD(T) energies (including the MP2 ZPEs) for the HCHO + OH and CH₃CHO + OH hydrogen-abstraction reactions are shown in Fig. 4.7. The formation of a stable reactant complex followed by a transition state whose energy is lower (CH₃CHO) or slightly higher (HCHO) than the energy of the reactants is clearly observed.

The calculated stabilization energies of the reactant complexes (Fig. 4.1) obtained at the PMP2 and the CCSD(T) levels agree to within 0.1 kJ/mol. The predicted stabilization energies at 0 K are 13.6 kJ/mol and 17.5 kJ/mol for the HCHO···OH and CH₃CHO···OH reactant complexes, respectively. Aloisio and Francisco[18] estimated binding energies at 0 K of 12.6 (HCHO···OH) and 16.7 kJ/mol (CH₃CHO···OH) at the B3LYP/6-311++(2d,2p) level, in very good agreement with the new calculations.

The PMP2 effective activation energies are overestimated; for these reactions, CCSD(T) seems to be the most appropriate method for obtaining activation energies and rate constants. Indeed, the CCSD(T) results agree remarkably well with the experimental values. For the OH hydrogen-abstraction reactions, the best value of the effective activation barrier at 298 K is calculated to be 0.1 for HCHO and −7.2 kJ/mol for CH₃CHO, in very good agreement with the experimental results (see

Table 4.3. Relevant barriers (E_a) and reaction enthalpies (ΔH), in kJ/mol, including zero-point vibrational corrections (ZPE), unless otherwise specified, for the OH addition to HCHO and the OH hydrogen-abstraction reaction from HCHO and CH₃CHO.

Basis set: 6-311++G(d,p)	$E_{a(2)}$	E_a^{eff}	$E_a^{eff\,(a)}$	ΔH	$\Delta H^{(a)}$
Addition: HCHO + OH					
PMP2	47.2	33.6	32.2	-67.9	-69.7
CCSD(T)	52.6	38.9	37.6	-71.8	-73.6

Basis set: 6-311++G(d,p)	$E_{a(-1)}$	$E_{a(-1)}^{(a)}$	$E_{a(2)}$	E_a^{eff}	$E_a^{eff\,(a)}$	ΔH	$\Delta H^{(a)}$
HCHO + OH							
PMP2	13.6	13.0	26.6	13.0	12.6	-142.0	-140.8
CCSD(T)	13.6	13.0	14.1	0.5	0.1	-118.9	-117.7
Previous calculations	12.6[b]			5.0[c] 23.0[d]	6.7[c]	-126.9[c] -139.4[e] -129.4[f]	
Experiment					-0.2[g] -1.9[h] 0.7[i]		-129.4[j] -130.7[k] -135.3[l]
CH₃CHO + OH							
PMP2	17.4	16.4	23.4	6.0	6.0	-134.7	-133.2
CCSD(T)	17.5	16.5	10.3	-7.2	-7.2	-115.0	-113.5
Previous calculations	16.7[b]		-5.4[m]				
Experiment					-2.6[n] -2.2[o] -4.7[p]		-125.3[j] -139.6[k,l]

[a] Including thermal correction (TCE) at 298.15 K; [b] Ref. 18 (2000); [c] Ref. 17 (1992); [d] Ref. 16 (1984); [e] Ref. 19 (2001); [f] Ref. 26 (1998); [g] Ref. 14a, b (1999, 1997); [h] Ref. 14d, g (1992, 1986); [i] Ref. 14f, k (1988, 1978); [j] Ref. 14a (1999); [k] Ref. 14b (1997); [l] Ref. 27 (1992); [m] Ref. 5 (1996); [n] Ref. 14a, b (1999, 1997), 5 (1996), 4c (1985); [o] Ref. 14c (1997); [p] Ref. 14d (1992)
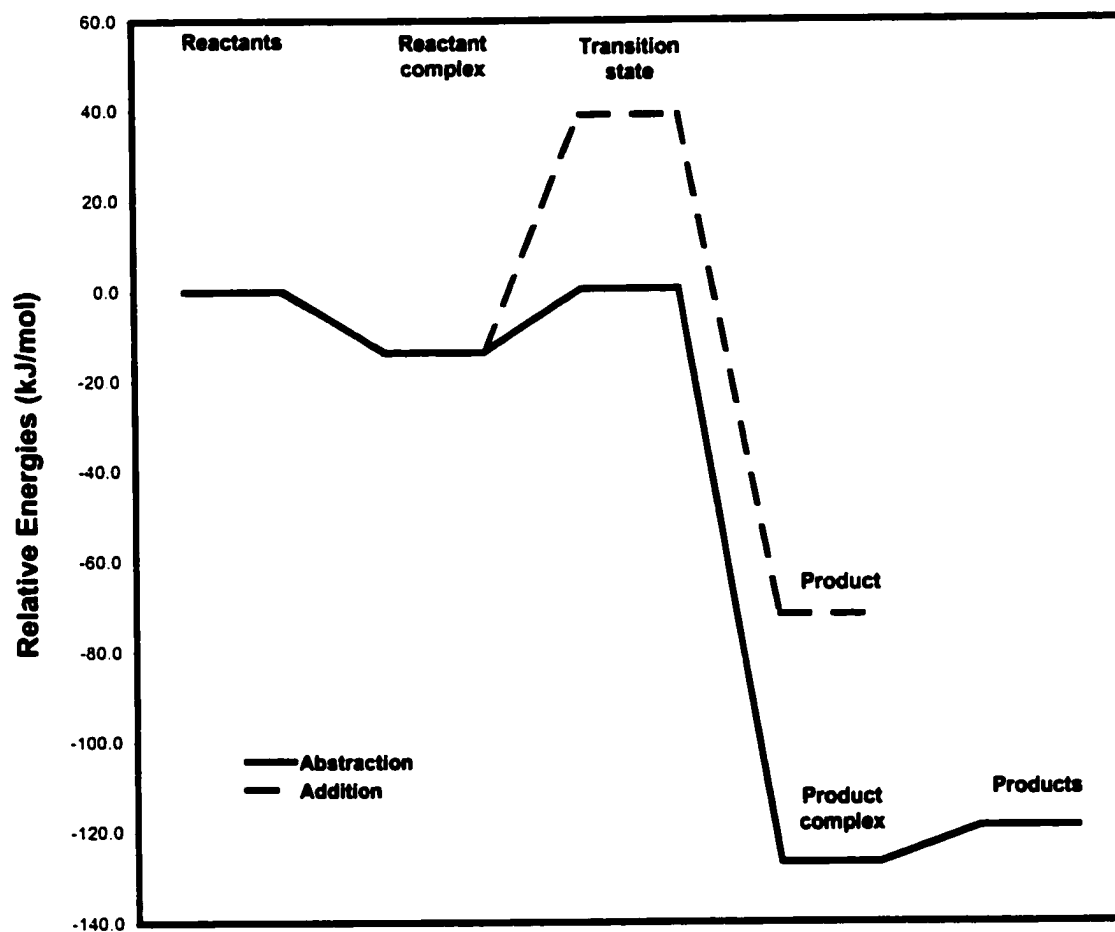
Figure 4.6. Schematic reaction profiles for the addition (PMP2 energies) and hydrogen-abstraction (CCSD(T) energies) in the HCHO + OH reaction, with the 6-311++G(d,p) basis set. ZPEs calculated at the MP2 level have been included.

RCHO + OH → RCO + H₂O   (R = H, CH₃)
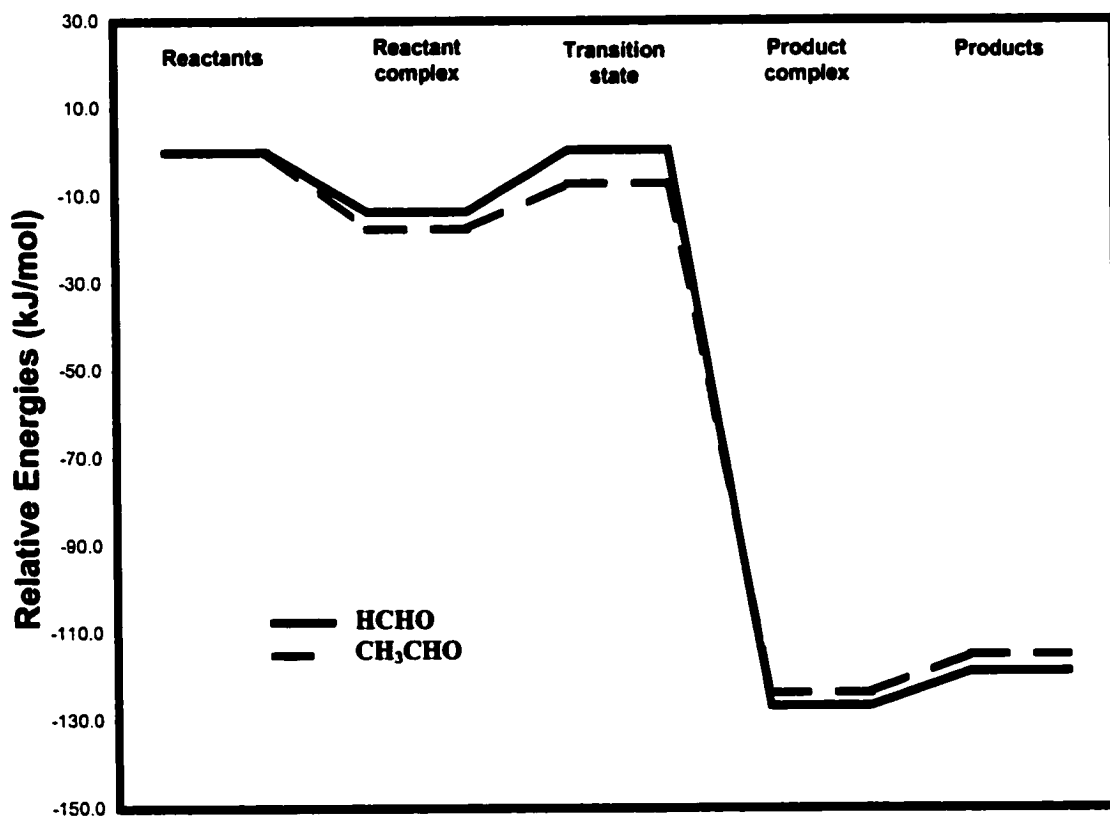
Figure 4.7. Schematic reaction profiles for the RCHO + OH (R = H, CH₃) using the calculated CCSD(T)/6-311++G(d,p) energy values, including the MP2(FC)/6-311++G(d,p) ZPEs.

Tables 4.1 and 4.2). At the same level, considering the formation of the reactant complex, the activation energy of the second step in the complex mechanism (E_a (2) at 0 K) is 14.1 for HCHO and 10.3 kJ/mol for CH₃CHO.

Product complexes (Fig. 4.3), which present hydrogen bonds between the water molecule and the aldehydic radicals, are about 8 kJ/mol more stable than the corresponding separated products at 0 K. The most recently reported heats of reaction for the hydrogen-abstraction processes[14a] lie between those obtained with the PMP2 and CCSD(T) calculations at 298 K. However, the theoretical methods employed reproduce correctly the observed trends.

The values of the partition functions needed for the calculation of the rate constants of the reactions studied at the MP2 level are given in Table 4.4, as well as the imaginary frequency of the TS. Three low frequencies (below 210 cm⁻¹) in addition to the imaginary frequency were calculated for the hydrogen-abstraction TSs. Of these, two were identified as internal rotations (or torsional vibrations) by visualization of the normal modes: frequencies 1 and 3 for both TSs. These harmonic modes correspond most closely to the two new internal rotors created in the TS (RCOH···OH and RCO···HOH), where the common axes for internal rotation are the ones linking the reactants and products, respectively, and were the axes considered in the calculation of the reduced moments of inertia. These harmonic modes were treated as free rotors in the calculation of the internal-rotation partition function of the TS (Q_{IR}^{TS}).[28,29] For CH₃CHO and its TS, the internal rotation around the C-C single bond was also considered and treated as a free rotor.

The harmonic contributions of these low frequencies were eliminated from the vibrational partition function in order to correct the total partition function of the TS (Q_{corr}^{TS}). For the OH reaction with CH₃CHO, Q_{corr}^{TS} is calculated as:

$$Q_{corr}^{TS} = \frac{Q^{TS} \; Q_{IR}^{TS}}{Q_{v=1} \; Q_{v=3} \; Q_{v=4}} \qquad (4.12)$$

Table 4.4. Total partition functions (Q) of the reactants and the TS, and imaginary frequency (v*
in cm⁻¹) of the TS of the OH hydrogen-abstraction reaction from HCHO and
CH₃CHO, calculated at the MP2(FC)/6-311++G(d,p) level.

System	HCHO + OH	CH₃CHO + OH
Q^{OH}	$6.02509 \cdot 10^7$	$6.02509 \cdot 10^7$
Q^{RCHO}	$4.63150 \cdot 10^9$	$3.11890 \cdot 10^{11}$ [a]
Q^{TS}	$7.94138 \cdot 10^{12}$	$1.44177 \cdot 10^{14}$
$\prod Q_{v=i}$ [d]	5.439 [b]	12.413 [c]
Q_{IR}^{TS} [e]	43.660	162.362
Q_{corr}^{TS} [f]	$6.37514 \cdot 10^{13}$	$1.88582 \cdot 10^{15}$
v^*	1522	1066
v^* [g]	3325	

[a] $Q_{corr}^{CH_3CHO} = 5.40018 \cdot 10^{11}$; [b] i=1, 3; [c] i=1, 3, 4;
[d] Vibrational components that were eliminated from the
calculation of Q_{corr}^{TS}; [e] Total internal-rotational partition
function of the TS; [f] Corrected total partition function of
the TS; [g] Ref. 17 (HF/6-31G(d))

Details of the calculation of the rate constants using the CCSD(T)/6-311++G(d,p)//MP2/
6-311++G(d,p) energy values and the MP2/6-311++G(d,p) frequency calculation, are
given in Table 4.5.

Thus, if the rate constant for the HCHO + OH reaction is calculated according to the
complex mechanism, a tunneling factor κ = 5.69 is obtained, and the rate constant is
calculated to be $6.65 \cdot 10^9$ L/mol·s, in excellent agreement with the experimental values
(see Table 4.1). If an elementary mechanism is assumed, κ is 0.724, so tunneling can be
neglected and the calculated rate constant is only $1.17 \cdot 10^9$ L/mol·s. The excellent

agreement obtained by Francisco[17] for the rate constant of this reaction (5.64·10⁹ L/mol·s) using the direct mechanism, is probably due to a cancellation of errors. The activation energy calculated by the author at 0 K is 5.0 kJ/mol and the tunneling correction is estimated to be 17.85. The direct barriers at 0 K used in the present study to calculate the Eckart tunneling corrections are 0.5 (κ = 0.724) and 14.1 (κ = 5.69) kJ/mol. Francisco's value of the Eckart tunneling correction should be intermediate between the two values reported above.

Table 4.5. Rate constants and tunneling parameters for the OH hydrogen-abstraction reaction from HCHO and CH₃CHO, calculated using CCSD(T)/6-311++G(d,p)//MP2(FC)/ 6-311++G(d,p) energies that include zero point corrections, for both the direct and complex mechanisms at 298.15 K. The frequency calculations were performed at the MP2(FC)/6-311++G(d,p) level.

	HCHO + OH	CH₃CHO + OH
Direct Mechanism		
κ	(a)	(a)
$\Delta s_{\frac{1}{2}}$ (Å)	(a)	(a)
k_D (L/mol·s)	1.17·10⁹	6.46·10⁹
Complex Mechanism		
κ	5.69	2.47
$\Delta s_{\frac{1}{2}}$ (Å)	0.30	0.38
k_{eff} (L/mol·s)	6.65·10⁹	1.59·10¹⁰
Experiment		
k (L/mol·s)	5.54·10⁹ [b]	9.55·10⁹ [b]
	6.03·10⁹ [c]	8.35·10⁹ [c]
Previous Calculation		
κ	17.85 [d]	
k (L/mol·s)	5.64·10⁹ [d]	5.11·10⁸ [e]

[a] κ < 1.0, so tunneling is ignored; [b] Ref. 14a, b (1999, 1997);
[c] Ref. 14c (1997); [d] Ref. 17 (1992); [e] Ref. 5 (1996)

The tunneling correction for the CH$_3$CHO + OH reaction assuming a complex mechanism is 2.47 and the rate constant is $1.59 \cdot 10^{10}$ L/mol·s, in good agreement with experiment (see Table 4.2). If the reaction were considered elementary, the forward barrier would be negative and the tunneling calculation meaningless.

The importance of considering the reactant complex formation when calculating the tunneling correction has been discussed by Sekušak and Sabljić[12] in the case of the hydrogen-abstraction reaction from haloethanes. However, these authors calculated the rate constants assuming a direct reaction mechanism, and hence they found significant discrepancies with the experimental results.

4.4. Conclusions

From the above discussion it is concluded that, when the RCHO + OH (R = H, CH$_3$) reaction occurs at atmospheric pressure, the following observations hold:

(i)   The addition of the OH radical to the carbonylic double bond is excluded because its activation energy is much higher than that for OH hydrogen-abstraction. The methyl H-atoms in CH$_3$CHO should be less reactive towards OH attack than the aldehydic H-atom. Hence, the reaction basically only involves the aldehydic hydrogen-abstraction.

(ii)   The OH hydrogen-abstraction reaction from aldehydes is not elementary.

(iii)   The overall rate depends on the rates of two competitive reactions: a reversible step where a reactant complex is formed, followed by the irreversible hydrogen-abstraction to form the products.

The proposed mechanism provides a clear explanation of the experimental behaviour. If $E_{a\ (-1)}$ is larger than $E_{a\ (2)}$, *i.e.*, the effective activation energy is negative, the decomposition of the reactant complex (step -1) will be relatively more favoured by an

increase in temperature than the hydrogen-abstraction process (step 2) and the overall rate will decrease. In the OH + aldehyde reactions, the effective negative activation energy is well founded and cannot be an artifact of the experimental method, as claimed by Benson and Dobis[30] for similar radical-molecule reactions.

The consideration of the reactant complex formation in the kinetic calculations has two important consequences: it explains the negative activation energies observed, and it also affects the rate constant calculations, as it determines the barrier height of the hydrogen-abstraction process and hence the value of the tunneling correction.

It is claimed in this study that the present results, together with those of Sekušak and Sabljić[12] and previous studies[11,13] have significant implications on the theory of transition states in general. In fact, it is well known that the reaction profile of any bimolecular reaction presents a minimum along the reaction coordinate, previous to the TS, which is commonly called the reactant complex, van der Waals complex or pre-reactive complex. This implies that, strictly speaking, in the gas phase there are no elementary bimolecular reactions, even though, in most cases, the possible formation of the complex is irrelevant. Nevertheless, the point corresponding to the reactant complex on the potential energy surface is especially important in radical-molecule reactions, many of which are known to occur with an apparent negative activation energy.

In the particular case of a reaction involving the migration of a hydrogen atom (or any other light particle for which tunneling must be considered), if the reactant complex is not considered, the height of the actual energy barrier is too small and the tunneling factor is underestimated, affecting the calculation of the rate constant. In the reactions studied both effects are present: a negative activation barrier and hydrogen atom migration.

4.5. References

1. Finlayson-Pitts, B.J.; Pitts, J.N. *Atmospheric Chemistry: Fundamentals and Experimental Techniques*, Wiley Interscience, New York, 1986.

2. Papagni, C.; Arey, J.; Atkinson, R. *Int. J. Chem. Kinet.* **2000**, *32*, 79.

3. The NIST Chemical Kinetics Database, NIST Standard Reference Database, U.S. Dept. of Commerce, Technology Administration, National Institute of Standards and Technology: Gaithersburg, MD, 17-2Q98.

4. (a) Horowitz, A.; Su, F.; Calvert, J.G. *Int. J. Chem. Kinet.* **1978**, *10*, 1099. (b) Atkinson, R.; Darnall, K.R.; Lloyd, A.C.; Winer, A.M.; Pitts, N.J.N., Jr. *Adv. Photochem.* **1979**, *11*, 375. (c) Michael, J.V.; Keil, D.G.; Klemm, R.B. *J. Chem. Phys.* **1985**, *83*, 1630.

5. Taylor, P.H.; Rahman, M.S.; Arif, M.; Dellinger, B.; Marshall, P. *Symp. Int. Comb. Proc.* **1996**, *26*, 497.

6. Niki, H.; Maker, P.D.; Savage, C.M.; Breitenbach, L.P. *J. Phys. Chem.* **1984**, *88*, 5342.

7. Butkovskaya, N.I.; Setser, D.W. *J. Phys. Chem. A* **1998**, *102*, 9715.

8. Atkinson, R. *J. Phys. Chem. Ref. Data* **1994**, Monograph 2, 1.

9. (a) Mozurkewich, M.; Benson, S.W. *J. Phys. Chem.* **1984**, *88*, 6429. (b) Mozurkewich, M.; Lamb, J.J.; Benson, S.W. *J. Phys. Chem.* **1984**, *88*, 6435. (c) Lamb, J.J.; Mozurkewich, M.; Benson, S.W. *J. Phys. Chem.* **1984**, *88*, 6441.

10. Singleton, D.L.; Cvetanovic, R.J. *J. Am. Chem. Soc.* **1976**, *98*, 6812.

11. (a) Sosa, C.; Schlegel, H.B. *J. Am. Chem. Soc.* **1987**, *109*, 4193. (b) Alvarez-Idaboy, J. R.; Díaz-Acosta, I.; Vivier-Bunge, A. *J. Comput. Chem.* **1998**, *88*, 811. (c) Sekušak, S.; Liedl, K.R.; Sabljić, A. *J. Phys. Chem. A* **1998**, *102*, 1583. (d) Díaz-Acosta, I.; Alvarez-Idaboy, J.R.; Vivier-Bunge, A. *Int. J. Chem. Kinet.* **1999**, *31*, 29. (e) Alvarez-Idaboy, J.R.; Mora-Diez, N.; Vivier-Bunge, A. *J. Am. Chem. Soc.* **2000**, *122*, 3715.

12. Sekušak, S.; Sabljić, A. *Chem. Phys. Lett.* **1997**, *272*, 353.

13. (a) Uc. V.H.; García-Cruz, I.; Hernández-Laguna, A.; Vivier-Bunge, A. *J. Phys. Chem.* **2000**, *104*, 7847. (b) Uc, V.H.; García-Cruz, I.; Vivier-Bunge, A. in *Quantum Systems in Chemistry and Physics*; Advanced Problems and Complex Systems, Vol. 2, Kluwer Academic Publishers: Great Britain, p. 241, 2000.

14.   (a) Atkinson, R.; Baulch, D.L.; Cox, R.A.; Hampson, R.F. Jr.; Kerr, J.A.; Rossi, M.J.; Troe, J. *J. Phys. Chem. Ref. Data* **1999**, *28*, 191. (b) Atkinson, R.; Baulch, D.L.; Cox, R.A.; Hampson, R.F., Jr.; Kerr, J.A.; Rossi, M.J.; Troe, J. *J. Phys. Chem. Ref. Data* **1997**, *26*, 521. (c) DeMore, W.B.; Sander, S.P.; Golden, D.M.; Hampson, R.F.; Kurylo, M.J.; Howard, C.J.; Ravishankara, A.R.; Kolb, C.E.; Molina, M.J. *JPL Publication* 97-4 **1997**. (d) Baulch, D.L.; Cobos, C.J.; Cox, R.A.; Esser, C.; Frank, P.; Just, Th.; Kerr, J.A.; Pilling, M.J.; Troe, J.; Walker, R.W.; Warnatz, J. *J. Phys. Chem. Ref. Data* **1992**, *21*, 411. (e) Yetter, R.A.; Rabitz, H.; Dryer, F.L.; Maki, R.G.; Klemm, R.B. *J. Chem. Phys.* **1989**, *91*, 4088. (f) Zabarnick, S.; Fleming, J.W.; Lin, M.C. *Int. J. Chem. Kinet.* **1988**, *20*, 117. (g) Tsang, W.; Hampson, R.F. *J. Phys. Chem. Ref. Data* **1986**, *15*, 1087. (h) Atkinson, R. *Chem. Rev.* **1986**, *86*, 69. (i) Stief, L.J.; Nava, D.F.; Payne, W.A.; Michael, J.V. *J. Chem. Phys.* **1980**, *73*, 2254. (j) Niki, H.; Maker, P.D.; Savage, C.M.; Breitenbach, L.P. *J. Phys. Chem.* **1978**, *82*, 132. (k) Atkinson, R.; Pitts, J.N., Jr. *J. Chem. Phys.* **1978**, *68*, 3581. (m) Morris, E.D., Jr.; Niki, H. *J. Chem. Phys.* **1971**, *55*, 1991.

15.   (a) Tyndall, G.S.; Staffelbach, T.A.; Orlando, J.J.; Calvert, J.G. *Int. J. Chem. Kinetics* **1995**, *27*, 1009. (b) Scollard, D.J.; Treacy, J.J.; Sidebottom, H.W.; Balestra-Garcia, C.; Laverdet, G.; LeBras, G.; MacLeod, H.; Teton, S. *J. Phys. Chem.* **1993**, *97*, 4683. (c) Balestra-Garcia, C.; LeBras, G.; Mac Leod, H. *J. Phys. Chem.* **1992**, *96*, 3312. (d) Dobe, S.; Khachatryan, L.A.; Berces, T. *Ber. Bunsenges. Phys. Chem.* **1989**, *93*, 847. (e) Semmes, D.H.; Ravishankara, A.R.; Gump-Perkins, C.A.; Wine, P.H. *Int. J. Chem. Kinet.* **1985**, *17*, 303. (f) Warnatz, J. *Combustion Chemistry*, W.C. Gardiner, Jr., Ed., Springer-Verlag, NY, 1984. (g) Kerr, J.A.; Sheppard, D.W. *Environ. Sci. and Technol.* **1981**, *15*, 960. (h) Morris, E.D., Jr.; Stedman, D.H.; Niki, H. *J. Am. Chem. Soc.* **1971**, *93*, 3570.

16.   Dupuis, M.; Lester Jr., W.A. *J. Chem. Phys.* **1984**, *81*, 847.

17.   Francisco, J.S. *J. Chem. Phys.* **1992**, *96*, 7597.

18.   Aloisio, S.; Francisco, J.S. *J. Phys. Chem. A* **2000**, *104*, 3211.

19.   Takahashi, H.; Hori, T.; Wakabayashi, T.; Nitta, T. *J. Phys. Chem. A* **2001**, *105*, 4351.

20.   Kleindiest, T.E.; Shepson, P.B.; Smith, D.F.; Hudgens, E.E.; Nero, C.M.; Cuppit, L.T.; Bufini, J.J.; Claxton, L.D. *Environ. Molecular Mutagen* **1990**, *16*, 70.

21.   (a) Scott, W.E.; Stephens, E.R.; Hanst, P.L.; Doerr, R.C. Paper presented at the 22nd Midyear Meeting of the American Petroleum Institute, Division of Refining, Philadelphia, Pennsylvania, May 14, 1957. (b) Temple, P.J.; Taylor, O.C. *Atmos. Environ.* **1983**, *17*, 1583.

22.   Eckart, C. *Phys. Rev.* **1930**, *35*, 1303; Shin, H. *J. Chem. Phys.* **1963**, *39*, 2934.

23.   Berkowitz, J.; Ellison, G.B.; Gutman, D. *J. Phys. Chem.* **1994**, *98*, 2744.

24.   Slagle, I.R.; Gutman, D. *J. Am. Chem. Soc.* **1982**, *104*, 4741.

25.   Alvarez-Idaboy, J.R.; Mora-Diez, N.; Boyd, R.J.; Vivier-Bunge, A. *J. Am. Chem. Soc.*, **2001**, *123*, 2018.

26.   Jursic, B.S. *J. Mol. Struct. (Theochem)* **1998**, *434*, 53.

27.   Atkinson, R.; Baulch, D.L.; Cox, R.A.; Hampson, R.F. Jr.; Kerr, J.A.; Troe, J. *J. Phys. Chem. Ref. Data* **1992**, *21*, 1125.

28.   Benson, S.W. *Thermochemical Kinetics*, 2nd Ed., Wiley & Sons, New York, p. 43, 1976.

29.   Chuang, Y-Y; Truhlar, D.G. *J. Chem. Phys.* **2000**, *112*, 1221.

30.   Benson, S.W.; Dobis, O. *J. Phys. Chem. A* **1998**, *102*, 5175.

Chapter 5. OH Hydrogen-Abstraction from FCHO and ClCHO

5.1. Introduction

Earlier experimental and theoretical studies on reactions between OH radicals and aldehydes have been performed.[1,2] In an earlier study[3] described in Chapter 4, the OH hydrogen-abstraction reaction from formaldehyde and acetaldehyde was examined. A complex mechanism in which the overall rate depends on the rates of two competitive reactions: a reversible step where a reactant complex is formed, followed by the irreversible hydrogen abstraction to form the products was considered. TST was applied for the calculation of the rate constants with successful results. Tunneling corrections were incorporated assuming an unsymmetrical Eckart barrier.

Consideration of the reactant complex formation has two important consequences in the kinetics calculations of these systems. It explains the negative activation barriers observed (especially for acetaldehyde) and it also affects the rate constant calculations, as it determines the barrier height of the hydrogen-abstraction process and hence the value of the tunneling correction. In view of the previous successful results, it was decided to extend these ideas to the OH hydrogen-abstraction reaction from FCHO and ClCHO, for which only experimental upper-bound rate constants have been reported and for which activation energy values are unknown.[1a,4,5]

Formyl fluoride (FCHO), one of the halogenated molecules in the upper stratosphere, is a major product of the degradation in the troposphere of CH_3CFH_2 (HFC-134a).[6] It is also a product of the subsequent dissociation of fluorinated radicals that originate in the atmosphere. Formyl chloride (ClCHO) is a reactive molecule that forms as an atmospheric degradation intermediate of several chlorinated hydrocarbons such as: CH_3Cl, CH_2Cl_2, $CHCl_3$, and hydrochlorofluorocarbons (HCFCs),[7] as well as from the tropospheric reaction of Cl atoms with volatile organic compounds such as isoprene.[8] The

reaction of FCHO and ClCHO with OH radicals is thought to be a tropospheric removal route for these compounds.

The OH reaction with the substituted aldehydes of interest was first examined theoretically by Francisco[9] in 1992. Activation energies and heats of reaction were estimated at the PMP4SDTQ(FC)/6-311++G(d,p)//MP2/6-311G(d,p) level. Vibrational frequencies were calculated at the HF/6-31G(d) level. TST was also employed for the rate-constant calculation and tunneling corrections were considered, assuming an unsymmetrical Eckart barrier. These reactions were considered to be elementary. The results obtained in the previous work will be shown together with the new data reported here, for comparison.

A DFT study on the FCHO + OH reaction was performed by Jursic,[10] who used hybrid functionals (B3LYP, B3P86 and B3PW91) to estimate the heat of reaction and the activation energy.

In the present study high-level *ab initio* calculations are performed to investigate the OH hydrogen-abstraction reaction from FCHO and ClCHO. In addition, TST is applied to the calculation of the rate constants and tunneling corrections are considered. The aim of this study is to show that the same complex mechanism can be applied to these reactions and to provide better theoretically-determined kinetics parameters.

5.2. Computational details

Geometries were optimized at the MP2(FC)/6-311++G(d,p) level. Energies at the CCSD(T)/6-311++G(d,p) level were calculated using the MP2 geometries. This is the same level of theory at which the reactions of HCHO and CH_3CHO with OH radicals were characterized.[3] The same two mechanisms previously considered in Chapter 4 will be taken into account in this study. TST with Eckart tunneling corrections will be applied for the calculation of the rate constants.

For the reactions under study the tunneling correction (κ) is the only factor that allows the quantitative differentiation between the two proposed mechanisms. It has been shown previously[3] that for the HCHO and CH$_3$CHO reactions with OH the present combination of methods (with all the approximations they imply) reproduce correctly the experimental kinetic parameters of these reactions. This fact demonstrates that the approximations are reasonable and that they can be used to predict similar kinetic parameters in reactions between the same kinds of compounds. The validity of this statement will be shown in the present study.

5.3. Results and discussion

The OH radical attack on FCHO and ClCHO seems to occur in a very similar way as described previously[3] for HCHO and CH$_3$CHO. The MP2 optimized geometries of the intermediate structures along the hydrogen-abstraction pathway are shown in Fig. 5.1 (FCHO + OH) and 5.2 (ClCHO + OH), where relevant geometrical parameters have been indicated. The reaction profiles for these four reactions (the results for the reactions with HCHO and CH$_3$CHO are included for comparison) using CCSD(T)/6-311++G(d,p) energies are shown in Fig. 5.3.

The reactant complexes for the FCHO + OH and ClCHO + OH reactions are calculated to be between 10 and 11 kJ/mol lower in energy than the isolated reactants, at 0 K. At 298 K their stabilization energies decrease by 2 kJ/mol. The structures of these complexes (Fig. 5.1a and 5.2a) are very similar to those calculated for the reactions with HCHO and CH$_3$CHO (Fig. 4.1), and are determined by dipole-dipole interactions, or more specifically by hydrogen bonding. The interaction established between the carbonylic oxygen atom and the hydrogen atom of the OH radical becomes weaker as the electron-withdrawing effect of the substituent increases (in the series: CH$_3$, H, Cl, and F) because this effect reduces the electronic density on the oxygen atom of the aldehyde. As a result, the distance between the carbonylic oxygen and the hydroxyl hydrogen in the complex increases from 1.947 Å in CH$_3$CHO$\cdots$OH to 2.136 Å in FCHO$\cdots$OH, and its stabilization energy is reduced. Consequently, the reactant complex of the FCHO + OH reaction is the least stable.

(a) FCHO···HO

2.136

3.111

(b) FCO···H···OH

171.3

1.214

1.273

(c) FCO···H₂O

3.399

2.742

3.252
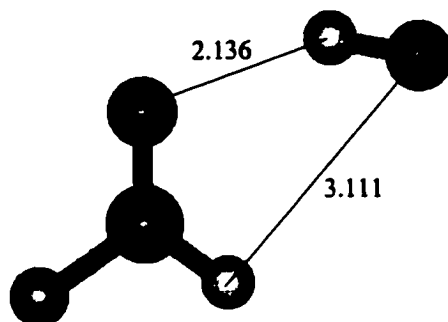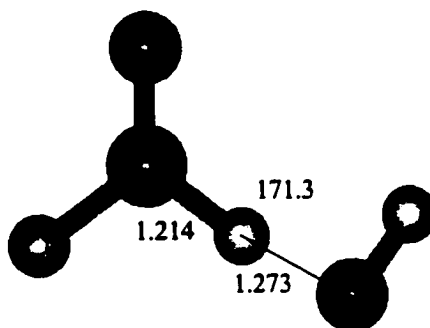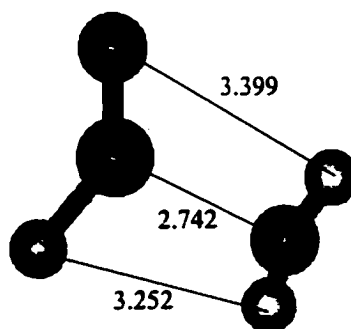
Figure 5.1. Optimized structures of the FCHO + OH hydrogen-abstraction reaction
(a) Reactant complex, (b) TS and (c) Product complex.
(Bond distances are given in Å and angles in degrees)

(a) ClCHO···HO
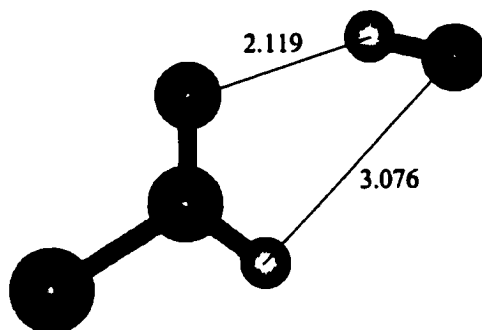
(b) ClCO···H···OH
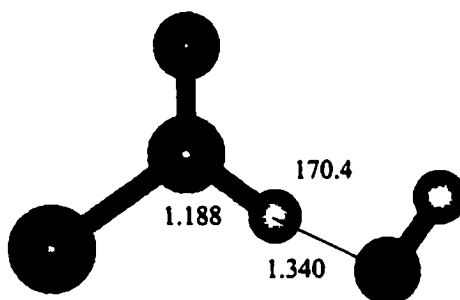
(c) ClCO···H₂O
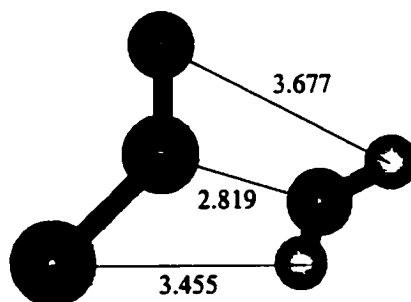
Figure 5.2. Optimized structures of the ClCHO + OH hydrogen-abstraction reaction
(a) Reactant complex, (b) TS and (c) Product complex.
(Bond distances are given in Å and angles in degrees)

$$XCHO + OH \longrightarrow XCO + H_2O \quad (X = F, Cl, H, CH_3)$$
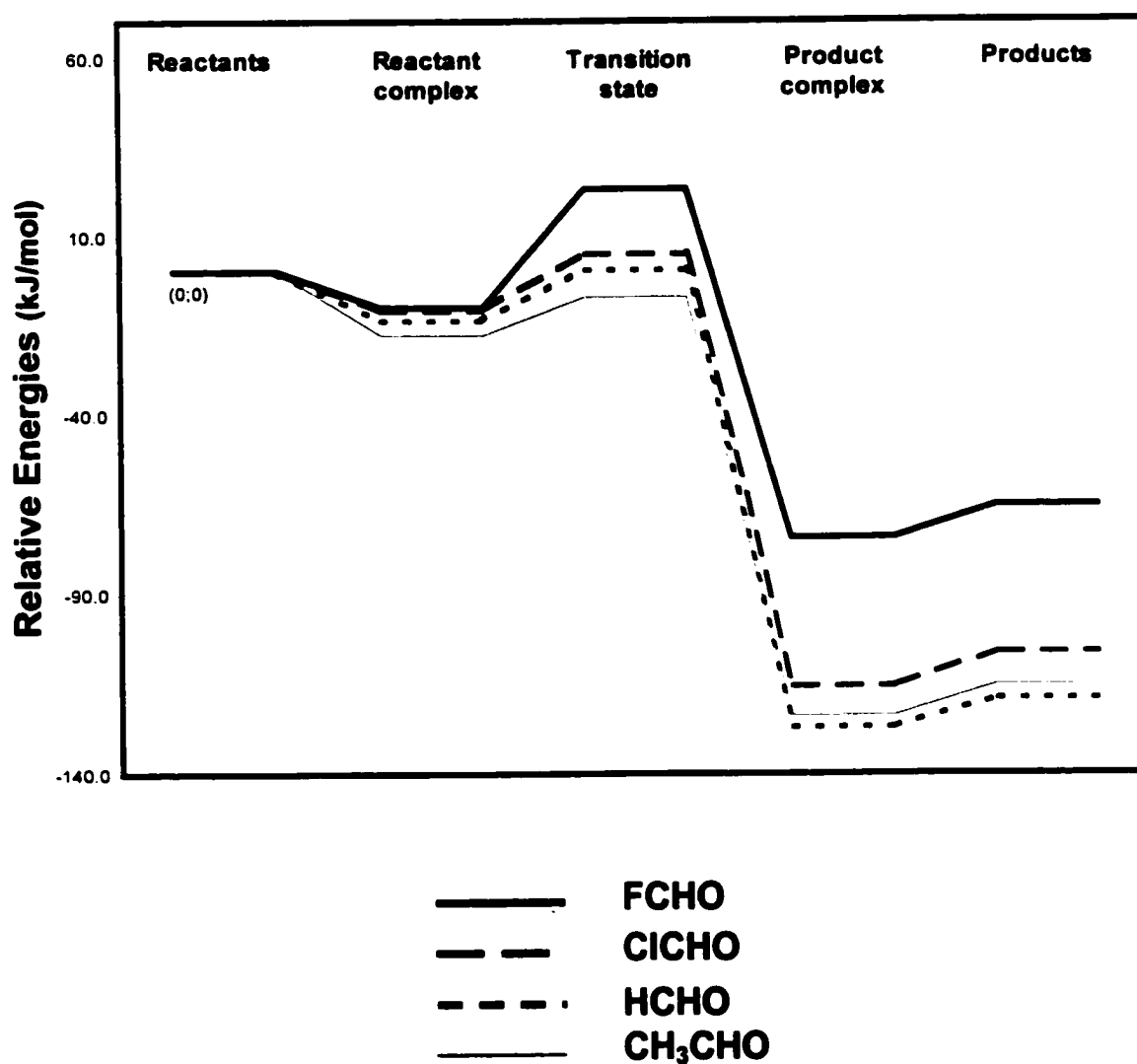
Figure 5.3. Schematic reaction profiles for the XCHO + OH (X = F, Cl, H, CH₃) hydrogen-abstraction reactions using the calculated CCSD(T)/6-311++G(d,p) energy values, including the MP2(FC)/6-311++G(d,p) zero-point energy corrections.

The symmetry of the TS for the OH reaction with FCHO and ClCHO is $^2A'$, implying that the unpaired electron is in the plane where the OH attack takes place. $^2A'$ is also the symmetry of the XCO radical generated.

The C···H and H···O distances in the TS (Fig. 5.1b and 5.2b) can be used to rationalize the electronic effects of these substituents (F and Cl) on the kinetics. The TS in the case of ClCHO is formed earlier since the C···H distance is smaller (and the O···H distance is larger). It resembles more closely the reactants and is consistent with the fact that Cl is less electron-withdrawing than F, and the electronic density at the carbonylic carbon is less reduced in ClCHO than in FCHO. Consequently, the abstraction of the hydrogen atom in ClCHO is more favoured since the TS is more stable and a smaller activation energy barrier is found (Fig. 5.3). The same reasoning explains why the radical product generated in the ClCHO reaction is more stable, and also explains the greater endothermicity of this reaction in comparison to that of the FCHO reaction.

In the series of substituents, CH₃, H, Cl and F, the TS is achieved later (the C···H distances in the case of CH₃CHO and HCHO are 1.171 and 1.177 Å, respectively, see Fig. 4.2) and a larger activation energy must be overcome. This trend is consistent with the decreasing electron-donating effect of these substituents that is also the cause for the decreasing reactivity of these aldehydes towards the OH hydrogen-abstraction reaction.

As the electron-withdrawing effect of the substituent (when going from CH₃ to F) increases, the activation energy of these reactions increases while the enthalpy of reaction and the stabilization energy of the reactant complex decreases.

A full discussion and tabulation of the geometrical information regarding the reactants and products of the reactions studied is not included because at the levels of theory used no significant differences were found with respect to the calculations reported by Francisco.[9]

The Cartesian coordinates of the optimized structures along the reaction pathway for the systems under study, as well as the calculated PMP2 and CCSD(T) total energies, zero-point and thermal (at 298.15 K) vibrational energy corrections (calculated at the MP2 level) of the species involved in the reaction of OH with FCHO and ClCHO, are available.[11]

For these reactions spin contamination is only significant (but small) at the TS: the expectation value of S^2 is 0.785 for the FCHO reaction and 0.780 for ClCHO, and in the MP2 calculation it is completely eliminated by projection. Hence, reliable results are expected when applying the CCSD(T) method to an MP2 optimized geometry.

The stabilization energy of the reactant complexes $(E_{a\,(-1)})$, the activation barriers of the second step of the complex mechanism $(E_{a\,(2)})$ and the effective activation energies (E_a^{eff}), calculated according to equation (4.4), are given in Table 5.1 at 0 K together with the reaction enthalpies, for the methods employed. Effective activation energies and stabilization energies of the reactant complexes at 298.15 K have also been included. Values previously calculated or measured are shown for comparison. The MP2 vibrational corrections were used to obtain the CCSD(T) energy differences.

The stabilization energies of the reactant complexes agree to within 0.5 kJ/mol in both cases with the two methods used. Based on the results obtained for the HCHO and CH₃CHO reactions,[3] the PMP2 effective activation energies should be overestimated and the best values should be the ones given by the CCSD(T) method. The effective activation energies calculated are 23.1 and 5.0 kJ/mol for the FCHO + OH and ClCHO + OH reactions, respectively. The MP4 energy parameters (activation energies and enthalpies of reaction) reported by Francisco[9] fall between the PMP2 and CCSD(T) results. His values at 298 K are between 4.7 and 7.0 kJ/mol larger than the CCSD(T) effective energy barriers calculated.

Table 5.1. Relevant barriers (E_a) and reaction enthalpies (ΔH), in kJ/mol, including zero-point vibrational corrections (ZPE), unless otherwise specified, for the OH hydrogen-abstraction reaction from FCHO and ClCHO.

Basis set: 6-311++G(d,p)	$E_{a(-1)}$	$E_{a(-1)}^{(b)}$	$E_{a(2)}$	E_a^{eff}	$E_a^{eff\,(b)}$	ΔH	$\Delta H^{(b)}$
FCHO + OH							
PMP2	9.5	7.6	39.5	30.0	29.8	-83.9	-82.7
CCSD(T)	10.0	8.0	33.1	23.1	23.0	-65.2	-64.0
Previous calculations [a]				25.1	27.7	-72.8	
[c]						-69.0, -71.1, -73.6	
Experiment [d]							-60.1
ClCHO + OH							
PMP2	10.1	8.2	25.5	15.4	15.2	-125.3	-123.8
CCSD(T)	10.6	8.7	15.6	5.0	4.8	-105.9	-104.4
Previous calculations [a]				9.6	11.8	-115.9	

[a] Ref. 9 (1992); [b] Including thermal correction (TCE) at 298.15 K; [c] Ref. 10 (1998); [d] Ref. 1a (1997)

The DFT barriers calculated by Jursic[10] for the FCHO + OH reaction are zero or negative, which shows the inability of DFT methods to predict the activation energy for this reaction. However, on the basis of calculations performed for a similar reaction with DFT and CCSD(T) methods, he estimated an activation energy of about 21 kJ/mol, in good agreement with the new calculations.

The best value for the heat of reaction of the FCHO + OH system is the one obtained from the CCSD(T) energies. It is -65.2 kJ/mol at 0 K and -64.1 at 298 K, in very good

agreement with the experimental value of –60.1 kJ/mol. The heat of reaction calculated for the ClCHO reaction is -105.9 kJ/mol at 0 K, and –104.5 at 298 K.

The values of the partition functions needed for the calculation of the rate constants of the reactions studied are given in Table 5.2, as well as the imaginary frequency of the TS. Three low frequencies (below 210 cm^{-1}) in addition to the imaginary frequency were calculated for the hydrogen-abstraction TS. Of these, two were identified as internal rotations (or torsional vibrations) by visualization of the normal modes: frequencies 1 and 3 for the FCHO–TS and frequencies 2 and 3 for the ClCHO–TS. These harmonic modes correspond most closely to the two new internal rotors created in the TS (XCOH···OH and XCO···HOH), where the common axes for internal rotation are the ones linking the reactants and products, respectively, and were the axes considered in the calculation of the reduced moments of inertia. These harmonic modes were treated as free rotors in the calculation of the internal-rotation partition function of the TS (Q_{IR}^{TS}).[12,13]

The harmonic contributions of these two low frequencies were eliminated from the vibrational partition function in order to correct the total partition function of the TS (Q_{corr}^{TS}). For the OH reaction with FCHO, Q_{corr}^{TS} is calculated as:

$$Q_{corr}^{TS} = \frac{Q^{TS} \ Q_{IR}^{TS}}{Q_{v=1} \ Q_{v=3}}$$

(5.1)

For the reaction with ClCHO, Q_{corr}^{TS} is calculated in a very similar way except that the vibrational components of frequencies 2 and 3 are the ones considered. This was also the procedure followed in the calculation of the internal-rotational partition function of the TS for the OH hydrogen-abstraction reaction from HCHO and CH$_3$CHO.

Inspection of the vibrational mode corresponding to the imaginary frequency of the TS of these reactions shows that this vibration can be approximated by the simple movement of a light atom (H) between two fixed heavier atoms (C and O). There is little heavy atom motion as the system moves along the reaction path.

Table 5.2. Total partition functions (Q) of the reactants and the TS, and imaginary frequency (v* in cm⁻¹) of the TS of the OH hydrogen-abstraction reaction from FCHO and ClCHO, calculated at the MP2(FC)/6-311++G(d,p) level.

System	FCHO + OH	ClCHO + OH
Q^{OH}	$6.02509 \cdot 10^7$	$6.02509 \cdot 10^7$
Q^{XCHO}	$1.14742 \cdot 10^{11}$	$3.87097 \cdot 10^{11}$
Q^{TS}	$3.64161 \cdot 10^{13}$	$8.57899 \cdot 10^{13}$
$\prod Q_{v=i}$ [a]	4.827 [e]	3.828 [f]
Q_{IR}^{TS} [b]	50.449	54.772
Q_{corr}^{TS} [c]	$3.80628 \cdot 10^{14}$	$1.22747 \cdot 10^{15}$
v^*	2455	1939
v^* [d]	3482	3535

[a] Vibrational components that were eliminated from the calculation of Q_{corr}^{TS}; [b] Total internal-rotational partition function of the TS; [c] Corrected total partition function of the TS; [d] Ref. 9 (HF/6-31G(d)); [e] i=1, 3; [f] i=2, 3

The best values for the activation energies and the rate constants for the reactions of HCHO and CH₃CHO with OH radicals were obtained with the CCSD(T) method using MP2 geometries. Therefore, the same level of theory has been used in the present study. The results of the rate constant calculations for the reactions of FCHO and ClCHO with OH radicals, at 298 K using the CCSD(T)/6-311++G(d,p) energy values are given in Table 5.3, for both the direct (k_D) and complex (k_eff) reaction mechanisms. Experimental upper bounds and the results calculated by Francisco[9] have been included for comparison. The tunneling corrections (κ) and the full width of each barrier at half its height (Δs½) have also been reported in Table 5.3.

Table 5.3. Rate constants and tunneling parameters for the OH hydrogen-abstraction reaction from FCHO and ClCHO, calculated using CCSD(T)/6-311++G(d,p)//MP2(FC)/6-311++G(d,p) energies that include zero point corrections, for both the direct and complex mechanisms at 298.15 K.

	FCHO + OH	ClCHO + OH
Direct Mechanism		
κ	70.12	2.60
$\Delta s_{1/2}$ (Å)	0.24	0.15
k_D (L/mol·s)	$2.10 \cdot 10^6$	$1.12 \cdot 10^8$
Complex Mechanism		
κ	244.30	12.10
$\Delta s_{1/2}$ (Å)	0.29	0.26
k_{eff} (L/mol·s)	$7.33 \cdot 10^6$	$5.21 \cdot 10^8$
Experiment		
k (L/mol·s)	$< 6.03 \cdot 10^6$ [a]	$< 3.01 \cdot 10^8$ [a]
	$< 2.41 \cdot 10^6$ [b]	$< 1.93 \cdot 10^8$ [c]
Previous Calculation [d]		
κ	13.83	16.26
k (L/mol·s)	$4.03 \cdot 10^5$	$1.89 \cdot 10^8$

[a] Ref. 1a (1997); [b] Ref. 4 (1993); [c] Ref. 5 (1990); [d] Ref. 9 (1992)

If the rate constant (all the rate constant values reported henceforth are expressed in units of Lmol^{-1}s^{-1}) is calculated according to the complex mechanism, tunneling factors (κ) of 244.30 (FCHO) and 12.10 (ClCHO) are obtained, and the effective rate constants are $7.33 \cdot 10^6$ (FCHO) and $5.21 \cdot 10^8$ (ClCHO), in very good agreement (just slightly greater) with the most recent upper-bound limits of $6.03 \cdot 10^6$ (FCHO) and $3.01 \cdot 10^8$ (ClCHO) reported by Atkinson *et al.*[1a] If an elementary mechanism is assumed, smaller tunneling factors are calculated (70.12 for FCHO and 2.60 for ClCHO) as expected, since the forward and reverse potential energy barriers of the elementary process in which the

hydrogen atom is abstracted are both reduced, but the forward barrier is reduced to a greater extent, and as a consequence, the direct rate constants are smaller ($2.10 \cdot 10^6$ for FCHO and $1.12 \cdot 10^8$ for ClCHO) than the effective rate constants. These values are in very good agreement (just slightly smaller) with the first reported upper-bound limits ($2.41 \cdot 10^6$ for FCHO[4] and $1.93 \cdot 10^8$ for ClCHO[5]). From the first experimental measurements[4,5] on these systems in 1990 and 1992, to the latest experimental results in 1997,[1b] the upper-bound limit reported for the rate constants has increased. Moreover, the values in best agreement with the latest experimental results are the ones obtained by considering a complex mechanism.

The rate constant reported by Francisco[9] for the ClCHO + OH reaction ($1.89 \cdot 10^8$) is in very good agreement with the first upper-bound value reported for this reaction, but the author's result for the FCHO + OH system is an order of magnitude smaller ($4.03 \cdot 10^5$). This discrepancy may be a consequence of the calculation of the tunneling factor. The energy barriers calculated by Francisco as well as the imaginary frequency of the TS (see Table 5.2) are greater than the new values reported in the present study, in accordance with the methods employed by the author. Hence, Francisco's tunneling factors (13.83 for FCHO and 16.26 for ClCHO) should be greater than the values reported for the direct mechanism, but that is not the case. Tunneling factors of 397.40 and 11.88 for the FCHO + OH and ClCHO + OH reactions, respectively, were calculated using the previously-mentioned program. An unsymmetrical Eckart barrier was assumed, with the forward and reverse potential energy barriers and the imaginary frequency of the TS reported by Francisco. Furthermore, the tunneling corrections reported by the author[9] decrease as the activation barriers increase (for the reactions of HCHO, ClCHO and FCHO with OH radicals) but the opposite is expected.[14]

Consideration of the results obtained for the direct and effective rate constants of the reactions with positive effective activation energies among the four reactions studied, indicates that it is possible to estimate the percentage by which these two rate constants differ due to an increase of the effective activation energy. The data in Table 5.4 shows

that the greater the effective activation energy (when going from HCHO to FCHO) the smaller the difference between the calculated rate constants. This shows that even for FCHO the discrepancy between considering an elementary or complex mechanism to describe the kinetics of its reaction with OH radicals is still significant. This difference tends to be reduced as the activation energy increases and the stabilization energy of the reactant complex decreases.

Table 5.4. Estimate of the difference between the effective and direct rate constants for the aldehyde + OH reactions studied with positive effective activation energies.

Adehyde + OH	$\left(\dfrac{k_{eff} - k_D}{k_{eff}}\right) \cdot 100\%$
HCHO	82.4
ClCHO	78.5
FCHO	71.3

5.4. Conclusions

The significance of considering the complex character of the kinetics of a radical-molecule reaction was shown in Chapter 4.[3] This chapter has focused on the reaction of OH with FCHO and ClCHO, systems for which there is very little experimental information available (only upper-bound limit rate constants).

By applying the same methodology it has been shown that the same complex mechanism considered for the reactions from HCHO and CH₃CHO can be applied to the OH hydrogen-abstraction reaction from FCHO and ClCHO, and furthermore (effective) activation energies and rate constants have been calculated successfully. The rate constants calculated in this study are in better agreement with experiment than previous

calculations performed on these reactions. Hence better activation energies and reaction enthalpies have been reported for which there is no experimental data.

It can also be rationalized from these results that the bigger the effective energy barrier for radical-molecule reactions, and the smaller the stabilization energy of the reactant complex, the more closely its behaviour resembles an elementary reaction. In other words, if the mechanism and the rate constant of another aldehyde much less reactive than FCHO, such as, perhaps, CF_3CHO, were to be calculated, the formation of the reactant complex could probably be ignored, since its consideration would provide no new qualitative or quantitative information about the mechanism. Hence, the assumption of an elementary mechanism should give similar results to those obtained by considering a complex mechanism.

Two extreme behaviours can be considered for a radical-molecule reaction: for systems with very low or negative activation energies the consideration of a complex mechanism is essential, but if the activation energy is significantly higher and the stabilization energy of the reactant complex is negligible, then the consideration of an elementary process is a satisfactory approximation.

5.5. References

1. (a) Atkinson, R.; Baulch, D.L.; Cox, R.A.; Hampson, R.F., Jr.; Kerr, J.A.; Rossi, M.J.; Troe, J. *J. Phys. Chem. Ref. Data* **1997**, *26*, 521. (b) DeMore, W.B.; Sander, S.P.; Golden, D.M.; Hampson, R.F.; Kurylo, M.J.; Howard, C.J.; Ravishankara, A.R.; Kolb, C.E.; Molina, M.J. *JPL Publication* 97-4 **1997**. (c) Taylor, P.H.; Rahman, M.S.; Arif, M.; Dellinger, B.; Marshall, P. *Symp. Int. Combust. Proc.* **1996**, *26*, 497, and references therein.

2. The NIST Chemical Kinetics Database, NIST Standard Reference Database, U.S. Dept. of Commerce, Technology Administration, National Institute of Standards and Technology: Gaithersburg, MD, 17-2Q98.

3. Alvarez-Idaboy, J.R.; Mora-Diez, N.; Boyd, R.J.; Vivier-Bunge, A. *J. Am. Chem. Soc.* **2001**, *123*, 2018.

4. Wallington, T.J.; Hurley, M.D. *Environ. Sci. Technol.* **1993**, *27*, 1448.

5. Libuda, H.G.; Zabel, F.; Fink, E.H.; Becker, K.H. *J. Phys. Chem.* **1990**, *94*, 5860.

6. (a) Wallington, T.J.; Hurley, M.D.; Ball, J.C.; Kaiser, E.W. *Environ. Sci. Technol.* **1992**, *26*, 1318. (b) Hasson, A.S.; Moore, C.M.; Smith, I.W.M. *Int. J. Chem. Kinet.* **1998**, *30*, 541.

7. (a) Sanhueza, E.C.; Heicklen, J. *J. Phys. Chem.* **1975**, *79*, 7. (b) Gay, B.W.; Hanst, P.L.; Bufalini, J.J.; Noonan, R.C. *Environ. Sci. Technol.* **1976**, *10*, 58. (c) Niki, H.; Maker, P.D.; Savage, C.M.; Breitenbach, L.P. *Int. J. Chem. Kinet.* **1980**, *12*, 1001. (d) Niki, H.; Maker, P.D.; Savage, C.M.; Breitenbach, L.P.; Martinez, R.I.; Herron J.T. *J. Phys. Chem.* **1982**, *86*, 1858. (e) Tuazon, E.C.; Atkinson R.; Aschmann, S.M.; Goodman, M.A.; Winer, A.M. *Int. J. Chem. Kinet.* **1988**, *20*, 241.

8. Fantechi, G.; Jensen, N.R.; Saastad, O.; Hjorth, J.; Peeters, J. *J. Atmos. Chem.* **1998**, *31*, 247.

9. Francisco, J.S. *J. Chem. Phys.* **1992**, *96*, 7597.

10. Jursic, B.S. *J. Mol. Struct. (Theochem)* **1998**, *434*, 53.

11. Mora-Diez, N.; Alvarez-Idaboy, J.R.; Boyd, R.J. *J. Phys. Chem.*, **2001**, in press.

12. Benson, S.W. *Thermochemical Kinetics*, 2nd Ed., Wiley & Sons, New York, p. 43, 1976.

13. Chuang, Y-Y; Truhlar, D.G. *J. Chem. Phys.* **2000**, *112*, 1221.

14. Johnston, H.S. *Gas Phase Reaction Rate Theory*, Ronald Press Company, New York, 1966.

Chapter 6. NO₃ Hydrogen-Abstraction from Aldehydes

6.1. Introduction

The consequences of the emission of aldehydes into the atmosphere or their formation in the troposphere from the decomposition or oxidation of other pollutants have been the object of several experimental and theoretical studies.[1] It is well known that during the daytime the photolysis of aldehydes and their reaction with OH radicals are the most probable processes.

The OH radical is the key species in the chemistry of the daytime troposphere. Since it is the most important oxidant, practically all organic and inorganic compounds are transformed by reaction with OH. The hydroxyl radical is formed mainly from three routes: the photolysis of O_3 and HONO, and from the reaction between HO_2 and NO (the most important source under noon-time conditions). In the absence of sunlight the OH radical concentration in the troposphere is very low.[2]

Numerous studies of the reaction of OH with aldehydes have been performed, both experimentally and theoretically.[3,4] Very recent theoretical studies[5] showed the importance of considering the formation of a reactant complex in the kinetics of the OH hydrogen-abstraction reaction from a series of aldehydes (XCHO: X = F, Cl, H, CH₃) at the level of theory chosen (geometries and energies were calculated at the MP2(FC) and CCSD(T) levels of theory, respectively, using the 6-311++G(d,p) basis set). The importance of aldehydes in the chemistry of the polluted atmosphere has been explained elsewhere.[3,5,6] TST[7] was applied successfully in the calculation of the rate constants. These calculations considered a complex mechanism in which the overall rate depends on the rates of two competitive reactions: a reversible step where a reactant complex is formed, followed by the irreversible hydrogen abstraction to form the products. Tunneling corrections were incorporated assuming an unsymmetrical Eckart barrier.[8]

Nitrate radicals were first detected in the stratosphere in 1978[9] and two years later were observed in the troposphere.[10] This free radical, as well as the OH radical, is a strong oxidizing agent and reacts with a number of atmospheric species.[11] The reaction of NO_3 radicals with atmospheric organic molecules can lead to the formation of undesirable compounds such as: HNO_3,[12] peroxyacyl nitrates (PANs)[13] and dinitrates.[14] The only primary source of NO_3 in the troposphere requires the simultaneous presence of NO_2 and O_3 in the same airmass,[2] but during the daytime NO_3 radicals photolize rapidly, thus its presence in the troposphere is only significant at night. Measurements made over the past 15 years show nighttime NO_3 concentrations near ground level over continental areas ranging up to $1.7 \cdot 10^{-4}$ mol L^{-1} ($1.0 \cdot 10^{10}$ molecule cm^{-3}).[11]

At night, NO_3 radicals play the same role as do OH radicals during the day.[15] Thus we should expect the reaction with NO_3 radicals to be an important nighttime tropospheric removal route for aldehydes, as has already been mentioned elsewhere.[16] The reaction of NO_3 radicals with unsaturated organic compounds (alkenes, halogenated alkenes, alcohols, terpenes) is also known to represent an important sink for these species in the nighttime troposphere, and a number of experimental and theoretical studies have been performed in this direction.[17] Experimental studies on the reaction between alkanes, aliphatic alcohols and ethers with NO_3 radicals have also been performed.[14,18]

There have been fewer kinetic studies on the reactions of NO_3 with aldehydes than on the corresponding reactions with OH radicals. This situation may be due to the differences in the reactivities of these two oxidant radicals, among other factors, as discussed below. Several experimental kinetic studies on the reactions between NO_3 radicals and aliphatic aldehydes (C_1-C_4, and certain C_5 and C_6 aldehydes, among others)[16a,19] have been performed although most of the activation energies and Arrhenius pre-exponential factors have not been reported. According to the NIST chemical kinetics database,[4] before the second half of 1998 the activation energy of the NO_3 reaction with CH_3CHO was the only one determined. Rate constants have been reported for HCHO and CH_3CHO,[3a,b,c,20,21] but no kinetic data is available for FCHO and ClCHO. Furthermore,

no previous theoretical determinations of the kinetic parameters for NO_3 reactions with aldehydes have been published.

Due to the lack of kinetic information concerning the reaction of NO_3 with aldehydes, it was decided to extend the previous studies[5] on the reactions with OH radicals to the NO_3 hydrogen-abstraction reactions with the same series of aldehydes:

$$\underset{\underset{X}{|}}{\overset{O}{\underset{\|}{C}}}\underset{H}{\diagdown} \quad + \quad {}^\bullet NO_3 \quad \longrightarrow \quad \underset{X}{\overset{O}{\underset{\|}{C}}}{}^\bullet \quad + \quad HNO_3$$

(XCHO: X = F, Cl, H, CH₃)

Previous calculations on the reaction of formaldehyde with OH[5a] show why the addition reaction of OH to the carbonylic double bond does not occur. Since the NO_3 radical is less reactive than the OH radical we should not expect the addition reaction of NO_3 to be of any importance. The abstraction mechanism has also been confirmed on the basis of the non-detection of NO_2 in the product mixture of the reaction and also because of the positive temperature dependence.[21b]

In the present study high-level *ab initio* calculations are performed to investigate the NO_3 hydrogen-abstraction reaction from FCHO, ClCHO, HCHO and CH_3CHO. In addition, TST is applied to the calculation of the rate constants and tunneling corrections are considered. The purpose of this study is to provide accurate theoretically determined kinetic parameters for these reactions.

6.2. Computational details

Geometries were optimized at the MP2(FC) and BH&HLYP[22] levels. Energies at the CCSD(T) level were calculated using the previous geometries and in all cases the 6-311G(d,p) basis set was used.

In Chapter 4,[5a] CCSD(T) energies obtained from MP2(FC) geometries using the 6-311++G(d,p) basis set were sufficient to reproduce experimental activation energies and rate constants for the reaction of OH radicals with HCHO and CH₃CHO. A later study on the HCHO + OH system,[23] that contains a comparative discussion on the performance of different levels of theory (MP2, MP4, B3LYP, BH&HLYP), showed that the CCSD(T)//MP2(FC) (the basis set will be omitted from this notation for simplicity) selection of methods gives the best results for this system and that the inclusion of diffuse functions on the hydrogen atoms does not change the results significantly. BH&HLYP, combined with a CCSD(T) single point calculation, works better for this system than the other hybrid DFT method, B3LYP. CCSD(T)//B3LYP barriers are too low, resulting in rate constants greater than expected. In addition, it should be mentioned that in previous studies[24] with DFT methods it was concluded that BH&HLYP is the best functional to characterize TS structures, vibrational frequencies and classical barrier heights for several reactions, including some hydrogen transfer processes. Furthermore, the addition of diffuse or polarization functions to the 6-311G(d,p) basis set has been shown to be unimportant.[24b] Therefore for the NO₃ reactions diffuse functions were not included in the basis set.

For reasons discussed below, the reactions were assumed to occur in a one-step mechanism:

$$XCHO + NO_3 \xrightarrow{\ k_D\ } XCO + HNO_3 \qquad (X = F, Cl, H, CH_3)$$

According to TST, the expression to calculate the direct rate constants, k_D, can be written as:

$$k_D = \kappa_D \ \frac{k_B T}{h} \ \frac{Q^{TS}}{Q^{React}} \ \exp\left(-\frac{\left(E^{TS} - E^{React}\right)}{RT}\right) \qquad (6.1)$$

The tunneling factor and $\Delta s_{\frac{1}{2}}$ were calculated by assuming an unsymmetrical Eckart barrier.[8]

6.3. Results and discussion

6.3.1. The NO₃ radical

There is a great deal of conflicting evidence both experimental and theoretical as to the ground electronic state and geometry of NO_3.[15] While the experimental evidence[16b,25] suggests a D_{3h} equilibrium ground state, quantum chemical studies are divided between D_{3h}[26] and C_{2v}[27] (or even C_s), depending on the applied method. Two C_{2v} structures have been considered in the theoretical calculations and these have been previously denoted as 1L2S and 1S2L,[27b] according to the number of short (S) and long (L) NO bonds. Discrepancies between these predictions are partly due to the inherent difficulties of treating NO_3 properly, since it is an open-shell molecule with partial double bonds and low-lying excited electronic states.

Several CC calculations of different types have led to contradictory results for the NO_3 ground-state equilibrium geometry. A Fock space multireference CCSD (FSMR-CCSD) calculation yielded the symmetric D_{3h} structure as the global minimum on the potential surface,[26g,h] whereas a quasirestricted Hartree-Fock CCSD (QHF-CCSD) calculation generated a C_{2v} (1L2S) ground state;[27c] the same result was obtained with Brueckner orbitals.[27a] In contrast, by including triple excitations in single-point calculations, the global minimum was found to be of D_{3h} symmetry.[26f]

A very interesting study on symmetry breaking and its effects on the potential surface of NO_3 was recently performed by Eisfeld and Morokuma.[26a] The authors refer to the symmetry breaking[28] of the electronic HF wavefunction as a problem frequently encountered in systems of high nuclear symmetry (see Section 2.5.2). This phenomenon leads to three different solutions for the ground electronic state of NO_3, corresponding to equilibrium geometries that are not connected on the same potential energy surface. Eisfeld and Morokuma's study concludes that the effective equilibrium geometry of the NO_3 radical is D_{3h}. Their calculations, performed at the MR-SDCI level with selected electronic configurations and an N-electron basis of CASSCF orbitals, showed that even CCSD and CCSD(T) cannot completely overcome the symmetry breaking of the

reference function and that three solutions with slightly different energies are obtained. Their study also confirmed previous observations[26f] about the inclusion of triplets in CC calculations.

It has been shown that spin-unprojected Møller-Plesset perturbation theory calculations (MP2 and MP4) predict the NO₃ ground state to be of D_{3h} symmetry,[27b] although MP2 results still suffer from artifactual symmetry breaking since three different results are obtained.[26a]

In general, DFT methods have been reported to yield D_{3h} symmetric densities and equilibrium geometries for the NO₃ radical.[26c,e,27b] A study by Sherrill *et al.*[26c] showed that DFT methods tend to avoid artifactual spatial symmetry breaking in the equilibrium geometry region even when unrestricted Hartree-Fock (UHF) fails. They also showed that the exchange functional seems to be more important than the correlation functional in determining whether or not a symmetry-broken solution is obtained, and that hybrid functionals which include large amounts of HF exchange lead to symmetry breaking.

The results obtained for the NO₃ radical at the levels of calculation employed in this work are listed in Table 6.1. At the MP2 level the D_{3h} structure is the minimum, while at BH&HLYP level the NO₃ molecule prefers a C_{2v} (1L2S) structure, the D_{3h} structure being a saddle point of second order. With both geometries, the CCSD(T) single point calculation predicts the D_{3h} structures to be of lower energy. The calculations on the NO₃ radical presented here are in agreement with the previous studies. The present study does not attempt to add new insight into the previous discussion about the NO₃ ground state symmetry. The above controversy will be used later in the chapter to justify the selection of computational methods.

Simple inspection of the reported activation energies and rate constants for the OH and NO₃ reactions from aldehydes[4] shows that NO₃ is a less reactive molecule. This situation can be justified by analyzing the spin-density distribution in the radicals. In the D_{3h} NO₃ molecule, the spin density is homogeneously distributed among the oxygen atoms, while

for the OH radical the spin density distribution is localized on oxygen. Another chemical reason to explain the smaller reactivity of the NO₃ radical can be found in its smaller hydrogen affinity, HA (see Table 6.2). The HA of NO₃ radicals is much smaller than that of OH, and not too much bigger than the HA of HCO and CH₃CO, radicals with which the NO₃ radicals have to compete.

Table 6.1. Calculations on the NO₃ radical at different levels of theory using the 6-311G(d,p) basis set. Atomic distances in Å, angles in degrees and energies in au.

Geometry	MP2(FC) - D₃ₕ	MP2(FC) - C₂ᵥ '1S2L'	MP2(FC) - C₂ᵥ '1L2S'
d(N,O¹)	1.244	1.181	1.380
d(N,O²), d(N,O³)	1.244	1.247	1.204
∠(O¹,N,O²)	120.0	127.0	113.6
E(PMP2)	-279.66345	-279.64122	-279.62950
E(CCSD(T)//MP2(FC))	-279.66671	-279.66367	-279.66343
NImag[a]	0	0	0

Geometry	BH&HLYP - D₃ₕ	BH&HLYP - C₂ᵥ '1S2L'	BH&HLYP - C₂ᵥ '1L2S'
d(N,O¹)	1.210	1.174	1.326
d(N,O²)	1.210	1.241	1.184
∠(O¹,N,O²)	120.0	126.2	114.3
E(BH&HLYP)	-280.12240	-280.12821	-280.13238
E(CCSD(T)//BH&HLYP)	-279.66323	-279.66297	-279.66251
NImag[a]	2	1	0

[a] Number of imaginary frequencies

Table 6.2. Calculation of the hydrogen affinities (HA, in kJ/mol) of some radicals of interest at the PMP2 level using MP2(FC)/6-311++d(d,p) geometries.

Radical (X)	HA [a]
OH	-508.2
NO₃	-389.5
HCO	-368.1
CH₃CO	-371.8

[a] $HA_X = E_{HX} - (E_H + E_X)$

As a result of the lower reactivity of NO₃ radicals less stable reactant complexes and higher activation energies to form the TS are expected, compared to the results obtained for the analogous OH-aldehyde reactions.[5]

6.3.2. The reaction of NO₃ radicals with HCHO and CH₃CHO

It is convenient to begin by explaining the selection of the best combination of methods that reproduce the experimental kinetics of the NO₃ hydrogen-abstraction reaction from CH₃CHO and HCHO. The experimental rate constants, Arrhenius pre-exponential factors and activation energies are listed in Tables 6.3 (CH₃CHO + NO₃) and 6.4 (HCHO + NO₃).

Previous calculations on the OH reaction with CH₃CHO[5a] showed that the abstraction of the aldehydic hydrogen atom is favoured. It has also been shown that the rate constant for the abstraction of one of the methyl hydrogen atoms is 10 times smaller.[3d] Since the NO₃ radicals are less reactive than the OH radicals, they should be more selective and the aldehydic hydrogen-abstraction should be the dominant process occurring in the reaction of NO₃ with CH₃CHO.

Table 6.3. Experimental kinetic results for the NO₃ reaction with CH₃CHO.

Ref. (Year)	$E_a^{(a)}$	$A^{(b)}$	$k^{(c)}$	T (K)	P (atm)
21a (2001)	16.3	-	$1.58 \cdot 10^6$	263 – 363	1
3a (1999)	15.5	$8.43 \cdot 10^8$	$1.64 \cdot 10^6$	260 – 370	(d)
3b (1997)	15.5	$8.43 \cdot 10^8$	$1.64 \cdot 10^6$	260 – 370	(d)
3c (1997)	15.8	$8.43 \cdot 10^8$	$1.44 \cdot 10^6$	200 – 300	(d)
20a (1991)	15.5	$8.67 \cdot 10^8$	$1.67 \cdot 10^6$	264 – 374	(d)
21b (1989)	15.5	$8.67 \cdot 10^8$	$1.69 \cdot 10^6$	264 – 374	(e)
13a (1986)	-	-	$1.26 \cdot 10^6$	299	0.921
20d (1984)	-	-	$8.07 \cdot 10^5$	298	0.974
21c (1974)	-	-	$7.23 \cdot 10^5$	300	0.987

(a) kJ/mol; (b) L/mol·s; (c) At 298 K, in L/mol·s; (d) Literature review; (e) 0.00132 – 0.00145 atm

Recently, a publication by D'Anna and coworkers[21a] reported the rate coefficient of the acetaldehyde reaction with NO₃ by the absolute rate fast-flow-discharge technique and by a relative method. They also optimized the TS of the aldehydic and methyl hydrogen-abstraction reactions at the MP2/cc-pVDZ level, although activation energies were not estimated theoretically. Their experimental and theoretical results point to the aldehydic hydrogen-abstraction as the only pathway for the NO₃ reaction with acetaldehyde under atmospheric conditions, in agreement with ideas derived from a previous work[16a] based on bond dissociation energies.

Energies obtained at different levels of theory were used to calculate the activation energy of the CH₃CHO + NO₃ reaction, and the values obtained are shown in Table 6.5,

along with the calculated reaction enthalpies, at 0 and 298 K. This is the only reaction among those studied for which activation energy values have been measured.

Table 6.4. Experimental kinetic results for the NO_3 reaction with HCHO.

Ref. (Year)	E_a [a]	A [b]	k [c]	T (K)	P (atm)
3a (1999)	20.2 [d]	$1.20 \cdot 10^9$ [d]	$3.49 \cdot 10^5$	298	[e]
3b (1997)	-	-	$3.49 \cdot 10^5$	298	[e]
3c (1997)	-	-	$3.49 \cdot 10^5$	298	[e]
20a (1991)	-	-	$3.49 \cdot 10^5$	298	[e]
20b (1988)	-	-	$3.25 \cdot 10^5$	295	0.974
20c (1985)	-	-	$3.79 \cdot 10^5$	298	0.921
20d (1984)	-	-	$1.95 \cdot 10^5$	298	0.974

[a] kJ/mol; [b] L/mol·s; [c] At 298 K, in L/mol·s; [d] Suggested in Ref. 3a(1999); [e] Literature review

The PMP2 barrier is overestimated, as usual. This time the CCSD(T) calculation using MP2 geometries gives barriers that are still too high in comparison with experiment. The BH&HLYP and CCSD(T)//BH&HLYP barriers are too low. It is well known that DFT predicted barrier heights are often much lower than those obtained with *ab initio* methods.[29] In order to correct these last two barriers, an estimate of the magnitude of the basis set superposition error (BSSE)[30] was calculated by applying the counterpoise (CP) method[31] to the TS, following the original procedure in which the "monomeric units" (the reactants) upon forming the "intermolecular complex" (the TS) are not further optimized, *i.e.*, the "monomers" are frozen in their supermolecular geometries (see Section 2.3.2).

The BSSE was calculated using BH&HLYP as well as CCSD(T) (only for the CH₃CHO-NO₃ TS) energies, and are denoted BSSE(BH&H) and BSSE(CC), respectively. When

these two corrections are added to the CCSD(T)//BH&HLYP barrier, activation energies in good agreement with experiment are obtained.

Table 6.5. Activation energy (E_a) and reaction enthalpy (ΔH), in kJ/mol, including zero-point (ZPE) or thermal vibrational corrections at 298.15 K (TCE), for the NO₃ hydrogen-abstraction reaction from CH₃CHO at different levels of theory.

Basis set: 6-311G(d,p)	$E_a^{(ZPE)}$	$E_a^{(TCE)}$	$\Delta H^{(ZPE)}$	$\Delta H^{(TCE)}$
PMP2	109.7	111.7	-32.4	-31.1
CCSD(T)//MP2(FC)	23.2	25.3	-75.6	-74.3
BH&HLYP	-0.3	1.9	-65.5	-65.1
CCSD(T)//BH&HLYP	5.3	7.5	-64.7	-64.3
BH&HLYP + BSSE(BH&H)	6.9	9.1		
CCSD(T)//BH&HLYP + BSSE(BH&H)	12.4	14.6		
CCSD(T)//BH&HLYP + BSSE(CC)	18.8	21.0		
CCSD(T)//BH&HLYP*	16.3	18.5	-53.6	-53.3
Experiment		16.3 [a] 15.5 [b] 15.8 [c]		-53.3 [d] -67.3 [e]

[a] Ref. 21a(2001); [b] Ref. 3a(1999), 3b(1997), 20a(1991), 21b(1989); [c] Ref. 3c(1997);
[d] Ref. 3a(1999); [e] Ref. 3b(1997)

Bearing in mind the uncertainty about the ground state symmetry of the NO₃ radical, another correction to the CCSD(T)//BH&HLYP barrier is considered. Since the lowest CCSD(T) energy for NO₃ is obtained at the MP2(FC)-D₃ₕ geometry (see Table 6.1), this result was combined with the previous CCSD(T)//BH&HLYP calculations. That is, BH&HLYP geometries are used in the single point CCSD(T) calculations except for NO₃ for which the MP2(FC)-D₃ₕ structure is used. Frequency calculations are performed at the BH&HLYP level. Results using this correction will be denoted CCSD(T)//BH&HLYP* throughout the text. The activation energy obtained (16.3 at 0 K and 18.5 at 298 K, in

kJ/mol) is in very good agreement with experiment (15.5-16.3 kJ/mol). The reaction enthalpy calculated in this way is -53.6 at 0 K, and -53.3 at 298K (in kJ/mol), also in very good agreement with the latest experimental value (-53.3 kJ/mol).

For the HCHO + NO₃ reaction the calculated activation energies and reaction enthalpies are reported in Table 6.6, at 0 and 298 K. For this reaction an activation energy of 20.2 kJ/mol has been suggested by analogy with the reaction of NO₃ with CH₃CHO.[3a] The best results are once again obtained at the CCSD(T)//BH&HLYP level after considering the above mentioned corrections (CCSD(T)//BH&HLYP + BSSE(BH&H) and CCSD(T)//BH&HLYP*). The reaction enthalpy obtained at the CCSD(T)//BH&HLYP* level (-59.1 kJ/mol) is in excellent agreement with experiment as well (-57.1 kJ/mol).

Table 6.6. Activation energy (E_a) and reaction enthalpy (ΔH), in kJ/mol, including zero-point (ZPE) or thermal vibrational corrections at 298.15 K (TCE), for the NO₃ hydrogen-abstraction reaction from HCHO at different levels of theory.

Basis set: 6-311G(d,p)	$E_a^{(ZPE)}$	$E_a^{(TCE)}$	$E_{a(-1)}^{(ZPE)}$	$E_{a(2)}^{(ZPE)}$	$\Delta H^{(ZPE)}$	$\Delta H^{(TCE)}$
PMP2	118.2	119.3	-70.0	48.2	-41.2	-40.2
CCSD(T)//MP2(FC)	32.4	33.6	10.7	43.2	-81.1	-80.1
BH&HLYP	3.2	3.9	5.1	8.3	-70.1	-70.0
CCSD(T)//BH&HLYP	11.3	12.0	6.7	18.0	-70.3	-70.2
BH&HLYP + BSSE(BH&H)	10.2	10.9				
CCSD(T)//BH&HLYP + BSSE(BH&H)	18.3	19.0				
CCSD(T)//BH&HLYP*	22.4	23.1	-4.4	18.0	-59.3	-59.1
Experiment	20.2 [a]					-57.1 [b] -58.4 [c]

[a] Suggested in Ref. 3a(1999), 3b(1997); [b] Ref. 3a(1999); [c] Ref. 3b(1997)

The values of the partition functions needed for the calculation of the TST rate constants of the reactions studied at MP2 and BH&HLYP levels of theory are given in Tables 6.7 and 6.8, respectively, as well as the imaginary frequency of the TS. Several low frequencies (below 300 cm^{-1}) in addition to the imaginary frequency were calculated for the hydrogen-abstraction TS. Of these, three were identified as internal rotations (or torsional vibrations) by visualization of the normal modes. These harmonic modes correspond most closely to the three new internal rotors created in the TS (XCOH···ONO₂, XCO···HNO₃ and XCOHO···NO₂), where the common axes for internal rotation are the ones linking the reactants, products, and one along the N-O bond with the oxygen atom abstracting the hydrogen. These were the axes considered in the calculation of the reduced moments of inertia. These harmonic modes were treated as free rotors in the calculation of the internal-rotation partition function of the TS (Q_{IR}^{TS}).[32,33] A similar procedure has been used in earlier related studies.[5,34]

The harmonic contributions of these low frequencies were eliminated from the vibrational partition function in order to correct the total partition function of the TS (Q_{corr}^{TS}):

$$Q_{corr}^{TS} = \frac{Q^{TS} \, Q_{IR}^{TS}}{\prod Q_{v=i}}$$

(6.2)

For CH₃CHO and its TS, the internal rotation around the C-C single bond was also considered and treated as a free rotor.

TST direct rate constants (k_D) at 298 K for the reactions of CH₃CHO and HCHO with NO₃ radicals, calculated at different levels of theory, are given in Tables 6.9 and 6.10, respectively. Some experimental results have been included for comparison. The tunneling corrections (κ) and $\Delta s_{\frac{1}{2}}$ are also reported.

Table 6.7. Total partition functions (Q) of the reactants and the TS, and imaginary frequency (v^* in cm^{-1}) of the TS of the NO₃ hydrogen-abstraction reaction from XCHO (X = F, Cl, H, CH₃), calculated at the MP2(FC)/6-311G(d,p) level of theory.

System	FCHO + NO₃	ClCHO + NO₃	HCHO + NO₃	CH₃CHO + NO₃
$Q^{NO_3}_{(D_{3h})}$	$1.70737 \cdot 10^{11}$	$1.70737 \cdot 10^{11}$	$1.70737 \cdot 10^{11}$	$1.70737 \cdot 10^{11}$
Q^{XCHO}	$1.13573 \cdot 10^{11}$	$3.90682 \cdot 10^{11}$	$4.61479 \cdot 10^{9}$	$2.97963 \cdot 10^{11}$ [a]
Q^{TS}	$3.90874 \cdot 10^{15}$	$1.44419 \cdot 10^{16}$	$7.39244 \cdot 10^{14}$	$1.53333 \cdot 10^{16}$
$\prod Q_{v=i}$ [f]	28.649 [b]	41.307 [c]	17.383 [d]	90.815 [e]
$Q_{IR}^{TS (g)}$	$4.78689 \cdot 10^{4}$	$8.51824 \cdot 10^{4}$	$1.55481 \cdot 10^{4}$	$1.64320 \cdot 10^{5}$
$Q_{corr}^{TS (h)}$	$6.53102 \cdot 10^{18}$	$2.97821 \cdot 10^{19}$	$6.61219 \cdot 10^{17}$	$2.77441 \cdot 10^{19}$
v^*	2703	2335	1395	998

[a] $Q_{corr}^{CH_3CHO} = 5.39632 \cdot 10^{11}$; [b] i=1, 3, 4; [c] i=1, 3, 4; [d] i=1, 2, 4; [e] i=1, 2, 4, 6; [f] Vibrational components that were eliminated from the calculation of Q_{corr}^{TS}; [g] Total internal-rotational partition function of the TS; [h] Corrected total partition function of the TS

Table 6.8. Total partition functions (Q) of the reactants and the TS, and imaginary frequency (v^* in cm^{-1}) of the TS of the NO₃ hydrogen-abstraction reaction from XCHO (X = F, Cl, H, CH₃), calculated at the BH&HLYP/6-311G(d,p) level of theory.[a]

System	FCHO + NO₃	ClCHO + NO₃	HCHO + NO₃	CH₃CHO + NO₃
$Q^{NO_3}_{(C_{2v})}$	$5.50530 \cdot 10^{11}$	$5.50530 \cdot 10^{11}$	$5.50530 \cdot 10^{11}$	$5.50530 \cdot 10^{11}$
Q^{XCHO}	$1.08003 \cdot 10^{11}$	$3.79813 \cdot 10^{11}$	$4.42745 \cdot 10^{9}$	$2.79523 \cdot 10^{11}$ [b]
Q^{TS}	$5.34208 \cdot 10^{15}$	$1.82529 \cdot 10^{16}$	$1.09900 \cdot 10^{15}$	$8.36021 \cdot 10^{16}$
$\prod Q_{v=i}$	33.585 [c]	48.383 [d]	23.921 [e]	393.66 [f]
Q_{IR}^{TS}	$4.68184 \cdot 10^{4}$	$8.46634 \cdot 10^{4}$	$1.38936 \cdot 10^{4}$	$1.66813 \cdot 10^{5}$
Q_{corr}^{TS}	$7.44708 \cdot 10^{18}$	$3.19401 \cdot 10^{19}$	$6.38324 \cdot 10^{17}$	$3.54265 \cdot 10^{19}$
v^*	1983	1503	239	141

[a] See footnotes of Table 6.7 for more details; [b] $Q_{corr}^{CH_3CHO} = 5.10774 \cdot 10^{11}$; [c] i=1, 3, 4; [d] i=1, 3, 4; [e] i=1, 2, 4; [f] i=1, 2, 4, 6

In both cases the CCSD(T)//BH&HLYP* calculation gives the best rate constants, $1.11 \cdot 10^6$ for CH$_3$CHO + NO$_3$ and $2.09 \cdot 10^5$ for HCHO + NO$_3$, in very good agreement with experimental values of $1.26 \cdot 1.69 \cdot 10^6$ for CH$_3$CHO + NO$_3$ and $1.95 \cdot 3.79 \cdot 10^5$ for HCHO + NO$_3$. Rate constants at other levels of calculation are not able to reproduce the order of the experimental values for both reactions. From this, it is concluded that CCSD(T)//BH&HLYP* is the best method for predicting kinetic parameters in these systems.

Table 6.9. Rate constants (in L/mol·s) and tunneling parameters for the NO$_3$ hydrogen-abstraction reaction from CH$_3$CHO, calculated at different levels of theory using the 6-311G(d,p) basis set, and considering a direct mechanism, at 298.15 K.

Level of Calculation:	κ_D[a]	$\Delta s_{1/2}$[b]	k_D
PMP2	3.33		$3.82 \cdot 10^{-10}$
CCSD(T)//MP2(FC)	2.81	0.70	$4.45 \cdot 10^5$
BH&HLYP	-		$8.69 \cdot 10^8$
CCSD(T)//BH&HLYP	1.02		$9.51 \cdot 10^7$
BH&HLYP + BSSE(BH&H)	1.02		$4.95 \cdot 10^7$
CCSD(T)//BH&HLYP + BSSE(BH&H)	1.02		$5.31 \cdot 10^6$
CCSD(T)//BH&HLYP + BSSE(CC)	1.02		$4.10 \cdot 10^5$
CCSD(T)//BH&HLYP*	1.02	3.57	$1.11 \cdot 10^6$
Experiment			$1.58 \cdot 10^6$ [c]
			$1.64 \cdot 10^6$ [d]
			$1.44 \cdot 10^6$ [e]
			$1.67 \cdot 10^6$ [f]
			$1.69 \cdot 10^6$ [g]
			$1.26 \cdot 10^6$ [h]

[a] Tunneling correction; [b] Full width of the barrier at half its height, in Å; [c] Ref. 21a(2001); [d] Ref. 3a(1999), 3b(1997); [e] Ref. 3c(1997); [f] Ref. 20a(1991); [g] Ref. 21b(1989); [h] Ref. 13a(1986)

Table 6.10. Rate constants (in L/mol·s) and tunneling parameters for the NO_3 hydrogen-abstraction reaction from HCHO, calculated at different levels of theory using the 6-311G(d,p) basis set, for both the direct and complex mechanisms at 298.15 K.

Level of Calculation:	Direct Mechanism			Complex Mechanism		
	$\kappa_D^{(a)}$	$\Delta s_\frac{1}{2}^{(b)}$	k_D	$\kappa^{(a)}$	$\Delta s_\frac{1}{2}^{(b)}$	k_{eff}
PMP2	23.16		$2.39 \cdot 10^{-10}$	11.97		$1.24 \cdot 10^{-10}$
CCSD(T)//MP2(FC)	8.96	0.51	$9.66 \cdot 10^4$	11.08	0.59	$1.19 \cdot 10^5$
BH&HLYP	1.05		$4.78 \cdot 10^8$	1.06		$4.81 \cdot 10^8$
CCSD(T)//BH&HLYP	1.06		$1.78 \cdot 10^7$	1.06		$1.78 \cdot 10^7$
BH&HLYP + BSSE(BH&H)	1.06		$2.86 \cdot 10^7$	1.06		$2.86 \cdot 10^7$
CCSD(T)//BH&HLYP + BSSE(BH&H)	1.06		$1.06 \cdot 10^6$	1.06		$1.06 \cdot 10^6$
CCSD(T)//BH&HLYP*	1.06	2.47	$2.09 \cdot 10^5$	1.06	2.22	$2.08 \cdot 10^5$
Experiment			$3.49 \cdot 10^{5 \ (c)}$ $3.25 \cdot 10^{5 \ (d)}$ $3.79 \cdot 10^{5 \ (e)}$ $1.95 \cdot 10^{5 \ (f)}$			

[a] Tunneling correction; [b] Full width of the barrier at half its height, in Å;
[c] Ref. 3a(1999), 3b, 3c (1997), 20a(1991); [d] Ref. 20b(1988); [e] Ref. 20c(1985); [f] Ref. 20d(1984)

6.3.2.1. Elementary or complex reactions?

The significance of considering the complex character of the kinetics of a radical-molecule reaction was one of the main conclusions of a recent work.[5a] Later it was shown that even for reactions with less stable reactant complexes and higher activation energies (FCHO + OH and ClCHO + OH),[5b] a complex mechanism should also be considered. Furthermore, it was shown that for these two reactions, the percentage difference between the elementary (direct) and complex (effective) rate constants was smaller than the

difference found for the HCHO + OH reaction, in which a smaller activation energy was found. It was rationalized that the bigger the effective energy barrier for radical-molecule reactions, and the smaller the stabilization energy of the reactant complex, the more closely its behaviour resembles an elementary reaction.

Intuitively, for the NO_3 reactions higher activation energies and less stable reactant complexes are expected. Hence, a smaller percentage of difference between the elementary and complex rate constants in comparison with the analogous OH reactions is also expected. In other words, the kinetic behaviour of the NO_3 reactions should resemble more closely an elementary reaction. Whether these reactions should be assumed elementary or whether the formation of the reactant complex must be considered, will be discussed in this section.

For the simplest system, the HCHO + NO_3 reaction, two possible mechanisms were considered: a direct mechanism, in which the hydrogen-abstraction takes place in an elementary step, and a two-step mechanism that involves a fast pre-equilibrium between the reactants and the reactant complex, followed by the irreversible hydrogen-abstraction that takes place in the reactant complex to form the products (product complex):

Step 1:   HCHO + NO_3 $\rightleftarrows$ [HCHO⋯NO_3]

Step 2:   [HCHO⋯NO_3] $\longrightarrow$ [HCO⋯HNO_3] $\longrightarrow$ HCO + HNO_3
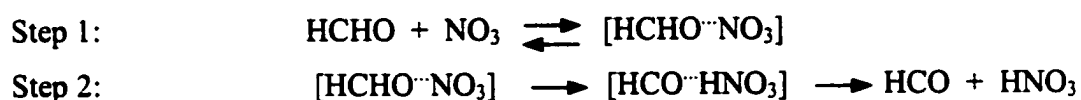
As shown before (Chapter 4) the overall rate constant for the complex mechanism (k_{eff}) can be calculated by:

$$k_{eff} = \kappa \ \frac{k_B T}{h} \ \frac{Q^{TS}}{Q^{React}} \ exp\left(-\frac{\left(E^{TS} - E^{React}\right)}{RT}\right)$$ (6.3)

The geometry of the reactant and product complexes of the HCHO + NO_3 reaction are shown in Figure 6.1, where some geometrical parameters have been indicated. These structures have been determined by dipole-dipole interactions.

(a) HCHO⋯NO₃

2.816
(2.778)

2.919
(2.802)

(b) HCO⋯HNO₃

1.944
(1.849)

2.708
(2.597)
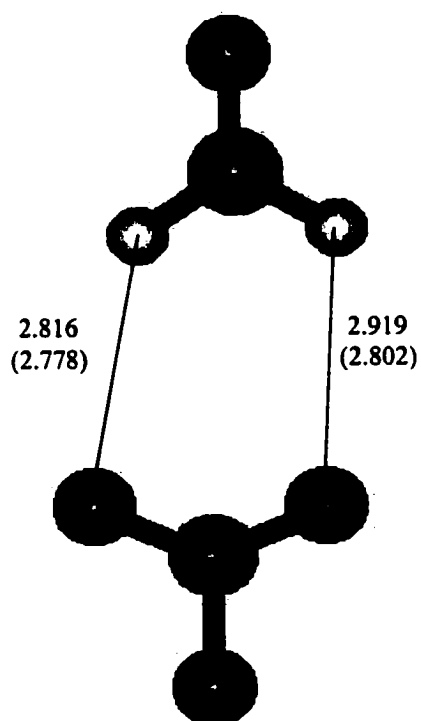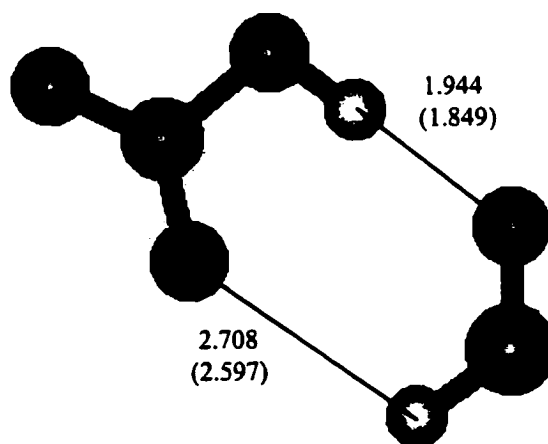
Figure 6.1. Optimized structures of the (a) reactant and (b) product complexes in the
HCHO + NO₃ hydrogen-abstraction reaction, as obtained at the MP2(FC)
(BH&HLYP) level with the 6-311G(d,p) basis set.
(Bond distances are given in Å)

The stabilization energy of the reactant complex ($E_{a(-1)}$) and the activation barrier of the second step of the complex mechanism ($E_{a(2)}$) at 0 K, are given in Table 6.6. At the CCSD(T)//MP2(FC) level the reactant complex is calculated to be 10.7 kJ/mol lower in energy than the isolated reactants. At this level, but using a slightly larger basis set: 6-311++G(d,p), the stabilization energy of the reactant complex for the HCHO + OH reaction is calculated to be 13.6 kJ/mol. The new complex is less stable, as expected. At the CCSD(T)//BH&HLYP level this energy is 6.7 kJ/mol. The actual reactant complex stabilization energy is expected to be between these two values (6.7 and 10.7 kJ/mol).

Rate constants calculated for the direct and complex mechanisms are reported in Table 6.10. At the CCSD(T)//MP2 level the difference is small. The percentage by which these two rate constants differ, calculated by:

$$\left(\frac{k_{eff} - k_D}{k_{eff}}\right) \cdot 100\% \qquad (6.4)$$

is 18.8%. For the OH hydrogen-abstraction reaction from the same series of aldehydes, this percentage difference is 71.3 for the FCHO reaction, the one with the highest activation energy and the least stable reactant complex (see Chapter 5). For the other calculations the difference between rate constants for the mechanisms considered is negligible. Hence, the assumption of an elementary mechanism for the NO₃ hydrogen-abstraction reaction from these aldehydes is valid.

6.3.3. Results and discussions on the NO₃ hydrogen-abstraction reactions

The optimized geometries of the TSs of these reactions are shown in Fig. 6.2, where relevant geometrical parameters have been indicated for the MP2 and BH&HLYP optimizations. The overall shape of these molecular systems did not change significantly at these two levels. The reaction profiles at the CCSD(T)/BH&HLYP* level of calculation are shown in Fig. 6.3.
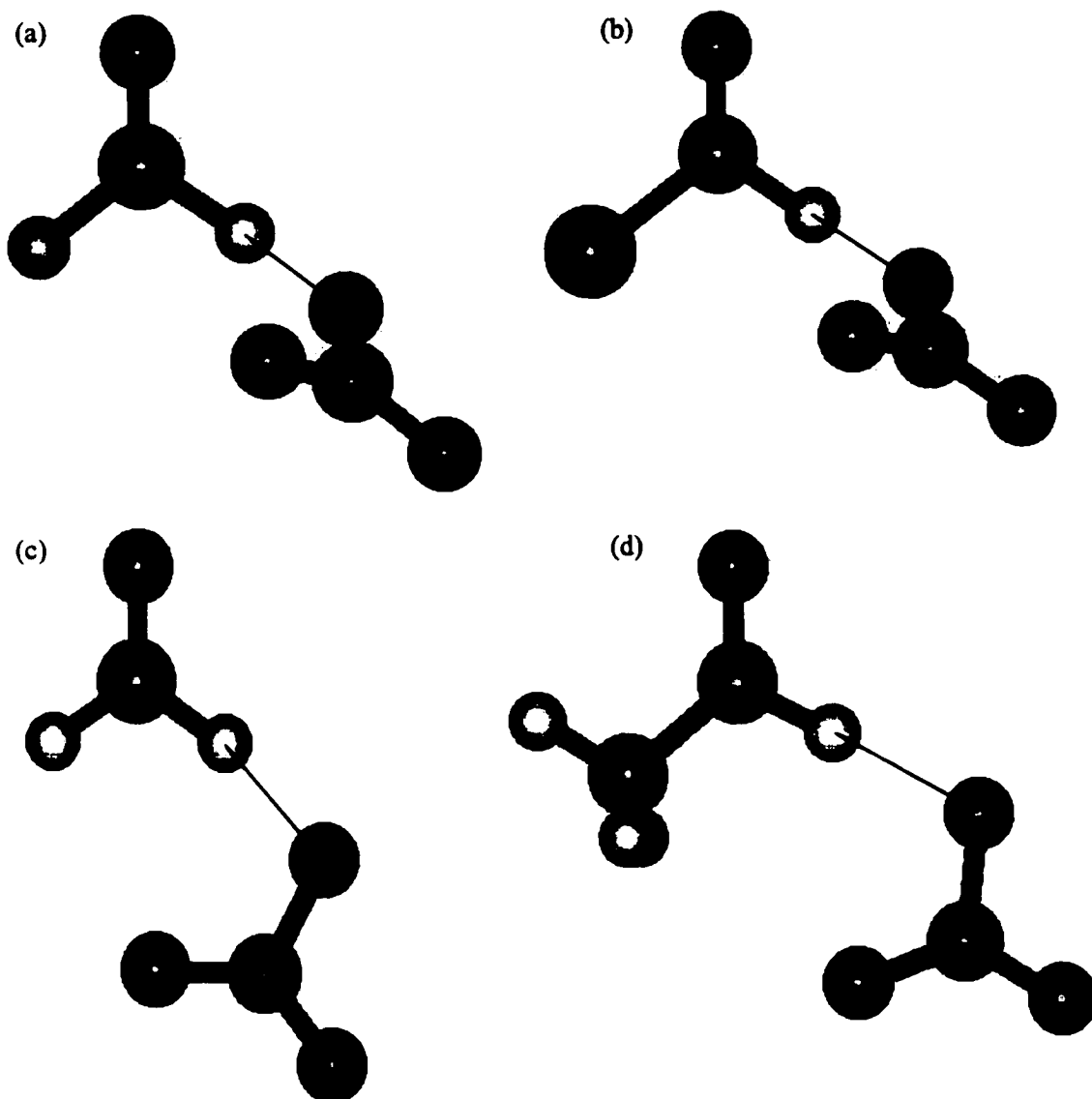
X(O)C···H···ONO₂	MP2(FC)/6-311G(d,p)			BH&HLYP/6-311G(d,p)		
X	d(C,H)	d(H,O)	∠(C,H,O)	d(C,H)	d(H,O)	∠(C,H,O)
F	1.195	1.359	174.3	1.240	1.287	174.9
Cl	1.178	1.424	176.7	1.200	1.372	177.9
H	1.164	1.563	168.9	1.146	1.617	165.3
CH₃	1.160	1.595	175.9	1.132	1.735	179.3

H F O N C Cl

Figure 6.2. Structure of the transition states of the hydrogen-abstraction reactions studied and some relevant geometrical parameters. (a) FCHO + NO₃, (b) ClCHO + NO₃, (c) HCHO + NO₃, (d) CH₃CHO + NO₃.
(Bond distances are given in Å and angles in degrees)

XCHO + NO₃ ⟶ XCO + HNO₃ (X = F, Cl, H, CH₃)
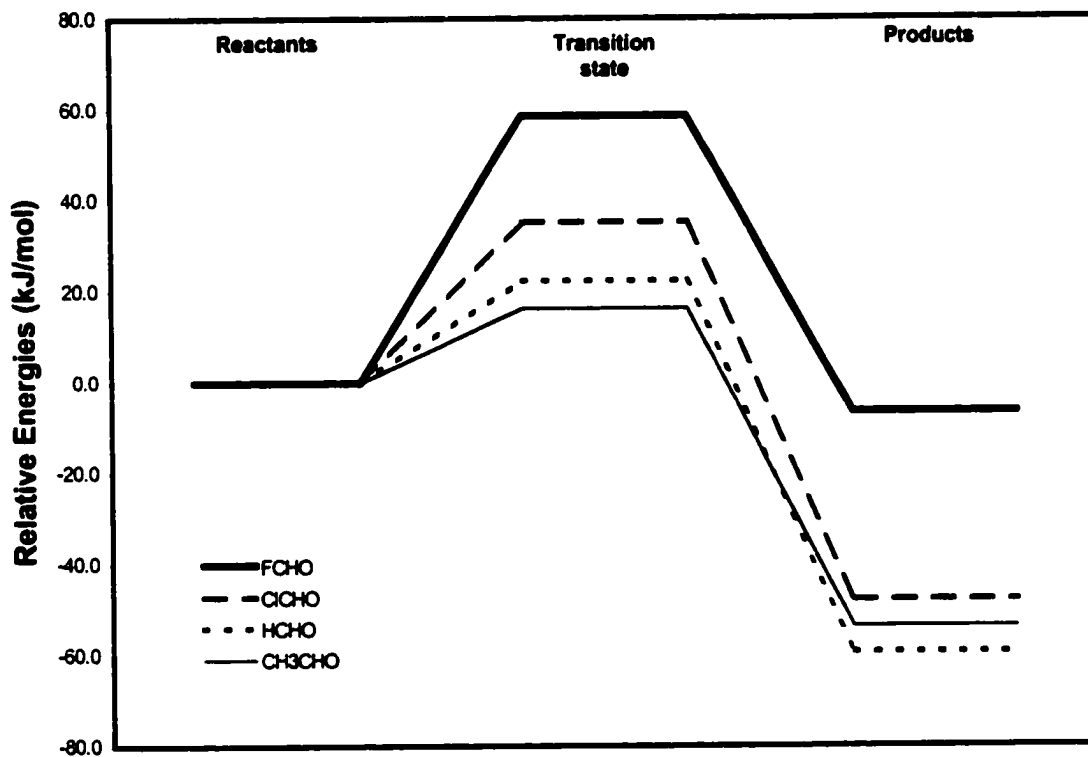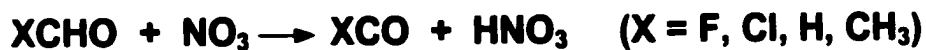
Figure 6.3. Schematic reaction profile for the XCHO + NO₃ (X = F, Cl, H, CH₃) hydrogen-Abstraction reactions using the calculated CCSD(T)/6-311G(d,p)//BH&HLYP/ 6-311G(d,p) energy values, including the BH&HLYP/6-311G(d,p) zero-point energy corrections.

Note: For the CCSD(T) calculation on the NO₃ radical the MP2(FC)-D₃ₕ geometry was employed.

The symmetry of the TS calculated for the NO₃ reaction with HCHO and CH₃CHO is ^{2}A', (C$_s$ point group) implying that the unpaired electron is in the plane where the NO₃ attack takes place. ^{2}A' is also the symmetry of the XCO radical generated. This corresponds to the TS structures obtained for the OH reactions.[5] However, for the FCHO and ClCHO hydrogen-abstraction reaction, the TSs possess C₁ symmetry. The oxygen atoms of the NO₃ radical avoid spatial interaction with the electronic cloud of the halogen atom of these aldehydes, and the best way of achieving this, without creating new destabilizing interactions, is by breaking the plane of symmetry. Hydrogen bonding interactions stabilize these structures. For HCHO and CH₃CHO the distance from the closest oxygen atom (of the two not directly implied in the abstraction process) of NO₃ to the aldehyde is 2.605 and 2.931 Å, respectively. For FCHO and ClCHO these distances are 3.172 and 3.611 Å, respectively. The larger the halogen atom the greater this interatomic distance. The structure of the TS of the CH₃CHO reaction reported in the work by D'Anna andcoworkers,[21a] calculated at the MP2/cc-pVDZ level of theory, agrees to within 0.01 Å with the MP2 results reported here.

In the series of substituents, F, Cl, H and CH₃, the TS is achieved earlier. Thus, the calculated C⋯H distances decrease in this order from 1.195 Å (FCHO) to 1.160 (CH₃CHO) at the MP2 level and from 1.240 to 1.132 Å at the BH&HLYP level; in a similar way the H⋯O distance increases. Furthermore, a larger activation energy has to be overcome. This trend is consistent with the decreasing electron-donating effect of these substituents that is also the cause of the decreasing reactivity of these aldehydes towards the NO₃ hydrogen-abstraction reaction. Similar results were discussed for the analogous OH reactions in Chapter 5.[5b]

Constant oscillations between energy related structures during the optimization of the TS, and the reactant and product complexes (in the case of the HCHO + NO₃ reaction) are difficult to overcome. These oscillations basically involve the stretching and enlargement of the NO bonds in the NO₃ radical, and may be related to the "symmetry dilemma" for this radical, discussed above.

Frequency calculations at MP2 level lead to imaginary frequencies of the TS where the transfer of the hydrogen atom between the carbon and oxygen atoms is easy to visualize for the four reactions. In a similar way the large amplitude vibrations were assigned to internal rotations and the axes were identified, as explained before in Section 6.3.2. At the BH&HLYP level the situation is quite different. Only the TS of the FCHO and ClCHO reactions showed imaginary frequencies like the one described above. However, for the HCHO and CH₃CHO reactions this vibrational mode exhibits features of an addition-elimination reaction. IRC calculations proved that the optimized structures are the TSs of the aldehydic hydrogen-abstraction reactions, and moreover, made possible the establishment of a relationship between the TS of the HCHO reaction and the corresponding reactant and product complexes referred to in Section 6.3.2.1. An analogous situation was encountered while studying the HCHO + OH hydrogen-abstraction reaction at the B3LYP level,[23] but at the BH&HLYP level this is not the case. This problem may be an artefact of the method.

In the series of substituents, F, Cl, H, CH₃, the imaginary frequency of the TS ($v^{\neq}$) decreases at both levels of theory, and thus the curvature of the calculated barrier is reduced as well; $\Delta s_{\frac{1}{2}}$ increases in the same order. In this series of aldehydes κ decreases in agreement with the fact that activation energies and imaginary frequencies decrease. At the MP2 and BH&HLYP levels of theory barriers are predicted to reduce in height and curvature on going from FCHO to CH₃CHO. This is also the case for the OH hydrogen-abstraction reactions.[5]

Barriers calculated using BH&HLYP geometries are predicted to be smaller and wider than those calculated with MP2 structures, as expected. Tunneling corrections for BH&HLYP geometries are significantly smaller than the values calculated with MP2 structures, since barriers and imaginary frequencies are also smaller.

Cartesian coordinates of the TS, reactant and product complexes at MP2 and BH&HLYP levels are available,[35] as well as the calculated total energies (PMP2, CCSD(T)//MP2, BH&HLYP and CCSD(T)// BH&HLYP), zero-point and thermal (at 298.15 K)

vibrational energy corrections (calculated at MP2 and BH&HLYP levels) of the species involved in the reaction of NO_3 with the aldehydes, and the BSSE calculated for the TS for these reactions.

The remaining parameters were calculated at the CCSD(T)//BH&HLYP* level, at which the experimental kinetic parameters and reaction enthalpies are reproduced. The predicted values of rate constant and activation energy for the NO_3 hydrogen-abstraction reaction from FCHO and ClCHO, at 298K, are: 60.2 kJ/mol and 10.30 L/mol·s for FCHO, and 37.0 kJ/mol and $9.01 \cdot 10^8$ L/mol·s for ClCHO. Reaction enthalpies are calculated to be -6.4 (FCHO) and –47.1 kJ/mol (ClCHO). These values, as well as activation energies and reaction enthalpies at 0 K and tunneling parameters calculated at various levels of theory are shown in Tables 6.11 and 6.12. The calculated partition functions and imaginary frequency of the TS at MP2 and BH&HLYP levels are given in Tables 6.7 and 6.8, respectively.

In order to obtain the CCSD(T) energy differences reported in Tables 6.5, 6.6 and 6.11, vibrational corrections at the level at which the geometries were optimized, MP2 or BH&HLYP, are used. For these reactions spin contamination at the TS is small; the highest expectation value of S^2 is 0.806 for the FCHO reaction at the MP2 level. Spin contamination is completely eliminated by projection at MP2 and BH&HLYP levels, hence CCSD(T) calculations may be considered reliable in this sense.

For the HCHO and CH_3CHO reactions with NO_3 radicals with geometries calculated at the BH&HLYP level, tunneling corrections are almost negligible (1.06 and 1.02, respectively). Hence, an Arrhenius behaviour is expected for these reactions at temperatures above T^*, the characteristic tunneling temperature below which tunneling is significant. T^* is equal to $hc\nu^*/(2\pi k_B)$; for the HCHO and CH_3CHO reactions, T^* is 55 and 32 K, respectively. Hence, classical Arrhenius parameters for these reactions for temperatures above T^* may be calculated from:

$$A = \frac{k_B T}{h} \frac{Q^{TS}}{Q^{React}} \tag{6.5}$$

Table 6.11. Activation energy (E_a) and reaction enthalpy (ΔH), in kJ/mol, including zero-point (ZPE) or thermal vibrational corrections at 298.15 K (TCE), for the NO₃ hydrogen-abstraction reaction from XCHO (X = F, Cl, H) at different levels of theory.

Basis set: 6-311G(d,p)	$E_a^{(ZPE)}$	$E_a^{(TCE)}$	$\Delta H^{(ZPE)}$	$\Delta H^{(TCE)}$
FCHO + NO₃				
PMP2	147.8	149.6	15.9	16.8
CCSD(T)//MP2(FC)	74.4	76.3	-28.2	-27.3
BH&HLYP	49.3	51.0	-13.4	-13.3
CCSD(T)//BH&HLYP	47.6	49.2	-17.5	-17.4
BH&HLYP + BSSE(BH&H)	58.5	60.1		
CCSD(T)//BH&HLYP + BSSE(BH&H)	56.7	58.4		
CCSD(T)//BH&HLYP*	58.6	60.2	-6.5	-6.4
ClCHO + NO₃				
PMP2	131.5	133.7	-25.1	-23.9
CCSD(T)//MP2(FC)	52.5	54.7	-68.7	-67.5
BH&HLYP	28.1	30.0	-55.5	-54.8
CCSD(T)//BH&HLYP	24.2	26.0	-58.8	-58.2
BH&HLYP + BSSE(BH&H)	37.3	39.1		
CCSD(T)//BH&HLYP + BSSE(BH&H)	33.3	35.2		
CCSD(T)//BH&HLYP*	35.2	37.0	-47.8	-47.1

Table 6.12. Rate constants (in L/mol·s) and tunneling parameters for the NO_3 hydrogen-abstraction reaction from FCHO and ClCHO, calculated at different levels of theory using the 6-311G(d,p) basis set, and considering a direct mechanism, at 298.15 K.

Level of Calculation:	FCHO + NO₃			ClCHO + NO₃		
	κ_D	$\Delta S_{1/2}$	k_D	κ_D	$\Delta S_{1/2}$	k_D
PMP2	$4.53 \cdot 10^7$		$1.23 \cdot 10^{-9}$	$1.11 \cdot 10^6$		$2.80 \cdot 10^{-8}$
CCSD(T)//MP2(FC)	$8.05 \cdot 10^4$	0.41	15.55	$1.34 \cdot 10^3$	0.39	$2.36 \cdot 10^3$
BH&HLYP	162.25		$2.85 \cdot 10^2$	11.19		$1.25 \cdot 10^5$
CCSD(T)//BH&HLYP	152.76		$5.49 \cdot 10^2$	9.66		$5.34 \cdot 10^5$
BH&HLYP + BSSE(BH&H)	273.18		11.92	14.76		$4.11 \cdot 10^3$
CCSD(T)//BH&HLYP + BSSE(BH&H)	260.34		23.42	13.19		$1.81 \cdot 10^4$
CCSD(T)//BH&HLYP*	244.78	0.50	10.30	13.95	0.49	$9.01 \cdot 10^3$

For $CH_3CHO + NO_3$ the pre-exponential factor (in units of L/mol·s) is calculated to be $7.83 \cdot 10^8$, in very good agreement with the experimental value ($8.43 - 8.67 \cdot 10^8$, see Table 6.3). For the $HCHO + NO_3$ reaction the Arrhenius parameter is predicted to be $1.63 \cdot 10^9$, basically twice the A value for the CH_3CHO reaction, as expected since in HCHO there are two equivalent sites of attack. The suggested value[3a] $1.20 \cdot 10^9$ is in agreement with this calculation.

For the FCHO and ClCHO reactions tunneling is significant. The calculated characteristic temperature (T^*) is 454 and 344 K, respectively. Calculations of Arrhenius parameters using the above expression and ignoring tunneling quantum effects would be erroneous. If the value of κ is included in the above expression, A for the FCHO and ClCHO

reactions would be $1.90 \cdot 10^{11}$ and $1.32 \cdot 10^{10}$, respectively. Although this is not the most appropriate way of estimating the quantum Arrhenius parameter, these values could be used as a reference when better determinations are made.

6.4. Conclusions

The NO₃ hydrogen-abstraction reaction from a series of aldehydes (XCHO: X = F, Cl, H, CH₃) has been studied by means of *ab initio* calculations. Optimizations at the MP2 and BH&HLYP levels followed by CCSD(T) single point calculations were performed using the 6-311G(d,p) basis set. Neither CCSD(T)//MP2 nor CCSD(T)//BH&HLYP calculations were successful in reproducing the kinetic and thermochemical data available for such reactions. Hence several corrections were considered to improve upon the CCSD(T)//BH&HLYP results, which were the closest to experiment. The use of the MP2-D₃ₕ geometry of the NO₃ radical (for which a lot of controversial results regarding its ground state symmetry have been published) in the CCSD(T) calculation reproduced the only 6 parameters for which experimental results exist: rate constants and reaction enthalpies for the CH₃CHO and HCHO reactions, as well as the activation energy and Arrhenius pre-exponential factor for the CH₃CHO reaction with NO₃ radicals. At this level of theory the remaining parameters were then predicted theoretically for the first time, since no previous theoretical studies have been reported for the reactions between aldehydes and NO₃ radicals.

It was shown that these reactions can be considered elementary. The consideration of a reactant complex as in previous studies (Chapters 4 and 5)[5] does not affect the calculated kinetic results at the chosen level of theory. These results complement a series of studies regarding radical-molecule reactions and prove that even though for some reactions with low or negative activation energies the formation of the reactant complex needs to be considered, another extreme case, such as the NO₃ reactions studied, can be found for which a one-step mechanism is a sufficient approximation for kinetic determinations.[5b]

6.5. References

1.   Finlayson-Pitts, B.J.; Pitts, J.N. *Atmospheric Chemistry: Fundamentals and Experimental Techniques*, Wiley Interscience, New York, 1986.

2.   Seinfeld, J.H.; Pandis, S.N. *Atmospheric Chemistry and Physics: From Air Pollution to Climate Change*, Wiley Interscience, New York, 1998.

3.   (a) Atkinson, R.; Baulch, D.L.; Cox, R.A.; Hampson, R.F. Jr.; Kerr, J.A.; Rossi, M.J.; Troe, J. *J. Phys. Chem. Ref. Data* **1999**, *28*, 191. (b) Atkinson, R.; Baulch, D.L.; Cox, R.A.; Hampson, R.F., Jr.; Kerr, J.A.; Rossi, M.J.; Troe, J. *J. Phys. Chem. Ref. Data* **1997**, *26*, 521. (c) DeMore, W.B.; Sander, S.P.; Golden, D.M.; Hampson, R.F.; Kurylo, M.J.; Howard, C.J.; Ravishankara, A.R.; Kolb, C.E.; Molina, M.J. *JPL Publication* 97-4 **1997**. (d) Taylor, P.H.; Rahman, M.S.; Arif, M.; Dellinger, B.; Marshall, P. *Symp. Int. Combust. Proc.* **1996**, *26*, 497. (e) Wallington, T.J.; Hurley, M.D. *Environ. Sci. Technol.* **1993**, *27*, 1448. (f) Francisco, J.S. *J. Chem. Phys.* **1992**, *96*, 7597. (g) Libuda, H.G.; Zabel, F.; Fink, E.H.; Becker, K.H. *J. Phys. Chem.* **1990**, *94*, 5860, and references therein.

4.   The NIST Chemical Kinetics Database, NIST Standard Reference Database, U.S. Dept. of Commerce, Technology Administration, National Institute of Standards and Technology: Gaithersburg, MD, 17-2Q98.

5.   (a) Alvarez-Idaboy, J.R.; Mora-Diez, N.; Boyd, R.J.; Vivier-Bunge, A. *J. Am. Chem. Soc.*, **2001**, *123*, 2018. (b) Mora-Diez, N.; Alvarez-Idaboy, J.R.; Boyd, R.J. *J. Phys. Chem.*, **2001**, in press.

6.   (a) Wallington, T.J.; Hurley, M.D.; Ball, J.C.; Kaiser, E.W. *Environ. Sci. Technol.* **1992**, *26*, 1318. (b) Hasson, A.S.; Moore, C.M.; Smith, I.W.M. *Int. J. Chem. Kinet.* **1998**, *30*, 541. (c) Sanhueza, E.C.; Heicklen, J. *J. Phys. Chem.* **1975**, *79*, 7. (d) Gay, B.W.; Hanst, P.L.; Bufalini, J.J.; Noonan, R.C. *Environ. Sci. Technol.* **1976**, *10*, 58. (e) Niki, H.; Maker, P.D.; Savage, C.M.; Breitenbach, L.P. *Int. J. Chem. Kinet.* **1980**, *12*, 1001. (f) Niki, H.; Maker, P.D.; Savage, C.M.; Breitenbach, L.P.; Martinez, R.I.; Herron J.T. *J. Phys. Chem.* **1982**, *86*, 1858. (g) Tuazon, E.C.; Atkinson R.; Aschmann, S.M.; Goodman, M.A.; Winer, A.M. *Int. J. Chem. Kinet.* **1988**, *20*, 241. (h) Fantechi, G.; Jensen, N.R.; Saastad, O.; Hjorth, J.; Peeters, J. *J. Atmos. Chem.* **1998**, *31*, 247.

7.   (a) Eyring, H. *J. Chem. Phys.* **1935**, *3*, 107. (b) Evans, M.G., Polanyi, M. *Trans. Faraday Soc.* **1935**, *31*, 875.

8.   (a) Eckart, C. *Phys. Rev.* **1930**, *35*, 1303. (b) Shin, H. *J. Chem. Phys.* **1963**, *39*, 2934.

9.   Noxon, J.F.; Norton, R.B.; Henderson, W.R. *J. Geophys. Res.* **1978**, *5*, 675.

10. (a) Platt, U.; Perner, D.; Winer, A.M.; Harris, G.W.; Pitts, N.J. *Geophys. Res. Lett.* **1980**, *7*, 89. (b) Noxon, J.F.; Norton, R.B.; Marovich, E. *Geophys. Res. Lett.* **1980**, *7*, 125.

11. Atkinson, R. *Atmos. Environ.* **2000**, *34*, 2063.

12. (a) Calvert, J.G.; Stockwell. W.R. *Environ. Sci. Technol.* **1983**, *17*, 428A. (b) Atkinson, R.; Plum, C.N.; Carter, W.P.L.; Winer, A.M.; Pitts, J.N., Jr. *J. Phys. Chem.* **1984**, *88*, 2361. (c) Seinfeld, J.H. *Science* **1989**, *243*, 745. (d) Schwartz, S.E. *ibid.*, 753. (e) McElroy, M.B.; Salawitch, R.J. *ibid.*, 763.

13. (a) Louw, R.; van Harm, J.; Nieboer, H. *J. Air Pollut. Contr. Ass.* **1973**, *23*, 716. (b) Cantrell, C.A.; Davidson, J.A.; Busarow, K.L.; Calvert, J.G. *J. Geophys. Res.* **1986**, *91*, 5347. (c) Miller, C.E.; Francisco, J.S. *J. Phys. Chem.* **2001**, *105*, 750.

14. Bandow, H.; Okuda, M.; Akimoto, H. *J. Phys. Chem.* **1980**, *84*, 3604.

15. Wayne, R.P.; Barnes, I.; Biggs, P.; Burrows, J.P.; Canosa-Mas, C.E.; Hjorth, J.; Le Bras, G., Moortgat, G.K.; Perner, D.; Poulet, G.; Restelli, G.; Sidebottom, H. *Atmos. Environ.* **1991**, *25A*, 1.

16. (a) D'Anna, B.; Nielsen, C.J. *J. Chem. Soc. Faraday Trans.* **1997**, *93*, 3479. (b) Monks, P.S.; Stief, L.J.; Krauss, M.; Kuo, S.C.; Zhang, Z.; Klemm, R.B. *J. Phys. Chem.* **1994**, *98*, 10017.

17. (a) Pérez-Casany, M.; Sánchez-Marín, J.; Nebot-Gil, I. *J. Am. Chem. Soc.* **2000**, *122*, 11585. (b) Pérez-Casany, M.; Nebot-Gil, I.; Sánchez-Marín, J. *J. Phys. Chem. A* **2000**, *104*, 6277, 10721, 11340. (c) King, M.D.; Canosa-Mas, C.E.; Wayne, R.P. *Phys. Chem. Chem. Phys.* **1999**, *1*, 2231, 2239. (d) Martínez E.; Cabañas, B.; Aranda, A.; Martín, P; Salgado, S. *J. Atmos. Chem.* **1999**, *33*, 265. (e) Martínez E.; Cabañas, B.; Aranda, A.; Martín, P; Salgado, S. *J. Phys. Chem. A* **1999**, *103*, 5321. (f) Fantechi, G.; Jensen, N.R.; Hjorth, J.; Peeters, J. *Atmos. Environ.* **1998**, *32*, 3547. (g) Pérez-Casany, M.; Nebot-Gil, I.; Sánchez-Marín, J. *J. Org. Chem.* **1998**, *63*, 6978. (h) Chew, A.A.; Atkinson, R.; Aschmann, S.M *J. Chem. Soc. Faraday Trans.*, **1998**, *94*, 1083. (i) Noremsaune, I.M.W.; Langer, S.; Ljungström, E.; Nielsen, C.J. *J. Chem. Soc. Faraday Trans.* **1997**, *93*, 525. (j) Hallquist, M.; Langer, S.; Ljungström, E.; Wängberg, I. *Int. J. Chem. Kinetics* **1996**, *28*, 467. (k) Martínez E.; Cabañas, B.; Aranda, A.; Wayne, R.P. *J. Chem. Soc. Faraday Trans.*, **1996**, *92*, 53, 4385. (l) Berndt, T; Boge, O. *J. Atmos. Chem.* **1995**, *21*, 275. (m) Galan, B.C.; Marston, G.; Wayne, R.P. *J. Chem. Soc. Faraday Trans.* **1995**, *91*, 1185. (n) Skov, H.; Benter, T.; Schindler, R.N.; Hjorth, J.;

Restelli, G. *Atmosph. Environ.* **1994**, *28*, 1583. (o) Grosjean, D.; Williams, E. *Atmos. Environ.* **1992**, *26A*, 1395.

18.   (a) Langer, S.; Ljungström, E. *Int. J. Chem. Kinetics* **1994**, *26*, 367. (b) Langer, S.; Ljungström, E. *J. Chem. Soc. Faraday Trans.* **1995**, *91*, 405.

19.   (a) Cabañas, B.; Salgado, S.; Martín, P; Baeza, M.T.; Martínez E. *J. Phys. Chem. A* **2001**, *105*, 4440. (b) Papagni, C; Arey, J.; Atkinson, R. *Int. J. Chem. Kinetics* **2000**, *32*, 79. (c) Ullerstam, M.; Langer, S.; Ljungström, E. *Int. J. Chem. Kinetics* **2000**, *32*, 294. (d) Alvarado, A; Arey, J.; Atkinson, R. *J. Atmos. Chem.* **1998**, *31*, 281. (e) Glasius, M; Calogirou, A; Jensen, N.R.; Hjorth, J.; Nielsen, C.J. *Int. J. Chem. Kinetics* **1997**, *29*, 527. (f) Hallquist, M; Wängberg, I.; Ljungström, E. *Environ. Sci. Technol.* **1997**, *31*, 3166.

20.   (a) Atkinson, R. *J. Phys. Chem. Ref. Data* **1991**, *20*, 459. (b) Hjorth, J.; Ottobrini, G.; Restelli, G. *J. Phys. Chem.* **1988**, *92*, 2669. (c) Cantrell, C.A.; Stockwell, W.R.; Anderson, L.G.; Busarow, K.L.; Perner, D.; Schmeltekopf, A.; Calvert, J.G.; Johnston, H.S. *J. Phys. Chem.* **1985**, *89*, 139. (d) Atkinson, R.; Plum, C.N.; Carter, W.P.L.; Winer, A.M.; Pitts, J.N., Jr. *J. Phys. Chem.* **1984**, *88*, 1210, 4446 (correction).

21.   (a) D'Anna, B.; Langer, S.; Ljungström, E.; Nielsen, C.J.; Ullerstam, M. *Phys. Chem. Chem. Phys.* **2001**, *3*, 1631. (b) Dlugokencky, E.J.; Howard, C.J. *J. Phys. Chem.* **1989**, *93*, 1091. (c) Morris, E.D., Jr.; Niki, H. *J. Phys. Chem.* **1974**, *78*, 1337.

22.   Frisch, A.; Frisch, M.J. *Gaussian 98 User's Reference*; Gaussian Inc.: Pittsburgh, PA, p. 65, 1998.

23.   Mora-Diez, N; Boyd, R.J., in preparation.

24.   (a) Zhang, Q.; Bell, R.; Truong, T.N. *J. Phys. Chem.* **1995**, *99*, 592. (b) Durant, J.L. *Chem. Phys. Lett.* **1996**, *256*, 595.

25.   (a) Kawaguchi, K.; Ishiwata, T.; Hirota, E.; Tanaka, I. *Chem. Phys.* **1998**, *231*, 193. (b) Wang, D.; Jiang, P.; Qian, X.; Hong, G. *J. Chem. Phys.* **1997**, *106*, 3003. (c) Ishiwata, T.; Tanaka, I.; Kawaguchi, K.; Hirota, E. *J. Mol. Spectrosc.* **1992**, *153*, 167. (d) Kawaguchi, K.; Ishiwata, T.; Tanaka, I.; Hirota, E. *Chem. Phys. Lett.* **1991**, *180*, 436. (e) Hirota, E.; Kawaguchi, K.; Ishiwata, T.; Tanaka, I. *J. Chem. Phys.* **1991**, *95*, 771. (f) Weaver, A.; Arnold, D.W.; Bradforth, S.E.; Neumark, D.M. *J. Chem. Phys.* **1991**, *94*, 1740. (g) Kawaguchi, K.; Hirota, E.; Ishiwata, T.; Tanaka, I. *J. Chem. Phys.* **1990**, *93*, 951. (h) Friedl, R.R.; Sander, S.P. *J. Phys. Chem.* **1987**, *91*, 2721. (i) Ishiwata, T.; Tanaka, I.; Kawaguchi, K.;

Hirota, E. *J. Chem. Phys.* **1985**, *82*, 2196. (j) Reuveni, A.; Luz, Z. *J. Magn. Res.* **1976**, *23*, 271.

26.   (a) Eisfeld, W.; Morokuma, K. *J. Chem. Phys.* **2000**, *113*, 5587. (b) Cao, X.Y.; Hong, G.Y.; Wang, D.X.; Li, L.M.; Xu, G.X. *Chinese J. Chem.* **2000**, *18*, 267. (c) Sherril, C.D.; Lee, M.S.; Head-Gordon, M. *Chem. Phys. Lett.* **1999**, *302*, 425. (d) Mayer, M.; Cederbaum, L.S.; Köppel, H. *J. Chem. Phys.* **1994**, *100*, 899. (e) Stirling, A.; Pápai, I.; Mink, J.; Salahub, D.R. *J. Chem. Phys.* **1994**, *100*, 2910. (f) Staton, J.F.; Gauss, J.; Bartlett, R.J. *J. Chem. Phys.* **1992**, *97*, 5554. (g) Kaldor, U. *Chem. Phys. Lett.* **1991**, *185*, 131. (h) Kaldor, U. *Chem. Phys. Lett.* **1990**, *166*, 599. (i) Ishiwata, T.; Fujiwara, L.; Nagure, Y.; Obi, K.; Tanaka, I. *J. Phys. Chem.* **1983**, *87*, 1349. (j) Lund. A.; Thuomas, K.-Å. *Chem. Phys. Lett.* **1976**, *44*, 569.

27.   (a) Crawford, T.D.; Lee, T.J.; Handy, N.C.; Schaefer III, H.F. *J. Chem. Phys.* **1997**, *107*, 9980. (b) Eriksson, L.A.; Wang, J.; Boyd, R.J.; Lunell, S. *J. Phys. Chem.* **1994**, *98*, 792. (c) Staton, J.F.; Gauss, J.; Bartlett, R.J. *J. Chem. Phys.* **1991**, *94*, 4084. (d) Boehm, R.C.; Lohr, L.L. *J. Comp. Chem.* **1991**, *112*, 119. (e) Morris, V.R.; Bhatia, S.; Hall, J.H., Jr. *J. Phys. Chem.* **1991**, *95*, 9203. (f) Kim, B.; Hammond, B.L.; Lester, W.A., Jr.; Johnston, H.S. *Chem. Phys. Lett.* **1990**, *168*, 131. (g) Morris, V.R.; Bhatia, S.; Hall, J.H., Jr. *J. Phys. Chem.* **1990**, *94*, 7414. (h) Boehm, R.C.; Lohr, L.L. *J. Phys. Chem.* **1989**, *93*, 3430. (i) Davy, R.D.; Schaefer III, H.F. *J. Chem. Phys.* **1989**, *91*, 4410. (j) Kim, B.; Johnston, H.S.; Clabo, D.A., Jr.; Schaefer III, H.F. *J. Chem. Phys.* **1988**, *88*, 3204. (k) Siegbahn, P.E.M. *J. Comput. Chem.* **1985**, *6*, 182. (l) Baird, N.C.; Taylor, K.F. *Chem. Phys. Lett.* **1981**, *80*, 83. (m) Dewar, M.J.S.; Rzepa, H.S. *J. Am. Chem. Soc.* **1978**, *100*, 784. (n) Olsen, J.F.; Burnelle, L. *J. Am. Chem. Soc.* **1970**, *92*, 3659. (o) Chantry, G.W.; Horsfeld, A.; Morton, J.R.; Wiffen, D.H. *Mol. Phys.* **1962**, *5*, 589.

28.   (a) Löwdin, P.-O. *Rev. Mod. Phys.* **1963**, *35*, 496. (b) Löwdin, P.-O. *Adv. Chem. Phys.* **1969**, *14*, 283.

29.   Johnson, B.G.; González, C.A.; Gill, P.M.W.; Pople, J.A. *Chem. Phys. Lett.* **1994**, *221*, 100.

30.   Kestner, N.R.; Combariza, J.E. in *Reviews in Computational Chemistry*, Volume 13, Lipkowits, K.B. and Boyd, D.B., Editors, Wiley-VCH, New York, p. 99, 1999.

31.   (a) Boys, S.F.; Bernardi, F. *Mol. Phys.* **1970**, *19*, 553. (b) Handy, N.C.; Pople, J.A.; Shavitt, I. *J. Phys. Chem.* **1996**, *100*, 6007 (This paper gives a biographical synopsis on Boys's work). (c) Jansen, H.B.; Ros, P. *Chem. Phys. Lett.* **1969**, *3*, 140.

32. Benson, S.W. *Thermochemical Kinetics*, 2nd Ed., Wiley & Sons, New York, p. 43, 1976.

33. Chuang, Y-Y; Truhlar, D.G. *J. Chem. Phys.* **2000**, *112*, 1221.

34. (a) Galano, A.; Alvarez-Idaboy, J.R.; Montero, L.A.; Vivier-Bunge, A. *J. Comp. Chem.* **2001**, *22*, 1138. (b) Alvarez-Idaboy, J.R.; Mora-Diez, N.; Boyd, R.J.; Vivier-Bunge, A. *J. Am. Chem. Soc.*, **2000**, *122*, 3715.

35. Mora-Diez, N.; Boyd, R.J. *J. Phys. Chem.*, **2001**, submitted.

PART 2

Chapter 7. Calculation of Excited States

The ground state of a system is the lowest energy configuration of the electrons within the various MOs. Excited states are stable, higher energy electronic configurations. Such states are produced when a sample is exposed to UV-visible (UV-vis) radiation. They are relevant to many areas of chemistry, including photochemistry and spectroscopy. Modeling excited states and predicting their properties is a very difficult task.[1]

7.1. Theoretical overview of UV-vis spectroscopy

The UV-vis absorption bands of organic molecules are commonly associated with electronic transitions in the valence shell. These bands are characterized by their position, intensity and shape. These will be discussed in this section.

Electronic absorption frequencies (v) at which UV-vis absorption bands appear can be obtained from the differences between the energies of the ground (E_i) and excited (E_f) states.

$$v = \frac{E_f - E_i}{h} \tag{7.1}$$

Frequency, wavelength (λ), and wavenumber ($\bar{v}$) are related by the following expressions:

$$c = \lambda v = \frac{v}{\bar{v}} \tag{7.2}$$

where c is the speed of light. They can be used to describe the position of electronic absorption bands.

Based on the HF approximation, electrons are considered to be in spin-orbitals, but actually due to the electronic correlation and the fact that electrons are fermions, it is better to say that they are in Fermi states that have major contributions of certain spin-orbitals. E_i and E_f would be the initial and final Fermi states.

157

As a consequence of Brillouin's theorem,[2] singly excited determinants $\left| \Phi_i^a \right\rangle$ (obtained by

a single replacement of an occupied spin-orbital χ_i with an unoccupied spin-orbital χ_a)

will not interact directly with a reference HF determinant $\left| \Phi_o \right\rangle$. They can mix indirectly

with $\left| \Phi_o \right\rangle$ through the doubly excited determinants. Hence, a CIS procedure cannot

improve the ground state HF energy ($E_{CIS} = E_{HF}$). However, the CIS treatment is

frequently used to calculate excited states from which electronic spectra, are predicted.

The energy required to promote an electron from an occupied orbital "i" to a virtual

orbital "a" is given by the expression:[3]

$$\Delta E = \varepsilon_a - \varepsilon_i - J_{ia} + 2K_{ia} \qquad (7.3)$$

where ε_a and ε_i are the energies of the initial and final orbitals; J_{ia} is the molecular

Coulomb integral:

$$J_{ia} = (ii \mid aa) = \int \phi_i^*(1)\phi_i(1)\frac{1}{r_{12}}\phi_a^*(2)\phi_a(2)d\tau_1 d\tau_2 \qquad (7.4)$$

and K_{ia} is the molecular exchange integral:

$$K_{ia} = (ia \mid ai) = \int \phi_i^*(1)\phi_a(1)\frac{1}{r_{12}}\phi_a^*(2)\phi_i(2)d\tau_1 d\tau_2 \qquad (7.5)$$

The expression (7.3) refers to the energy associated with singlet-singlet transitions. For

singlet-triplet transitions the corresponding expression is:[3]

$$\Delta E = \varepsilon_a - \varepsilon_i - J_{ia} \qquad (7.6)$$

These latter transitions will not be treated in this work because usually they do not appear

in the electronic spectrum.

Excited states calculated from HF orbitals are in poor agreement with experiment because

virtual orbitals are not well optimized, a consequence of the fact that there is no

electronic density associated with them. However, they are of great importance in the

calculation of spectroscopic data. To improve the calculation of spectra once the ground

state has been obtained in a previous geometry optimization (yielding MO coefficients

and eigenvalues), a CI calculation must follow.

A single-point calculation (*i.e.*, the calculation of the energy of the system at a specified configuration) on an optimized structure allows us to determined the HF reference electronic configuration associated with the (singlet) ground state of a molecular system. A CIS calculation mixes all single determinant wavefunctions that can be obtained from the ground state by exciting electrons from a subset of the occupied spin-orbitals to a subset of the unoccupied spin-orbitals. These subsets can be specified as a fixed number or by an energy criterion associated with the energy difference between the occupied and unoccupied spin-orbitals. The degree of mixing of states depends primarily upon the energy differences among them. Generally, configurations of high energy do not interact strongly with the reference configuration, and the higher the maximum energy, the greater the number of configurations to be included in the CIS calculation.[4] The Hamiltonian matrix elements between the singly excited determinants are computed, and the matrix is diagonalized to get the spectrum of electronic CIS states, which are expressed (for singlet transitions) as a linear combination of the normalized singly excited Slater determinants:

$$\Psi_{CIS} = 2^{-\frac{1}{2}} \sum_i c_i \left(\left|\Phi_i^{\bar{s}}\right\rangle - \left|\Phi_i^s\right\rangle \right) \tag{7.7}$$

$\left|\Phi_i^{\bar{s}}\right\rangle$ represents the excitation of an electron between the β spin-orbitals χ_i and χ_a, and

$\left|\Phi_i^s\right\rangle$ represents the corresponding excitation between the α spin-orbitals χ_i and χ_a. Triplet CIS states are also obtained but will not be included in this discussion. The coefficients c_i are determined variationally to obtain the lowest CIS energies. The difference in energy between the ground and CIS states determines the energy of the calculated excited electronic states. If N singly excited determinants are considered, N CIS wavefunctions and excited states are obtained.

Detailing the composition of the CIS states, the nature of the calculated electronic transitions (*e.g.* $\sigma\sigma^*$, $\pi\pi^*$, $n\sigma^*$, $n\pi^*$, etc.) can be determined, although there are cases where this assignment is not possible due to a mixture of a great number of states (MOs). The symmetry of the MOs (σ, π, n) implied in the single excitations of the determinants with higher square of the CIS coefficients (c_i^2) will determine the nature of the UV-vis

bands. For a normalized wavefunction, $\sum_i c_i^2 = 1$, that is the reason c_i^2 is the magnitude

usually reported, instead of c_i. The symmetry of the MOs can be deduced by considering how they are localized in the molecule, or by analyzing the nature of the AOs that make a major contribution to the MOs.

Various schemes have been proposed to denote the states of a molecule and the absorption bands that correspond to transitions between these states. Some of these schemes are collected in Table 7.1.[5]

Table 7.1. Labeling of electronic transitions.[a]

System	State Symbol		Example
Enumerative	S_0	Singlet ground state	$S_0 \rightarrow S_1$
	$S_1, S_2, S_3, ...$	Excited singlet states	$S_1 \rightarrow S_2$
	$T_1, T_2, T_3, ...$	Triplet states	$T_1 \rightarrow T_2$
Group theory	A, B, E, T	Irreducible representation of	$^1A_1 \rightarrow {}^1B_2$ [b]
	(with indices g, u, 1, 2,',")	the point group of the molecule	$^1A_{1g} \rightarrow {}^3E_{1u}$
Kasha	$\sigma, \pi, n,$	Ground state orbitals	$\pi \rightarrow \pi^*$
	σ^*, π^*	Excited state orbitals	$n \rightarrow \sigma^*$
Platt	A	Ground state	$^1A \rightarrow {}^1B_a$ [b]
	B, L	Excited states	$^1A \rightarrow {}^1L_b$
	(with indices a, b)		
Mulliken	N	Ground state	$V \leftarrow N$
	Q, V, R	Excited states	$Q \leftarrow N$
Clar	α, p, β	Intensity and band shape	

[a] Reproduced from reference 5; [b] The upper left index indicates the multiplicity

In theoretical calculations the intensity of a transition is given by a dimensionless quantity called the oscillator strength (f):

$$f_{i \to f} = \left(\frac{8\pi^2 m_e}{3e^2 h^2} \right) (E_f - E_i) |\mu_{fi}|^2 \tag{7.8}$$

where μ_{fi} is the electric dipole transition moment, e and m_e are the charge and rest mass of the electron, respectively, and h is Planck's constant.

The oscillator strength[6] may be interpreted as the ratio of the observed intensity to the intensity of radiation absorbed or emitted by a harmonically bound electron in an atom. For strongly allowed transitions, (*e.g.* $\sigma\sigma^*$, $\pi\pi^*$) f is close to 1; for symmetry forbidden transitions (*e.g.* $n\pi^*$, $n\sigma^*$) f is often close to 0.1, and for spin forbidden transitions (*e.g.* singlet→triplet) f is close to 10^{-5}. The oscillator strength is measured experimentally by determining the integrated absorption intensity, the greater the area under the absorption curve, the greater the intensity of the transition. In practice, the magnitude used to characterize the intensity of an absorption is the molar absorption or extinction coefficient, ε.

The energies of the initial and final states of transitions are determined by the CIS eigenvalues, and the transition dipole moments are obtained by using the CIS eigenvectors, that is,

$$\mu_{fi} = \left\langle \Psi_{CIS} \left| \sum_k \hat{m}_k \right| \Phi_o \right\rangle, \qquad \hat{m}_k = -|e| r_k \tag{7.9}$$

where k is the sum over electrons. Ψ_{CIS} and Φ_o are the total wavefunctions of the final and initial states. The orientation of μ_{fi} with respect to the molecular axis system is frequently called the absolute polarization direction. It is determined by its highest component.[5]

Absorption occurs only if the light can interact with a transient molecular charge or current distribution characterized by μ_{fi}. The transition dipole moment may be thought of as the dipole moment of the transition density $\left\langle \Psi_{CIS}^* \Phi_o \right\rangle$. The square of the transition

dipole moment is a measure of the change in charge distribution as a result of the electronic transition. The higher $|\mu_{fi}|^2$, the higher the probability of the transition and the greater its intensity.

Selection rules[5] establish the conditions under which the dipole moment of the transition vanishes and allow us to differentiate between formally "allowed" and "forbidden" transitions. A transition with a vanishing transition moment is referred to as forbidden and should have zero intensity. The transition moment of an allowed transition, although non-vanishing, can still be very small, whereas a forbidden transition may be observed in the spectrum with finite intensity if the selection rule is relaxed by an appropriate perturbation.

The shape of a UV-vis absorption band depends on the number and relative intensity of its vibrational components (fine structure). The Franck-Condon principle[7] explains the spectral intensity distribution of the vibrational transitions between two different electronic states of a molecule. This principle states that, because the electron mass is much less than that of the nuclei, the electronic transition in a molecule takes place much more rapidly in comparison to the vibrational motion. As a consequence, the nuclear rearrangement takes place after, not during, the electronic transition. The quantum mechanical basis for the Franck-Condon principle is the extent of overlap between the vibrational wavefunctions of the two electronic states: the more the overlap, the stronger the transition.

Frequently, because of the differences in the bonding characteristics of the upper and the lower states, the potential energy curves are displaced with respect to each other. Consequently, a transition can occur to more than one vibrational level in the excited electronic state (Fig. 7.1). Solvent effects can also alter the shape (besides its position and intensity) of absorption bands, but they will not be discussed in this section.

The accuracy of the computed spectrum depends on the size (*i.e.*, orbital active space) of the CIS calculation (if this is the method employed). In general, the ordering of excited

states is affected only by singly and doubly excited configurations. However, the actual values for the state energies, intensities and polarization directions, are sensitive to higher configurations.[5] Therefore, rational methods for selecting configurations are of great importance. Energy criteria alone are not sufficient for this purpose. Rather, rough estimates of the matrix elements $\left\langle \Phi_s \left| \sum_k \hat{m}_k \right| \Phi_o \right\rangle$ are needed in order to decide which configurations affect the computed values. Such a scheme was developed, for example, by Downing at *al.*[8]
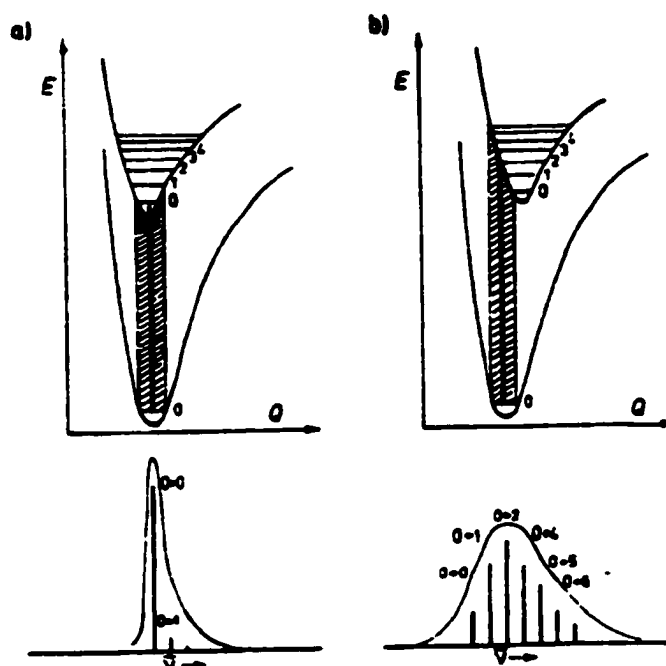
Figure 7.1. Schematic representation of the band shape expected from the Franck-Condon principle: a) approximately equal equilibrium internuclear distances in the ground and excited states; b) internuclear distance in the excited state larger than that of the ground state.
Reproduced from reference 5

7.2. The absorption spectra of PAHs

The UV-vis absorption spectra of organic compounds containing π electrons are easy to observe experimentally. The electronic spectra of cyclic conjugated π systems depend

inherently on the number of π electrons. Benzenoid hydrocarbons constitute a class of compounds whose UV-vis spectra have been investigated extensively both experimentally and theoretically. [5,9,10]

Typical UV-vis spectra of aromatic hydrocarbons are shown in Fig. 7.2. For these compounds the notation scheme introduced by Platt[11] is widely used (among others). These spectra contain absorption bands that fall into three categories according to their intensity. Bands of the first type (^1L_b) are of low intensity ($\epsilon = 10^2$-10^3), may be hidden by the other bands, and often possess a complicated vibrational structure. Bands of the second type (^1L_a or ^1B_a) are moderately intense ($\epsilon \approx 10^4$); ^1L_a bands usually show a regular vibrational structure. Bands of the third type (^1B_b) are very strong ($\epsilon > 10^5$) and have little vibrational structure.[5]

As can be seen from Fig. 7.2, the increment in size of the π system from naphthalene to tetracene leads to an extension of the conjugation and consequently, all absorption bands are shifted bathochromically (*i.e.*, to longer wavelengths) and their intensities are also enhanced. Fig. 7.3 shows how the experimentally observed wavelengths for two series of PAHs, the linearly annelated *acenes* and the angularly annelated *phenes*, change with increasing number of benzene rings. The shifts in the ^1L_b and ^1B_b positions are parallel to one another in both series, whereas the bathochromic shift of the ^1L_a band (whose excitation energy is related to the HOMO-LUMO energy difference) of acenes upon annelation is so pronounced that even in anthracene it masks the ^1L_b band.

7.2.1. Substituent effects on the spectra of PAHs

In general, the long-wavelength bands of the spectra of aromatic compounds are most sensitive to substituents. In spite of changes due to substituents, the spectra of substituted derivatives nevertheless possess some resemblance to those of the unsubstituted aromatic hydrocarbon both in the position of bands and in intensity values, although there are exceptions (*e.g.*, quinones, anhydrides, phthalimides, etc.). The spectrum produced by a particular functional group depends to some extent on the position of the substituent. The

substituent position effects are less in molecules of lower symmetry, such as phenanthrene and chrysene, than in molecules of greater symmetry, such as naphthalene, anthracene and pyrene. Moreover, modifications due to position are usually not so great as the difference between the various polynuclear systems.[10]
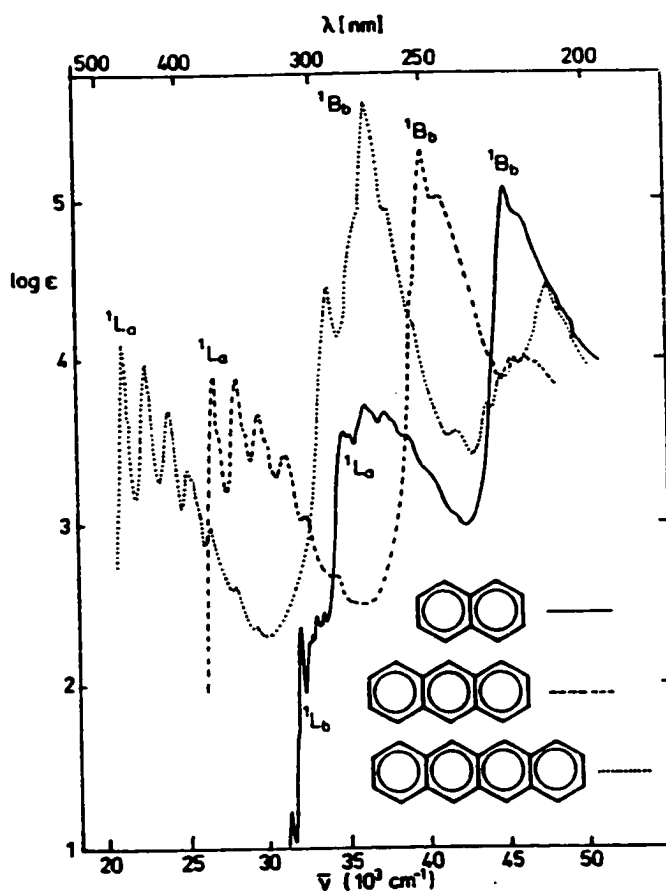
Figure 7.2. Examples of typical absorption spectra of PAHs. Reproduced from reference 5

Alkyl substituents shift bathochromically all the transitions, and sometimes alter the total number of spectral bands but these changes usually occur in the very weak bands at long wavelengths. The presence of more than one alkyl group increases the bathochromic shift, but usually not as much as a single alkyl group does. Friedel and Orchin,[10] after

examining the spectra of various alkyl-substituted naphthalenes and 1,2-benzanthracenes, have also stated the non-existence of a correlation between the size of the shift and the number of substituents, or their position on the ring. Askew[12] has indicated that alkylphenanthrenes substituted in the 1-position generally give the greatest bathochromic shift.
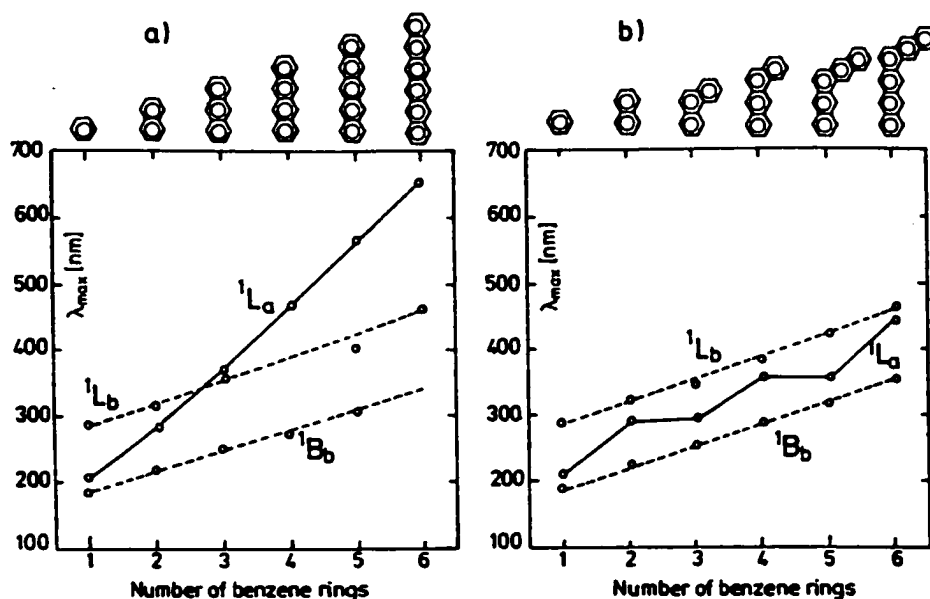
Figure 7.3. Wavelengths of ^1L_b, ^1L_a or ^1B_b bands of condensed aromatic hydrocarbons plotted versus the number of benzene rings
a) linearly annelated and, b) angularly annelated aromatics.
Reproduced from reference 5

The difference in chain length of the alkyl substituent on PAHs has little effect. In the series methylbenzene to n-hexylbenzene, there is a slight shift and decrease of fine structure with increasing size of alkyl group, and this effect becomes progressively less as one approaches n-hexylbenzene.[13] In more highly condensed aromatic systems, alkyl groups of various sizes have little or no effect because of the relatively large size of the aromatic nucleus.[5]

Partially hydrogenated aromatic rings are compounds in which at least one non-aromatic ring (with or without olefin bond) is attached to an aromatic skeleton (Fig. 7.4). Steric hindrance cannot appreciably affect the resonance in this class of olefins because the ring structure compels the olefin bond to remain approximately in the same plane as the aromatic system.[5]
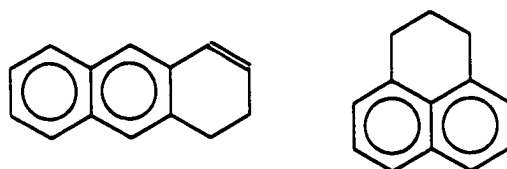
Figure 7.4. Examples of partially hydrogenated aromatic rings.

7.3. *Ab initio* methods for the calculation of excited states

Quantum chemical calculations of excitation energies and transition dipole moments vary according to the level of sophistication. Several *ab initio* and semi-empirical methods have been developed for this purpose.

For a detailed *ab initio* description of excited states[5] it is necessary to use diffuse basis functions. In addition, electron correlation effects for the ground state and the open-shell excited state must be considered. A widely used scheme for such calculations is the MRD-CI (multi-reference double excitation CI), which considers all doubly excited configurations with respect to a number of reference configurations. The number of elements in the CI matrix may easily exceed $5 \cdot 10^5$. The CI expansion is therefore truncated by appropriate selection criteria and energy extrapolations are used to approximate the contributions from omitted configurations.[14]

The most accurate data for excited states are obtained from CASSCF calculations[1,15] and a subsequent step is the use of the second-order perturbation theory with the CASSCF wavefunction as a reference state.[16]

In general, these methods lead to very good agreement between calculated and observed values. Rydberg states (unoccupied orbitals outside of the valence shell, characterized by high quantum number orbitals, which are much more extended than valence orbitals) are also described well. For $\pi\pi^*$ transitions, agreement with experiment is more difficult to achieve.

Modeling excited states as combinations of single substitutions from the HF ground state at the *ab initio* level, that is, without parameterizations and solving explicitly all the integrals and matrix elements, give rise to a method to which reference has been made in previous sections, CIS. This method is comparable to HF theory for ground state systems in that it is qualitatively accurate if not always highly quantitatively predictive. Like HF theory, CIS is an inexpensive method that can be applied to large systems.[1,17]

Time-dependent calculations often result in obtaining a wavefunction that oscillates between the ground and first excited states. From this solution, it is possible to extract both these states.[18] Time-dependent HF (TD-HF) is the HF approximation for the time-dependent Schrödinger equation:

$$\hat{H}\Psi = i\frac{h}{2\pi}\left(\frac{\partial\Psi}{\partial t}\right)$$ (7.10)

TD-HF, together with other time-dependent methods, is also used in computing non-linear optical properties.[19]

In the last several years, time-dependent DFT has emerged as an attractive method for the calculation of excited states.[20] Its success in predicting excited states for PAHs has also been demonstrated.[21] At its simplest, TD-DFT is the translation of the random phase approximation (RPA, a time-dependent *ab initio* method with a formulation and results equivalent to TD-HF)[18] into DFT.[22]

7.4. Semi-empirical methods for the calculation of excited states

Over the past decades the semi-empirical MO methods of quantum chemistry have been widely used in computational studies. SCF π-electron calculations have been carried out since the 1950s and valence-electron calculations since the 1960s. Several books[23] and reviews[24,25] describe the underlying theory, the variants of semi-empirical methods, and the numerical results in much detail. Section 2.7 covers this topic in a general way.

The HMO[26] model is the easiest way of calculating excited states, but the spectra of PAHs cannot be well reproduced. Excited states are described by just one singly excited configuration (this is frequently possible to a good approximation for transitions from the highest occupied MO (HOMO) into the lowest unoccupied MO (LUMO)), and because electronic repulsions are not explicitly considered, the formulae for the excitation energies (linearly related to orbital energy differences) and the transition moments are considerably simplified.

The PPP method[27,23a] was an important stage in the calculation of electronic excitation properties of organic molecules. This theory was designed for the correlation and prediction of the wavelengths and intensities of the first main UV-vis absorption bands and other properties of complex unsaturated molecules. CI and SCF procedures are combined in a simple and economical way, and although it is limited to π electrons, it has been used extensively and with great success.

The inclusion of all valence electrons in the framework of semi-empirical procedures to calculate excited states of organic molecules occurred 15 years later, when del Bene and Jaffé published the papers related to their CNDO/S method[28] (spectroscopic CNDO) after the development of CNDO-INDO routines by Pople et al. in 1965.[23c] It is a modified CNDO/2 method extended to spectroscopic calculations. A new empirical parameter is introduced to differentiate resonance integrals between σ orbitals from those between π orbitals, and the semi-empirical Coulomb integrals are substituted with similar integrals to those used in the PPP method. The changes introduced in this method made possible

the study of nπ^* transitions and calculations for non-planar π systems, for which the PPP method was not applicable. When limited CI including singly and doubly excited configurations is considered,[29] fairly good agreement between computed and experimental results is obtained for singlet as well as triplet excitation energies. Some applications to excited state calculations of aromatic hydrocarbons are cited in reference 30.

CNDOL[31] is another approach, based on the CNDO approximation, which has been used to calculate excited states.[32] This method only uses parameters that are chosen *a priori*: STO exponents, valence state ionization potentials and electron affinities of each *l* azimuthal quantum number type of valence atomic orbital. That is, no parameters are empirically adjusted to fit results to experimental or previous accurate theoretical data. This method is combined with a single CI variational procedure.

The PCILO (perturbative CI using totally localized orbitals) method[33] is one of the methods which bypass the SCF stage by using a perturbational CI scheme in its place. This non-iterative method is based on the idea of treating a molecule as a system of localized bonds. First, the bond orbitals are obtained from a standard STO basis by minimizing the bond-bond overlap through construction of hybrid orbitals. Next, the various integrals over the resulting hybrid AOs are determined either by approximation formulae (semi-empirical method) or *ab initio*.[34] In particular, it is possible to adopt the ZDO approximation at the CNDO or INDO[35] levels. The PCILO method is especially interesting in the case of highly localized systems, where the bond-orbital description is quite satisfactory.

Another semi-empirical alternative for the calculation of ionization potentials and electronic transition energies of valence electrons is called LNDO/S (LNDO for spectroscopy).[36] This method is distinguished by explicit inclusion of electron correlation in a semi-empirical frame on the basis of large CI calculations. Simplifications in the SCF part of the method are achieved by use of the LNDO (local neglect of differential overlap) approximation. It is an approximation intermediate between CNDO and INDO

on the one hand and NDDO on the other. The basic idea is contained in the application of the ZDO approximation in the local instead of the molecular coordinate system. In this approximation all integrals except the Coulomb integrals are set equal to zero. Moreover, different types of Coulomb integrals may be used. This method has shown promising results.[36,37]

A frequent problem in excited-state applications of semi-empirical valence-electron methods including CI with multiply excited configurations is that the parameterization already may have been determined so as to include correlation effects for the ground-state results, and these are thus counted twice. Thiel in 1981 proposed the semi-empirical MNDOC method,[38] a reparameterization of the MNDO model[39] with explicit inclusion of electron correlation (C for correlation) by CI. Together with appropriate selection criteria for truncating the CI and with the possibility of using different reference configurations for different states, this method is well suited for calculating excitation energies, potential energy surfaces, and hence geometries of excited states,[40] but the basic shortcomings of the ZDO approximation remain in effect and again lead to excitation energies that are usually too small.[5,24]

7.4.1. The INDO/S method

INDO/S[41] (spectroscopic INDO, also called ZINDO/S or ZINDO) has been designed for calculating electronic spectra, particularly vertical excitation energies at given ground-state geometries. It is a semi-empirical CI method parameterized at the CIS level, like the CNDO methods previously mentioned, that employs the INDO approximation.[42] Without using an extensive parameterization, it has been quite successful in calculating electronic spectra of large molecules.[41,43] ZINDO often gives poor results when used for geometry optimizations.

The INDO approximation includes the one-centre exchange integrals (neglected in the CNDO approximation) necessary in accurately separating different terms from within a configuration (e.g., the singlet and triplet states arising from $n\pi^*$ transitions are degenerate within the CNDO approximation). In addition, it has been found[41a] that these

integrals increase the interaction between states arising from $\pi\pi^*$ and $\sigma\sigma^*$ transitions, in many cases reducing the calculated transition energies and oscillator strengths.

Under the CNDO approximation the two electron integrals:

$$(ij \mid kl) = \int \phi_i^*(1)\phi_j(1)\frac{1}{r_{12}}\phi_k^*(2)\phi_l(2)d\tau_1 d\tau_2 = \sum_{\alpha\beta\gamma\delta} C_{i\alpha}C_{j\beta}C_{k\gamma}C_{l\delta}(\alpha\beta \mid \gamma\delta) \qquad (7.11)$$

(where the indices i, j, k, l refer to MOs; the α, β, γ, δ, refer to AOs) reduce to:

$$(ij \mid kl)_{CNDO} = \sum_{\alpha\gamma} C_{i\alpha}C_{j\alpha}C_{k\gamma}C_{l\gamma}\gamma_{\alpha\gamma} \qquad (7.12)$$

This term is equal to zero when α and γ are σ and π orbitals, respectively.

Under the INDO approximation many terms of equation (3.10) do not reduce to zero, as indeed they should not:

$$(ij \mid kl) = \sum_{\alpha\neq\beta,\gamma\neq\delta} C_{i\alpha}C_{j\beta}C_{k\gamma}C_{l\delta}(\alpha\beta \mid \gamma\delta)\delta^{AB}\delta^{CD}\delta^{AC} + \sum_{\alpha\gamma} C_{i\alpha}C_{j\alpha}C_{k\gamma}C_{l\gamma}\delta^{AC}\Delta_{\alpha\gamma} + (ij \mid kl)_{CNDO} \qquad (7.13)$$

$$\alpha \in A, \beta \in B, \gamma \in C, \delta \in D$$

$$\Delta_{\alpha\gamma} \equiv (\alpha\alpha \mid \gamma\gamma) - F^0(\alpha\gamma)$$

The first term refers to the situation when α, β, γ and δ are all on one centre; the second term refers to the situation when α and γ are on the same centre. $F^0(\alpha\gamma)$ represents the one-centre two-electron integrals.

The transition energies calculated with equation (7.3) are the diagonal elements of the CI Hamiltonian matrix, $\left\langle {}^1\Phi_{i\rightarrow a} \middle| \hat{H} \middle| {}^1\Phi_{i\rightarrow a} \right\rangle$. The off-diagonal elements are:

$$\left\langle {}^1\Phi_o \middle| \hat{H} \middle| {}^1\Phi_{i\rightarrow a} \right\rangle = 0 \quad \text{(Brillouin's theorem)}$$

$$\left\langle {}^1\Phi_{i\rightarrow a} \middle| \hat{H} \middle| {}^1\Phi_{j\rightarrow b} \right\rangle = 2(ai \mid jb) - (ab \mid ij) \qquad (7.14)$$

During the parameterization of the method several factors appear. The developers of ZINDO found that the parameters required to reproduce orbital energy orderings and UV-vis spectra are different from those required to reproduce accurate structures by geometry

optimizations. Empirical overlap weighting factors (f_π and f_σ) are introduced to account for this. They are used to scale down the π-π two-centre interactions, and scale up the σ-σ interactions. Their effect is to modify the resonance integrals for the off-diagonal elements of the Hamiltonian matrix.[41a]

In semi-empirical formulations, resonance integrals account for σ and π bonding patterns in molecules. These one-electron two-centre integrals represent the kinetic and electron-nuclear attraction energies associated with a charge distribution that lies between two atoms (overlap distribution). The actual magnitude of the resonance integral is proportional to the overlap integral $S_{\mu\nu}$. There are two types of atomic orbital overlap: σ-σ and π-π. The σ-π overlap is generally absent due to orthogonality conditions. Adjusting the weights provides a mechanism to account for the relative contributions of σ versus π bonding.

Usually a value of 1.267 is given to f_σ.[41b] Several different values have been used in the literature for f_π, for UV-vis spectra and orbital eigenvalues of organic molecules, 0.585 is commonly used,[26c] and for transition metal complexes,[41c] 0.640 has been recommended. As in many computational methods trends and differences are determined more accurately than absolute values. ZINDO calculations on several substituted benzenes underestimate the wavelengths of the major UV absorption by about 20 nm, but the relative values are very well reproduced.[4]

Sophisticated *ab initio*-CI methods for excited states calculations are available, but their computational cost is too high. Such calculations are not expected to become routine for large molecules in the near future. Therefore the semi-empirical valence-electron procedures continue to present an important way out of this dilemma.

7.5. References

1.   Foresman, J.B.; Frisch, Æ. *Exploring Chemistry with Electronic Structure Methods*, 2nd edition, Gaussian, Inc., 1996.

2.   Szabo, A.; Ostlund, N.S. *Modern Quantum Chemistry: Introduction to Advanced Electronic Structure Theory*, Dover, New York, 1989.

3.   Ridley, J.; Zerner, M.C. *Theor. Chim. Acta* 1973, *32*, 111.

4.   *HyperChem: Computational Chemistry*, Hypercube Inc., 1996.

5.   Klessinger, M.; Michl, J. *Excited States and Photochemistry of Organic Molecules*, VCH Publishers, 1995.

6.   Atkins, W. *Quanta: A Handbook of Concepts*, 2nd Edition, Oxford University Press, 1991.

7.   (a) Franck, J. *Trans. Faraday Soc.* **1925**, *21*, 536. (b) Condon, E.U. *Phys. Rev.* **1928**, *32*, 858. (c) Herzberg, G. *Spectra of Diatomic Molecules*, D. Van Nostrand: Princenton, NJ, 1950. (d) Ahmed, F. *J. Chem. Edu.* **1987**, *64*, 427.

8.   Downing, J.W.; Michl, J.; Jørgensen, P.; Thulstrup, E.W. *Theor. Chim. Acta* **1974**, *32*, 203.

9.   Platt, J.R. and co-workers, *Systematics of the Electronic Spectra of Conjugated Molecules: A Source Book*, Wiley, New York, 1964.

10.   Friedel, R.A.; Orchin, M. *Ultraviolet Spectra of Aromatic Compounds*, Wiley: New York, 1951.

11.   Platt, J.R. *J. Chem. Phys.* **1949**, *17*, 484.

12.   Askew, F.A. *J. Chem. Soc.* **1935**, 509.

13.   Pestemer, M.; Gubitz, O. *Monatsh.* **1934**, *64*, 426. (in Ref. 5)

14.   Peyerimoff, S.D.; Buenker, R.J. *Adv. Quantum Chem.* **1975**, *9*, 69.

15.   Roos, B.O. *Int. J. Quantum Chem.: Quantum Chem. Symp.* **1980**, *14*, 175.

16.   Roos, B.O.; Andersson, K.; Fülscher, M.P.; Malmqvist, P.; Serrano-Andrés, L.; Pierloot, K.; Merchán, M. in *Advances in Chemical Physics*, Prigogine, I. and Rice, S.A. (Editors), Vol. XCIII, Wiley, New York, p. 219, 1996.

17. Foresman, J.B.; Head-Gordon, M.; Pople, J.A.; Frisch, M.J. *J. Phys. Chem.* **1992**, *96*, 135.

18. Young, D.C. *Computational Chemistry: A Practical Guide for Applying Techniques to Real-World Problems*, John Wiley & Sons, New York, 2001.

19. Kurtz, H.A.; Dudis, D.S. *Rev. Comput. Chem.* **1998**, *12*, 241.

20. (a) Bauernschmitt, R.; Ahlrichs, R. *Chem. Phys. Lett.* **1996**, *256*, 454. (b) Bauernschmitt, R.; Haser, M.; Treutler, O.; Ahlrichs, R. *Chem. Phys. Lett.* **1997**, *264*, 573. (c) Bauernschmitt, R.; Ahlrichs, R.; Hennrich, F.H.; Kappes, M.M. *J. Am. Chem. Soc.* **1998**, *120*, 5052. (d) Casida, M.E.; Jamorski, C.; Casida, K.C.; Salahub, D.R. *J. Chem. Phys.* **1998**, *108*, 4439. (e) Stratmann, R.E.; Scuseria, G.E.; Frisch, M.J. *J. Chem. Phys.* **1998**, *109*, 8218. (f) Nguyen, K.A.; Day, P.N.; Pachter, R. *J. Phys. Chem.* **1999**, *103*, 9378. (g) Rosa, A.; Baerends, E.J.; van Gisbergen, S.J.A.; van Lenthe, E., Groeneveld, J.A.; Snijders, J.G. *J. Am. Chem. Soc.* **1999**, *121*, 10356. (h) Broclawik, E.; Borowski, T. *Chem. Phys. Lett.* **2001**, *339*, 433. (i) Nguyen, K.A.; Pachter, R. *J. Chem. Phys.* **2001**, *114*, 10757.

21. (a) Hirata, S.; Lee, T.J.; Head-Gordon, M. *J. Chem. Phys.* **1999**, *111*, 8904. (b) Heinze, H.H.; Gorling, A.; Rosch, N. *J. Chem. Phys.* **2000**, *113*, 2088. (c) Kwon, O.; McKee, M.L. *J. Phys. Chem. A* **2000**, *104*, 7106. (d) Adamo, C.; Barone, V. *Chem. Phys. Lett.* **2000**, *330*, 152. (e) Weisman, J.L.; Lee, T.J.; Head-Gordon, M. *Spectrochim. Acta A* **2001**, *57*, 931.

22. Tozer, D.J.; Handy, N.C. *Phys. Chem. Chem. Phys.* **2000**, *2*, 2117.

23. (a) Parr, R.G. *The Quantum Theory of Molecular Electronic Structure*, W.A. Benjamin, New York, 1963. (b) Salem, L. *The Molecular Orbital Theory of Conjugated Systems*, W.A. Benjamin, New York, 1966. (c) Pople, J.A.; Beveridge, D.L. *Approximate Molecular Orbital Theory*, McGraw Hill, New York, 1970. (d) Clark, T. *A Handbook of Computational Chemistry*, Wiley, New York, 1985.

24. Thiel, W. in *Advances in Chemical Physics*, Prigogine, I. and Rice, S.A. (Editors), Vol. XCIII, Wiley, New York, p. 703, 1996.

25. (a) Dewar, M.J.S. *Science* **1975**, *187*, 1037. (b) Jug, K. *Theor. Chim. Acta* **1980**, *54*, 263. (c) Dewar, M.J.S. *J. Phys. Chem.* **1985**, *89*, 2145. (d) Thiel, W. *Tetrahedron* **1988**, *44*, 7393. (e) Stewart, J.J.P. in *Reviews in Computational Chemistry*, Lipkowitz, K.B. and Boys, D.B. (Eds.), Vol. 1, VCH, New York, p. 45, 1990.

26. Hückel, E.P. *Z. Physik* **1931**, *70*, 204.

27. (a) Pariser, R.; Parr, R.G. *J. Chem. Phys.* **1953**, *21*, 466, 767. (b) Pople, J.A. *Trans. Faraday Soc.* **1953**, *49*, 1475.

28. Del Bene, J.; Jaffé, H.H. *J. Chem. Phys.* **1968**, *48*, 1807, 4050.

29. (a) Colditz, R.; Grebner, D.; Helbig, M.; Rentsch, S. *Chem. Phys.* **1995**, *201*, 309. (b) Negri, F.; Orlandi, G. *J. Chem. Phys.* **1998**, *108*, 9675.

30. (a) Jorgensen, P.; Poulsen, J.C. *J. Phys. Chem.* **1974**, *78*, 1420. (b) Gudipati, M.S. *Chem. Phys. Lett.* **1992**, *196*, 481. (c) Swiderek, P.; Hohlneicher, G. *THEOCHEM J. Mol. Struct.* **1992**, *94*, 187. (d) Gudipati, M.S.; Maus, M.; Daverkausen, J.; Hohlneicher, G. *Chem. Phys.* **1994**, *186*, 289. (e) *ibid.* **1995**, *192*, 37. (f) Kumar, P.; Garg, R.K.; Parkash, O.; Ram, R.S.; Zaidi, Z.H. *Spectrochim. Acta A* **1997**, *53*, 151. (g) Garg, R.K.; Kumar, P.; Ram, R.S.; Zaidi, Z.H. *Spectrosc. Lett.* **1998**, *31*, 1013. (h) Maus, M.; Rettig, W.; Depaemelaere, S.; Onkelinx, A.; De Schryver, F.C.; Iwai, K. *Chem. Phys. Lett.* **1998**, *292*, 115.

31. Montero, L.A.; Alfonso, L.; Alvarez, J.R.; Pérez, E. *Int. J. Quantum Chem.* **1990**, *37*, 465.

32. (a) Díaz, I; Montero, L.A.; Muñoz, F.; Donoso, J. *THEOCHEM J. Mol. Struct.* **1998**, *433*, 279. (b) Mora-Diez, N.; Montero, L.A.; Fabian, J. *THEOCHEM J. Mol. Struct.* **1998**, *453*, 49. (c) Montero, L.A.; Esteva, A.M.; Molina, J.; Zapardiel, A.; Hernández, L.; Márquez, H.; Acosta, A. *J. Am. Chem. Soc.* **1998**, *120*, 12023.

33. (a) Diner, S. *Theor. Chim. Acta* **1969**, *13*, 1. (b) *ibid.* **1969**, *15*, 100. (c) Langlet, J.; Malrieu, J.P. *Theor. Chim. Acta* **1973**, *30*, 59. (d) Langlet, J. *idib.* **1975**, *38*, 199.

34. Del Re, G.; Berthier, G.; Serre, J. in *Lecture Notes in Chemistry*, Vol. 13, Springer-Verlag, 1980.

35. (a) Douady, J.; Ellinger, Y.; Subra, R. Bull. Soc. Chim. Belg. **1976**, *85*, 1009. (b) *Chem. Phys. Lett.* **1978**, *56*, 58. (c) Douady, J.; Barone, V.; Ellinger, Y.; Subra, R. *Int. J. Quantum Chem.* **1980**, *17*, 211.

36. Lauer, G.; Schulte, K.-W.; Schweig, A. *J. Am. Chem. Soc.* **1978**, *100*, 4925.

37. (a) Schulz, R.; Schweig, A.; Zittlau, W. *Chem. Phys. Lett.* **1984**, *106*, 467. (b) *idem. THEOCHEM J. Mol. Struct.* **1985**, *22*, 115. (c) Heidenreich, A.; Munzel,

N.; Schweig, A. *Z. Naturforsch A* **1986**, *41*, 1415. (d) Hanekamp, G.; Heidenreich, A.; Schweig, A. *J. Mol. Struct.* **1994**, *327*, 193.

38.   Thiel, W. *J. Am. Chem. Soc.* **1981**, *103*, 1413, 1420.

39.   Dewar, M.J.S.; Thiel, W. *J. Am. Chem. Soc.* **1977**, *99*, 4899.

40.   (a) Schweig, A.; Thiel, W. *J. Am. Chem. Soc.* **1981**, *103*, 1425. (b) Reinsch, M.; Howeler, U.; Klessinger, M. *THEOCHEM J. Mol. Struct.* **1988**, *44*, 301. (c) Klessinger, M.; Pötter, T.; van Möllen, C. *Theor. Chim. Acta* **1991**, *80*, 1.

41.   (a) Ridley, J.; Zerner, M.C. *Theor. Chim. Acta* **1973**, *32*, 111. (b) *ibid.* **1976**, *42*, 223. (c) Bacon, A.D.; Zerner, M.C. *Theor. Chim. Acta* **1979**, *53*, 21. (d) Zerner, M.C.; Loew, G.H.; Kirchner, R.F.; Mueller-Westerhoff, U.T. *J. Am. Chem. Soc.* **1980**, *102*, 589.

42.   (a) Pople, J.A.; Beveridge, D.L.; Dobosh, P.A. *J. Chem. Phys.* **1967**, *47*, 2026. (b) Nanda, D.N.; Jug, K., *Theor. Chim. Acta* **1980**, *57*, 95. (c) Jug, K.; Iffert, R.; Schulz, J. *Int. J. Quantum Chem.* **1987**, *32*, 265.

43.   (a) Ridley, J.E.; Zerner, M.C. *J. Mol. Spect.* **1974**, *50*, 457. (b) Krogh-Jespersen, K.; Ratner, M. *Theor. Chim. Acta* **1978**, *47*, 283. (c) Canuto, S.; Zerner, M.C.; Diercksen, G.H.F. *Astrophys. J.* **1991**, *377*, 150. (d) Du, P.; Salama, F.; Loew, G.H. *Chem. Phys.* **1993**, *173*, 421. (e) Zimmermann, R. *J. Mol. Struct.* **1996**, *377*, 35.

Chapter 8. Effects of Alkyl Substituents on the Excited States of Naphthalene

8.1. Introduction

The petroleum industry is vitally interested in the identification and quantification of polycyclic aromatic compounds (PACs).[1] Such species interfere with refining operations and many of them possess carcinogenic or mutagenic properties. There are thousands of PACs in petroleum-related samples and their characterization is extremely difficult because of the structural similarities. Even if complete separation were possible, identification would still be difficult because in many cases standards are not available. State-of-the-art chromatographic methods have to be employed, mainly using UV-visible, fluorescence and mass spectrometric detectors.

It has been proposed that PACs in oil sands samples are basically alkylated polycyclic aromatic hydrocarbons (PAHs), mainly methyl- and ethyl- substituted PAHs, although it has also been suggested that partially hydrogenated PAHs (maybe with reduced rings as substituents) may be present as a consequence of the reduction process undergone by the samples during industrial treatment.[2] Furthermore, mono-aromatic compounds with reduced rings have been found in chromatographic studies of heavy distillates.[3] The presence of alkyl groups causes some problems in the identification of these species because the greater the number of rings the larger the number of possible alkylated isomers and the harder the labour of separation, identification and quantification.

The present study focuses on the effect of alkyl substituents on the excited states of naphthalene, the smallest PAH. The effect of methyl and reduced-ring substituents (cyclic substituents which are completely reduced) on the electronic spectrum of naphthalene is examined. The effect of the successive addition of methyl and reduced-ring substituents on the UV-visible spectrum of naphthalene, will be reported. The calculated electronic spectra of all the reduced derivatives with 2, 3 and 4 substituents are

compared with the spectra of their methylated analogues. The calculated excited states of several reduced derivatives with 7 and 8 substituents are also compared.

The electronic spectrum of naphthalene has been widely studied, in both the vapor phase[4] and in solution.[5] Furthermore, a variety of theoretical calculations have been performed at different levels of theory, semi-empirical[6] and *ab initio*.[7] Polymethyl naphthalenes have also been broadly studied in solution, but few UV-visible spectra of reduced-ring naphthalene derivatives have been reported.[8,5b-d] The effects of -OH, -NH$_2$, -CN and -CHO substituents on the electronic spectra of naphthalene have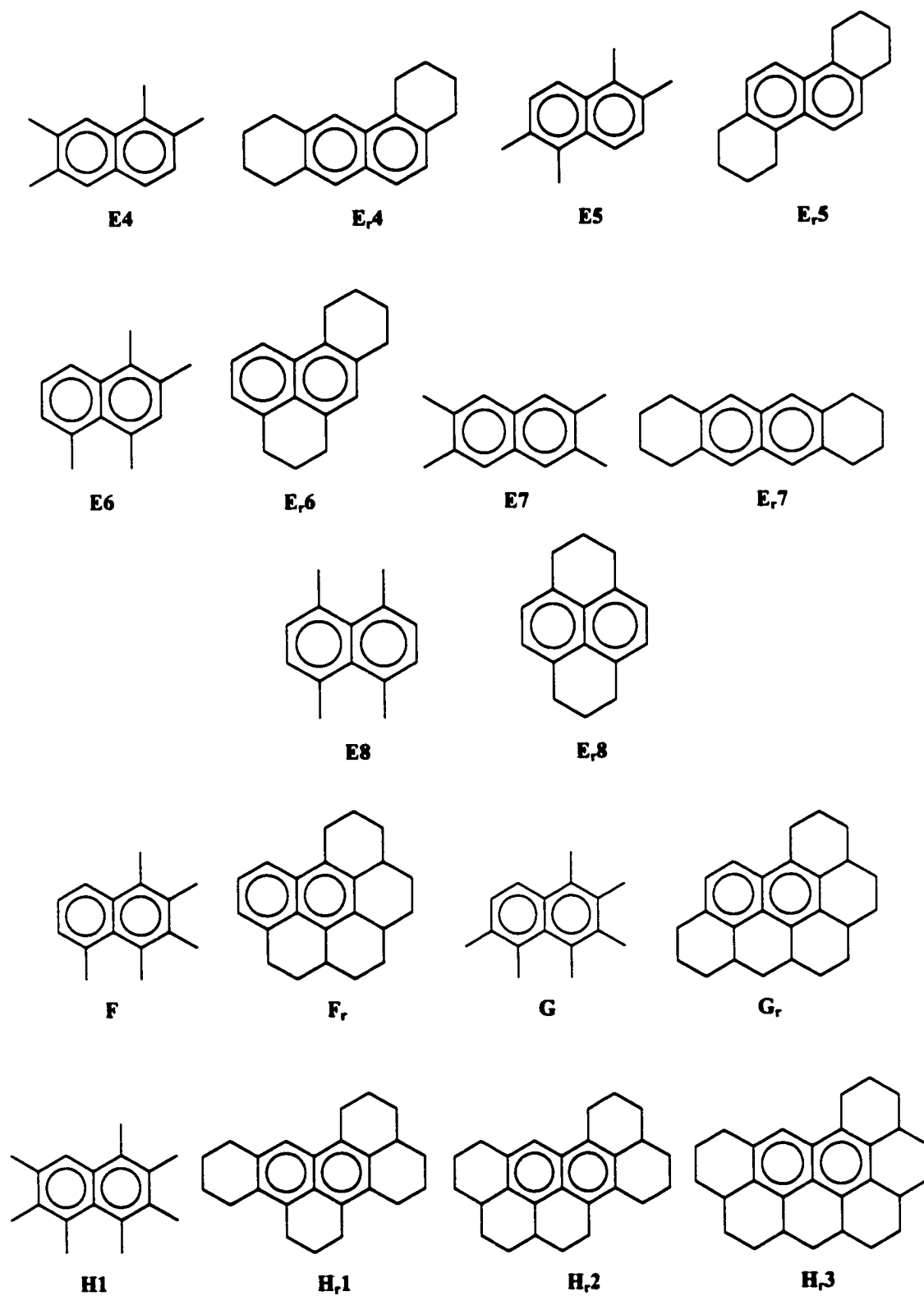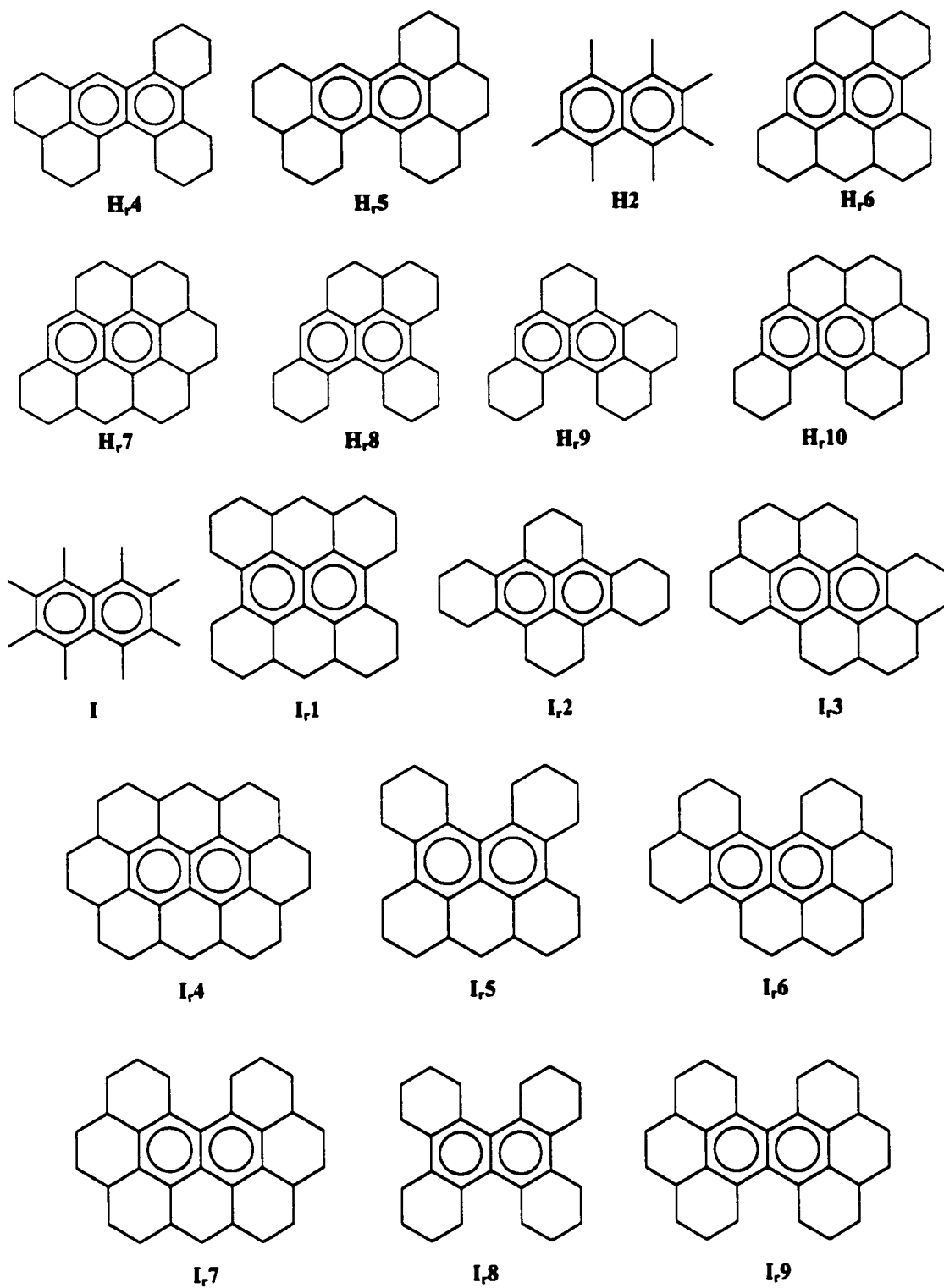 been theoretically analyzed and interpreted by the method of configuration analysis.[9] A systematic theoretical study of the effects of alkyl substituents on the excited states of naphthalene has not been previously reported.

Alkylated naphthalenes are used as a test case study to locate properties of the electronic spectra with respect to individual substituent positions. These results could be useful in the study of larger systems where the wavelengths are longer and a change in the position of alkyl substituents is more likely to be detected and identified.

A total of 57 compounds, listed in Fig. 8.1, were included in this study. For ease of identification these compounds were labeled in alphabetical order according to the number of substituents in the ring. Methylated isomers have also been identified with a number. To distinguish between a methylated naphthalene and its reduced analogues (a reduced naphthalene with the same number and position of substituents linked to the ring) the same letter and number is used, but a subscript is added to the label of the reduced compounds. Hence, labels such as E2, E$_r$2 and E$_r$2' identify a methylated compound (E2) and its reduced analogues (E$_r$2 and E$_r$2'), all with four substituents connected to the ring in the same positions. For molecules of the series H and I, the same subscript is used for the reduced analogues, but the number in the label of the reduced compounds has no relation with the alkylated analogues.
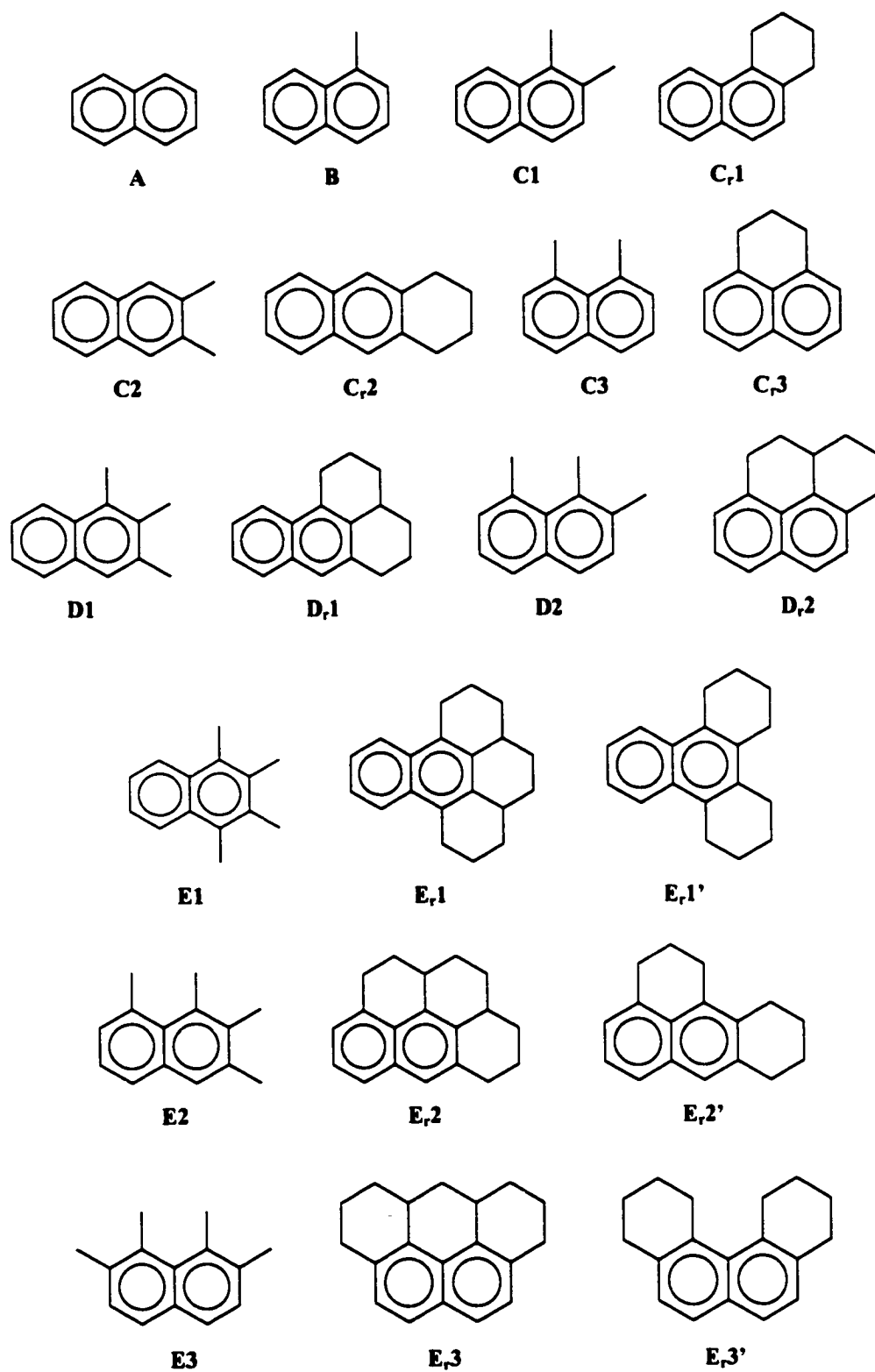
Figure 8.1. Molecules studied and their labels.

E4   E,4   E5   E,5

E6   E,6   E7   E,7

E8   E,8

F   F,   G   G,

H1   H,1   H,2   H,3

Figure 8.1. Molecules studied and their labels. (Cont.)

H₄4   H₄5   H2   H₄6

H₄7   H₄8   H₄9   H₄10

I   I₄1   I₄2   I₄3

I₄4   I₄5   I₄6

I₄7   I₄8   I₄9

Figure 8.1. Molecules studied and their labels. (Cont.)

8.2. Computational details

Because of the size of the molecules chosen for this study (up to 32 heavy atoms), a semi-empirical SCF-MO Hamiltonian was selected for the geometry optimizations of all substituted naphthalenes. Various semi-empirical techniques have previously been used for the geometry optimization of naphthalene.[6c] The AM1[10] optimized geometry of naphthalene is closest to experiment and therefore all the naphthalene derivatives are optimized at the AM1 level as implemented in the MOPAC v.6.0 program package.[11]

Excited electronic states of naphthalene are calculated using the semi-empirical methods for which the appropriate software is available: CNDO/S,[12] CNDOL[13] and ZINDO/S (also known as INDO/S),[6b,14] employing the AM1 optimized geometry. For the CNDO/S and CNDOL methods, as implemented in the program NDOL,[15] 48 lowest-energy singly excited configurations (the maximum number of configurations possible due to constraints of the program) are considered in the CIS procedure. For the ZINDO/S method, as implemented in HyperChem v.5.0,[16] values of 1.267 and 0.585 are employed for the empirical overlap weighting factors f_σ and f_π,[6b] respectively. Moreover, an energy criterion of 13.0 eV for the maximum excitation energy (MEE) of the configurations included in the CIS procedure (this selection will be explained in the following section) is chosen.

Excited states of naphthalene are also calculated by means of *ab initio* CIS,[17,18] time-dependent Hartree-Fock (TD-HF) and density functional theory (TD-DFT),[19] as implemented in Gaussian 98,[20] with Pople's 6-31+G(d) basis set. The DFT calculations are performed using Becke's three-parameter exchange functional (B3)[21] in combination with the Lee, Yang and Parr correlation functional (LYP).[22]

For the cases where experimental results are available, calculations are compared with experimentally determined $\overline{v}_{max}$ (or λ_{max}) rather than $\overline{v}_{o-o}$ (λ_{o-o}) values.[6b]

For the substituted naphthalenes the calculation of excited states is performed with the ZINDO/S method using the specifications previously mentioned. The MEE is set to 12 eV for those compounds with more than three non-aromatic rings (series F, G, H and I), and for the rest of the molecules the MEE is equal to 13 eV. This change is made in order to include approximately the same number of singly excited configurations for each compound.

To simplify the notation for the orbitals, the occupied MOs in the ground state configuration will be called H, H1, H2, ... starting from the HOMO, and the unoccupied MOs by L, L1, L2, ... starting from the LUMO. Thus, H1 denotes the HOMO-1 orbital, and L2 denotes the LUMO+2 orbital.

8.3. Results and Discussion

8.3.1. Excited states of naphthalene

All the singlet transitions calculated at several semi-empirical levels with excitation energies (ΔE) smaller than 5.30 μm^{-1} are reported in Table 8.1, along with their intensities in terms of the oscillator strength (f). For the *ab initio* calculations the first eight singlet excited states are reported. Some experimental results in the vapor phase are also summarized.

The *ab initio* (CIS and TD-HF) calculations give higher excitation energies than the semi-empirical methods. TD-DFT excitation energies are in good agreement with experiment but the intensities are not well reproduced. Many more transitions than those observed are predicted with CNDO/S and CNDOL, and their agreement in position and intensity with experiment is not as good as those predicted with ZINDO/S. Hence, the excited states of the alkylated naphthalenes are studied with the ZINDO/S method.

It was previously shown that a singles only CI calculation (CIS) using the ZINDO/S approximation accurately reproduces the optical spectrum of naphthalene.[6b,c,e] In references 6b and 6c, single excitations that lie within ~6.50 μm^{-1} of the ground state

were included in the CI calculation, as well as some additional selected configurations of the symmetry type of interest (50-70 configurations). In reference 6e a full CIS calculation (including all possible singly excited configurations within the 24 occupied and 24 unoccupied MOs of naphthalene) was performed, but results were in poorer agreement with experiment (Table 8.2). The symmetry of the calculated excited states is also related to the number of configurations included.

Due to these differences, a study of the energy criterion for the selection of single excitations is performed in order to determine the best conditions (considering the quality of the results and the computational time) under which the ZINDO/S method gives results closest to experiment for the excited states of naphthalene. Thus, calculations are performed including singly excited configurations at 11 different maximum excitation energies (MEEs), and within 15-15 (15 occupied MOs and 15 unoccupied MOs) and 20-20 subsets of MOs. The number of configurations (# Conf.) considered in each calculation has also been included in Table 8.3.

When the number of configurations included in the CIS procedure is increased, the calculated excitation energies decrease. However, the energy does not decrease variationally (*i.e.*, excitation energies are not closer to the exact value when an improved procedure is used), since the ZINDO/S single point calculation uses a parameterized (semi-empirical) Hamiltonian. The inclusion of more than the 'necessary' configurations is useless because the calculated excited states are in poorer agreement with experiment. Thus it is important to determine the number of singly excited configurations that have to be included in the CIS procedure. It was also found in this study that the position and intensity of the calculated bands are very dependent on the values given to the overlap weighting factors, especially f_π.

The best agreement with experiment at the lowest computational cost was found to occur with a MEE of 13 eV. Details of the calculated spectrum with this MEE are reported in Table 8.2. These results are in excellent agreement with those reported by Ridley and Zerner[6b,c] and with the five π-π^* transitions observed in the vapor spectrum.[4c] The

Table 8.1. Position (ΔE in μm^{-1}) and intensity (f) of calculated and experimental (in vapor phase) excited states of naphthalene.

	Calculated						Experimental	
	CIS(FC) 6-31+G(d)	TD-HF 6-31+G(d)	TD-DFT B3LYP/6-31+G(d)	CNDO/S (48 conf.)[a]	CNDOL (48 conf.)[a]	ZINDO/S (63 conf.)[a]	Absorption (vapor)[b]	Neon matrix[c]
	4.16(0.090)	3.91(0.015)	3.55(0.009)	3.54(0.006)	3.34	3.26(0.006)	3.20(0.002)	3.21(0.07)
	4.29	4.12	3.63	3.91(0.101)	3.89	3.72(0.162)	3.75(0.102)	3.58(0.13)
	5.00	4.99	4.41	4.36	3.90	4.46		
	5.20	5.08	4.44	4.44	3.92(0.001)	4.60(1.956)	4.75(1.0)	4.73(1.72)
	5.30	5.29	4.66	4.74	3.93(0.028)	4.62		
	5.32	5.29(0.301)	4.73	4.76	3.96	4.91(0.676)	4.95(0.3)	4.91(0.60)
	5.60(2.154)	5.31	4.96	4.78(0.902)	4.24(0.002)	5.05	5.26(0.1)	
	5.62(0.062)	5.50(0.094)	5.02(0.003)	4.86	4.46	5.22		
				4.87	4.50			
				5.03	4.60			
				5.18(0.357)	4.63			
				5.25	4.81			
					4.91			
					4.93(0.018)			
					5.02			
					5.18			
					5.28			

[a] Number of configurations included in the CIS calculation; [b] Ref. 4c; [c] Ref. 4f

Table 8.2. ZINDO/S calculations on naphthalene.

State	Configurations	This work (MEE = 13eV) (63 Conf.)[a]				Ref. 7b,c (50-70 Conf.)[a]		Ref. 7e (Full-CIS) (1153 Conf.)[a]		Experiment[d]	
		Conf.[b] (c^2)	Type	λ (nm)	ΔE[e] (f)	State	ΔE[e] (f)	State	ΔE[e] (f)	State	ΔE[e] (f)
$^1B_{2u}$	$1a_u \rightarrow 2b_{2g}$ $2b_{3u} \rightarrow 2b_{1g}$	H-L1 (0.55) H1-L (0.43)	ππ*	307.2	3.26(0.006)	$^1B_{2u}$	3.25(0.002)	$^1B_{3u}$	3.23(0.003)	$^1B_{2u}$	3.20(0.002)
$^1B_{1u}$	$1a_u \rightarrow 2b_{1g}$	H-L (0.88)	ππ*	268.6	3.72(0.162)	$^1B_{1u}$	3.77(0.148)	$^1B_{2u}$	3.39(0.166)	$^1B_{1u}$	3.75(0.102)
^1A_g	$2b_{3u} \rightarrow 3b_{3u}$ $1b_{2g} \rightarrow 2b_{2g}$	H1-L2 (0.56) H2-L1 (0.28)	ππ*	224.1	4.46	^1A_g	4.48	$^1B_{3u}$	4.28(1.590)		
$^1B_{2u}$	$1a_u \rightarrow 2b_{2g}$ $2b_{3u} \rightarrow 2b_{1g}$	H-L1 (0.42) H1-L (0.55)	ππ*	217.5	4.60(1.956)	$^1B_{2u}$	4.58(1.866)	$^1B_{1g}$	4.29	$^1B_{2u}$	4.75(1.0)
$^1B_{3g}$	$1a_u \rightarrow 3b_{3u}$	H-L2 (0.80)	ππ*	216.6	4.62	$^1B_{3g}$	4.67	^1A_g	4.45		
$^1B_{1u}$	$2b_{3u} \rightarrow 2b_{2g}$	H1-L1 (0.87)	ππ*	203.7	4.91(0.676)	$^1B_{1u}$	4.86(0.672)	$^1B_{2u}$	4.53(0.563)	$^1B_{1u}$	4.95(0.3)
$^1B_{1g}$	$1a_u \rightarrow 5b_{1u}$	H-L4 (0.95)	πσ*	198.1	5.05	$^1B_{1g}$	5.27	$^1B_{3g}$	4.93		
$^1B_{3g}$	$1b_{2g} \rightarrow 2b_{1g}$	H2-L (0.96)	ππ*	191.5	5.22	$^1B_{3g}$	5.27	$^1B_{1g}$	4.95	$^1B_{2u}$	5.26(0.1)

[a] Number of configurations included in the CIS calculation; [b] Dominant configurations of each CIS state; [c] Units are μm^{-1}; [d] Ref. 4c

Table 8.3. ZINDO/S excited states of naphthalene using various energy criteria for the selection of the singly excited configurations.

MEE[a] (eV)	9.0	9.5	10.0	10.5	11.0	11.5	12.0
# Conf.[b]	7	11	11	17	23	29	41
ΔE (f) (in μm^{-1})	3.31 (0.002)	3.31 (0.002)	3.31 (0.002)	3.31 (0.002)	3.31 (0.002)	3.30 (0.004)	3.30 (0.004)
	3.89 (0.501)	3.75 (0.185)	3.75 (0.185)	3.75 (0.185)	3.75 (0.185)	3.75 (0.185)	3.74 (0.163)
	4.64 (2.068)	4.64 (2.068)	4.64 (2.068)	4.62	4.53	4.53	4.46
		4.64	4.64	4.64 (2.068)	4.62	4.60 (1.968)	4.60 (1.968)
		4.95 (0.932)	4.95 (0.932)	4.89	4.64 (2.068)	4.62	4.62
				4.95 (0.932)	4.95 (0.932)	4.95 (0.932)	4.91 (0.676)
				5.23	5.09	5.09	5.05
					5.23	5.23	5.23

MEE[a] (eV)	13.0	14.0	15.0	16.0	15-15[c]	20-20[c]
# Conf.[b]	63	85	123	171	451	801
ΔE (f) (in μm^{-1})	3.26 (0.006)	3.22 (0.003)	3.21 (0.003)	3.21 (0.003)	3.21 (0.003)	3.21 (0.004)
	3.72 (0.162)	3.72 (0.161)	3.71 (0.163)	3.70 (0.164)	3.65 (0.183)	3.53 (0.176)
	4.46	4.46	4.46	4.46	4.41 (1.711)	4.33 (1.723)
	4.60 (1.956)	4.60 (1.966)	4.54 (1.837)	4.53 (1.833)	4.46	4.43
	4.62	4.62	4.62	4.61	4.53	4.45
	4.91 (0.676)	4.91 (0.677)	4.86 (0.646)	4.86 (0.643)	4.71 (0.623)	4.61 (0.630)
	5.05	4.98	4.98	4.94	4.92	4.91
	5.22	5.22	5.22	5.21	5.09	5.01

[a] Maximum excitation energy; [b] Number of configurations considered; [c] Occupied and unoccupied MOs included in the production of singly excited determinants

calculations indicate a forbidden π-σ^* band at 5.05 μm^{-1} ($^1B_{1g}$), and forbidden π-π^* bands at 4.46 μm^{-1} (^1A_g), 4.62 μm^{-1} ($^1B_{3g}$), and 5.22 μm^{-1} ($^1B_{3g}$).

The only difference between experiment and calculation is the symmetry assigned to a band reported at 5.26 μm^{-1} by George and Morris.[4c] On the basis of PPP calculations,[6a] and the intensity of the band, it was assigned as $^1B_{2u}$. However, Ridley and Zerner[6b] explain this band by suggesting that it is $^1B_{3g}$, and that it borrows intensity from the $^1B_{1u}$ band at 4.91 μm^{-1} through one of the b_{2u} modes.

Although Rydberg states have been identified to appear from 5.40 μm^{-1} for naphthalene,[4c] the assignment of the last two excited states (Table 8.2) in terms of dominant singly excited configurations could change if more flexible and computationally expensive ab initio methods with proper one-electron basis sets including Rydberg functions are used. Even the assignment to the other excited states would change if other levels of theory are employed[7c,d] or if more singly excited configurations are included in the CIS procedure.[6c] This situation would also be applicable to the excited states of the naphthalene derivatives studied.

8.3.2. Effects of alkyl substituents on the excited states of naphthalene

Since the degree of reproducibility of the excited states of naphthalene with the chosen method was excellent, it is expected that calculations on alkylated naphthalenes will also be in good agreement with experiment if a similar number of singly excited configurations are included in the CIS procedure, because the π framework is the same. Hence, the main characteristics of the UV-visible spectrum of naphthalene, in terms of the dominant configurations in each CIS state, should be reproduced.

Vapor phase spectra have not been reported for any of the naphthalene derivatives included in this study. Experimental results for polymethylnaphthalenes in hydrocarbons[8] have been used to compare the quality of the calculations. In Table 8.4 the absorption

band maxima reported for some di- and trimethylnaphthalenes are shown along with the ZINDO/S results.

Table 8.4. Absorption band maxima of some di- and trimethylnaphthalenes: ZINDO/S calculations and experimental results

Substitution	Compound	Calculated		Experimental [d]	
		λ (nm) [c]	f	λ_{max} (nm)	log ε
$\alpha\alpha$	1,4-dmn. [a]	281	0.200	289	3.88
	1,5-dmn.	278	0.213	287	3.96
	1,8-dmn.	281	0.223	285	3.85
$\alpha\beta$	1,2-dmn.	278	0.179	285	3.77
	1,3-dmn.	276	0.174	283	3.78
	1,6-dmn.	275	0.161	281	3.80
	1,7-dmn.	276	0.176	280	3.80
$\beta\beta$	2,3-dmn.	273	0.123	278	3.71
	2,6-dmn.	272	0.141	274	3.67
	2,7-dmn.	272	0.118	275	3.69
$\alpha\alpha\alpha$	1,4,5-tmn. [b]	286	0.241	292	3.90
$\alpha\alpha\beta$	1,4,6-tmn.	281	0.184	290	3.82
$\alpha\beta\beta$	1,3,6-tmn.	277	0.142	284	3.70
$\beta\beta\alpha$	2,3,5-tmn.	278	0.149	284	3.89
$\alpha\beta\beta$	1,3,7-tmn.	277	0.175	280	3.74
$\beta\beta\beta$	2,3,6-tmn.	275	0.109	-	-

[a] dmn. = dimethylnaphthalene; [b] tmn. = trimethylnaphthalene; [c] H-L transition; [d] Ref. 8a (dmn.'s), 8d (tmn.'s), 8e (2,3,5-tmn.)

The ZINDO/S calculations are in very good agreement with experimental results. Small differences can be attributed to the presence of solvent (even non-polar solvents can alter slightly the spectra of PAHs). Qualitative changes in the position and intensity of the maxima reported are very well described. The bathochromic and hyperchromic displacements exhibited due to increasing the number of substituents in α positions (see

Fig. 8.2(a)), are very well reproduced.[8b,23] The excited states of alkylated naphthalenes can also be calculated accurately with the ZINDO/S method.
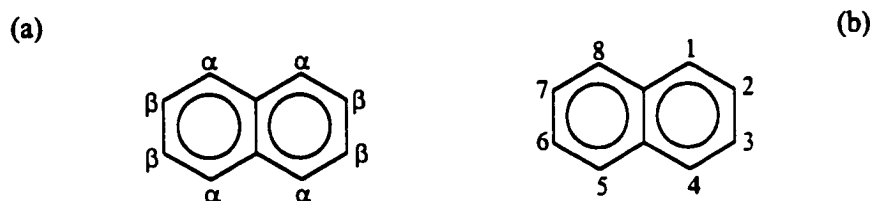
Figure 8.2. Substitution positions in naphthalene.

8.3.2.1. Methylated and reduced series of substituents

The first eight singlet excited states of the series of methylated and reduced-ring naphthalenes were calculated. Alkylation starts from position 1 and continues successively to position 8 (see Figure 8.2(b)). The displacement of the calculated UV-visible bands when increasing the number of alkyl substituents on the naphthalene ring is shown in Figures 8.3 and 8.4, for both series. Every transition has been identified in terms of the dominant singly excited configurations (*e.g.*, H-L1/H1-L, H-L, etc).

In order to obtain more information about the effects of alkyl substituents on the MOs of naphthalene, the ZINDO/S orbital energies of H2, H1, H, L, L1, L2, L4 and L5 of both series, are plotted, as well as the calculated transition energies (based on orbital energy differences) of the dominant configurations of the excited states (the transition H-L5 is also included). This information appears in Figures 8.5 and 8.6.

The composition of the calculated CIS states for all the compounds studied is basically the same as that obtained for naphthalene, although there are some differences in position, intensity and CIS coefficients, as expected. This situation made possible the comparative study of the excited states of naphthalene upon substitution.

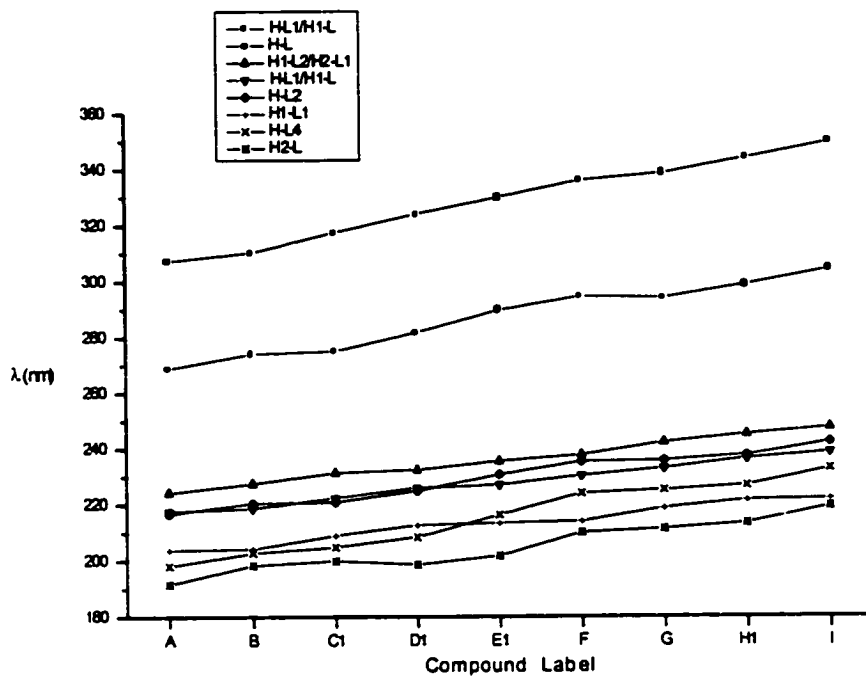**Figure 8.3.** Displacement of the calculated transitions of the methylated series of naphthalenes.
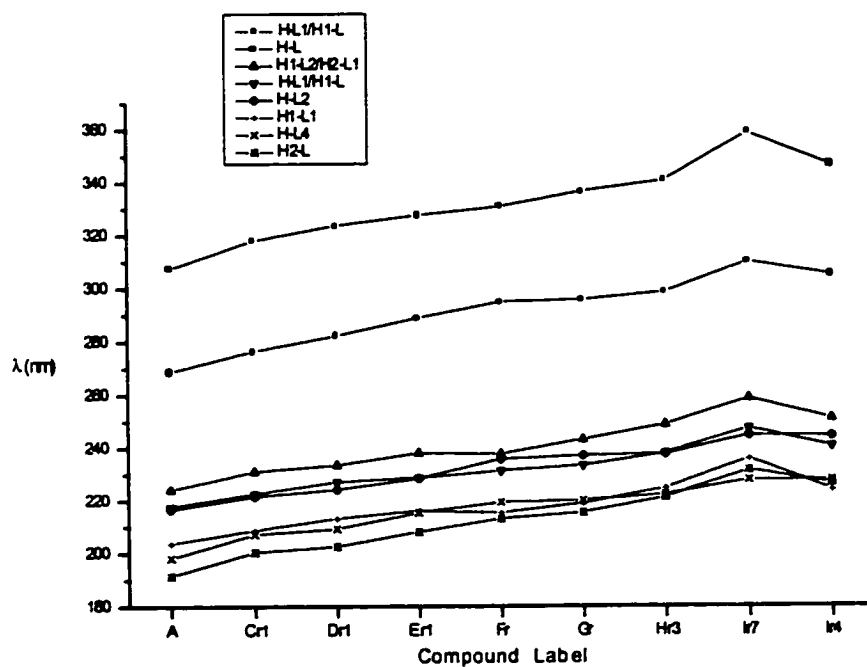

Figure 8.4. Displacement of the calculated transitions of the reduced series of naphthalenes.
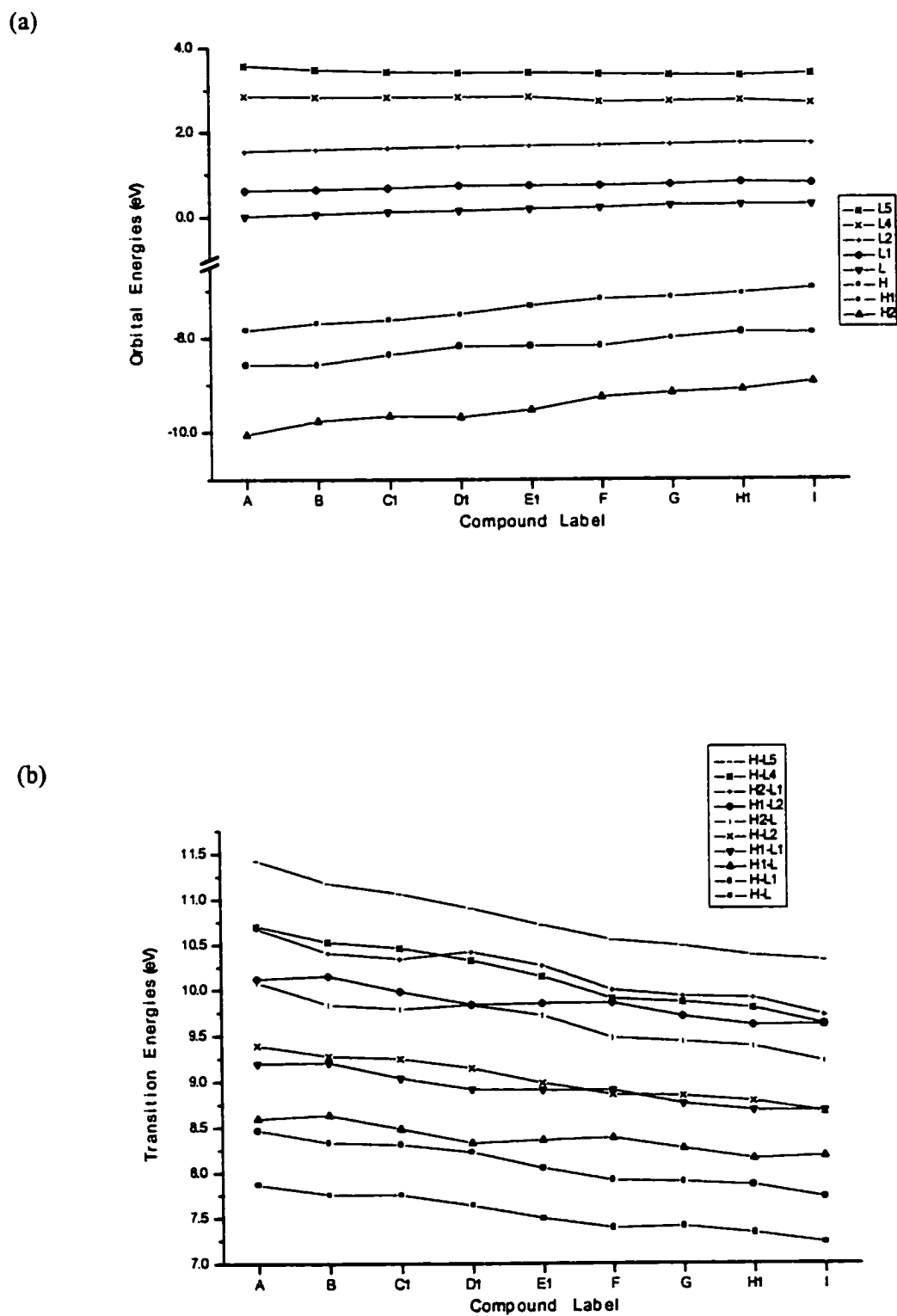
(a)

(b)

Figure 8.5. Orbital (a) and transition energies (b) of the methylated series of naphthalenes.
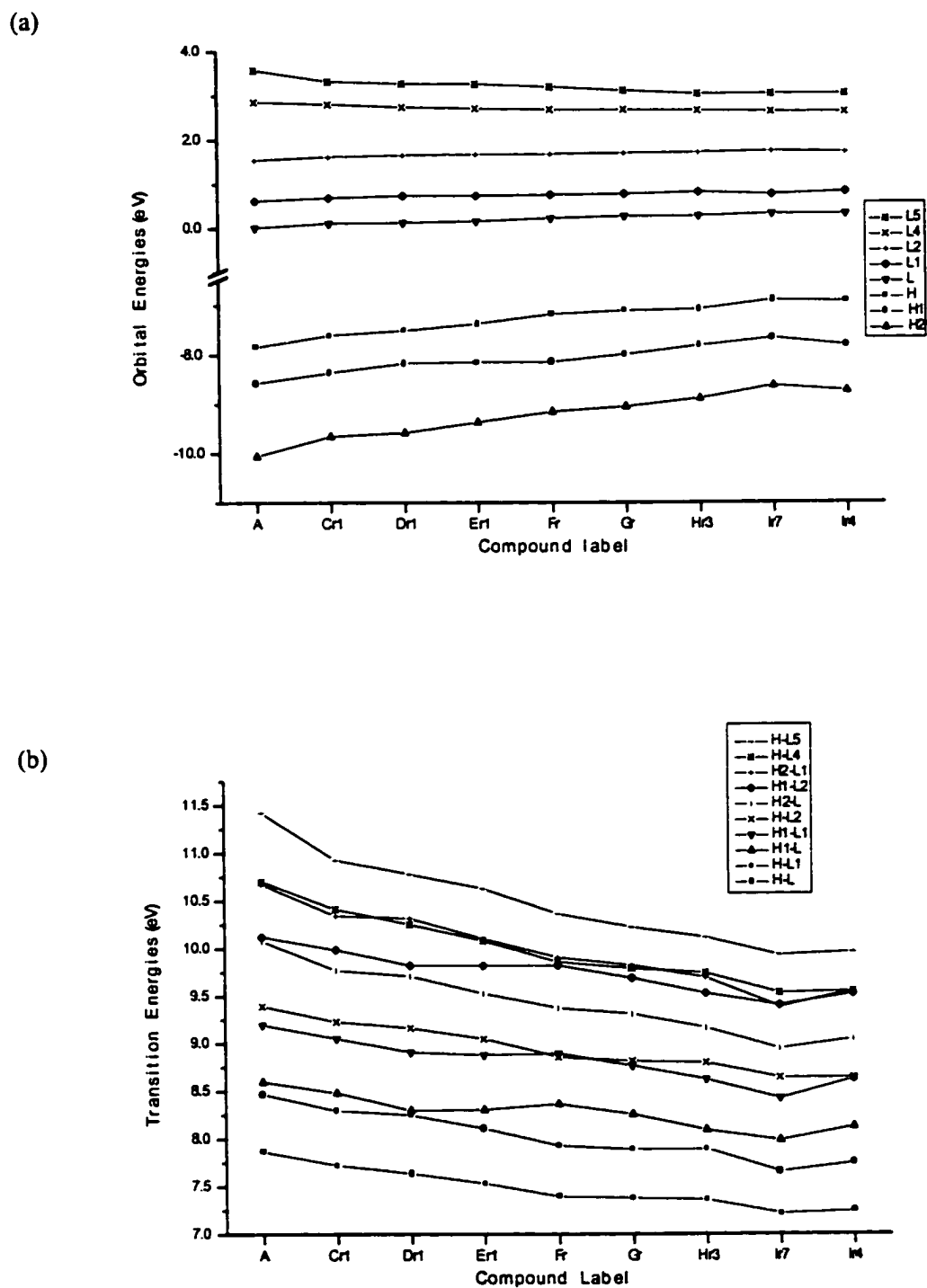
(a)

(b)

Figure 8.6. Orbital (a) and transition energies (b) of the reduced series of naphthalenes.

As the number of substituent alkyl groups increases there is a general shift towards longer wavelengths, in accordance with observations of Mosby[8b] and Laszlo[8c] on methylnaphthalenes, and Askew on methylphenanthrenes.[24] The greatest bathochromic change is obtained in the long-wavelength bands of the spectra, as reported from experiments.[5d]

In these substituents all C atoms have sp^3 hybridization. The atom connected to the naphthalene ring is linked to an sp^2 C atom. The latter is more electronegative than the former since the "s" content in sp^2 hybrid orbitals is higher than in sp^3 orbitals. Hence, a positive inductive effect transfers electronic density from the substituents to the ring, increasing the energy of the MOs and destabilizing the molecule from a kinetic point of view, e.g., reactivity towards electrophilic aromatic substitution reactions is increased.

As can be seen from Figs. 8.5(a) and 8.6(a), the energy of the occupied MOs (H, H1 and H2) increases with the number of substituents. The unoccupied MOs L, L1 and L2 (of π symmetry) also increase in energy but not by as much as the occupied orbitals, and L4 and L5 (unoccupied MOs of σ symmetry) show a slight decrease in energy.

From equation (7.3), the transition energy for excitation from an occupied orbital to a virtual orbital is given by the difference in energy of the two molecular orbitals, plus the exchange and Coulomb terms. So for a transition dominated by one such excitation, the difference in energy of the molecular orbitals is a useful first-order approximation to the transition energy. As a consequence of the changes produced in the energy of the MOs of these molecules with an increase in the number of substituents (Figs. 8.5(a) and 8.6(a)), the energy of the electronic transitions decreases (Figs. 8.5(b) and 8.6(b)) and bathochromic displacements of the calculated UV-visible bands are obtained (Figs. 8.3 and 8.4).

In the methylated series, it can also be seen (Fig. 8.3) that the addition of methyl groups to positions 2 and 6 provokes less pronounced (or almost zero) red-shifts in those states where H and H2 are the only dominant initial MOs (transitions H-L, H-L2, H-L4 and H2-

L). Something similar occurs in the reduced series (Fig. 8.4) when position 6 is occupied (when going from F_r to G_r). The same situation is observed when the transition energies are analyzed (Figs. 8.5(b) and 8.6(b)). Transitions from H and H2 show very little change in energy while a much greater decrease in energy is obtained for transitions from H1. This is very important since it could be possible to determine from some absorption bands if positions 2 or 6 are alkylated even in molecules with different numbers of alkyl substituents, *e.g.* 2,6,7-trimethylnaphthalene (equivalent to 2,3,6-trimethylnaphthalene) and 2,7-dimethylnaphthalene (see the calculated transitions in Table 8.4). This situation corroborates the fact that the strength of the electronic interaction between a substituent and the aromatic ring, as well as the perturbation of MOs, is very dependent on the position being substituted.[8b,23]

Another important observation is the difference found between I_r7 and I_r4 (Fig. 8.4). It is expected that the wavelengths of I_r7 will be smaller (following the trends noted above) or equal (since they have the same number of substituents on the naphthalene ring) to the values obtained for I_r4. The only structural difference between these compounds is the planarity of the aromatic area. Four dihedral angles can be defined to characterize the coplanarity (or non-coplanarity) of the fused rings in naphthalene. These angles and their absolute values for the reduced series of compounds are displayed in Table 8.5. All the methylated naphthalenes included in this study are assumed to be planar. From these results it can be inferred that the contrasting distortion from planarity in I_r7 (maximum of 17°) is the cause of the "anomalous" (higher than expected) wavelength values. In I_r7 orbital energies of occupied MOs are higher than in I_r4 and the overall effect causes the reduction of the transition energy values and CIS energies. It seems that the presence of the alkyl bridge between the fused rings in naphthalene (in I_r4), equilibrates the tensions provoked by the six-member rings, and favours a more planar conformation of the aromatic skeleton. In cases where greater distortions from planarity are obtained, greater differences between the position of the UV-visible bands should be found. This will be discussed further in the next section.

8.3.2.2. Comparison of the effects of methyl and reduced substituents

In order to compare the effects of methyl and reduced substituents on the excited states of naphthalene, the absorption spectra of all possible reduced derivatives with 2, 3 and 4 substituents on the aromatic ring, as well as their methylated analogues, were calculated. The wavelengths of the calculated bands are shown in Figs. 8.7 and 8.8. The values of the dihedral angles that define the fusion of the benzene rings in naphthalene are shown in Table 8.6.

Table 8.5. Dihedral angles (in degrees) of the optimized structures of the methylated and reduced series.

Label	C_r1	D_r1	E_r1	F_r	G_r	H_r3	I_r7	I_r4
d(a,b,c,d)	179.7	179.2	177.4	179.4	178.4	179.2	163.0	176.1
d(b,c,d,e)	177.9	179.2	179.3	178.9	176.8	176.6	169.0	172.9
d(f,g,h,i)	179.3	178.6	177.5	179.5	176.7	173.2	172.9	174.0
d(g,h,i,j)	179.3	179.8	178.9	175.6	175.5	167.3	178.7	175.0
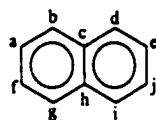
Table 8.6. Dihedral angles (in degrees) of the optimized structures of the reduced series C, D and E.

Label	C_r1	C_r2	C_r3	D_r1	D_r2	E_r1	E_r1'	E_r2
d(a,b,c,d)	179.7	179.9	179.7	179.2	179.7	177.4	178.9	179.8
d(b,c,d,e)	177.9	180.0	179.7	179.2	177.2	179.3	177.8	175.7
d(f,g,h,i)	179.3	179.8	179.8	178.6	179.1	177.5	178.9	179.9
d(g,h,i,j)	179.3	179.9	179.8	179.8	179.1	178.9	177.8	178.5

Label	E_r2'	E_r3	E_r3'	E_r4	E_r5	E_r6	E_r7	E_r8
d(a,b,c,d)	179.6	177.3	169.0	179.3	179.8	179.8	179.7	179.9
d(b,c,d,e)	177.6	177.3	169.0	177.7	176.7	177.4	179.8	179.8
d(f,g,h,i)	179.4	178.0	177.7	179.4	176.7	178.9	179.8	179.9
d(g,h,i,j)	179.0	178.0	177.7	179.8	179.9	178.9	179.8	179.9

It can be seen from the series C, D and E (in the methylated and reduced derivatives) that an increase in the number of α substituents leads to longer wavelengths, especially in those transitions where H and H2 are the only dominant initial MOs, *e.g.* in the order C2, C1 to C3, with their respective reduced derivatives; also from D1 to D2, and in the order E7, E4, E5, E6 to E8. This situation has been experimentally observed for methyl-naphthalenes[8b] and it has been explained in terms of the conjugating power[25] of the various positions.

When an energy cut-off is used to determine the number of configurations to include, the smaller the difference in energy between the occupied and virtual orbitals, the greater the number of configurations that will be considered important. The excited states of the reduced compounds of the series C, D and E are calculated with more configurations than their methylated analogues, using the same energy criterion (MEE = 13 eV). It could be expected that the MOs in the former are closer in energy and the transition energies also are smaller. However, there are no significant differences or trends in the wavelengths of methylated and reduced derivatives in these series (Figs. 8.7 and 8.8). Furthermore, these figures show that there are no major shifts of the energies of the π MOs and that the σ MOs become closer in energy due to the presence of reduced substituents. Moreover, small distortions from planarity are observed in the reduced molecules (Table 8.6), especially in the series C and D (maximum distortion of 2.8°). In the molecules with greater distortion: E_r5 (3.3°), E_r2 (4.3°) and E_r3' (11°), longer wavelengths are obtained in most of the calculated transitions (although the differences are small). The greater the distortion, the greater the red-shift of the calculated bands.

In those cases where a reduced cycle forms a bridge between the fused benzene rings (*e.g.*, C_r3, D_r2, E_r2', E_r3, E_r6 and E_r8), the wavelengths are slightly shorter than in the methylated analogues. In E_r8 the change is greater since reduced cycles are present in both bridge positions. In E_r2 this situation is not observed, perhaps due to the slight distortion from planarity.
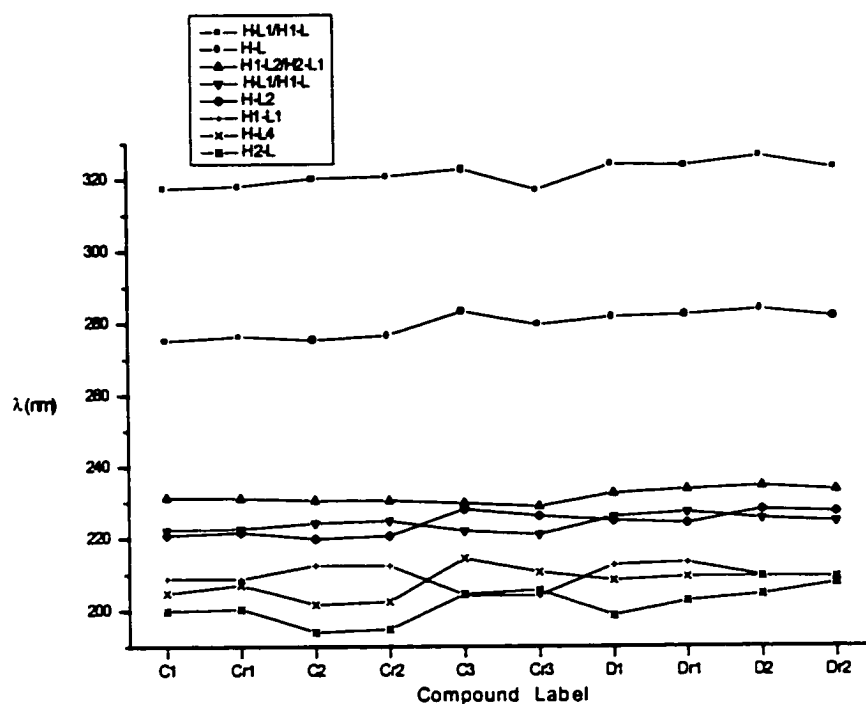
Figure 8.7. Displacement of the calculated transitions of the series C and D.

The wavelengths of the reduced analogues of the same methylated compound, with more cycles (E_r1, E_r2) are longer than the wavelengths of their partners (E_r1', E_r2'). For E_r3 and E_r3' this situation is inverted due to the distortion from planarity observed in E_r3' (11°).

For the reduced molecules with 2, 3 and 4 substituents significant distortions from planarity are not observed (except for E_r3' where up to 11° of distortion is obtained). In order to explore the possible relationship between the planarity of the substituted naphthalene skeleton and the bathochromic displacement of the calculated UV-visible bands upon substitution, derivatives with 7 and 8 substituents (series H and I) were

studied. The greater the number of methyl groups, the greater the number of reduced analogues that can be found. Moreover, the greater the number of reduced substituents, the greater the probability of distortion from planarity of the aromatic skeleton. Only a subset of all possible reduced compounds with 7 and 8 substituents was examined. It is expected that the degree of distortion will depend on the number and positions of the reduced substituents present.
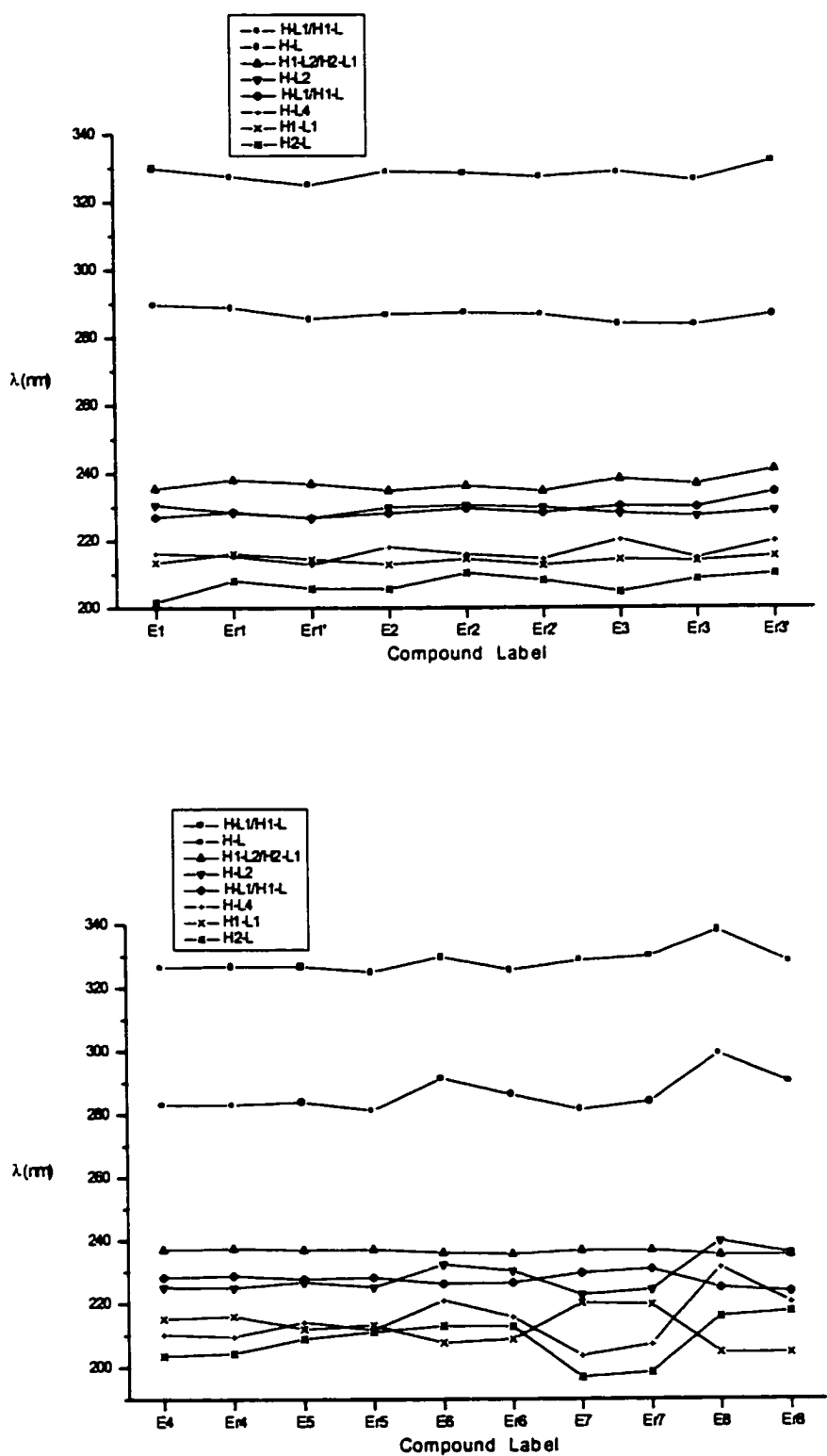
The calculated transitions for the series H (H1 and H2) and I, are shown in Figs. 8.9 and 8.11. Orbital energies are displayed in Figs. 8.10 and 8.12. Dihedral angles that define the degree of planarity of the naphthalene centre and the distances between the farthest points in naphthalene (another criterion to measure distortion from planarity) are reported in Table 8.7.

Compounds of the series H1, H2 and I are labeled from the shortest to the longest wavelengths. The geometrical parameters that characterize the degree of planarity of the aromatic centre show that, in general, the greater the distortion, the greater the red-shift of the calculated transitions.

Values of the dihedral angles far from 180° or values of the distances between the farthest points in naphthalene smaller than those found in the methylated analogues (H1, H2 and I) are measures of the distortion from planarity of these compounds. There are cases where the comparison of the distortions is not evident but, in general, greater distortions are accompanied by greater bathochromic displacements and higher energies of the occupied orbitals.

The biggest wavelength changes are found in the series I, as expected, since all available positions in naphthalene are occupied and greater distortions are possible. Bathochromic displacements of up to 35 nm (0.27 μm^{-1}) were calculated for the most affected transition of the compound with greatest distortion.

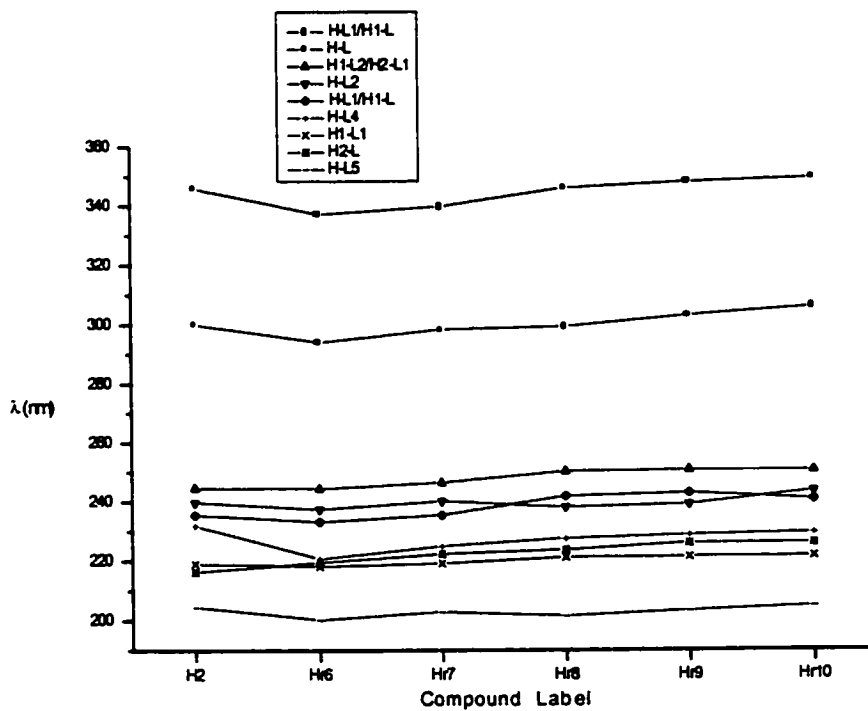**Figure 8.8.** Displacement of the calculated transitions of the series E.

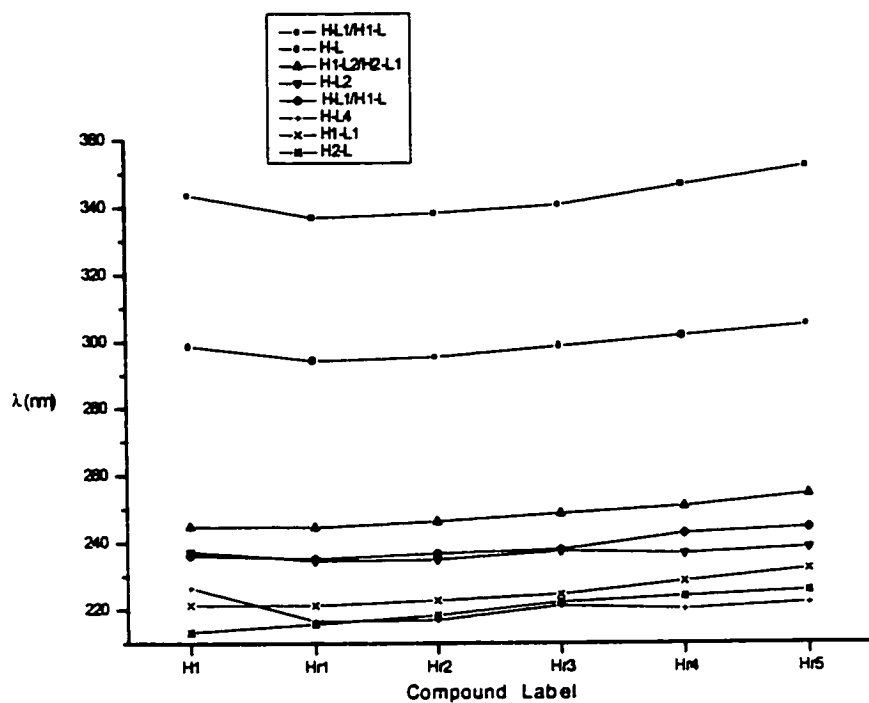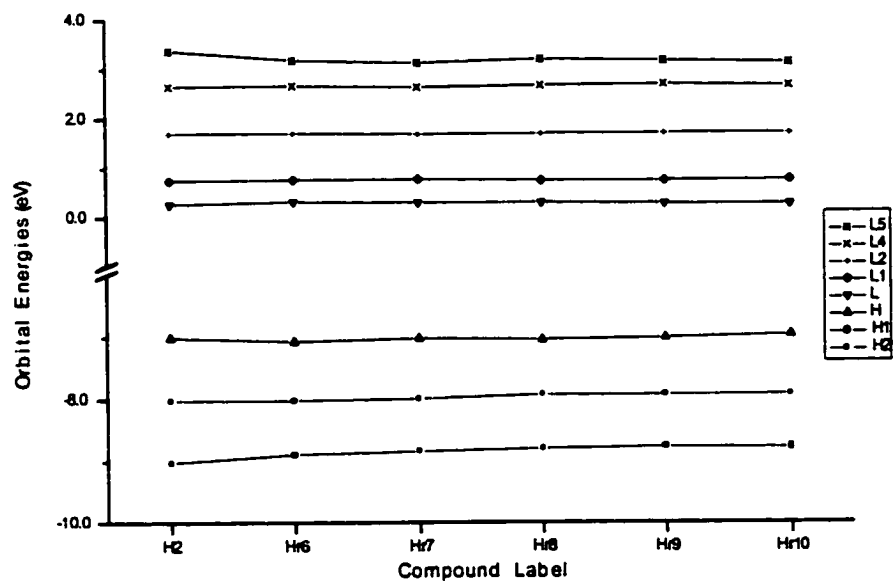**Figure 8.9.** Displacement of the calculated transitions of the series H.
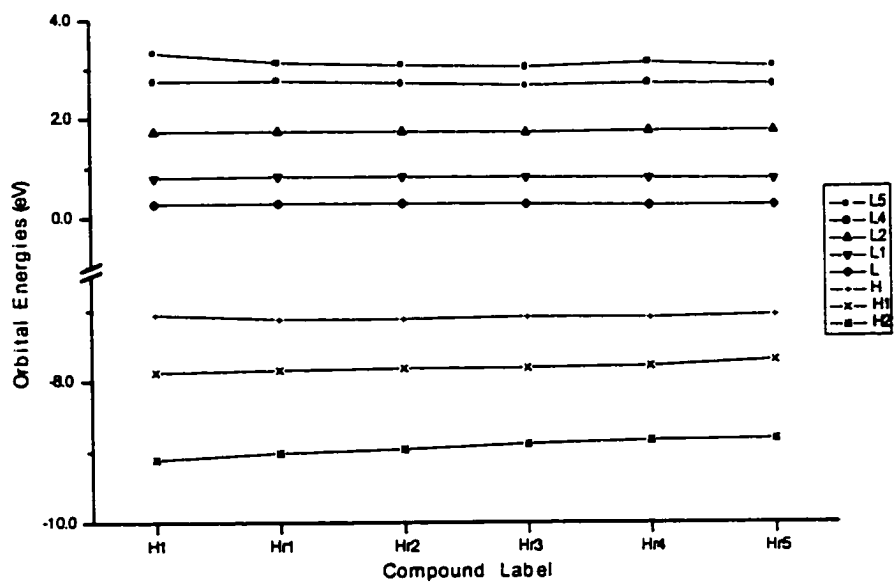
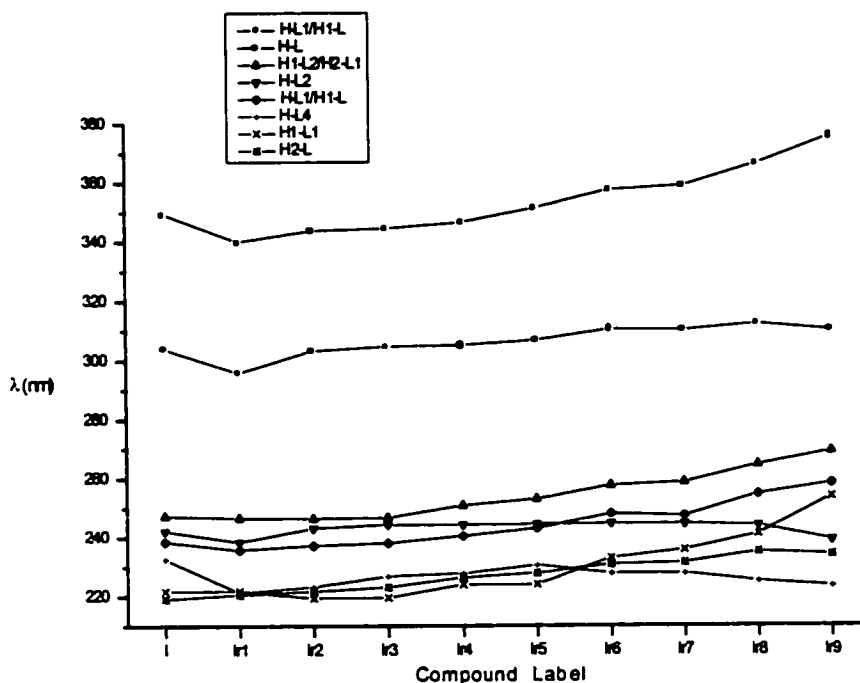**Figure 8.10.** Orbital energies of the series H.

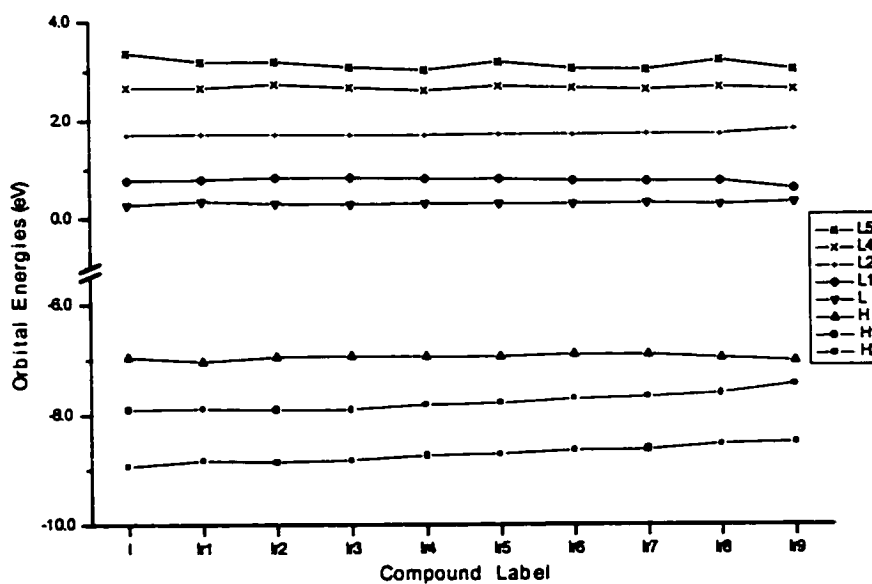**Figure 8.11.** Displacement of the calculated transitions of the series I.


Figure 8.12. Orbital energies of the series I.

Table 8.7. Dihedral angles (in degrees) and distances (Å) of the optimized structures of the series H and I

Label	H1	H,1	H,2	H,3	H,4	H,5
d(a,b,c,d)	180.0	177.7	179.7	179.2	174.4	176.3
d(b,c,d,e)	180.0	178.5	177.7	176.6	171.9	170.7
d(f,g,h,i)	180.0	177.7	175.4	173.2	166.2	160.1
d(g,h,i,j)	180.0	177.9	177.8	174.6	167.3	172.7
r(a,j)	5.100	5.079	5.079	5.081	5.073	5.055
r(f,e)	5.118	5.084	5.083	5.092	5.082	5.084

Label	H2	H,6	H,7	H,8	H,9	H,10
d(a,b,c,d)	180.0	179.1	178.4	178.6	176.0	173.5
d(b,c,d,e)	180.0	177.8	177.6	170.7	173.2	178.1
d(f,g,h,i)	180.0	177.2	176.4	163.0	164.0	169.4
d(g,h,i,j)	180.0	178.9	175.5	175.3	169.7	163.9
r(a,j)	5.085	5.070	5.069	5.044	5.053	5.068
r(f,e)	5.122	5.088	5.084	5.085	5.083	5.073

Label	I	I,1	I,2	I,3	I,4
d(a,b,c,d)	180.0	179.0	176.9	176.4	176.1
d(b,c,d,e)	180.0	179.0	176.8	176.1	172.9
d(f,g,h,i)	180.0	179.0	174.7	176.2	174.0
d(g,h,i,j)	180.0	179.0	174.7	176.3	175.8
r(a,j)	5.125	5.093	5.091	5.082	5.078
r(f,e)	5.121	5.093	5.091	5.092	5.088

Label	I,5	I,6	I,7	I,8	I,9
d(a,b,c,d)	161.7	159.4	163.0	154.3	163.0
d(b,c,d,e)	170.1	171.1	169.0	175.8	163.0
d(f,g,h,i)	179.9	178.1	172.9	175.8	163.0
d(g,h,i,j)	174.6	177.1	178.7	154.3	163.0
r(a,j)	5.081	5.084	5.072	5.070	5.025
r(f,e)	5.088	5.066	5.079	4.986	5.025
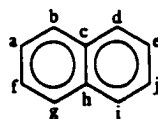
Another important observation is that greater distortions are obtained in those molecules where a maximum of one reduced ring is located in the bridge positions. Reduced substituents in the bridge positions lead to less distortion of the aromatic backbone of the molecule, resulting in shorter wavelengths in comparison with compounds which have reduced groups in other positions. The loss of planarity could be a consequence of the torsional strain in the reduced substituents. The instability provoked by strained substituents is not compensated for by the stability of a completely planar π system.

In some of these compounds (*e.g.*, H_r9, I_r5, I_r6, I_r9, etc) the composition of some of the CIS states is slightly changed. New configurations become dominant making the selection of the transitions to be followed difficult. This could be a reason for the non-uniform change in the displacement of some excited states. The most intense excited states in naphthalene (usually the most intense excited states of the substituted compounds), *i.e.*, the first, second, fourth and sixth transitions, increase in wavelength (decrease in energy) with increasing distortion from planarity. In order to find an explanation for this situation, the ground states of the molecules of series H and I were examined.

To compare the thermodynamic stability of different molecules, their total energies must be compared. But this comparison is only correct when considering molecules with the same type and number of atoms, that is, isomers. In the series H and I there are three sets of isomers, without mixing molecules of different series. These are $H_r1/H_r8/H_r9$, H_r2/H_r10 and I_r1/I_r3. Their total energies as calculated by MOPAC (AM1) and HyperChem (ZINDO/S) are reported in Table 8.8. Although ZINDO/S is not a method designed to obtain ground-state energies, these values were included to show that the AM1 order of stability is also reproduced at the ZINDO/S level.

AM1 and ZINDO/S results are in agreement. Both show that the greater the distortion from planarity, the higher the ground state energy of these molecules. This increase in ground state energy is a consequence of the higher orbital energies of the occupied orbitals.

Table 8.8. Total energies (in au) of the isomers of the series H and I.

Label	E$_T$(AM1)	E$_T$(ZINDO/S)
H$_r$1	-205.22784	-155.76287
H$_r$8	-204.96818	-155.74892
H$_r$9	-204.95961	-155.74745
H$_r$2	-221.74352	-168.66345
H$_r$10	-221.44898	-168.64511
I$_r$1	-238.43199	-181.58033
I$_r$3	-238.30161	-181.56582

Since the energy difference between the ground and excited states becomes smaller with greater distortions from planarity (UV-visible bands are displaced to longer wavelengths), and it has been shown that the ground state energy increases with distortion, it can be inferred that excited states do not increase in energy relative to the ground state as a consequence of the distortion from planarity.

From the calculations presented in this section it can be said that distortions from planarity of the aromatic centre (due to the number and position of the reduced substituents) increase the ground state energy of the naphthalene derivatives more than the corresponding excited states. This is translated into bathochromic displacements of their UV-visible bands with respect to the position of the corresponding bands of other non-distorted derivatives.

The calculated ZINDO/S spectra in terms of position (λ), intensity (f) and composition of the calculated transitions above 200 nm of the compounds included in the present study, and tables with the plotted magnitudes (orbital, transition energies, and wavelength of the calculated bands), are available.[26]

8.4. Conclusions

The effects of methyl and reduced-ring substituents on the electronic excited states of naphthalene have been studied at a semi-empirical level. Successive addition of alkyl substituents on naphthalene leads to bathochromic displacements of its UV-visible bands because of the greater raising of the occupied MOs relative to the unoccupied orbitals. The red-shifts of these bands are a consequence of a relative destabilization of the ground state with respect to the excited states. This slow and steady increase in wavelength with the number of substituents may help to distinguish between a long alkyl chain at one position and several short alkyl substituents.

Analysis of substituent effects on absorption bands corroborates the fact that substituent positions in naphthalene are not equivalent.[8b] Certain substituent positions have zero (or near zero) effect on important bands. Red-shifts obtained when positions 2 and 6 (or only 6 for the reduced derivatives) are occupied are smaller than in other positions in excited states where the only dominant initial MO is H or H2. This may help to identify the substituent positions of an unknown alkylated PAH.

In those cases where no significant distortion from planarity is produced in the aromatic centre of the reduced compounds, very small differences are found between the calculated electronic spectra of these compounds and their methylated analogues. Where the number and position of the reduced substituents affect the planarity of the naphthalene skeleton, the calculated position of the absorption bands among derivatives with the same number of substituents (with methyl or reduced rings) differs greatly. Distorted rings lead to unusually longer wavelengths. The greater the distortion, the greater the bathochromic displacement of the bands. This displacement is a consequence of the destabilization of the ground state with respect to the excited states. This situation can also be extended to larger PAHs, the bigger the PAH the greater the distortion from planarity to be expected due to the presence of reduced-ring substituents. PAHs with reduced rings at bridgehead positions are not as distorted as ones with reduced rings at other positions. These theoretical observations may be useful criteria to assist with the

separation and identification of PACs in complex oil-sands samples, in combination with other analytic techniques, *e.g.* mass spectrometry. Moreover, the retention behavior of electron-acceptor and electron-donor charge-transfer phases for the separation of PAH isomers and methyl-substituted PAHs has been previously studied,[27] and in all cases planar compounds were retained in preference to corresponding non-planar analogues.

The conclusions derived from alkylated naphthalenes could be transferred to larger PAHs for which absorption bands occur at longer wavelengths and these effects are more likely to be detected. Small changes in the energy of the transitions will result in a large change in the (observable) wavelength of the absorption spectrum.

8.5. References

1. Vo-Dinh, T. *Chemical Analysis of Polycyclic Aromatic Compounds*, Wiley, New York, 1989.

2. Information obtained through private correspondence with Michael Potvin and Drs. L. Ramaley and R.D. Guy, Dalhousie University.

3. Robbins, W.K. *J. Chromatogr. Sci.* **1998**, *36*, 457.

4. (a) Purvis, J.E. *J. Chem. Soc.* **1912**, *101*, 1315. (b) Sponer, H.; Cooper, C.D. *J. Chem. Phys.* **1955**, *23*, 646. (c) George, G.A.; Morris, G.C. *J. Mol. Spect.* **1968**, *26*, 647. (d) Huebner, R.H.; Mielczarek, S.R.; Kuyatt, C.E. *Chem. Phys. Lett.* **1972**, *16*, 464. (e) Hasnain, S.S.; Brint, P.; Hamilton, T.D.S.; Munro, I.H. *J. Mol. Spect.* **1978**, *72*, 349. (f) Salama, F.; Allamandola, L.J. *J. Chem. Phys.* **1991**, *94*, 6964.

5. (a) Hartley, W.N. *J. Chem. Soc.* **1881**, *39*, 153. (b) *UV Atlas of Organic Compounds*, Verlag Chemie, Weiheim, Butterworths, London, 1966. (c) *The Sadtler Handbook of Ultraviolet Spectra*, Ed. Simons, W.W., Heydin & Son Ltd., 1979. (d) Friedel, R.A.; Orchin, M. *Ultraviolet Spectra of Aromatic Compounds*, Wiley: New York, 1951.

6. (a) Pariser, R. *J. Chem. Phys.* **1956**, *24*, 250. (b) Ridley, J.; Zerner, M.C. *Theor. Chim. Acta* **1973**, *32*, 111. (c) Ridley, J.E.; Zerner, M.C. *J. Mol. Spect.* **1974**, *50*, 457. (d) Åsbrink, L.; Fridh, C.; Lindholm, E. *Z. Naturforsch.* **1978**, *33a*, 172. (e)

Du, P.; Salama, F.; Loew, G.H. *Chem. Phys.* **1993**, *173*, 421. (f) Grimme, S. *J. Comput. Chem.* **1994**, *15*, 424.

7. (a) Buenker, R.J.; Peyerimhoff, S.D. *Chem. Phys. Lett.* **1969**, *3*, 37. (b) Matos, J.M.O.; Roos, B.O. *Theor. Chim. Acta* **1988**, *74*, 363. (c) Rubio, M.; Merchan, M.; Orti, E.; Roos, B.O. *Chem. Phys.* **1994**, *179*, 395. (d) Hashimoto, T.; Nakano, H.; Hirao, K. *J. Chem. Phys.* **1996**, *104*, 6244.

8. (a) Heilbronner, E.; Fröhlicher, U.; Plattner, Pl.A. *Helv. Chim. Acta* **1949**, *32*, 2479. (b) Mosby, W.L. *J. Am. Chem. Soc.* **1952**, *74*, 2564. (c) de Laszlo, H. Z. *Phys. Chem.* **1925**, *118*, 369. (d) Bailey, A.S.; Bryant, K.C.; Hancock, R.A.; Morrell, S.H.; Smith, J.C. *J. Inst. Petroleum* **1947**, *33*, 503. (e) Morton, R.A; de Gouveia, A.J.A. *J. Chem. Soc.* **1934**, 916.

9. (a) Baba, H.; Suzuki, S. *Bull. Chem. Soc. Jap.* **1967**, *40*, 2457. (b) Fujii, T.; Suzuki, S.; Takemura, T. *J. Chem. Phys.* **1969**, *50*, 2078. (c) Suzuki, S.; Fujii, T.; Baba, H. *J. Mol. Spect.* **1973**, *47*, 243. (d) Suzuki, S.; Fujii, T.; Ishikawa, T. *J. Mol. Spect.* **1975**, *57*, 490. (e) Suzuki, S.; Fujii, T. J. Mol. Spect. **1976**, *61*, 350.

10. Dewar, M.J.S.; Zoebisch, E.; Healy, E.F.; Stewart, J.P.P. *J. Am. Chem. Soc.* **1985**, *107*, 3902.

11. Stewart, J.J.P. MOPAC: QCPE Program No. 455 (v.6.0).

12. Del Bene, J.; Jaffé, H.H. *J. Chem. Phys.* **1968**, *48*, 1807, 4050.

13. Montero, L.A.; Alfonso, L.; Alvarez, J.R.; Pérez, E. *Int. J. Quantum Chem.* **1990**, *37*, 465.

14. (a) Ridley, J.; Zerner, M.C. *Theor. Chim. Acta* **1976**, *42*, 223. (b) Bacon, A.D.; Zerner, M.C. *Theor. Chim. Acta* **1979**, *53*, 21. (c) Zerner, M.C.; Loew, G.H.; Kirchner, R.F.; Mueller-Westerhoff, U.T. *J. Am. Chem. Soc.* **1980**, *102*, 589.

15. Montero, L.A.; Guevara, N.; Mora-Diez, N. Program NDOL for PC computers and Unix environments, 1985-1996.

16. HyperChem (v.5.0), Hypercube, Inc., 1996.

17. Foresman, J.B.; Head-Gordon, M. *J. Phys. Chem.* **1992**, *96*, 135.

18. Foresman, J.B.; Frisch, Æ. *Exploring Chemistry with Electronic Structure Methods*, 2nd edition, Gaussian, Inc., Pittsburgh, PA, 1996.

19. (a) Bauernschmitt, R.; Ahlrichs, R. *Chem. Phys. Lett.* **1996**, *256*, 454. (b) Casida, M.E.; Jamorski, C.; Casida, K.C.; Salahub, D.R. *J. Chem. Phys.* **1998**, *108*, 4439. (c) Stratmann, R.E.; Scuseria, G.E.; Frisch, M.J. *J. Chem. Phys.* **1998**, *109*, 8218.

20. Gaussian 98, (Revision A.4), Frisch, M.J.; Trucks, G.W.; Schlegel, H.B.; Scuseria, G.E.; Robb, M.A.; Cheeseman, J.R.; Zakrzewski, V.G.; Montgomery, J.A.; Stratmann, R.E.; Burant, J.C.; Dapprich, S.; Millam, J.M.; Daniels, A.D.; Kudin, K.N.; Strain, M.C.; Farkas, O.; Tomasi, J.; Barone, V.; Cossi, M.; Cammi, R.; Mennucci, B.; Pomelli, C.; Adamo, C.; Clifford, S.; Ochterski, J.; Petersson, G.A.; Ayala, P.Y.; Cui, Q.; Morokuma, K.; Malick, D.K.; Rabuck, A.D.; Raghavachari, K.; Foresman, J.B.; Cioslowski, J.; Ortiz, J.V.; Stefanov, B.B.; Liu, G.; Liashenko, A.; Piskorz, P.; Komaromi, I.; Gomperts, R.; Martin, R.L.; Fox, D.J.; Keith, T.; Al-Laham, M.A.; Peng, C.Y.; Nanayakkara, A.; Gonzalez, C.; Challacombe, M.; Gill, P.M.W.; Johnson, B.; Chen, W.; Wong, M.W.; Andres, J.L.; Head-Gordon, M.; Replogle, E.S.; Pople, J.A. Gaussian, Inc.: Pittsburgh PA, 1998.

21. Becke, A.D. *J. Chem. Phys.* **1993**, *98*, 1372.

22. Lee, C.; Yang, W.; Parr, R.G. *Phys. Rev. B* **1988**, *37*, 785.

23. (a) Badger, G.M. *J. Chem. Soc.* **1949**, 2500. (b) Badger, G.M.; Pearce, R.S.; Petit, R. *ibid.* **1952**, 1112.

24. Askew, F.A. *J. Chem. Soc.* **1935**, 509.

25. Coulson, C.A.; Longuet-Higgins, H.C. *Proc. Roy. Soc. A* **1947**, *191*, 39; **1948**, *195*, 188.

26. Mora-Diez, N; Boyd, R.J.; Heard, G.L. *J. Phys. Chem. A* **2000**, *104*, 1020.

27. Sander, L.C.; Parris, R.M.; Wise, S.A.; Garrigues, P. *Anal. Chem.* **1991**, *63*, 2589.

PART 3

Chapter 9. Global Conclusions and Future Work

9.1. OH and NO₃ hydrogen-abstraction reactions from aldehydes

9.1.1. Global conclusions

The main conclusion of this study is that in the gas phase there are no elementary bimolecular reactions (in which a TS is formed) because a reactant complex is always initially formed, even though in some cases its formation is irrelevant. The consideration of the reactant complex formation is especially important in radical-molecule reactions, many of which are known to occur with an apparent negative activation energy.

It can also be rationalized from the present results that the bigger the effective energy barrier for radical-molecule reactions, and the smaller the stabilization energy of the reactant complex, the more closely its behaviour resembles an elementary reaction. In other words, two extreme behaviours can be considered for a radical-molecule reaction: for systems with very low or negative activation energies the consideration of a complex mechanism is essential (as in the case of the OH + aldehyde reactions), but if the activation energy is significantly higher and the stabilization energy of the reactant complex is negligible, then the consideration of an elementary process will be a satisfactory approximation. This situation was made evident in the study of the NO₃ hydrogen-abstraction reactions for which it was shown that the formation of the reactant complex could be ignored.

After being able to establish computational methodologies to reproduce the experimental kinetic and thermodynamic parameters of the two groups of reactions studied, better or new theoretically determined quantities were obtained for reactions for which incomplete or no kinetic information is available. The predictive capability of the combination of *ab initio* methods with TST, considering Eckart corrections for tunneling, has been demonstrated.

212

9.1.2. Suggestions for future work

Even though only TST with Eckart tunneling corrections were applied in these studies, it would be interesting to test how other more sophisticated theories behave in predicting the rate constants of the reactions studied.

If the equilibrium constant for the reactant complex formation, K_{eq}, and the rate constant of the hydrogen-abstraction process, k_2, were to be reported, they need to be corrected by considering the internal rotations generated in the reactant complex.

The incorporation of tunneling effects in the calculation of activation energies and pre-exponential factors for the reactions in which tunneling was estimated to be significant, would be interesting. It will require the calculation of rate constants at temperatures around 298 K and the construction of a lnk *versus* 1/T plot (or by obtaining the corresponding analytical expression). From the slope and the intercept of the tangent to the above mentioned curve at the desired temperature, the Arrhenius parameters may be determined. This procedure will allow the determination of the pre-exponential factors for the reactions of FCHO and ClCHO with OH and NO_3, which are not known experimentally. In fact, such a program was written by the author in FORTRAN language but still needs to be tested for systems in which free internal rotations are considered to correct the total partition function of the TS. This program has already been used to obtain Arrhenius plots for the intramolecular hydrogen transfer in polymers, as a project in collaboration with Dr. Jesus M. Ugalde at the University of the Basque Country, in Spain.

Preliminary calculations on the NO_3 radical at the B3LYP/6-311G(d,p) level show that the D_{3h} structure is predicted to be the ground state minimum. CCSD(T) single point calculations using the previous geometry and basis set gives a similar result, although the difference in energy with the other C_{2v} structures is very small. This result is in correspondence with the fact that in the B3 functional less HF exchange is considered in comparison with the BH&H functional. This suggests that maybe B3LYP optimized

geometries and frequencies could be used for kinetic studies on reactions with the NO_3 radical. For the reaction of acetone with NO_3, only an upper bound rate constant has been reported, hence, this could be another interesting system to work on.

9.2. Effects of alkyl substituents on the excited states of naphthalene

9.2.1. Suggestions for future work

A series of mono-, di-, tri- and tetra-methylnaphthalenes have already been studied in order to determine if there is a correlation between the pattern of substitution, the degree of perturbation of the molecular orbitals, and the UV-visible bands of these compounds. Geometry optimizations were performed at different levels of theory: AM1, HF and B3LYP, and excited states were obtained by means of the semiempirical ZINDO/S method. Principal component analysis (PCA), a multivariate technique, has been shown to provide important insight into establishing such correlations when large sets of theoretical data are analysed. Isomers with the same pattern of substitution have shown very similar UV-visible spectra because their MOs are perturbed in a similar way. The above study could be extended to all the tri- and tetra-methylnaphthalenes.

The probability densities of certain MOs and the composition of the calculated excited states (in terms of the dominant singly excited configurations) can also help rationalize the effects of different substituent positions on the perturbation of MOs and the position of the UV-visible maxima.

Ultraviolet detection in high performance liquid chromatography (HPLC) is particularly useful for PACs, especially in non-polar solvents. Fluorescence detection in HPLC is a more frequently used technique for these compounds than UV-visible detection. Hence, the prediction (calculation) of fluorescence spectra of PACs would be very useful to assist in the separation and identification of these compounds, particularly since all the standards needed to validate the identifications are not available.

When absorption spectra are measured in solvents of increasing polarity it is found that the position and intensity of absorption bands change. Fluorescence spectra are more dependent on the environment and greater changes are produced with the change of solvent. Solvent effects have been ignored in this study (calculations have been done in the gas phase), but more realistic predictions require their consideration.